Synthesis and exploration of resorcinol derivatives as *Plasmodium falciparum* Hsp90 inhibitors

A thesis presented by

Théoneste UMUMARARUNGU

in fulfilment of the requirements of the degree

of

PhD in Pharmacy

The Faculty of Pharmacy, Rhodes University

6140 Grahamstown

December 2015

Abstract

 In this research project, we have synthesized a series of nine dimethyl ether resorcinol analogues of NMS-E973 (L-1) **38**, a potent Hsp90 inhibitor. These analogues were chosen because they share the same pharmacophore with NMS-E973 (L-1) **38** and were thus expected to have a similar biological activity. Moreover, it is generally easier to synthesize the dimethyl ether resorcinol analogues of NMS-E973 (L-1) **38** as compared to their demethylated counterparts. Since other Hsp90 inhibitors such as geldanamycin **19** have demonstrated anti-plasmodial activity, we also expected our compounds to be Hsp90 inhibitors and to possess anti-plasmodial activity. However, our compounds were tested for growth inhibitory activity of *Plasmodium falciparum* and not for *P. falciparum* Hsp90 (*Pf*HSP90) inhibitory activity.

The synthesis involved a series of steps that led to the formation of the ester compound TU-011 (L-7) **43** that was then used as a precursor for different NMS-E973 (L-1) **38** analogues. The choice of analogues to be synthesized was dictated by binding affinity predictions obtained from molecular docking.

 The chosen synthetic analogues were active against chloroquine-sensitive *Plasmodium falciparum* (3D7 strain) in a *Plasmodium* lactate dehydrogenase assay and they were not generally cytotoxic to human cervical adenocarcinoma cell line HeLa. The most active of our compounds was TU-018 (L-103) **50** with an IC_{50} value of approximately 1.830 μM as compared to the standard, chloroquine, with an IC_{50} value of 0.01062 μM. Some of the compounds showed mild cytotoxicity towards HeLa cells with IC_{50} values higher than 25 μM as compared to the standard apoptosis inducer drug, emetine that had an IC_{50} value of 0.09948 μM.

These results highlight the fact that the synthesized analogues are novel relatively non-toxic anti-plasmodial agents.

Acknowledgments

Dedication

Dedicated to my mom

Table of Contents

List of figures

List of tables

Abbreviations

17-AAG	17-(allylamino)-17-demethoxygeldanamycin
17-DMAG	17-Dimethylaminoethylamino-17-demethoxygeldanamycin
ACT	Artemisinin combination therapies
ADP	Adenosine diphosphate
Aha1	Activator of heat shock protein 90 ATPase homology 1
ATP	Adenosine triphosphate
CDCl$_3$	Deuterated chloroform
COSY	Correlation spectroscopy
cRaf1	CD40 Receptor associated factor 1
DEPT	Distortionless enhancement by polarization transfer
DHFR	Dihydrofolate reductase
DHPS	Dihydropteroate synthetase
DIPEA	*N,N*-diisopropylethylamine
DMA	*N,N*-dimethylacetamide
DMF	Dimethylformamide
DMSO	Dimethyl sulfoxide
DMSO-d$_6$	Deuterated dimethyl sulfoxide
DNA	Deoxyribonucleic acid
Erb2	Estrogen receptor b2

ESI   Electron-spray ionisation

HMBC   Heteronuclear multiple bond correlation

HRMS   High Resolution Mass Spectrometry

Hsp90   Heat shock protein 90

HSQC   Heteronuclear single quantum coherence

IC_{50} The half maximal inhibitory concentration

IRS   Indoor residual spraying

ITN   Insecticide-treated mosquito nets

Ki   Constant of inhibition

NBT/PES   Nitro blue tetra-zolium + phenazine ethosulphate

NMR   Nuclear magnetic resonance

NOESY   Nuclear Overhauser effect spectroscopy

PDB   Protein Data Bank

*Pf*CRT   *Plasmodium falciparum* chloroquine resistance transporter

*Pf*Hsp90   *Plasmodium falciparum* Hsp90

PLDH   *Plasmodium* lactate dehydrogenase

ppm   Parts per million

QSAR   Quantitative structure activity relationship

RPMI   Roswell Park Memorial Institute

Sti1/Hop   Stress inducible 1/Hsp70-Hsp90 organizing protein

TBTU   *N,N,N',N'*-tetramethyl-O-(benzotriazol-1-yl)uronium tetrafluoroborate

THF   Tetrahydrofuran

UV   Ultraviolet

WHO   World Health Organization

Chapter One: Introduction

Different diseases affect the world population and some of these diseases such as malaria are infectious while others such as cardiovascular diseases are non-infectious. The health risk associated with these diseases and the economic burden imposed by their treatment imply that there is a constant need to look for different ways of overcoming these diseases. Amongst the methods used in fighting different diseases are treatment with therapeutic drugs and the use of preventative methods to combat the infections. In the case of infectious diseases such as malaria, the causative agents, for example, *Plasmodium falciparum*, generally develop resistance over the course of time, which implies a permanent need to develop new drugs with a novel mode of action to efficiently overcome the rising number of cases of multidrug resistance.

1.1. Malaria and Plasmodium falciparum

1.1.1. Overview of Malaria and *Plasmodium falciparum*

Malaria is one of the deadliest infectious diseases.[1] It is estimated that 198 million cases of malaria occurred globally and that 584000 lives were lost due to malaria in 2013.[2] The disease affects particularly the African continent where 90% of malarial deaths occurred in 2013. Young children accounted for 78% of all malarial deaths in the same year.[2] In 2013, 82% of cases that occurred were in the WHO African Region, 12% were in the WHO South-East Asia Region and 5% were in the WHO Eastern Mediterranean Region.[2] In response to these alarming figures, different malaria control programs have been put in place and thus far they have yielded impressive results. For example, the global malaria mortality rates decreased by 47% between 2000 and 2013.[2] The control programs include vector control through the use of insecticide-treated mosquito nets (ITNs) or indoor residual spraying (IRS), chemoprevention, and case management which consists of the diagnosis and treatment of infections.[2]

Malaria is spread from one person to another through the bite of an infected female *Anopheles* mosquito.[3,4] Infection in humans is caused by five species that belong to the genus *Plasmodium*: *P. falciparum*, *P. vivax*, *P. malariae*, *P. ovale* and *P. knowlesi*.[1,3] Although cases of malaria in humans due to *P. knowlesi* have been recorded in recent years, it

normally causes malaria in monkeys and it is found in some forested areas of South-East Asia.[2] The most dangerous malaria causing species is *P. falciparum*.[3] *P. vivax* is geographically more widespread than *P. falciparum* due to its ability to resist harsh conditions. *P. vivax* has the capability to develop in *Anopheles* mosquitoes at lower temperatures and to survive at higher altitudes and in cooler climates than the other species.[3] It has a dormant liver stage called hypnozoite that enables it to survive when *Anopheles* mosquitoes are not present, e.g. during winter.[3]

Although *P. vivax* occurs throughout Africa, the risk of infection is low due to the absence of the Duffy gene in many African populations.[2] The Duffy gene produces the protein necessary for *P. vivax* to invade the red blood cells.[2] While *P. falciparum* is the most prevalent on the African continent, infections due to *P. vivax* are more common in many areas outside Africa.[2]

1.1.2. The life cycle of *Plasmodium*

The life cycle of *Plasmodium* can be divided into three stages as illustrated in **Figure 1**. It is complex and involves both the female *Anopheles* mosquito host and the human host. Only 30 of the 400 different species of *Anopheles* mosquitoes are considered major vectors.[2] The life cycle of *Plasmodium* can be divided into three stages as illustrated in **Figure 1**.

1.1.2.1. The liver stage

After the female *Anopheles* mosquito has injected the parasites in the form of sporozoites into the blood stream of the human host, they migrate into the liver within 30 minutes where they replicate.[1] Inside the hepatocyte, the sporozoites develop into schizonts, which in turn develop over a period of a week to give tens of thousands of merozoites.[5] In the case of *P. vivax* and *P. ovale*, the parasite can stay dormant in the liver for many years in the form of hypnozoites which can later cause the relapses of infections.[1,2,5,6] In order for the merozoites inside the hepatocytes to invade erythrocytes, they first need to escape the host immune system.[7] The merozoites escape the macrophages (Kupffer cells) in the sinusoids by hiding inside hepatocyte-derived structures called merosomes which bulge into the liver sinusoids and release merozoites into the bloodstream.[7]
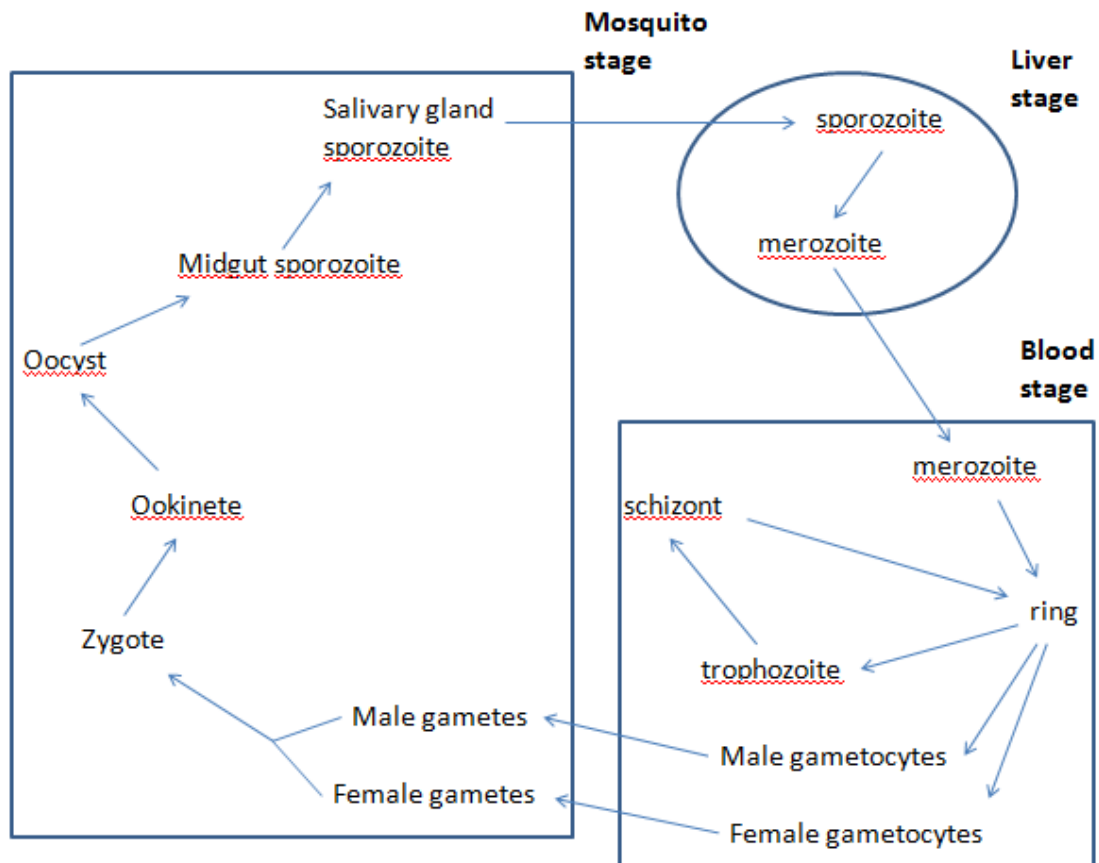
Figure 1: *Plasmodium falciparum* life cycle[4]

1.1.2.2. The blood stage

After five to ten days, the hepatocytes burst and release merozoites which invade new red blood cells (erythrocytes) and rapidly proliferate, causing malaria symptoms.[1] It is thought that the merozoite invasion of red blood cells takes place in steps. First, a random contact between any surface of the free merozoite and the human red blood cell is mediated by merozoite surface proteins (the apical organelles).[8] The merozoite then re-orientates itself such that the apical end makes a tight junction with the red blood cell surface.[8] Subsequently, the merozoite invades the cell using an actin-myosin motor and the intraerythrocytic development cycle follows.[8] Inside the erythrocytes, the merozoites go through various forms (the ring form, the trophozoite form and the schizont form) which lead to the formation of about 20 new daughter merozoites.[1] These daughter merozoite are released in the blood stream and infect new red blood cells.[1]

Each intraerythrocytic asexual cycle of *P. falciparum* lasts approximately 48 hours.[9] These daughter merozoites are released in the blood stream and infect new red blood cells.[1] After several asexual reproductions in the erythrocytes, some of the merozoites differentiate into female and male gametocytes, which only contain a half set of chromosomes.[1] Gametocytes go through five stages of maturation and only stage V is capable of infecting the mosquitoes.[1]

1.1.2.3. The mosquito stage

During a blood meal, the gametocytes are taken up by the mosquito and once inside, they differentiate into gametes that fuse to give a zygote.[10] Only mature gametocytes survive inside the mosquito after being taken up in a blood meal.[11] While gametocytes development is arrested for many days in the blood stream of the vertebrate host, they are activated within seconds after being taken up by a mosquito in a blood meal.[12] The activation of gametocytes inside the mosquito's gut lumen is stimulated by the change in environmental conditions as they pass from the human host into the mosquito host.[13] Inside the mosquito's gut, the gametocytes experience an increase in Ca^{2+} ions concentration, a drop in temperature (from 37 °C inside the human host to $20 - 25$ °C inside the mosquito) and a rise in pH as well as the presence of xanthurenic acid.[12] After nuclear fusion in the zygote, DNA replication and meiosis ensue and the zygote later changes into an elongated and highly motile form called an ookinete that then crosses the midgut epithelium and forms an oocyst on the haemocoel side of the midgut wall.[12,14,15]

1.1.3. Treatment and prevention of malaria

Despite decades of research on the development of an efficacious malaria vaccine, providing long-term protection, one has not yet been found.[16] Currently, the most advanced vaccine that has been developed is RTS,S/AS01, a recombinant protein candidate malaria vaccine whose phase III clinical trials were recently published.[16] It was found that RTS,S/AS01 substantially prevented clinical malaria in young infants and children over a period of 3 - 4 years with or without a booster dose, with its protective effect enhanced by the administration of a booster dose.[17] Thus, malaria chemotherapy remains a viable option for treatment and prevention of malarial infections.

1.1.3.1. Old and new antimalarial drugs

There are different anti-malarial drugs that can be grouped according to their chemical structures, their targeted stage of the parasite development or their mode of action. Some of the drugs used as anti-malarials are used as prophylactic treatment. They target the liver stage of the *Plasmodium* parasite and prevent the disease from developing.[1] In the case of *P. vivax* and *P. ovale* which can both switch into an active form after months or years in a dormant stage (hypnozoite), the drugs that target the liver provide what is known as a radical cure.[1] In 2013, primaquine **1** was being used to treat the hypnozoite stage of malaria in more than 50 countries with transmission of *P. vivax* malaria.[2] Despite its high cost, the combination of atovaquone **2**/proguanil **3** (a prodrug for cycloguanil **4**), is preferred as prophylactic treatment because it is well tolerated.[1]
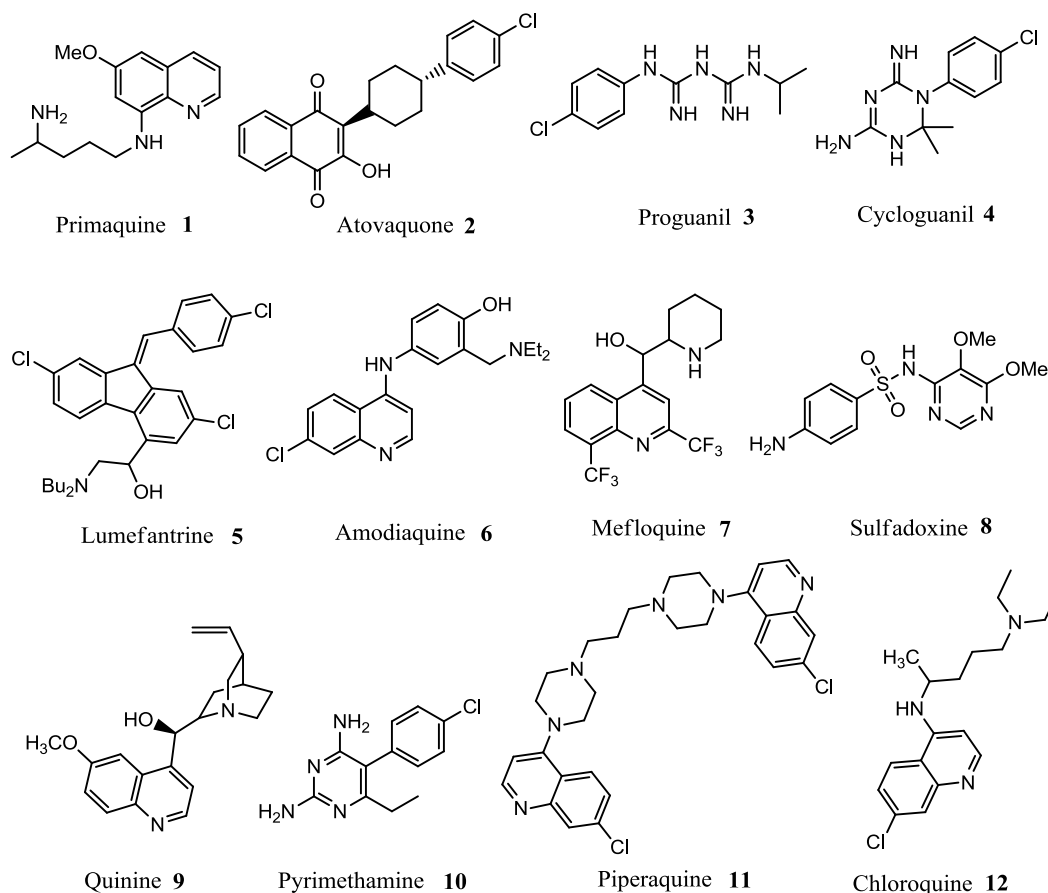
Figure 2: Structures of some non-peroxide anti-malarial drugs in use[1,10,18]

5

Most of the currently approved anti-malarial drugs target the blood stage of *P. falciparum* in general in order to help control the symptoms of malaria.[1,11] However, some of these drugs also target the gametocytes and help prevent the transmission of the parasite between humans.[1,11] Typical examples of gametocytocidal drugs belong to the class of 8-aminoquinolones with primaquine **1** being the only known drug effective against mature gametocytes.[10] However, it is less active against the intraerythrocytic forms of *P. falciparum* and it is generally recommended that it be used in combination with drugs that are active against the intraerythrocytic these forms.[10] The other drawback is that primaquine **1** causes haemolytic anaemia in people who are deficient in glucose-6-phosphate dehydrogenase.[19]

Artemisinin **13**   Artemether **14**   Artesunate **15**   Dihydroartemisinin **16**

OZ439 **17**   OZ277 **18**
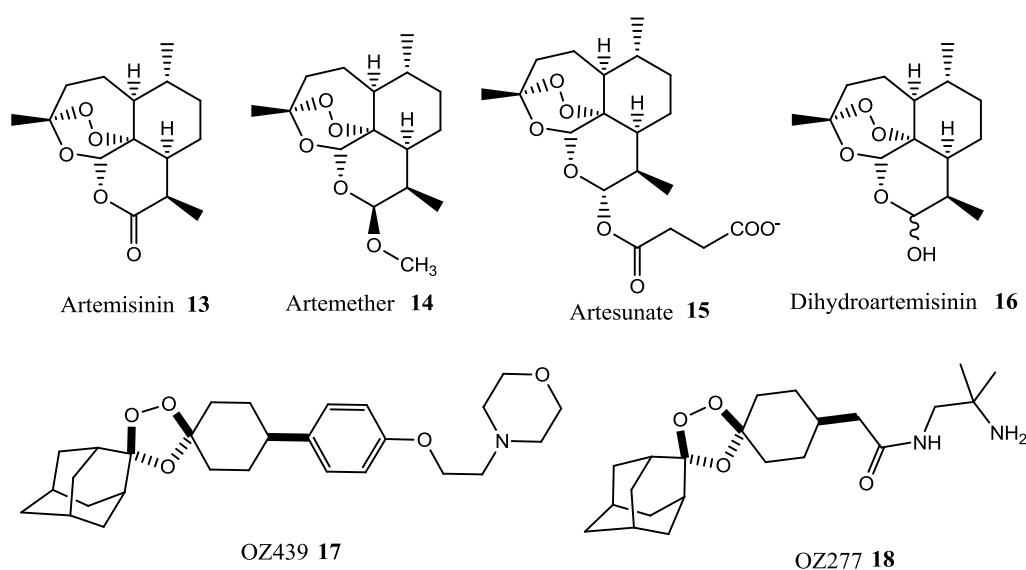
Figure 3: Structures of some peroxide-based anti-malarial drugs in use or in development[1,10,18]

Artemisinin combination therapies (ACTs) are the WHO recommended first line treatment for uncomplicated *P. falciparum*.[3] ACTs have been found to be highly efficacious in treating uncomplicated malaria as exemplified by the study done by Bukirwa *et al*.[20] in Tororo (Uganda), an area with very high malaria transmission. In areas where transmission is high, severe malaria is treated with quinine **9** or an artemisinin derivative.[18] Artemisinin **13** is produced by the plant *Artemisia annua*.[1,10] Despite their short plasma half-lives, artemisinins are good therapeutic options because of their rapid action and safety.[20-23] Due to their active uptake by *Plasmodium* parasites, artemisinins are highly toxic against the parasites at nanomolar concentrations while micromolar concentrations are needed for their toxicity to

mammal cells.[21] Once most of the parasite mass has been eliminated by an artemisinin **13**, the remaining parasites are eliminated by a partner drug that has a longer plasma half-life.[10] Artemisinins are active against gametocytes in the early stages of development which contributes to the reduction of the gametocytes that reach the mature stage necessary for transmission to the mosquito.[6] The current WHO policy about the use of ACTs recommends that the preferred choice of an ACT be dictated by the therapeutic efficacy of that ACT in the intended area of use.[3] Artemether **14** should be combined with lumefantrine **5**, artesunate **15** with amodiaquine **6** or mefloquine **7** or sulfadoxine **8**-pyrimethamine **10**, and dihydroartemisinin **16** with piperaquine **11**.[3]

The success of the currently used artemisinins has prompted interest in the synthesis of more structurally diverse artemisinin derivatives and synthetic analogues of artemisinin. Some of them have been found *in vitro* more active than artemisinin **13**.[24] For example, some of the semi-synthetic artemisinins were tested *in vitro* against chloroquine-sensitive (3D7) and chloroquine-resistant (K1) strains and found to be three times more potent than artemisinin **13** with high therapeutic indexes.[24] Semi-synthetic artemisinins also completely cured mice infected with multidrug resistant *P. yoeliinigeriensis*.[24] Moreover, the synthetic peroxide OZ439 **17** cures mice infected with malaria in a single dose of 20 mg/kg, which cannot be achieved using artemisinin **13** without a partner drug.[25] In preclinical embryo-foetal development studies, the synthetic peroxides OZ439 **17** and OZ277 **18** were found to have a safety margin which was approximately 100 times higher than that of an artemisinin derivatives.[11]

1.1.3.2. Resistance to existing anti-malarials

Although the use of a combination of drugs reduces the emergence of resistance, it also sometimes fails, which highlights a constant need for new drugs.[1] Ideally, the new drug should be rapid acting, amenable to a single dose, well tolerated especially in pregnant women and children and also adress the drug resistance problem.[1] Mefloquine **7** is the only anti-malarial drug that acts effectively in a single dose when administered as a single agent.[1] It is preferable that the new molecule be chemically different from the existing drugs as this may avert the development of cross-resistance by the parasites.[18] Due to its efficacy, low cost and safety, chloroquine **12** was a gold standard treatment for malaria for many years

starting from the late 1940s.[26] Its massive use for treatment and prevention led to the emergence of chloroquine-resistant strains with resistance associated with the *P. falciparum* chloroquine resistance transporter (*Pf*CRT).[19] To sustain their development, *Plasmodium* parasites degrade approximately 70% of the haemoglobin of the erythrocytes, which results in the release of the heme that is highly toxic to the parasites.[27] In order, to survive and maintain progress, the parasite detoxifies the heme by crystallizing it into a non-toxic structure called hemozoin.[27] Chloroquine **12** acts by binding to the heme and preventing its detoxification.[19] *Pf*CRT-associated chloroquine resistance is thought to involve active efflux of the drug from the parasite's food vacuole where it accumulates.[28] However, both chloroquine-sensitive and chloroquine-resistant *P. falciparum* parasites possess chloroquine carriers and they only differ by their efficacy, with the chloroquine-resistant parasite having the most efficacious carrier.[28]

After emergence of resistance to chloroquine **12**, it was replaced in many countries with a sulfadoxine **8**–pyrimethamine **10** combination as the first line treatment.[19] This combination was also very effective, low cost and safe.[19] Sulfadoxine **8** and pyrimethamine **10** act synergistically to inhibit two important enzymes of *Plasmodium*, namely dihydrofolate reductase (DHFR) and dihydropteroate synthetase (DHPS).[23,29] Unfortunately, point mutations in DHFR and DHPS genes make *P. falciparum* resistant to pyrimethamine **10** and sulfadoxine **8** respectively.[29] After the emergence of resistance to sulfadoxine **8**-pyrimethamine **10** and many other existing antimalarial drugs, artemisinins were recommended by the WHO as the first line treatment.[2,19]. However, resistance to artemisinin **13** and its derivatives has been recently observed along the Thai-Cambodian border, which highlights the need for antimalarial drugs with a novel mode of action to counteract the rising cases of drug resistance.[2,19] It is thought that resistance resulted from the use of artemisinin **13** derivatives as monotherapy.[19] Some novel drugs are being investigated as possible substitutes to artemisinins and these include synthetic peroxides and drugs previously developed for other diseases such as heat shock protein 90 (Hsp90) inhibitors previously developed for the treatment of cancer.[1,30,31]

1.2. Heat shock protein 90 (Hsp90)

1.2.1. Overview of Hsp90

Heat shock protein 90 belongs to a superfamily of proteins which also include histidine kinases, gyrase and MutL proteins. They all have a novel ATP-binding pocket named the Bergerat fold in common.[32] These proteins also share an ATP-lid region which serves as a rotatable cover for the ATP-binding pocket and differs in length and tertiary structure as well as its predominance of closed or open states from one protein to another.[32,33] The heat shock protein 90 family are ubiquitous molecular chaperones that play a key role in protein folding, stabilization and activation of a wide range of proteins including those involved in signal transduction, cell cycle regulation and steroid hormone responsiveness.[34,35] An *in silico* analysis done by Pavithra *et al*.[36] suggested that *P. falciparum* Hsp90 (*Pf*Hsp90) might be involved in chromatin remodelling and protein translation.

Hsp90 works closely with the ubiquitin-proteasome machinery to maintain protein homeostasis.[35] The 26S proteasome needs the ATP (adenosine triphosphate) activity of Hsp90 for its assembly both *in vivo* and *in vitro*.[35] The 26S proteasome is involved in the degradation of most cellular proteins in eukaryotic cells usually after they have been tagged by covalent bonding with polyubiquitin.[37] Hsp90 is the most abundant of all molecular chaperones present in the cytosol of eukaryotic cells.[38] Hsp90 molecular chaperones differ from other chaperones in that they do not bind to nascent or unfolded polypeptides and that they interact with a large number of co-chaperones. In contrast, Hsp90 binds to a limited number of partially folded client proteins.[38] These client proteins belong to different protein families and do not have any clear structural nor conformational similarity between them. However, they all have an intrinsic instability and a need to undergo conformational changes in order to achieve their active states in common.[38]

The increased ATPase activity of the Hsp90 of cancer cells is very important for their increased proliferation and survival.[39] Hsp90 is essential for the survival of a number of protozoan parasites in harsh environmental conditions and these parasites include those of the genera *Plasmodium*, *Leishmania*, *Eimeria*, *Toxoplasma* and *Trypanosoma*.[31,40-43] Hsp90 is secreted by normal cells in response to various stressing conditions such as heat, hypoxia and UV light.[38] It is also secreted as a response to tissue injury where it stimulates wound closure.[38] Its function is regulated by a number of co-chaperones which are classified into

three groups: client recruiter co-chaperones, remodelling co-chaperones and late-acting co-chaperones.[38] The client recruiter co-chaperones favour the open conformation of the protein and, except for the sgt1 co-chaperone, slow down its ATPase activity thus making it ready to receive client proteins and other co-chaperones.[38] The most studied client recruiter co-chaperone is sti1/Hop (stress inducible 1/Hsp70-Hsp90 organizing protein) which delivers substrates from Hsp70 to Hsp90.[38] However, the remodelling function of co-chaperones is not well understood, but they generally serve to stabilize particular conformations of Hsp90. For example, the Aha1 (Activator of heat shock protein 90 ATPase) promotes conformational changes that lead to the closed state of Hsp90.[38] The late acting co-chaperones seem to be involved in later stages of client maturation as well as its release.[38]

1.2.2. Structure of Hsp90

The Hsp90 molecular chaperone is a dimeric protein with dynamic conformations.[35] Each Hsp90 monomer is composed of three domains: the N-terminal domain that accommodates the ATP binding pocket and co-chaperone interacting motifs, the middle domain that contains binding sites for co-chaperones and client proteins, and the C-terminal domain that contains the dimerization domain.[35] Although there is general sequence conservation between human Hsp90 and *Pf*Hsp90, they differ significantly in their linker region with *Pf*Hsp90 having a unique 30-amino acid-long stretch adjoining the ATP binding domain.[31] A high homology is observed among all Hsp90s.[34] For example, 69% of yeast and human Hsp90 sequences are identical. The tertiary structures of their N-terminal domains are also very similar.[34] In both cases, the N-terminal domain consists of a highly twisted β sheet with eight strands covered on one face with α helices.[34] However, their quaternary structures crystallize differently with the yeast N-terminal domain crystallizing as a dimer while the human one crystallizes as a monomer.[34]

There are three residues substitutions inside the ATP binding pocket when comparing *Pf*Hsp90 with human Hsp90. [33] In addition to the Arg-98/Lys-112 substitution, Ala-38 of *Pf*Hsp90 is substituted with a serine in human Hsp90 and Ile-173 is substituted with a valine.[33] Of these three substitutions, only the Arg-98/Lys-112 substitution constitutes a potential useful difference for the design of species specific inhibitors.[33] The substitution of Ala-38 by a serine does not make any great difference because the residue is also masked by

structural water molecules that mediate hydrogen bonds between Asp-79 and Asp-37 and that it is also only substituted in human Hsp90α but not in Hsp90β.[33,34] In the case of Ile-173, the only difference between it and valine is that valine has one extra methyl group, which is unlikely to cause any great difference to the structure of the surrounding network of water molecules inside the ATP binding pocket.[33]

However, it has been suggested that due to several slight differences between *Pf*Hsp90 and human Hsp90, it should be possible to design selective *Pf*Hsp90 inhibitors.[44] For example, Met84 of *Pf*Hsp90 adopts a different side chain rotamer than the human counterpart Met98, which leads to two different shapes of the ceiling of the binding pocket in *Pf*Hsp90 and human Hsp90.[45]

Analysis of a geldanamycin **19** bound human Hsp90 showed that the geldanamycin **19** binding pocket is 15 Å deep and 12 Å wide near its entrance.[44] The pocket is 8 Å in its middle and is wide enough to accommodate three molecules of water at its bottom, thus giving an overall structure of a flat-bottomed cone.[44] Nevertheless, the size and accessibility of the pocket change as the Hsp90 undergoes conformational changes leading to either the open or the closed conformation of the chaperone.[44] It is only the open conformation that is compatible with geldanamycin **19** binding.[44]

1.2.3. Hsp90 function and corresponding inhibitors

*Pf*Hsp90 has the highest ATPase activity of all reported Hsp90 ATPase activities and it is 6 times higher than that of human Hsp90.[31] 17-(allylamino)-17-demethoxygeldanamycin (17-AAG) **20** or tanespimycin **20**, a geldanamycin derivative (**Figure 4**) is 15 to 25 fold more effective against cancer cells where the Hsp90 ATPase activity is higher than in a normal healthy cell.[39] Geldanamycin **19** binds *Pf*Hsp90 with high affinity robustly inhibits its ATPase activity. The whole cell lysate assay of *P. falciparum* also demonstrated that the *in vivo* activity of geldanamycin **19** is through *Pf*Hsp90 inhibition.[31] 17-AAG **20** (**Figure 4**) inhibits *P. falciparum* growth and prolongs the lifespan of a preclinical rodent model of malaria. Geldanamycin **19** also specifically binds *Trypanosoma evansi* Hsp90 (*Te*Hsp90) both in its purified form and in its whole cell lysate.[31] Furthermore, 17-AAG **20** inhibited *T. evansi* growth and cured mice infected with *T. evansi*.[31]

Geldanamycin **19** (**Figure 4**) belongs to a class of natural products called benzoquinone ansamycins, which all have an aliphatic chain bonded to an aromatic ring in a metacyclophane manner.[46] Different benzoquinone ansamycins have been reported to inhibit Hsp90 and some of them such as macbecin I **21** (**Figure 4**) are more potent than geldanamycin **19** in inhibiting the ATPase activity of Hsp90.[46] The respective binding affinities are K_d = 0.24 μM for macbecin I **21** and K_d = 1.2 μM for geldanamycin **19**. Herbimycins and TAN compounds also belong to this class of compounds.[46]
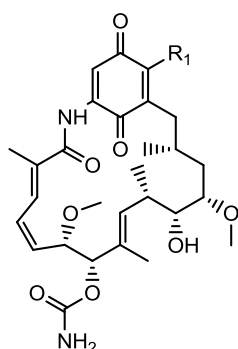
Geldanamycin **19**, R_1= OCH$_3$
17-AAG **20** R_1= NHCH$_2$CHCH$_2$
17-DMAG **22**, R_1= NHCH$_2$CH$_2$N(CH$_3$)$_2$
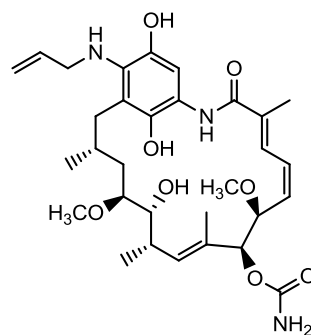
IPI-504 (Dihydro-17-AAG) **23**
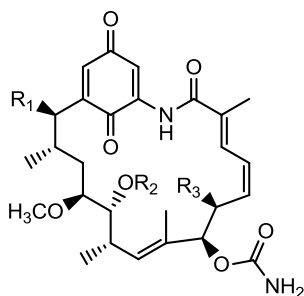
Macbecin I **21**, R_1= OCH$_3$, R_2= CH$_3$, R_3= CH$_3$
Herbimyin A **24**, R_1= OCH$_3$, R_2=CH$_3$, R_3= OCH$_3$
Herbimycin B **25**, R_1= H, R_2= H, R_3= OCH$_3$
Herbimycin C **26**, R_1= OCH$_3$, R_2= H, R_3= OCH$_3$
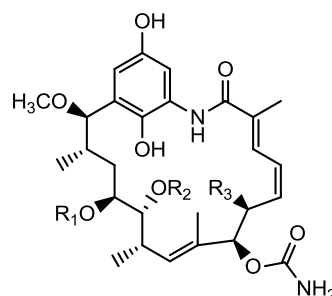
Macbecin II **27**, R_1= CH$_3$, R_2= CH$_3$, R_3= CH$_3$
TAN-420A **28**, R_1= H, R_2= H, R_3= OCH$_3$
TAN-420C **29**, R_1= H, R_2= CH$_3$, R_3= OCH$_3$
TAN-420E **30**, R_1= CH$_3$, R_2= CH$_3$, R_3= OCH$_3$
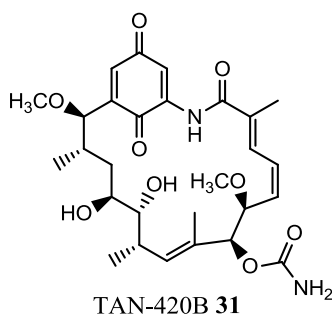
TAN-420B **31**
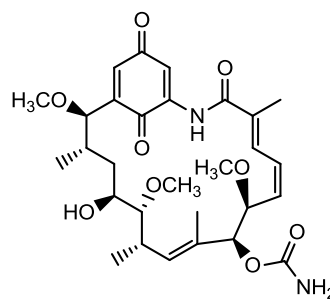
TAN-420D **32**

Figure 4: Chemical structures of the ansamycin class of Hsp90 inhibitors[46]

*Pf*Hsp90 and *Te*Hsp90 are potential drug targets and in general there is a possibility to treat protozoan infections by inhibiting the protozoan Hsp90s.[31] For example, geldanamycin **19** blocks the ring to trophozoite stage progression during *P. falciparum* development.[40] Other phases of *P. falciparum* growth such as the progression from trophozoites to schizont, the release of merozoites from schizonts and the reinvasion of erythrocytes by the newly released merozoites are not affected by geldanamycin **19**. Banumathy *et al.*[40] The difference might be due to the fact that the trophozoite is the most active phase and that the progression from ring to trophozoite might depend greatly on *Pf*Hsp90, hence its great sensitivity to inhibition by geldanamycin **19**. In fact, *Pf*Hsp90 production is maximal during the progression from ring to trophozoite.[40]

Geldanamycin **19** acts by binding to the ATP binding site in the N-terminal domain of Hsp90, thus blocking the maturation of the client protein and consequently leading to its degradation.[31] The anti-tumour activity of macbecin I **21** is due to the degradation of Hsp90 oncogenic client proteins ErB2 (Estrogen receptor b2) and cRaf1 (CD40 Receptor associated factor 1) following the inhibition of Hsp90.[46] The Western blot analysis of protein expression in lysates of the prostate cancer cell line DU145 following incubation with macbecin shows that Hsp90 proteins are still present when ErB2 and cRaf1 disappear.[46] These two sets of observations about geldanamycin **19**[31] and macbecin I **21**[46] lead to the conclusion that Hsp90 inhibitors might inhibit cell growth by causing the degradation of its client proteins.

A sequence alignment of different Hsp90 from protozoan parasites revealed that the residues required for geldanamycin **19** binding are conserved across the parasites.[31] This highlights the possibility of using Hsp90 inhibitors to treat different protozoan infections in both animals and humans.[31] The sequences of human Hsp90 and *Pf*Hsp90 revealed that their binding sites complexed with geldanamycin **19** differ only by the substitution of Lys-112 in human Hsp90 with Arg-98 in *P. falciparum*.[31] However, this slight difference cannot be linked to the small increase in geldanamycin **19** binding affinity of *Pf*Hsp90 as compared to human Hsp90. [31] In spite of *Pf*Hsp90 and human Hsp90 having identical sequence alignments, *Pf*Hsp90 has a distinct extension which differs from its human counterpart through its tertiary structure. These structural differences between *Pf*Hsp90 and human

Hsp90 were exploited to design a new generation of *Pf*Hsp90 selective inhibitors based on compound IND31119 **34** (**Figure 5**).[33]

Radicicol **33**	IND31119 **34**	SST0116CL1 **35**
Harmalol **36**	NVP-AUY922 **37**	NMS-E973 **38**
PU-H71 **39**	Harmine **40**	CPUY201112 **45**
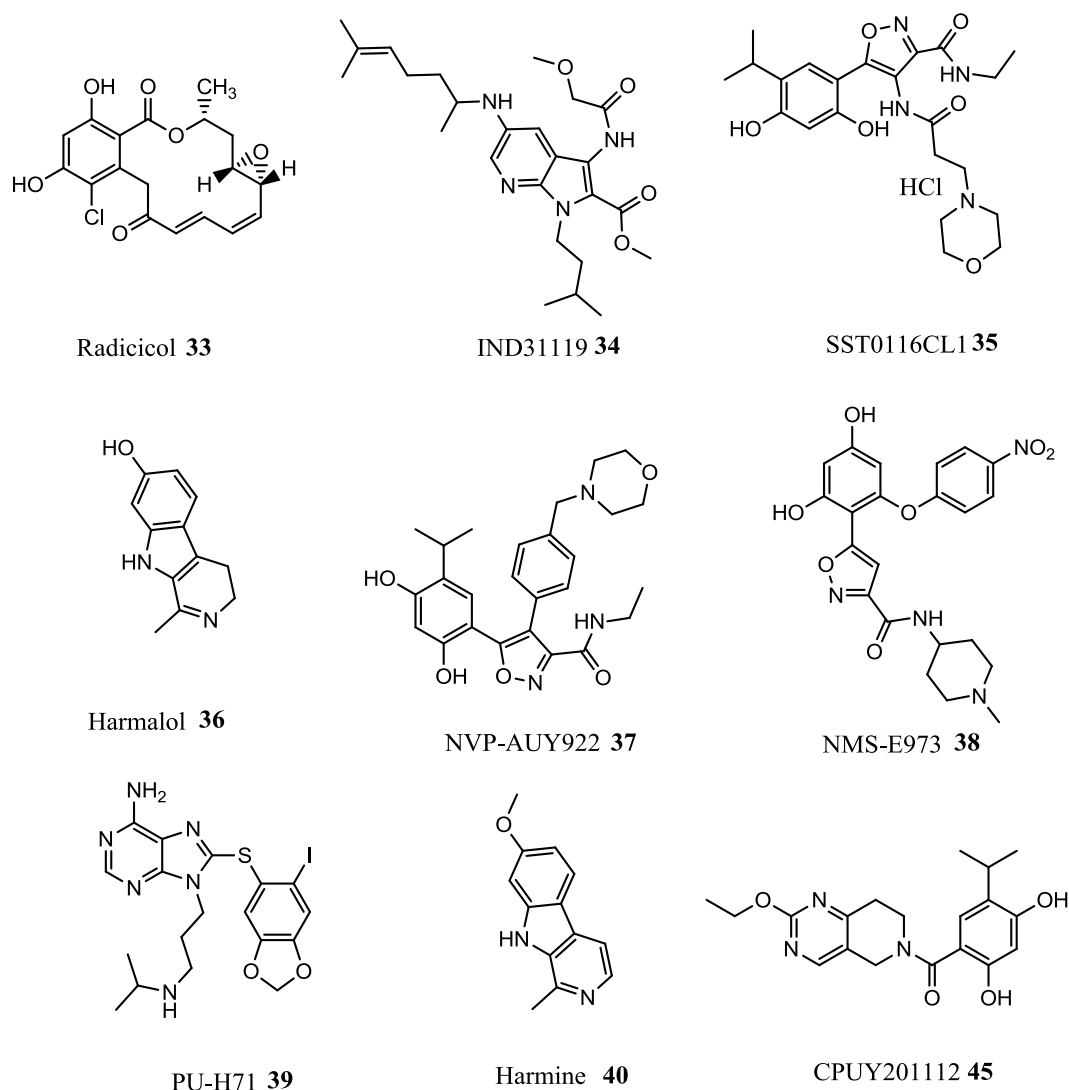
Figure 5: Miscellaneous Hsp90 inhibitors[47-53]

Furthermore, the substitution of Arg-98/Lys-112 can potentially be exploited to design selective inhibitors of different Hsp90s of various protozoan parasites over the human Hsp90.[33]

Due to the flexibility of the Arg-98 side chain, the selective inhibitors of protozoan Hsp90s would need to interact with hydrophobic residues surrounding Arg-98 for stronger binding.[33] The hydrophobic region of the ATP binding pocket of *P. falciparum* consists of a glycine-rich hinge loop (G118 to G123) and amino acid residues G100, T101 and F104. Two studies,

one with geldanamycin **19** and another with IND31119 **34** (**Figure 5**), that were carried out to assess whether the homologous substitution Arg-98/Lys-112 was important for drug-protein interactions concluded that this substitution has no significant effect on the binding affinity or on the selectivity of the drugs for the Hsp90.[31,33]

However, harmine **40** showed selectivity for *Pf*Hsp90 while its derivative harmalol **36** (**Figure 5**) showed selectivity for human Hsp90. [54] On one hand, when Arg-98 was substituted with Lys in *Pf*Hsp90 and Lys-112 in human Hsp90 was replaced with Arg, harmine **40** showed better binding for human Hsp90 compared to *Pf*Hsp90. On the other hand, the analogous harmalol **36** showed better binding for *Pf*Hsp90 than for human Hsp90.[54] This was also corroborated by docking studies suggesting that the methoxy group of harmine **40** interacts with the guanidinium moiety of Arg-98 while the hydroxyl group of harmalol **36** mediates polar interactions with Lys-112.[54] Hsp90 inhibitors have the advantage that mutations that would render a pathogen resistant by modifying the ATP binding pocket would also compromise the pathogen's viability since ATP binding and hydrolysis are essential for the Hsp90 function.[55]

Asp-79 is essential for the binding of ATP and ADP (adenosine diphosphate) in the N-terminal domain of Hsp90.[55] Mutation of Asp-79 to Asn results in the complete loss of Hsp90 function.[55] In fact, the side-chain carboxylate of Asp-79 forms a direct hydrogen bond with the exocyclic N6 of the adenine moiety and the bonding environment is such that when Asp-79 is mutated to Asn, this leads to a strong repulsive interaction with the adenine.[55] The mutations of Glu33 to Ala in yeast Hsp90 leads to a significant decrease in the Hsp90 ATPase activity. Although the Glu33-Ala mutant retains ATP binding capabilities, its Hsp90 ATPase activity is reduced to less than 1% of the wild type's ATPase activity.[55] Thus, Asp79-Asn and Glu33-Ala mutations compromise the yeast's viability and highlights the importance of ATP binding and hydrolysis for the Hsp90 function.[55] A superimposition of the bound structures of Hsp90 with the inhibitors geldanamycin **19** and radicicol **33** revealed that the inhibitors mimic ADP binding in shape and interactions with the protein and water molecules, and that in particular they conserve the hydrogen bonding to Asp-79 side chain carboxylate.[56]

*Pf*Hsp90 inhibitors such as geldanamycin **19**, 17-AAG **20**, PU-H71 **39** and harmine **40** act in synergy with chloroquine **12** *in vitro* and *in vivo* experiments indicating that *Pf*Hsp90 inhibitors might reverse drug resistance of chloroquine-resistant *P. falciparum.*[57] In fact, *Pf*Hsp90 is essential for the folding of proteins involved in drug-resistance and virulence in the infected cells.[57] In erythrocytes, geldanamycin **19** alone was active against chloroquine-sensitive and chloroquine-resistant strains of *P. falciparum.*[30] When it is combined with chloroquine **12**, the two drugs act in synergy, reducing their IC_{50} values 5-10 fold.[30] Harmine **40** inhibits *Pf*Hsp90 and has a synergistic effect *in vitro* with either one of chloroquine **12** and artemisinin **13**.[54] After the identification of the Hsp90 inhibitors geldanamycin **19**, 17-AAG **20** and other semi-synthetic ansamycin derivatives, more Hsp90 inhibitors with new scaffolds have been synthesized. These include for example the compounds SST0116CL1 **35**[58], NVP-AUY922 **37**[59], CPUY201112 **45**[60], NMS-E973 (L-1) **38** [61] and their analogues.
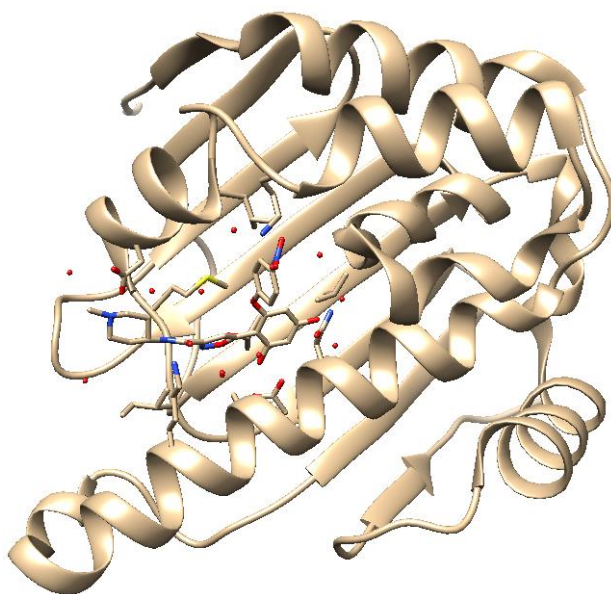
Figure 6 : Crystal structure of NMS-E973 (L-1) 38 bound to human Hsp90 (PDB: 4B7P)

Some of these synthetic Hsp90 inhibitors such as compound SST0116CL1 **35**[50,62] have anti-plasmodial and anti-trypanosomal activity. The anti-tumour activity and the physicochemical properties of our lead molecule NMS-E973 (L-1) **38** and its analogues depend on some particular moieties.[61] For example, the nitro group maintains their binding to Hsp90 and the two hydroxyl groups are also important for Hsp90 affinity. The carboxamide and its side-chains are important for potency and solubility can be increased by simply adding a

hydrophilic moiety to the molecule.[61] Thus, the analysis of structure-activity relationship is important in order to identify a suitable inhibitor lead molecule from its analogues.

1.3. Modern approaches to rational drug discovery

1.3.1. Introduction

A drug is generally defined as a chemical substance that can change the way a given tissue responds to its surroundings.[63] Traditionally, drugs used to be discovered by trial and error by which chemical substances were assessed for their capability to produce the desired effect *in vitro* and/or *in vivo*.[63] Although those methods were based on the assumption that receptors existed, in many cases their presence and locality still remained unknown to researchers.[63]

In order to increase our knowledge of protein structure and functions, new techniques such as high-throughput protein purification, x-ray crystallography and nuclear magnetic resonance spectroscopy have been employed.[64] These techniques coupled to the completion of the human genome project have contributed to the amount of biological data available. This information, combined with empirical studies, led to the increased use of computer based methods to facilitate the study of chemical entities that are capable of influencing the molecular interactions that govern life.[64,65] In contrast to classically used random screening methods, the modern process of drug discovery typically starts with the identification of a suitable drug target such as a receptor or an enzyme.[66] The relevance of the drug target is then validated.[66] This is followed by the identification of the modulators (agonists or antagonists of the receptor, enzyme inhibitors etc.) of the drug target.[66] The next stage comprises the development of an appropriate assay to assess the effect of newly designed ligands on the drug target.[66] The lead molecule is then identified based on its relative selectivity for the target molecule, and it is optimized for potency, selectivity, physicochemical properties as well as pharmacokinetic and toxicity properties.[66] After lead optimization, the lead compound is assessed in animal studies and then progress to clinical trials.[66]

1.3.2. Virtual screening

Virtual screening is one of the approaches used in rational drug discovery in order to speed up the process of finding the hit compounds. Modern drug discovery methods rely on the knowledge of the conformation of the receptor when complexed with the ligand.[67] The information obtained from the ligand-receptor complex is used to design and synthesize analogues of the ligand. The results of bioassays on the synthesized analogues are then used to improve the ligand until a better potency and specificity is obtained.[67] *In silico* methods (virtual screening) used in rational drug design are gaining popularity and can currently be used for different purposes such as virtual high throughput screening and even predictive toxicology.[66] Virtual screening is performed using docking software such as AutoDock Vina, Autodock 4, Dock, FlexX, Fred, Glide, Gold, LigFit, etc.[64,68,69] Docking involves prediction of the conformation of the ligand within the binding site, its position and orientation as well as the corresponding binding affinity.[64] AutoDock Vina is one of the most recently developed docking software packages with a proven accuracy in predicting the binding mode of the ligands to their target proteins.[69] Its speed is approximately two orders of magnitude higher than that of Autodock 4, another widely used docking program.[69] The virtual high throughput screening has the advantage that it is cost-effective.[66] However, it is important to remember that the scores assigned by the docking software are simply approximation and that increased accuracy also requires expensive computational time.[70]

1.3.3. Structure and ligand based drug design

Two approaches are followed in rational drug design namely structure-based drug design and ligand-based drug design. In the case of structure-based drug design, the bioactive conformation of the ligand in complex with its receptor is known. The researcher can modify the ligand in such a way that the new ligand keeps key interactions with the receptor but that less important interactions are replaced with new interactions that give to the ligand more potency and specificity.[67] This gives the researcher the capability to design completely new analogue molecules based on the structure activity relationship of the bioactive ligand-receptor conformation. In some cases when a group of ligands for a protein is known while the structure of the target protein is not known, a ligand-based approach is used in order to

discover new ligands of the target protein.[64] This approach uses methods such as pharmacophore modelling and quantitative structure activity relationship (QSAR).[64]

1.3.4. Combinatorial chemistry and high throughput screening

Combinatorial chemistry and high-throughput screening are of great interest in experimental drug design. Typically, combinatorial chemistry involves the synthesis of large-scale libraries of compounds based on a few available building blocks.[65] For example, a large number of different peptides can be obtained by combining differently 7 of the 20 coded amino acids.[65] Combinatorial chemistry is used in parallel with high throughput screening. Due to the large size of combinatorial libraries, it is impractical to analyse them manually. Scientists therefore rely on automated screening systems that can assay up to a 100 000 thousand compounds a day.[66] This technique is termed high throughput screening and has gained widespread popularity amongst drug discovery scientists in the last two decades.[66]

1. 4. Aims and objective of the project

The fact that compounds such as geldanamycin **19**[31], 17-AAG **20**[31] and SST0116CL1 **35**[50,62], which manifest anti-tumour activity, also exhibit anti-plasmodial activity, we sought to prove that the analogues of the anti-tumour Hsp90 inhibitor NMS-E973 (L-1) **38**[61] could be 'switched' for possible anti-plasmodial activity.

Our primary aim was to synthesize a series of compounds based on a NMS-E973 (L-1) **38** template as potential *Pf*Hsp90 inhibitors and then evaluate their potential *in vitro* anti-malarial activity against a selection of *P. falciparum* strains. We also aimed to use docking studies in order to assess whether these compounds would interact with the *Pf*Hsp90 target in the same way as known inhibitors such as geldanamycin **19** in order to prioritise compounds to be synthesized. Finally, we aimed to show that these compounds were non-toxic.

Chapter Two: Results and discussion

2.1. Introduction

Resorcinol derivatives have been found to inhibit Hsp90, which has applications in treating diseases associated with Hsp90 malfunction such as cancer[59,61,71-73] and neurodegenerative diseases.[72,73]. Resorcinol derivatives are attractive chemical scaffolds that could be potentially used as alternative treatment against human parasites such as *Tryapanosoma brucei rhodesiense* and *Plasmodium falciparum*.[74] Recently, the group of Brasca reported the discovery of a potent inhibitor, NMS-E973 (L-1) **38**, of Hsp90 protein which showed good anticancer activity.[61] Taking into consideration that Hsp90 inhibitors have also been shown to exhibit anti-parasitic activity,[74] it was worth resynthesizing analogues of NMS-E973 (L-1) **38** and repurposing them as potential anti-plasmodial agents.

Since the synthesis of compounds requires much work and implies a high cost of reagents and solvents, we used molecular docking to screen the library of molecules synthesized by Brasca *et al.*[61] in order to select appropriate molecules for synthesis. The molecules were assessed based on their calculated binding energies deduced from the predictions of their binding affinity.

^{1}H NMR (Nuclear magnetic resonance), ^{13}C NMR, COSY (Correlation spectroscopy), HSQC (Heteronuclear single quantum coherence spectroscopy) and HMBC (Heteronuclear multiple bond correlation) data and in some cases also NOESY (Nuclear Overhauser effect spectroscopy) and Mass Spectrometry were obtained for most of the molecules that were synthesized in order to confirm their structures. In this chapter, we will only give a brief description of the collected data. The full spectral assignments of the molecules we synthesized can be found in Chapter Three and in the supplementary data.

2.2. Results and discussion

2.2.1. Docking studies (virtual screening)

Our molecular docking studies were aimed at selecting molecules from those synthesized by Brasca *et al.*[61] as well as close analogues that would potentially have selective interactions with *Pf*Hsp90 as compared to human Hsp90. We used the ADP-bound crystal structures of

human Hsp90 (PDB (Protein Data Bank) code: 1BYQ) and *Pf*Hsp90 (PDB code: 3K60) for our docking studies. Based on their inhibition constants (Ki) for human Hsp90 and *Pf*Hsp90, three molecules L-31 **63**, L-62 **64**, and L-63 **65** were identified as potential selective inhibitors of *Pf*Hsp90. The full list of molecules screened by docking and the values of binding affinity and inhibition constants obtained can be found in appendix III. The inhibition constants were calculated according to the equation: $\Delta G = -RT\ln Ki$, where ΔG = Gibbs free energy of binding, R = the gas constant and T = 298.15 K.

Table 1: NMS-E973 (L-1) 38 analogues potential selective inhibitors of *Pf*Hsp90 and their constants of inhibition

Code	Molecules	Smiles	M.W.	1BYQ Ki (μM)	3K60 Ki (μM)
NMS-E973 (L-1) **38** (lead molecule)		O=C(C1=NOC(C2=C(OC3=CC=C([N+]([O-])=O)C=C3)C=C(O)C=C2O)=C1)NC4CCN(C)CC4	454.43	0.1	0.3
L-31 **63**		O=C(C1=NOC(C2=C(OC3=CC=C([N+]([O-])=O)C=C3)C=C(O)C=C2O)=C1)NC4CCN(C(C)C)CC4	482.49	1.1	0.2
L-62 **64**		OC1=CC(OC2=CC=C([N+]([O-])=O)C=C2)=C(C3=CC(C(NC4CC(C)(C)N(C)C(C)(C)C4)=O)=NO3)C(O)=C1	510.54	0.8	0.2
L-63 **65**		OC1=CC(OC2=CC=C([N+]([O-])=O)C=C2)=C(C3=CC(C(NC4CCN(C(C)=O)CC4)=O)=NO3)C(O)=C1	482.44	0.8	0.1

The analysis of the docking results of these three molecules L-31 **63**, L-62 **64** and L-63 **65** shows that they all have three particular hydrogen bonds interactions in common with three amino acid residues (Ile-96, Thr-101 and Asn-92) of *Pf*Hsp90. These H-bonds are not found in the docking results of NMS-E973 (L-1) **38** to *Pf*Hsp90. However, it should be remembered that these molecules do not only interact with *Pf*Hsp90 through hydrogen bonds, but other interactions such as hydrophobic interactions are also observed. Moreover, our docking results do not show any interaction mediated by the water solvent molecules since they were all removed from the protein before docking.
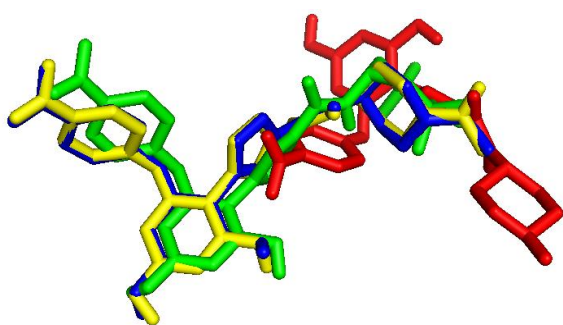
Figure 7: Conformations and positions of NMS-E973 (L-1) 38 (red), L-31 63 (blue), L-62 64 (green) and L-63 65 (yellow) after docking to *Pf*Hsp90
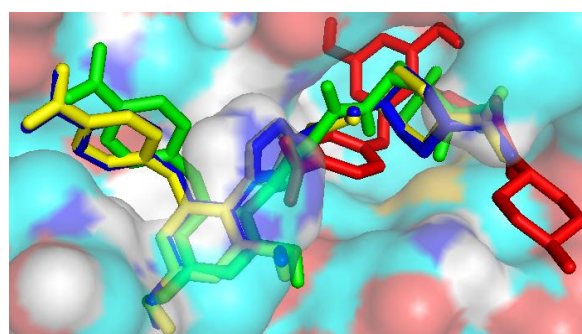
Figure 8: Conformations and positions of NMS-E973 (L-1) 38 (red), L-31 63 (blue), L-62 64 (green) and L-63 65 (yellow) inside the binding site after docking to *Pf*Hsp90

The analysis of the conformations and positions of the ligands NMS-E973 (L-1) **38**, L-31 **63**, L-62 **64** and L-63 **65** (**Figure 7** and **Figure 8**) shows that apart from ligand **L-1 (38)**, the other ligands occupy the same position and adopt similar conformations inside the *Pf*Hsp90 binding pocket.

23
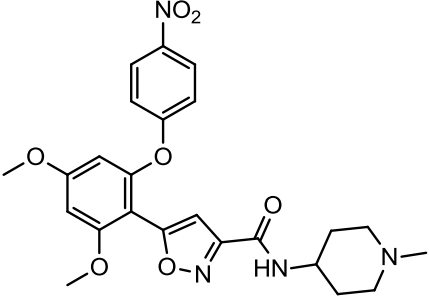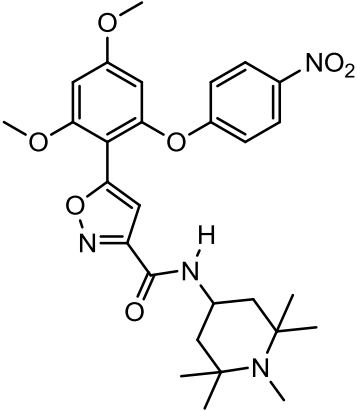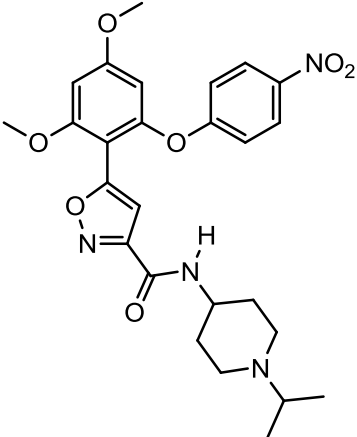
Table 2: Analysis of the interaction between *Pf*Hsp90 and its potential selective inhibitors analogues of NMS-E973 (L-1) 38

	Residues of *Pf*Hsp90 involved in H-bonds with the ligand	Bond length (Å)
NMS-E973 (L-1) **38**	Arg-98	3.09
	Arg-98	3.01
	Asp-37	3.14
	Asp-79	2.78
	Lys-44	2.89
	Thr-171	3.04
L-31 **63**	Ile-96	3.17
	Thr-101	3.10
	Asn-92	2.84
	Arg-98	3.19
	Asn-37	3.13
L-62 **64**	Ile-96	3.12
	Thr-101	3.19
	Asn-92	2.82
L-63 **65**	Thr-101	3.17
	Ile-96	3.11
	Asn-92	2.87
	Arg-98	6.90
	Asn-37	3.08
	Lys-44	3.12

From our docking results, we identified three potential inhibitors that could preferentially select *Pf*Hsp90 above human Hsp90. Based on the ease of synthesis, we choose two compounds, L-31 **63** and L-62 **64** and synthesized their respective dimethyl ether resorcinol analogues, TU-019 (L-104) **51** and TU-017 (L-102) **61**. We also synthesized TU-016 (L-14) **60**, the dimethyl ether resorcinol analogue of our lead molecule, NMS-E973 (L-1) **38** in order to use it for comparison. Our docking results (**Table 3**) for these dimethyl ether resorcinol analogues indicate that they do not selectively bind to *Pf*Hsp90 in the presence of human

Hsp90. In comparison, docking studies clearly predict that their non-methylated analogues could be selective for *Pf*Hsp90.

Table 3: Dimethyl ether resorcinol analogues of NMS-E973 (L-1) 38 potential inhibitors of *Pf*Hsp90 and their constants of inhibition

Code	Molecules	Smiles	M.W.	1BYQ Ki (μM)	3K60 Ki (μM)
TU-016 (L-14) **60**		O=C(C1=NOC(C2=C(OC3=CC=C([N+]([O-])=O)C=C3C=C(OC)C=C2OC)=C1)NC4CCN(C)CC4	482.49	0.7	0.6
TU-017 (L-102) **61**		COC1=CC(OC2=CC=C([N+]([O-])=O)C=C2)=C(C3=CC(C(N([H])C4CC(C)(C)N(C)C(C)(C)C4)=O)=NO3)C(OC)=C1	538.59	0.2	0.5
TU-019 (L-104) **51**		COC1=CC(OC2=CC=C([N+]([O-])=O)C=C2)=C(C3=CC(C(N([H])C4CCN(C(C)C)CC4)=O)=NO3)C(OC)=C1	510.54	0.8	0.8

Since *Pf*Hsp90 has the highest ATPase activity of all known Hsp90 ATPase's[31] and 17-AAG **20** inhibits 15 to 25 fold more effectively cancer cells because of their higher ATPase

25

activity as compared to normal healthy cells,[39] we suggest that, based on our docking results, dimethyl ether resorcinol analogue compounds are more effective growth inhibitors of *P. falciparum* than HeLa cells because *Pf*Hsp90 has higher ATPase activity. This is based on the assumption that growth inhibition is mediated by the inhibition of the *Pf*Hsp90 chaperones.

The analysis of the H-bond interactions between the dimethyl ether resorcinol analogues in **Table 4** with their counterparts in **Table 3** indicates that they do not mediate the same interactions, which is likely the source for the observed difference in their selectivity for *Pf*Hsp90.

Table 4: Analysis of the interaction between *Pf*Hsp90 and its potential inhibitors dimethyl ether resorcinol analogues of NMS-E973 (L-1) 38

	Residues of *Pf*Hsp90 involved in H-bonds with the ligand	Bond length (Å)
TU-016 (L-14) **60**	Ala-38	3.17
	Lys-44	3.16
	Asn-92	3.00
TU-017 (L-102) **61**	Arg-98	3.06
	Arg-98	3.22
	Arg-98	5.76
TU-019 (L-104) **51**	Lys-44	3.24
	Phe-124	3.00

A visualization of the docking results (**Figure 9** and **Figure 10**) of the ligands in **Table 4** illustrates that each molecule adopts a different conformation and position inside the binding pocket of *Pf*Hsp90, which is not the case for the ligands in **Table 2**.
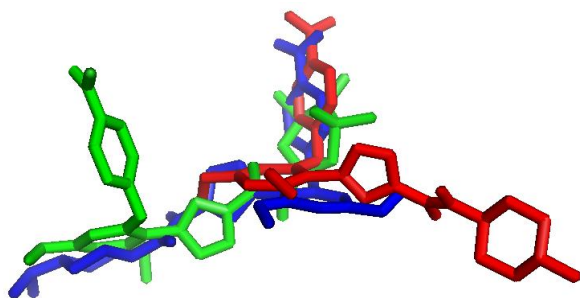
Figure 9: Conformations and positions of TU-016 (L-14) 60 (red), TU-017 (L-102) 61 (blue) and TU-019 (L-104) 51 (green)
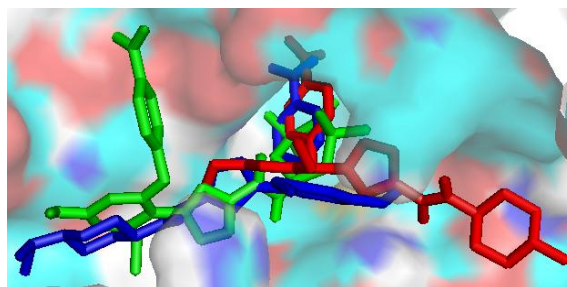
Figure 10: Conformations and positions of TU-016 (L-14) 60 (red), TU-017 (L-102) 61 (blue) and TU-019 (L-104) 51 (green) inside the binding site after docking to *Pf*Hsp90

In addition to compounds TU-016 (L-14) **60**, TU-017 (L-102) **61** and TU-019 (L-104) **51**, we also synthesized compounds TU-013 (L-98) **57** and TU-015 (L-100) **59** based on our docking studies. They are variations of our series of compounds and based on their docking results, it was thought that they would assist in the exploration of the effects of other binding fragments. Compounds TU-007 (L-96) **55** was also added to the study as it had the resorcinol moiety cyclised into a benzofuran ring which made it unique. Benzofurans are known bioactive molecules.[75] All the above compounds and their synthetic intermediates in our synthesis which shared the same pharmacophore were submitted for PLDH and cytotoxicity assays.

2.2.2. Synthesis of diaryl ethers

Diaryl ethers constitute an important class of natural bioactive compounds.[76] They have therefore attracted the attention of many researchers who have synthesized them for various applications such as potential anticancer agents,[61] antiplasmodial and antibacterial agents,[77] anti-arthropods and anti-helminths.[78] They are also widely used in polymer chemistry.[76]

The synthesis of NMS-E973 (L-1) **38** and its analogues involved a series of steps starting from the synthesis of the diaryl ether **41**.[61] Different amides that share a common diaryl ether isoxazole substructure were then synthesized from this precursor.
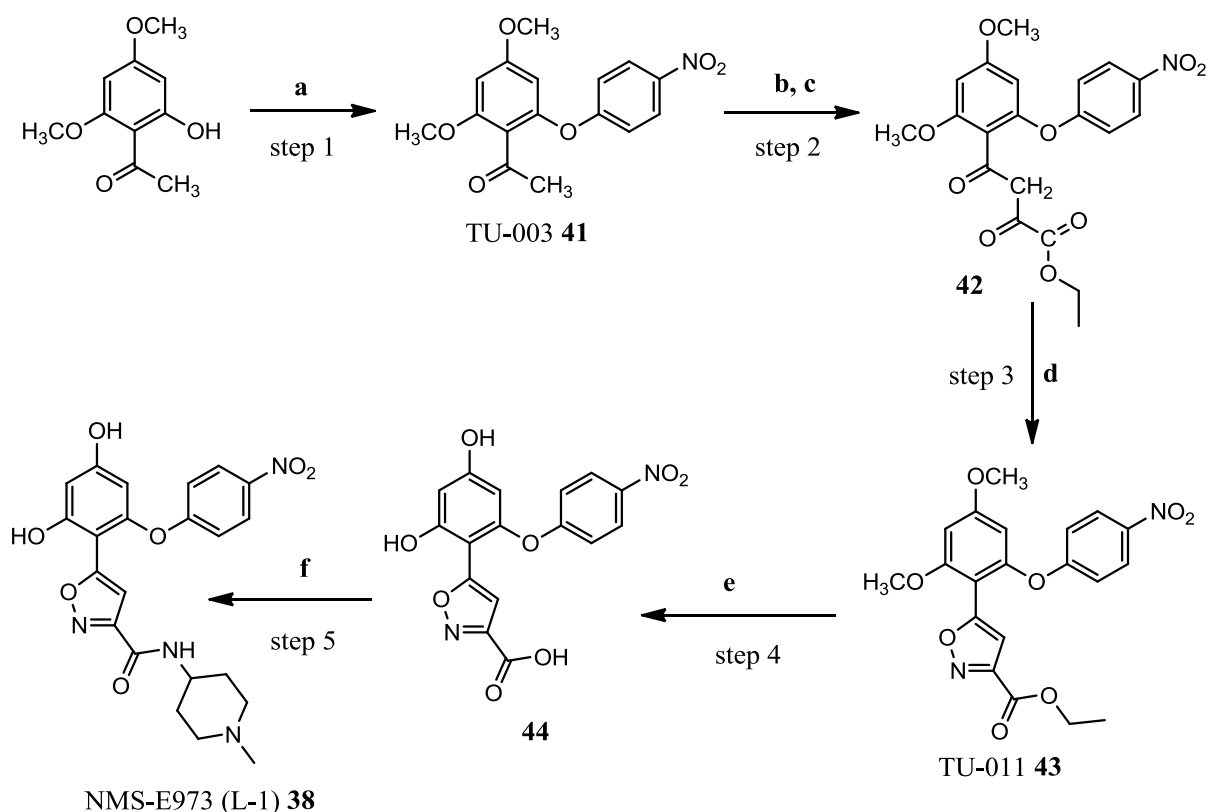
(a)1-fluoro-4-nitrobenzene, K_2CO_3, 55 °C, (b)1M lithium bis(trimethylsilyl) amide in THF, -50 °C
(c) diethyl oxalate, room temperature, (d) $NH_4OH.HCl$, ethanol, reflux (e) 1 M BBr_3 in DCM, room temperature, (f) 1-methylpiperidine-4-amine, DIPEA, TBTU, DMA, room temperature

Scheme 1: Synthesis of compound NMS-E973 (L-1) **38**

The most common way of preparing diaryl ethers involves a reaction of a phenol with an aryl halide in the presence of a catalytic amount of copper or iron.[76,79,80] However, *ortho*-nitrofluorobenzene and *para*-nitrofluorobenzene react with phenols without a catalyst in DMSO or DMF and in the presence of K_2CO_3 as a base and temperatures ranging from room temperature to 110 °C.[61,73,81] The obtained yields can be as high as 90%.[81] The treatment of *para*-bromonitrobenzene with *para*-methoxyphenol without a catalyst gave the desired compound in 89% yield with a longer reaction time (18 h).[79]

Taking into consideration that the product TU-003 **41** of the first step (**scheme 1, page 29**) of our synthesis was a diaryl ether and that the mechanism involved in its formation is an aromatic nucleophilic substitution (**scheme 2, page 30**), we first tested similar reactions using 3,5-dimethylphenol with 1-fluoro-4-nitrobenzene and with 1-(4-fluorophenyl)ethanone. In nucleophilic aromatic substitution where addition-elimination mechanism is involved, the intermediate species is stabilized by electron-withdrawing groups positioned *ortho* or *para* to

the site of substitution.[82] Such substituents activate the aromatic ring to nucleophilic substitution and the strongest effect is observed when the substituent is a nitro group.[82] Cyano and carbonyl groups also favour nucleophilic aromatic substitution, but are less reactive than a nitro group.[82] A fluoride ion is the best leaving group in most aromatic nucleophilic substitution reactions.[83]
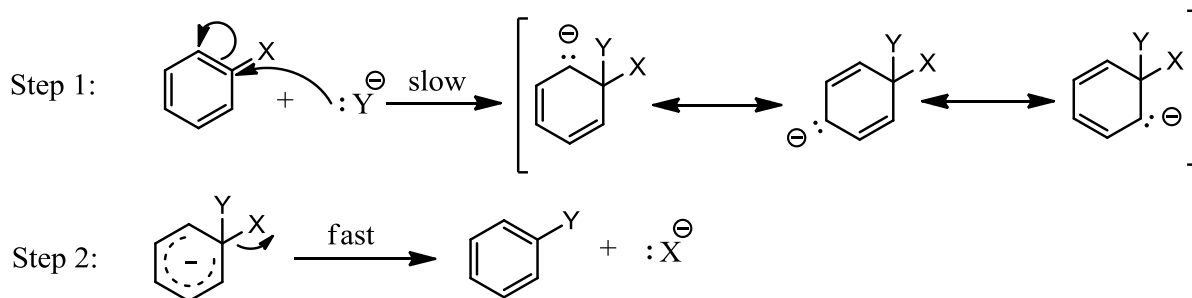
Scheme 2: The most important mechanism for nucleophilic aromatic substitution[83]

The reaction between 3,5-dimethylphenol and 1-fluoro-4-nitrobenzene in the presence of K$_2$CO$_3$ yielded compound TU-001 **46 (Scheme 3, page 31)** with a yield of 96% after purification. The melting point 68 °C - 70 °C was lower than the one of 59 °C reported in the litarature.[76] We attribute this to different degrees of purity of the product. The yield of 96% was obtained without using a catalyst and the best yield (99%) was obtained using a nickel-based catalyst.[84] This is comparable to the yields (88% - 95%) obtained by using copper-based catalysts,[76,80,85,86] iron-based catalysts[76,80] or palladium-based catalysts[87] with halides (Cl, Br, I) other than fluoro (F) as leaving groups.
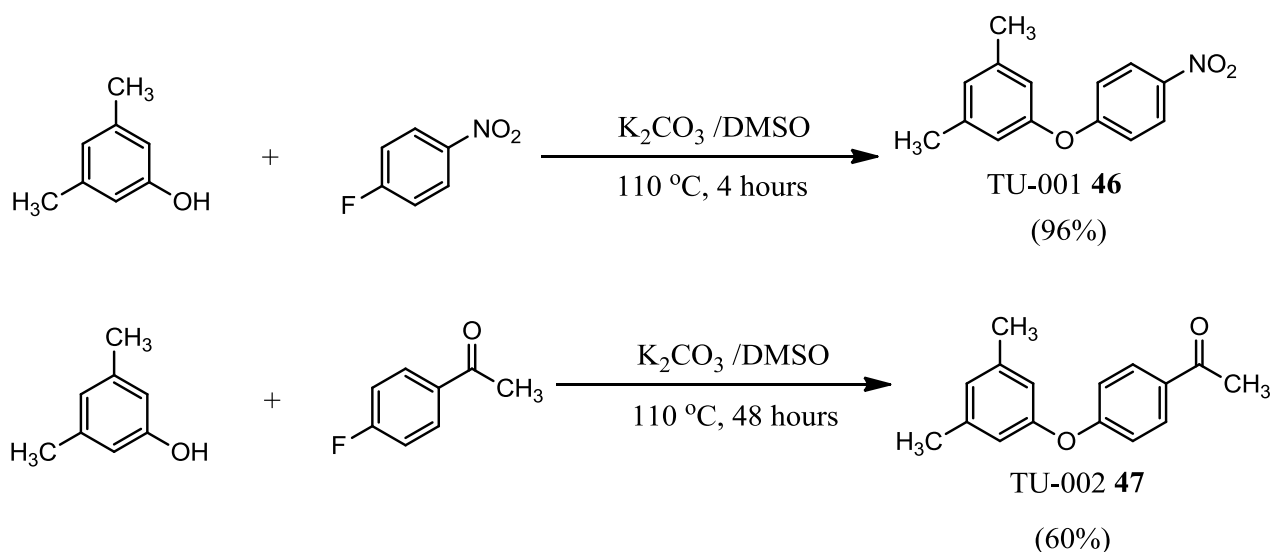
Scheme 3: Synthesis of TU-001 **46** and TU-002 **47**

29

The ^{1}H NMR (**Figure 11**) of compound TU-001 **46** has signals representing the protons of the two methyl groups at 2.33 ppm (parts per million) and the protons of the nitro substituted aromatic ring at 7.00 ppm and 8.17 ppm. The electron density and consequently the shielding of a nucleus are affected by inductive and mesomeric effects which also depend on the electron shells of that nucleus and its direct neighbours.[88] The protons (3'-H and 5'-H) on the para substituted benzene ring that are *ortho* with respect to the nitro substituent are therefore less shielded due to its electron-withdrawing effect and their signals have chemical shift values of 8.17 ppm whereas 2'-H and 6'-H have signals at 7.00 ppm. The two sets of signals appear as doublets because the protons of each set have only one neighbouring proton each. The signals of two equivalent protons *ortho* to the ether moiety of the tri-substituted benzene ring are at 6.71 ppm. They are singlets since each one has no neighbouring proton. The signal of the remaining proton on the tri-substituted benzene ring is a singlet at 6.89 ppm.
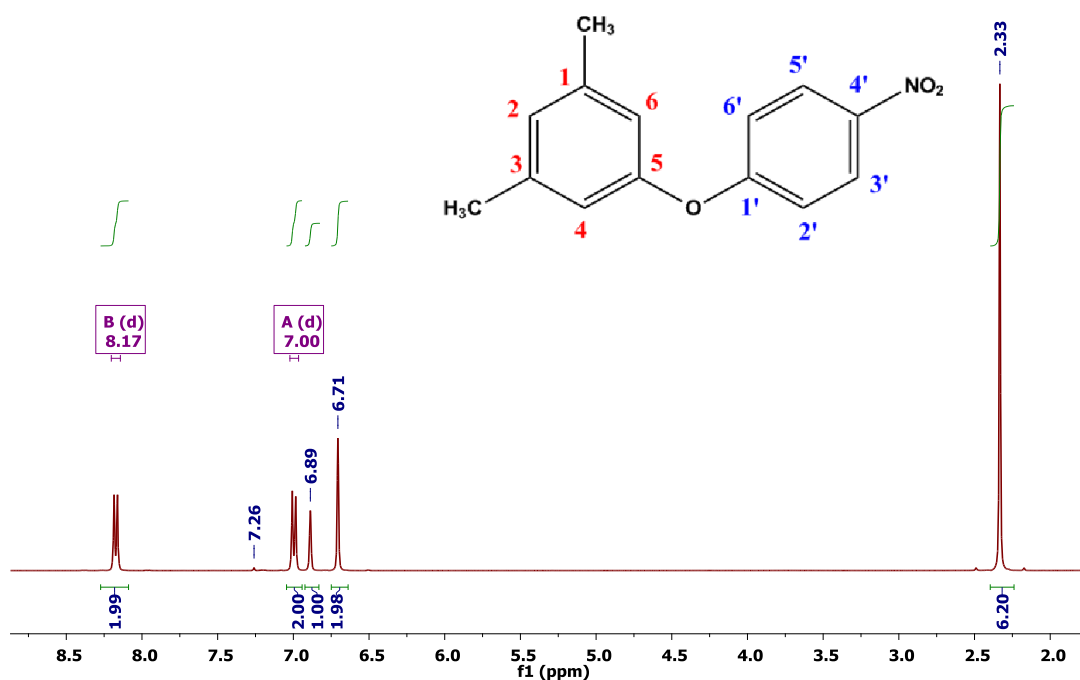
Figure 11: ^{1}H NMR spectrum of TU-001 46 in CDCl$_3$ (deuterated chloroform)

The ^{13}C NMR spectrum (**Figure 12**) has nine peaks representing the nine non-equivalent carbon nuclei. The signals for the two equivalent methyl groups are at 21.2 ppm and the

signals of the carbon nuclei of the aromatic rings are in the region of 110 ppm – 170 ppm as expected.
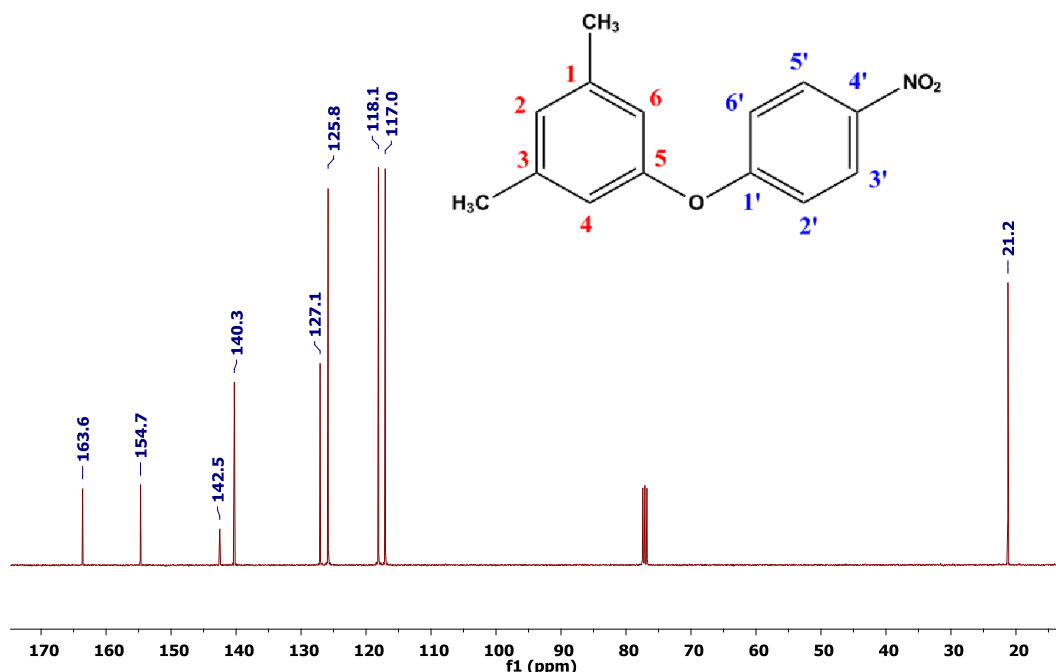
Figure 12: ^{13}C NMR spectrum of TU-001 46 in CDCl$_3$

An HSQC experiment **(Figure 8)** was used to assign the signals of carbon nuclei directly attached to the protons of TU-001 **46**. For example, the signals of the protons of the methyl groups which appear at 2.33 ppm in the ^{1}H NMR spectrum form a cross peak with the signals of the carbon nuclei of the methyl groups at 21.2 ppm. The cross-peak (6.89 ppm, 127.04 ppm) that links 2-H to 2-C is also illustrated in **Figure 8**. An HMBC experiment was used to assign the peaks of non-hydrogen substituted carbon nuclei situated two or three bonds away from protons.
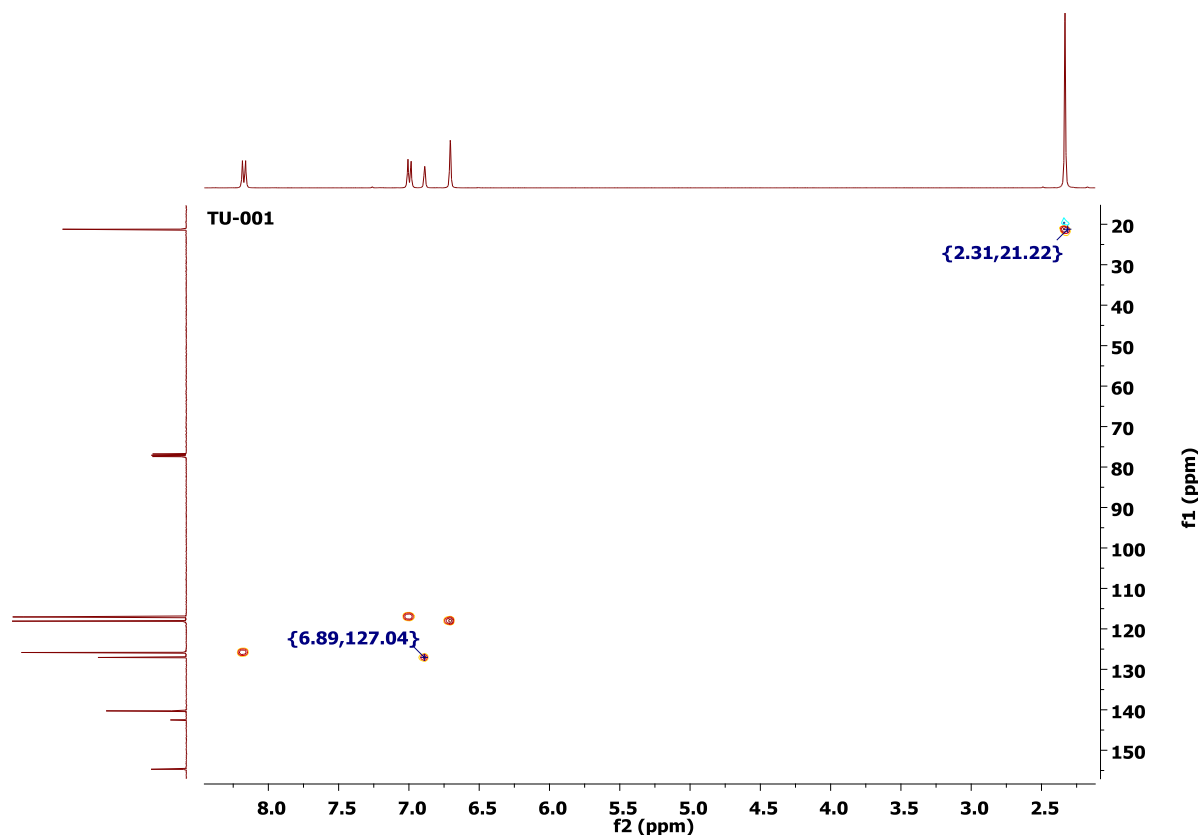
Figure 13: HSQC spectrum of TU-001 46 in CDCl₃

For the synthesis of TU-002 **47**, while we obtained 60 % of the desired product using 3,5-dimethylphenol and 1-(4-fluorophenyl)ethanone without a catalyst, better yields (88% - 95%) were obtained by Keller *et al*. [89] and Xia and Taillefer [90] who used the less reactive 1-(4-bromophenyl)ethanone and 1-(4-chlorophenyl)ethanone respectively, but in the presence of ligands and copper catalysts. The use of the more active 1-(4-fluorophenyl)ethanone is advantageous in that it is not as costly as the other methods that require the catalysts.

An analysis of the ¹H NMR of the product TU-002 **47** (**Figure 14**) shows 6 protons of the two equivalent methyl groups at 2.31 ppm and three protons of the acetyl at 2.57 ppm. The protons of the aromatic ring substituted with acetyl show up as doublets at 6.99 ppm and 7.93 ppm. The same as in the case of the nitro substituent, the acetyl group also reduces the shielding of the protons close to it due to the inductive and mesomeric effects. Therefore, the protons that appear at 7.93 ppm are those close to the acetyl group whereas their close neighbours appear at 6.99 ppm. Their corresponding signals show up as doublets because each one of the protons has one neighbour. The two equivalent protons of the ring substituted

32

with methyl groups appear as a singlet at 6.68 ppm and the remaining proton (4''-H) appear at 6.83 ppm.

TU-002
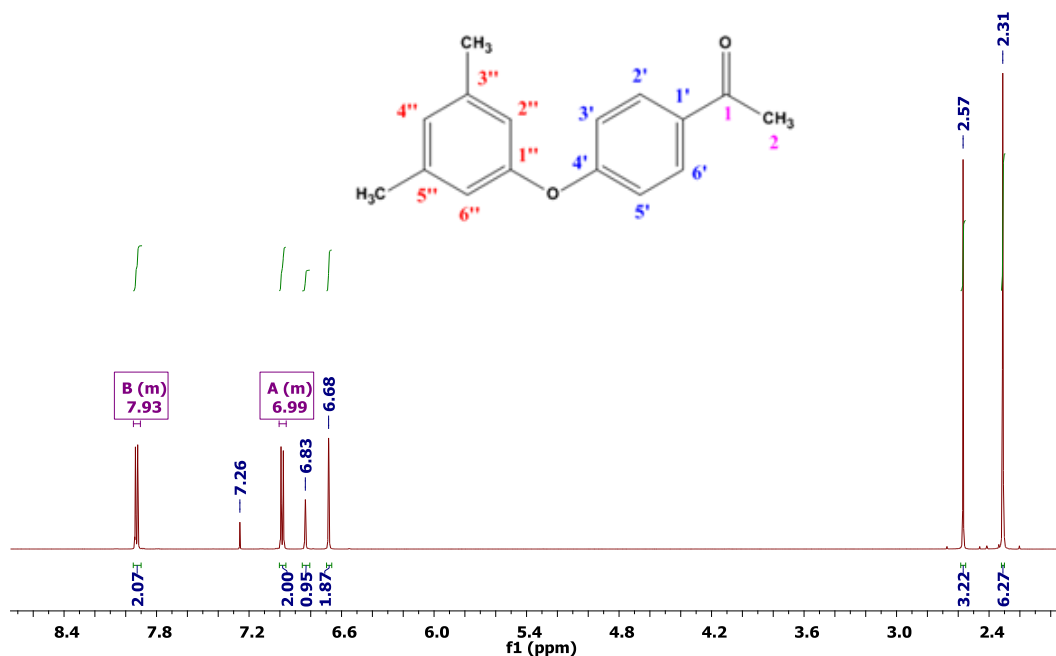
Figure 14: ^{1}H NMR spectrum of TU-002 47 in CDCl$_3$

The ^{13}C NMR spectrum of TU-002 **47** shows 11 carbons as expected with the carbons of the two equivalent methyl groups and the carbon of the methyl of acetyl appearing between 20 ppm and 30 ppm. The carbonyl of the acetyl substituent appears at 196.8 ppm and the carbons of the aromatic rings appear between 110 ppm and 170 ppm as previously observed for TU-001 **46**.
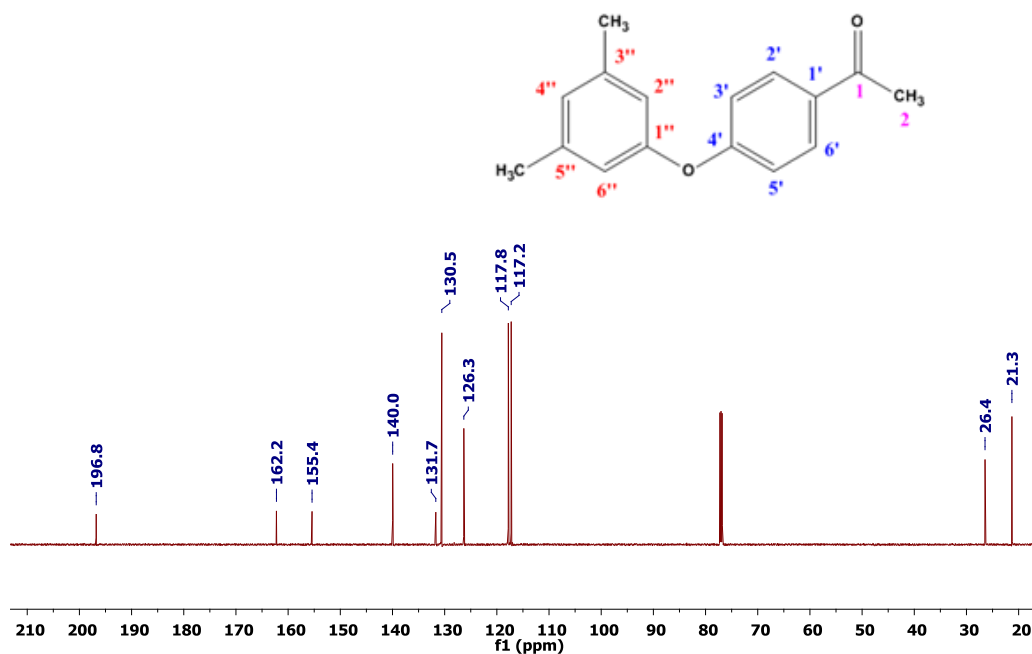
Figure 15: ^{13}C NMR spectrum of TU-002 47 in CDCl$_3$

In the HMBC spectrum (**Figure 16**) the cross peak that links the signals of the three protons of the acetyl group to the signal carbonyl carbon of the acetyl substituent assisted in their differentiation from the signals of the protons of the methyl groups directly attached to the aromatic ring. The protons of the methyl groups directly attached to the aromatic ring are too far from the carbonyl carbon of the acetyl substituent to form any significant HMBC cross peaks.
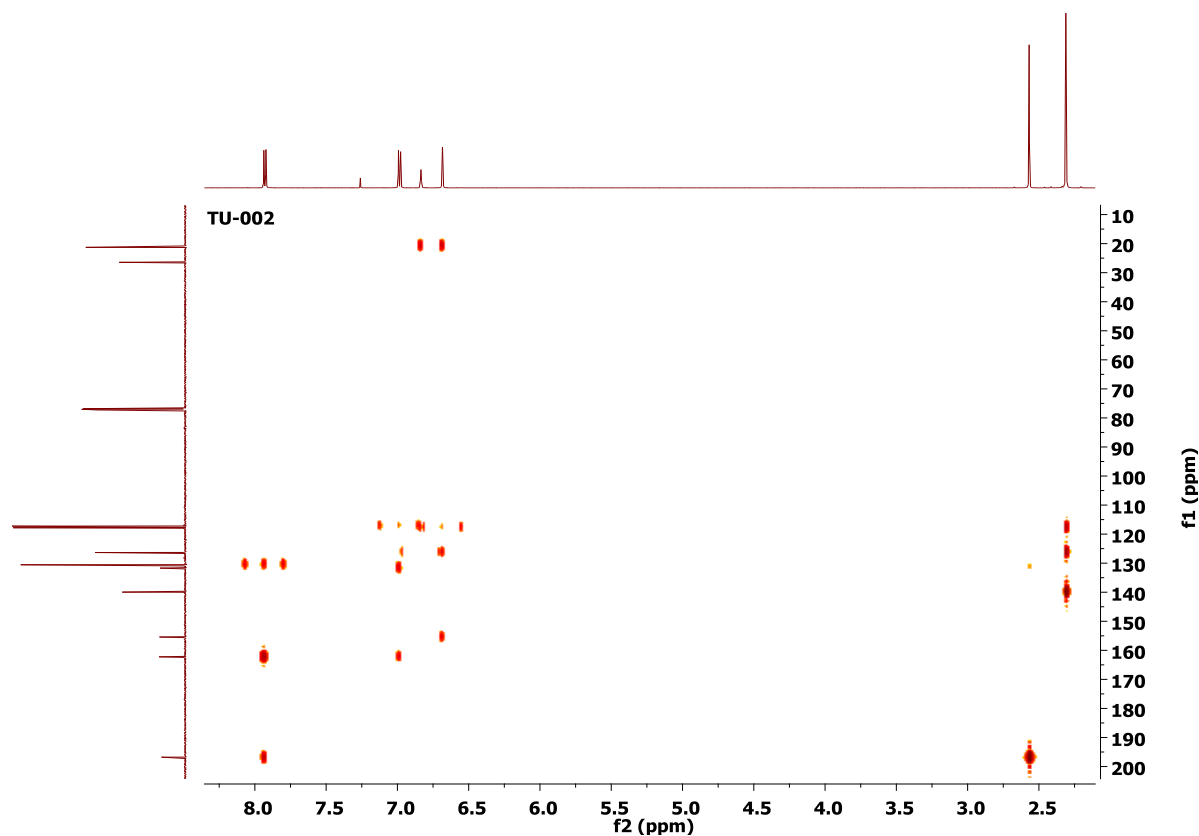
Figure 16: HMBC spectrum of TU-002 47 in CDCl₃

TU-003 **41** was synthesized by stirring the reaction mixture for two hours at 110 °C giving lower yields than the reported 63%[61]. The reaction conditions were changed to stirring the reaction mixture for four hours at 45 °C and the yield was improved to 88%. (**Scheme 4, page 40**)

The ¹H NMR spectrum of TU-003 **41** (**Figure 17**) has a signal of the acetyl substituent at 2.33 ppm and signals for the methoxy groups at 3.78 ppm and 3.86 ppm. Peaks of protons of the ring substituted with the nitro group appear as multiplets at 7.00 ppm and 8.19 ppm. As in the previous cases, the signals of the protons that are direct neighbours of the nitro substituent are at 8.19 ppm due to the deshielding effect of the nitro group whereas the signals of their neighbours are at 7.00 ppm.

The HMBC spectrum (**Figure 19**) assisted in the differentiation of the proton peak of the acetyl group from proton peaks of the methoxy groups. The protons of the acetyl group couple with the carbon nucleus of the carbonyl group through two bonds resulting in a cross-peak.

35

The protons of the methoxy groups couple to the carbon nuclei of the aromatic ring through three bonds forming cross-peaks on the HMBC spectrum.
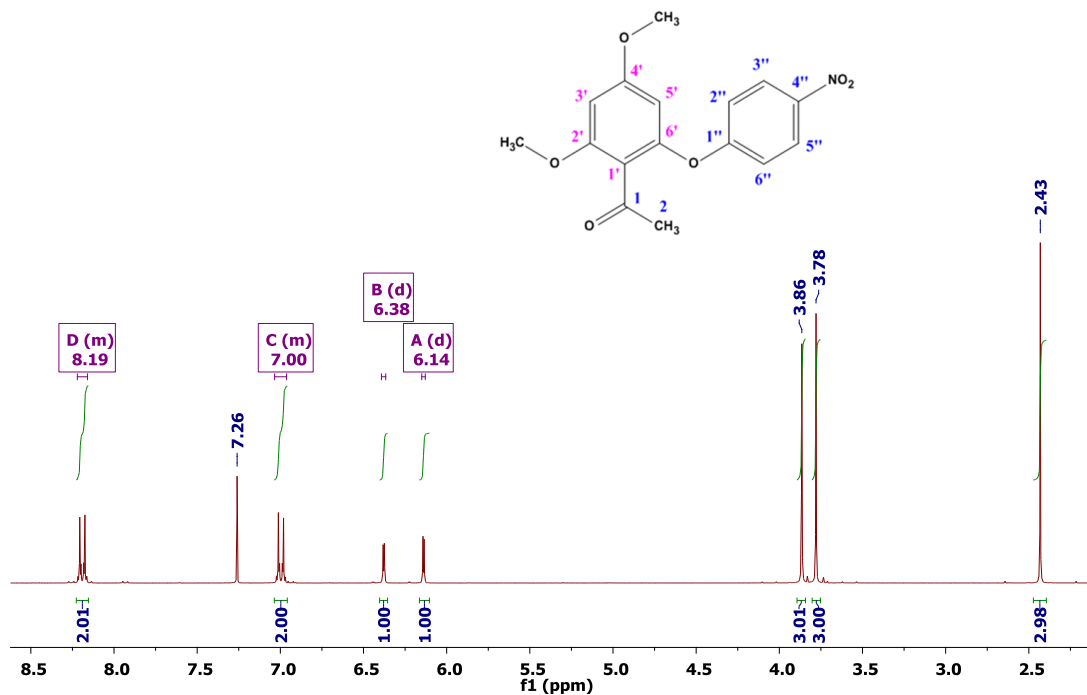
Figure 17: 1H NMR spectrum of TU-003 41 in CDCl₃

TU-003 **41** has sixteen carbon atoms but because there are two groups of equivalent carbon atoms (3''-C and 5''-C, 2''-C and 6''-C) on the nitro-substituted ring, only fourteen carbon peaks are observed on the ^{13}C NMR spectrum. The peak of the carbonyl carbon of the acetyl is at 199.4 ppm and is confirmed by its coupling with the protons of the acetyl group in the HMBC spectrum (**Figure 19**).
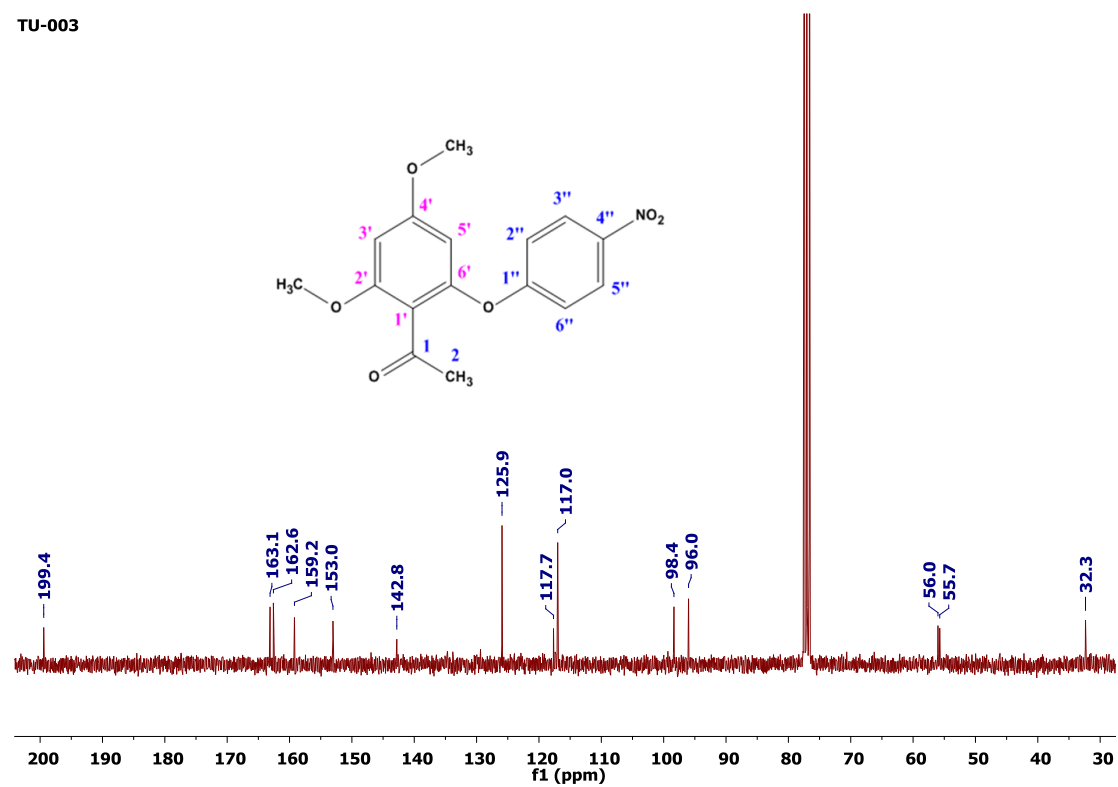
Figure 18: ^{13}C NMR spectrum of TU-003 41 in CDCl$_3$
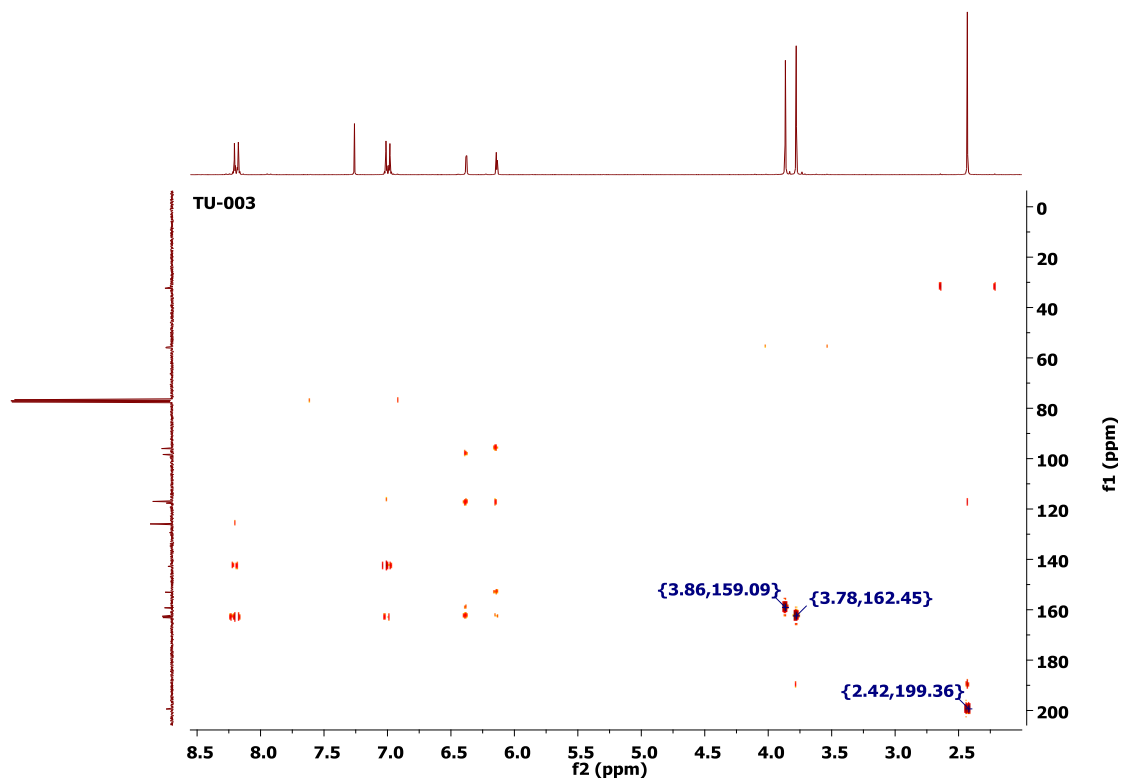
Figure 19: HMBC spectrum of TU-003 41 in CDCl$_3$

37
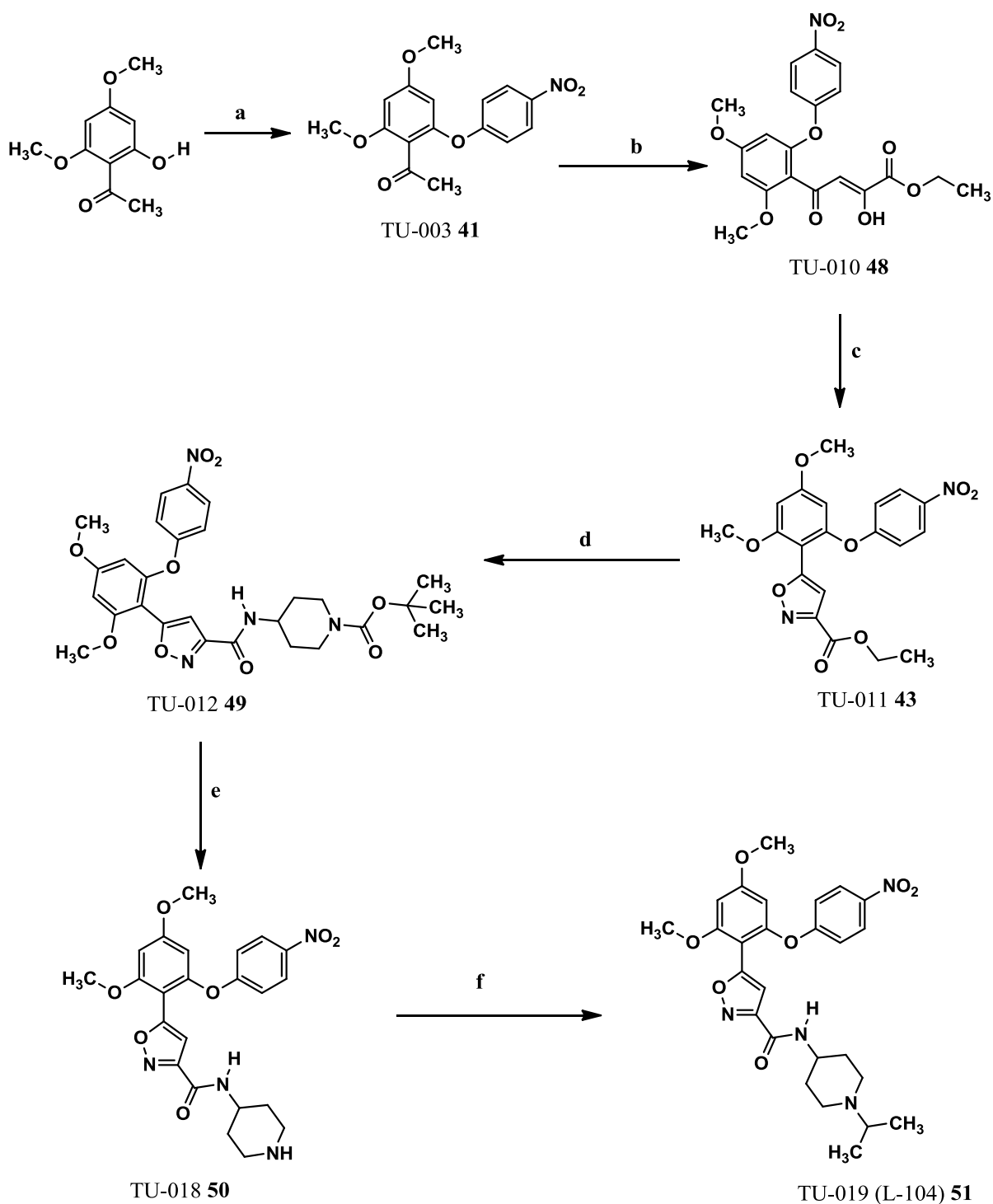
(**a**) 1-fluoro-4-nitrobenzene, K$_2$CO$_3$, 45 °C, 4 hours, DMSO; (**b**) 1 M lithium bis (trimethylsilyl) amide in THF, - 5° C, 10 min, then diethyl oxalate, room temperature, overnight; argon (**c**) Hydroxylamine hydrochloride, ethanol, reflux, 5 hours; (**d**) 4-amino-1-Boc-piperidine, 90 °C, 36 hours; (**e**) 4.0 M HCl in dioxane, overnight, argon, then KOH; (**f**) Acetone, sodium triacetoxyborohydride, 24 hours.

Scheme 4: Synthesis of different dimethyl ether resorcinol analogues of NMS-E973 (L-1) **38** without a coupling agent

When we synthesized TU-003 **41** at 55 °C, we obtained TU-003 **41** (65%) andTU-004 **52** (7%). The formation of TU-004 **52** could be the result of the keto-enol tautomerism (**Scheme 5, page 41**) of our starting material. The species that reacted to yield TU-004 **52** was an enolate while in the case of the formation of TU-003 **41**, the reacting species was a phenolate. Normally, in the case of keto-enol tautomerism, the keto form is the predominant form due to the fact that it is thermodynamically more stable than the enol form.[83] The melting point of TU-004 **52** was 124 °C - 126 °C as compared to the reported value of 150 °C. The difference in the melting points is very likely due to different degrees of purity of the two samples. Another reason for this could be the fact that some compounds crystallize in different forms (crystallographic polymorphism) and crystallographic polymorphs normally have different physical properties such as melting points.[91]
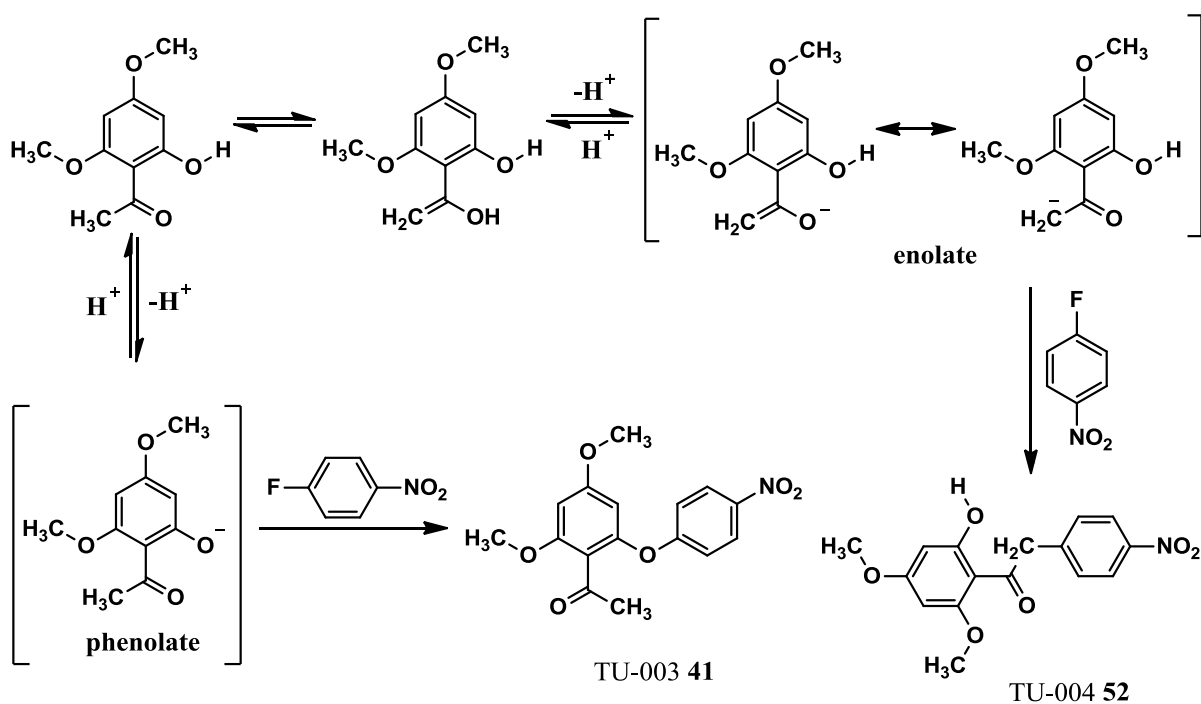
Scheme 5: The formation of TU-003 **41** and TU-004 **52** from the same starting material

The ^{1}H NMR spectrum of TU-004 **52** (**Figure 20**) has two singlets representing the two methoxy groups at 3.83 ppm and 3.86 ppm. The signal of the two protons of the methylene group is a singlet at 4.43 ppm and the signals of the two protons of the aromatic ring substituted with methoxy groups are doublets at 5.94 ppm and 6.09 ppm respectively. The peaks representing the two aromatic protons are doublets due to the coupling between them.

The protons of the nitro substituted ring appear as multiplets at 7.38 ppm and 8.19 ppm and the phenolic proton shows up at 13.65 ppm.
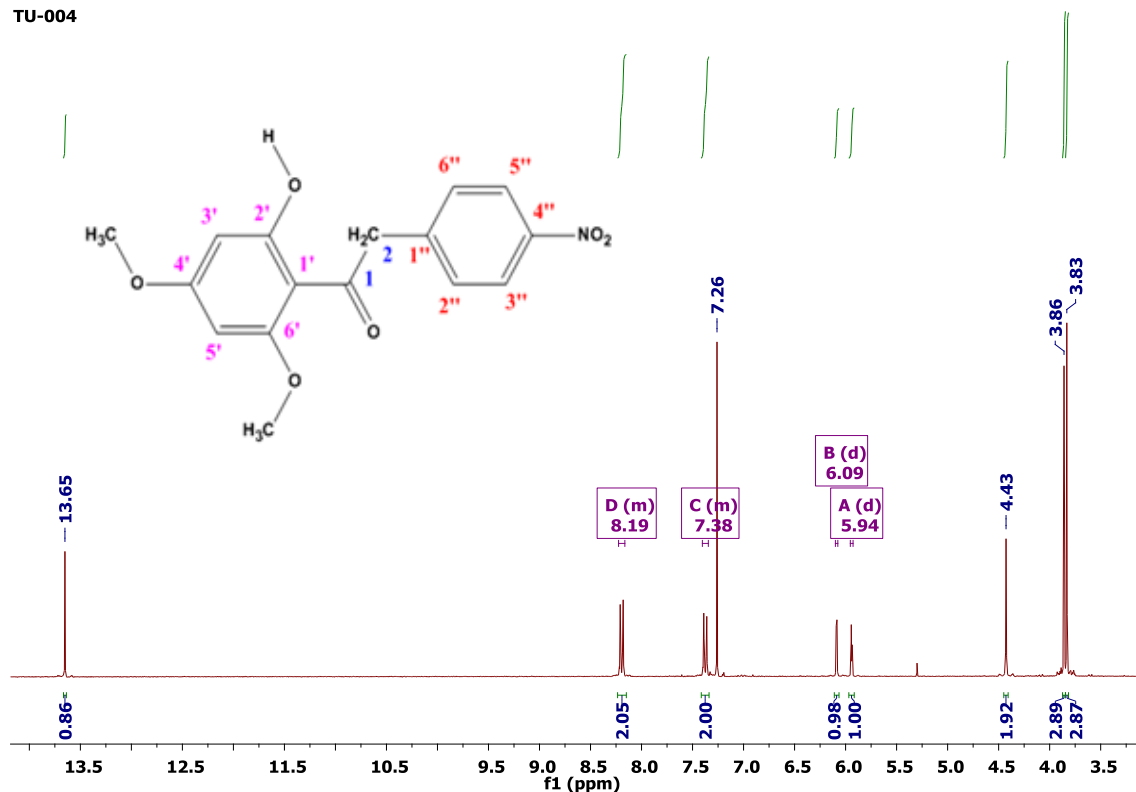
Figure 20: ^{1}H NMR spectrum of TU-004 52 in CDCl$_3$

The ^{13}C NMR spectrum of TU-004 **52** has only 13 carbon peaks because the signals of the carbon nuclei of the two methoxy groups overlapp despite the fact that they do not seem to be equivalent.
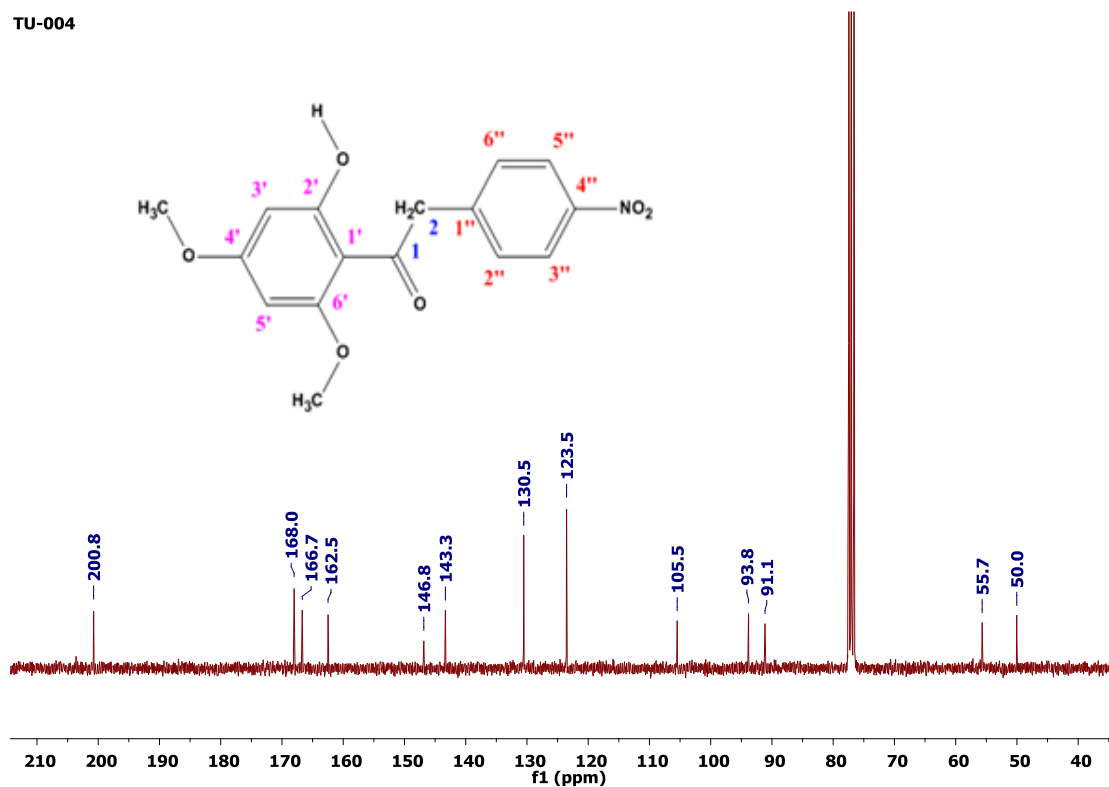
Figure 21: ^{13}C NMR of TU-004 52 in CDCl$_3$

The main cross peak on the HMBC spectrum of TU-004 **52** (**Figure 22**) is the one (4.43 ppm, 200.63 ppm) which indicates the coupling between the two protons of the methylene group and the adjacent carbon nucleus of the carbonyl group. The phenolic proton also couples with three neighbouring carbon nuclei (1'-C, 2'-C and 3'-C). One carbon nucleus (1'-C) is immediately assigned due to the fact that it couples with the two protons of the corresponding ring in addition to coupling with the phenolic proton. The coupling is observed because it is located three bonds away from each of the protons. The peak for 1'-C is at 105.5 ppm on the ^{13}C NMR spectrum (**Figure 21**).

41
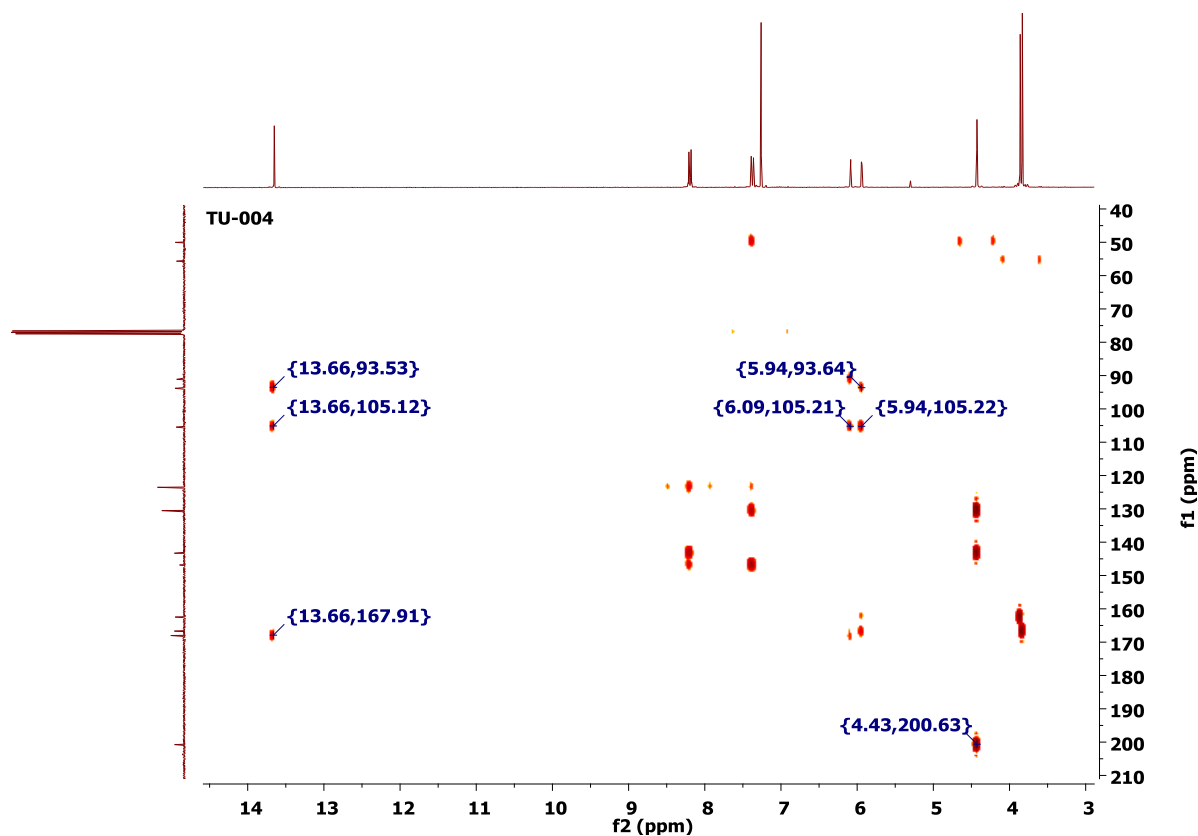
Figure 22: HMBC spectrum of TU-004 52 in CDCl₃

Markers on the spectrum:
- {13.66,93.53}
- {13.66,105.12}
- {13.66,167.91}
- {5.94,93.64}
- {6.09,105.21}
- {5.94,105.22}
- {4.43,200.63}

2.2.3. Synthesis of β-diketones

β-diketones are usually prepared from a methylketone and an aliphatic ester in the presence of a strong base in an anhydrous medium (**Scheme 6, page 45**).[61,92,93] Some of the bases include sodium hydride,[93-95] sodium amide,[92,93,96] lithium amide,[93] sodium ethoxide,[59,92,97,98] sodium methoxide,[97] metallic sodium,[92,98] lithium bis(trimethylsilyl)amide,[61] and sodium *tert*-butoxide.[61] When diesters are used instead of monoesters, a di-ketoester is obtained (**Scheme 6, page 45**).[61]
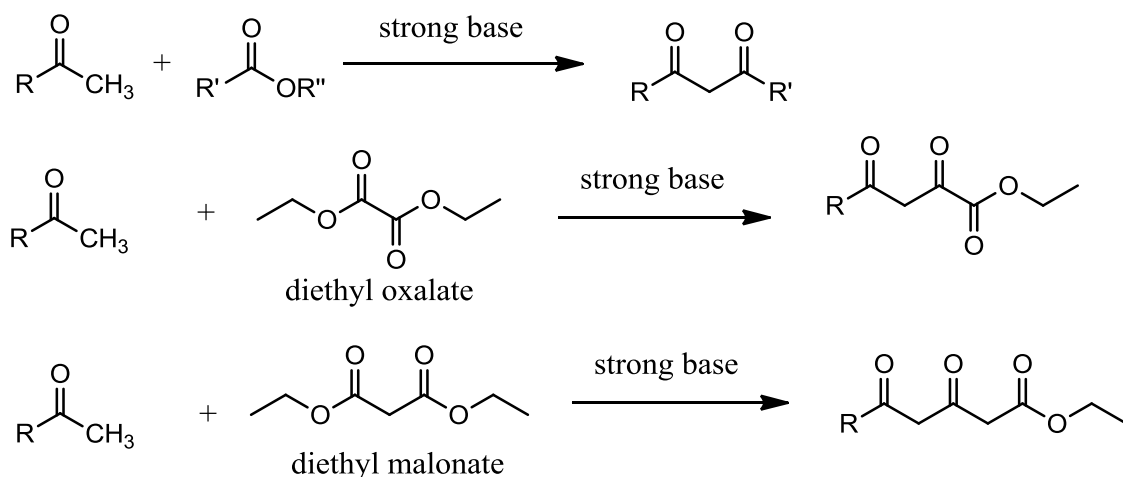
Scheme 6: General reactions for the preparation of β-diketones and β-diketoesters

We attempted to synthesize compound **42** by reacting TU-003 **41** with sodium (**scheme 1, page 29**) as similar reactions had previously been reported[98] Instead of obtaining the desired compound, the starting material was cleaving to give a new compound TU-006 **53**. The cleavage of aryl ethers in the presence of alkali metals has been previously reported[99]. It has also been reported[100] that a similar reaction takes place when using both an alkaline base and a triethylsilane. Based on this information, we suggest that TU-003 **41** was also being cleaved by the same sodium used to carry out the acylation of TU-003 **41** with diethyl oxalate.

It has been found that these reactions depend on the type and the number of equivalents of the base used.[92] For example, acylation with sodium amide is quicker and gives better yields than sodium ethoxide and metallic sodium.[92] Lithium amide also gives better yields than sodium amide, which in turn gives better yields than sodium hydride.[93] The yields obtained using two equivalents of sodium amide for one equivalent of the ketone are twice as high as when one equivalent of the base is used, usually yielding less than 50%.[92] However, using metallic sodium results in a 95% yield in the formation of a di-ketoester. Excess ester does not have any significant effect on the yield.[92] In our study, we did not even detect traces of our desired product when metallic sodium was used as the base.
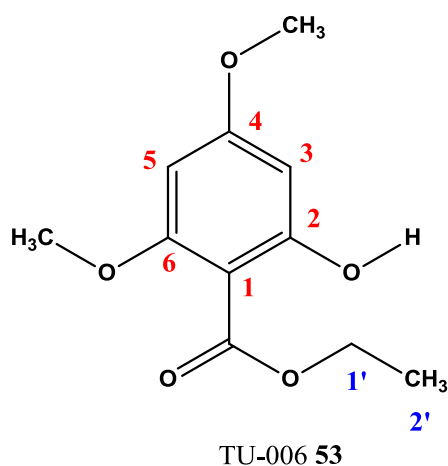
TU-006 **53**

The ^{1}H NMR spectrum of TU-006 **53** has a triplet at 1.39 ppm which corresponds to three protons and a quartet corresponding to two protons at 4.37 ppm. The two groups of peaks have the same coupling constant (7.09 Hz), which indicates that the two sets of protons are on neighbouring carbon atoms and represent the ethyl moiety of the ester in TU-006 **53**. The signals of the methoxy groups of TU-006 **53** partially overlap and are singlets at 3.80 ppm and 3.81 ppm. The signals of the aromatic protons are coupled doublets at 5.95 ppm and 6.10 ppm and the signal of the phenolic proton is a singlet at 12.09 ppm.
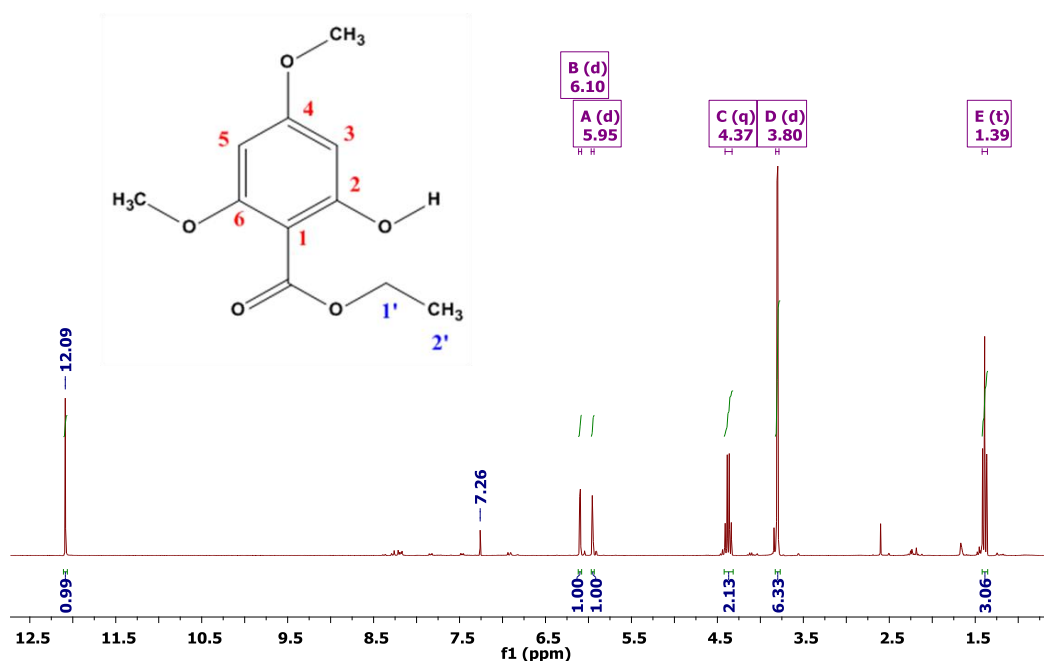
Figure 23: 1H NMR spectrum of TU-006 53 in CDCl3

The ^{13}C NMR spectrum of TU-006 **53** has eleven peaks representing the 11 non-equivalent carbon nuclei. The peak of 2'-C is at 14.2 ppm and the peaks at 55.4 ppm and 56.0 ppm correspond to the carbon nuclei of the two methoxy groups. The peak at 61.2 ppm represents the methylene carbon nucleus of the ethyl substituent. The rest of the peaks represent the aromatic carbon nuclei and carbonyl carbon nucleus of the ester moiety.
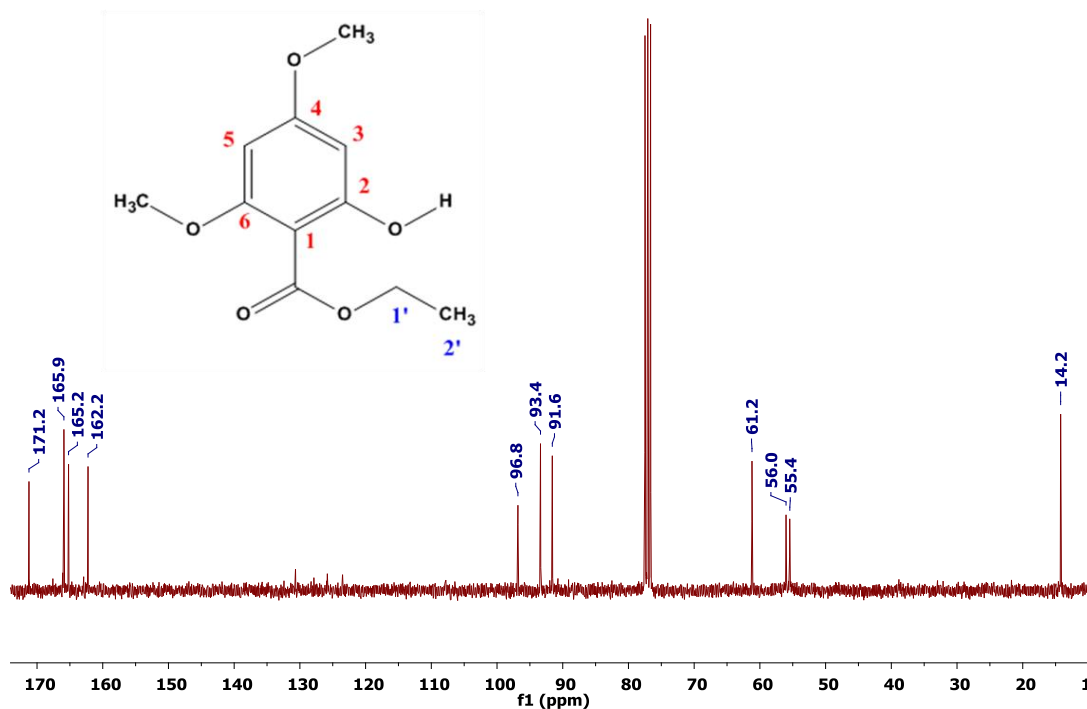
Figure 24: ^{13}C NMR spectrum of TU-006 53 in CDCl$_3$

After observing that sodium was cleaving TU-003 **41** instead of giving the desired product, we benzylated 1-(2-hydroxy-4,6-dimethoxyphenyl)ethanone with 1-(bromomethyl)-4-nitrobenzene and obtained compound TU-005 **54**. The same protecting group has been used previously.[98]

TU-005 **54**
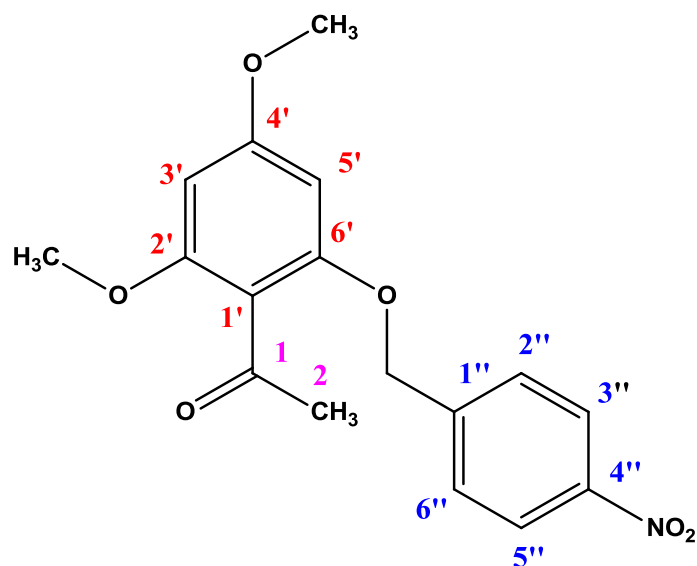
The peak of the protons of the acetyl group is a singlet at 2.49 ppm, peaks of the protons of the methoxy groups are singlets at 3.80 ppm and 3.81 ppm, the peak of the methylene protons is a singlet at 5.15 ppm and the peaks of the protons of the ring substituted by methoxy groups are doublets at 6.08 ppm and 6.14 ppm. The doublets at 7.56 ppm and 8.23 ppm correspond to the protons of the nitro-substituted ring with protons *ortho-* with respect to the nitro group at 8.23 ppm.
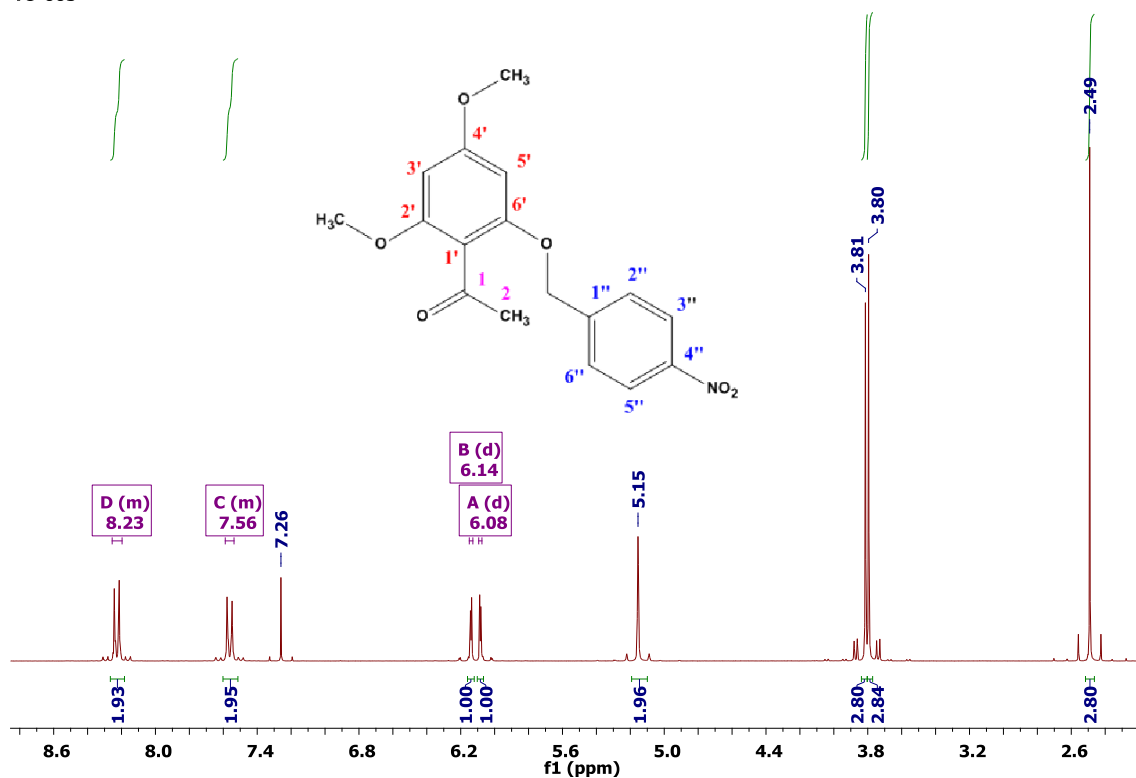
Figure 25: ^{1}H NMR spectrum of TU-005 54 in CDCl$_3$

The ^{13}C NMR spectrum of TU-005 **54** has fifteen peaks corresponding to fifteen non-equivalent carbon nuclei. The peak of the carbonyl carbon nucleus of the acetyl substituent is at 201.6 ppm and the peak of the methyl group of the acetyl substituent is at 32.7 ppm. The peaks of the methoxy groups are at 55.5 ppm and 55.9 ppm and the peak of the methylene group of the benzyl moiety is at 69.2 ppm. The peaks between 90 ppm and 170 ppm correspond to the carbon nuclei of the aromatic rings.
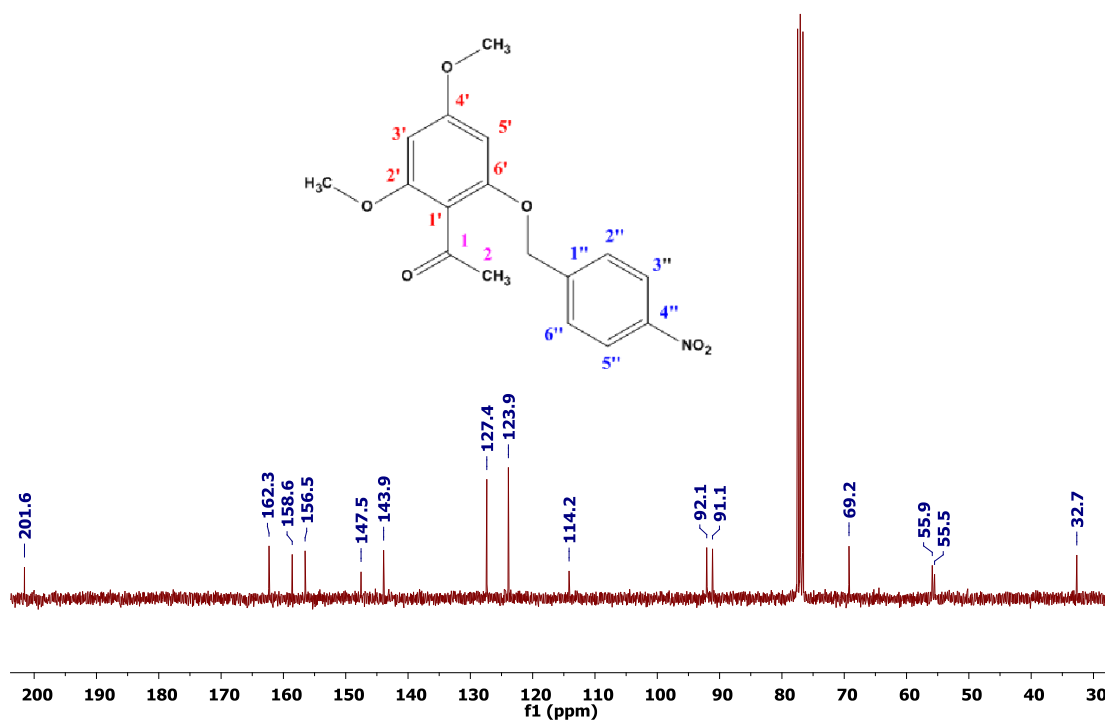
Figure 26: ^{13}C NMR spectrum of TU-005 54 in CDCl$_3$

Acetylation of the methyl ketone group of TU-005 **54** with diethyl oxalate in the presence of sodium, yielded an unexpected product TU-007 (L-96) **55**. Upon inspection of the ^{1}H and the ^{13}C NMR spectra of TU-005 **54** and TU-007 (L-96) **55** we noticed that the peak of the methylene of TU-005 **54** which is at 5.15 ppm in the ^{1}H NMR spectrum was not present in the ^{1}H NMR spectrum of TU-007 (L-96) **55** whereas all other proton peaks were present. Moreover, the peak of the carbonyl group of TU-005 **54** which is at 201.6 ppm was not present in the ^{13}C spectrum of TU-007 (L-96) **55** whereas the number of carbons remained the same for both compounds. This led us to the conclusion that TU-005 **54** had undergone a cyclisation and a condensation to give TU-007 (L-96) **55**, which was supported by NMR and mass spectrometry data.

48
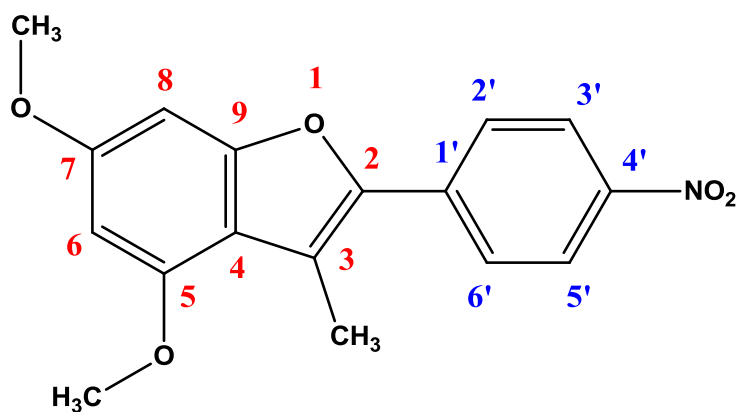
TU-007 **55**

The ^{1}H NMR spectrum of TU-007 (L-96) **55** has the peak representing the protons of the methyl substituent at 2.65 ppm and the peaks of the protons of the methoxy groups are at 3.86 ppm and 3.90 ppm. The signals for the two aromatic protons of the ring substituted with methoxy groups are at 6.29 ppm and 6.61 ppm and peaks of the protons of the nitro-substituted ring are at 7.85 ppm and 8.27 ppm. The peaks of 6-H and 8-H appear as doublets because of *meta*-coupling in the aromatic ring. This is supported by the magnitude of the coupling constant ($J = 1.92$ Hz).
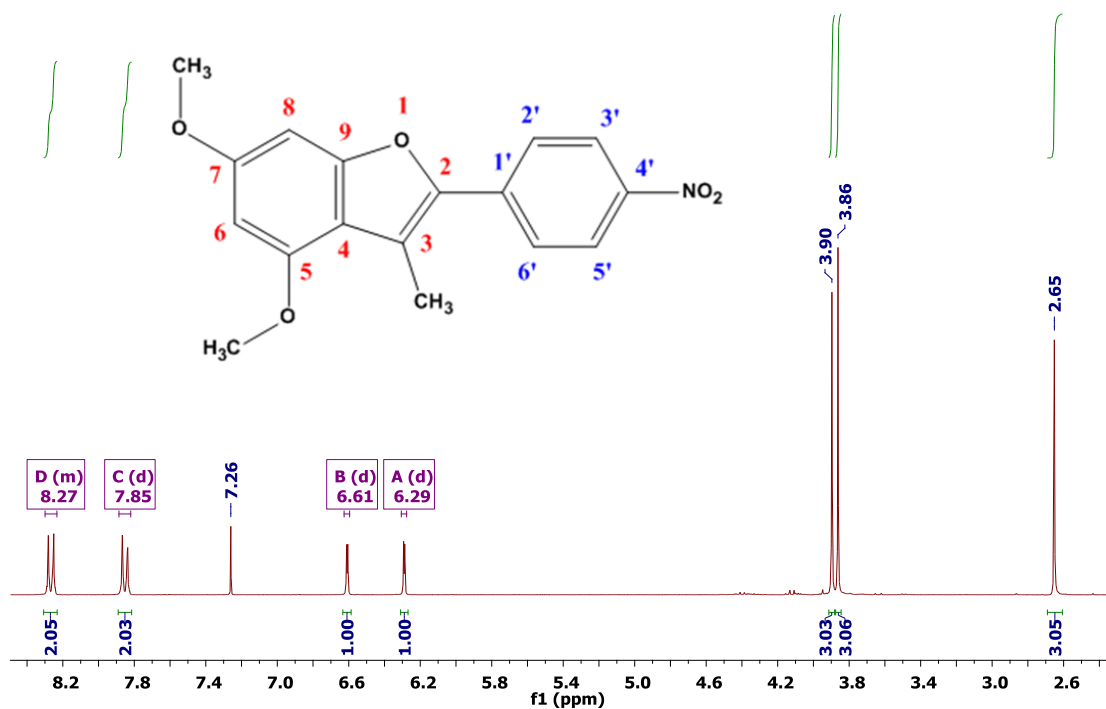
Figure 27: ^{1}H NMR spectrum of TU-007 (L-96) 55 in CDCl$_3$

Three peaks are easily identifiable in the ^{13}C NMR of TU-007 (L-96) **55**. The peak at 11.6 ppm corresponds to the methyl group whereas the peaks at 55.5 ppm and 55.8 ppm correspond to the methoxy groups. All other peaks between 80 ppm and 170 ppm represent the aromatic carbon nuclei.
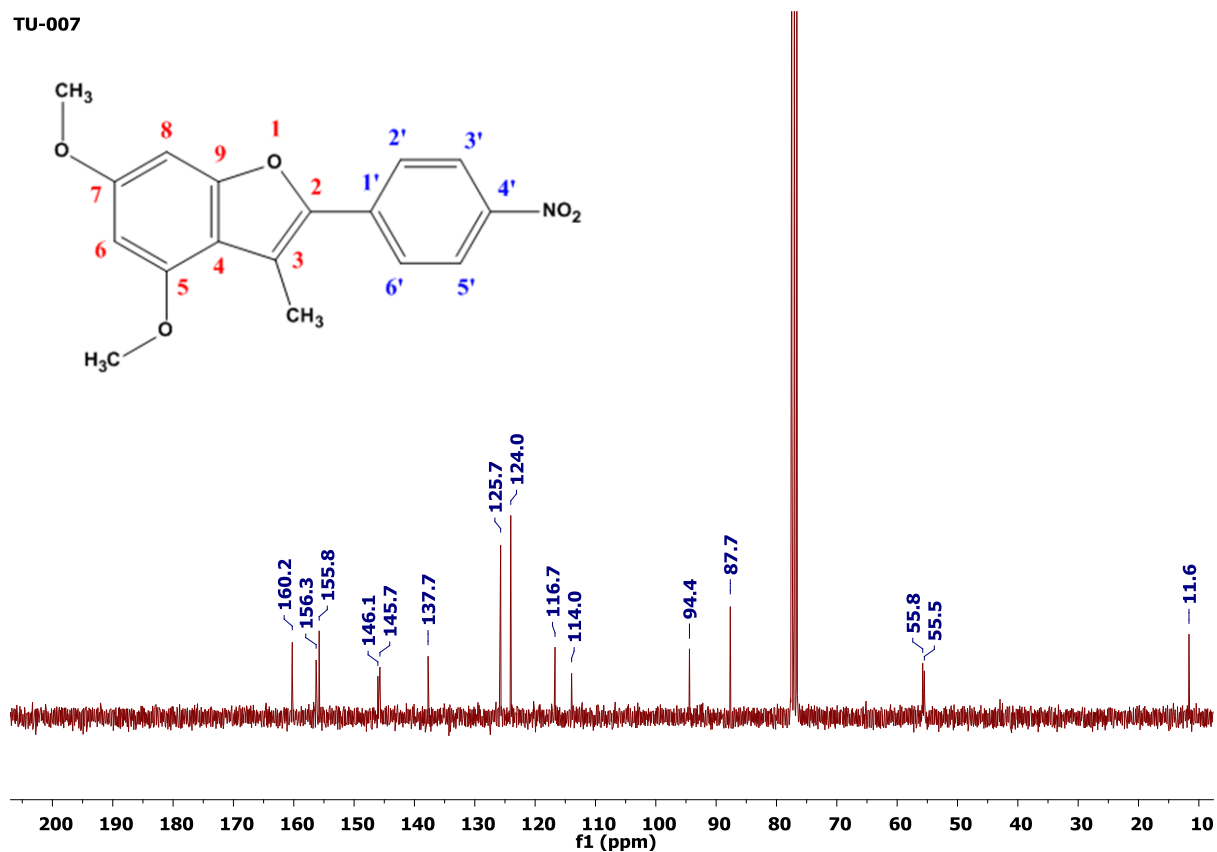
Figure 28: ^{13}C NMR spectrum of TU-007 (L-96) 55 in CDCl₃

High resolution mass spectrometry (HRMS) (ESI) of TU-007 (L-96) **55** indicated that the calculated mass of [M+H]⁺ is m/z = 314.1028 and the experimentally obtained mass is m/z = 314.1039. (**Figure 29**)

Mass	Calc. Mass	mDa	PPM	DBE	Formula	i-FIT	i-FIT Norm	Fit Conf %	C	H	N	O	Si
314.1039	314.1037	0.2	0.6	5.5	C8 H20 N7 O Si3	371.7	19.000	0.00	8	20	7	1	3
	314.1042	-0.3	-1.0	15.5	C18 H12 N5 O	357.1	4.490	1.12	18	12	5	1	
	314.1033	0.6	1.9	9.5	C16 H20 N O2 Si2	370.0	17.320	0.00	16	20	1	2	2
	314.1033	0.6	1.9	6.5	C9 H16 N7 O4 Si	365.1	12.478	0.00	9	16	7	4	1
	314.1028	1.1	3.5	10.5	C17 H16 N O5	352.9	0.229	79.51	17	16	1	5	
	314.1024	1.5	4.8	0.5	C7 H24 N3 O5 Si3	371.6	18.911	0.00	7	24	3	5	3
	314.1020	1.9	6.0	1.5	C8 H20 N3 O8 Si	366.1	13.442	0.00	8	20	3	8	1
	314.1060	-2.1	-6.7	5.5	C13 H20 N O6 Si	365.7	13.072	0.00	13	20	1	6	1
	314.1060	-2.1	-6.7	2.5	C6 H16 N7 O8	364.1	11.475	0.00	6	16	7	8	

Figure 29: HRMS (ESI) spectrum of TU-007 (L-96) 55

After realizing that the attempted acylation of TU-005 **54** with diethyl oxalate in the presence of sodium did not produce the desired product, we tested whether we would obtain the desired product if the hydroxyl of 1-(2-hydroxy-4,6-dimethoxyphenyl)ethanone were protected with a methyl. By reacting 1-(2-hydroxy-4,6-dimethoxyphenyl)ethanone with iodomethane, we obtained the compound TU-009 **56**.

TU-009 **56**

51
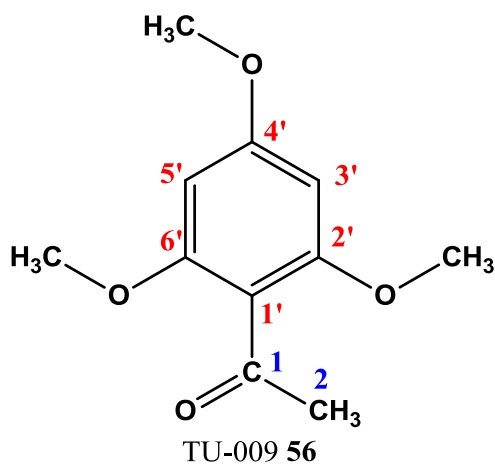
The ^{1}H NMR spectrum of TU-009 **56** (**Figure 30**) has a peak representing the acetyl protons at 2.46 ppm, the peak of the two equivalent methoxy groups are at 3.79 ppm, the peak of the remaining methoxy is at 3.82 ppm and the peak of the equivalent aromatic protons is at 6.10 ppm.
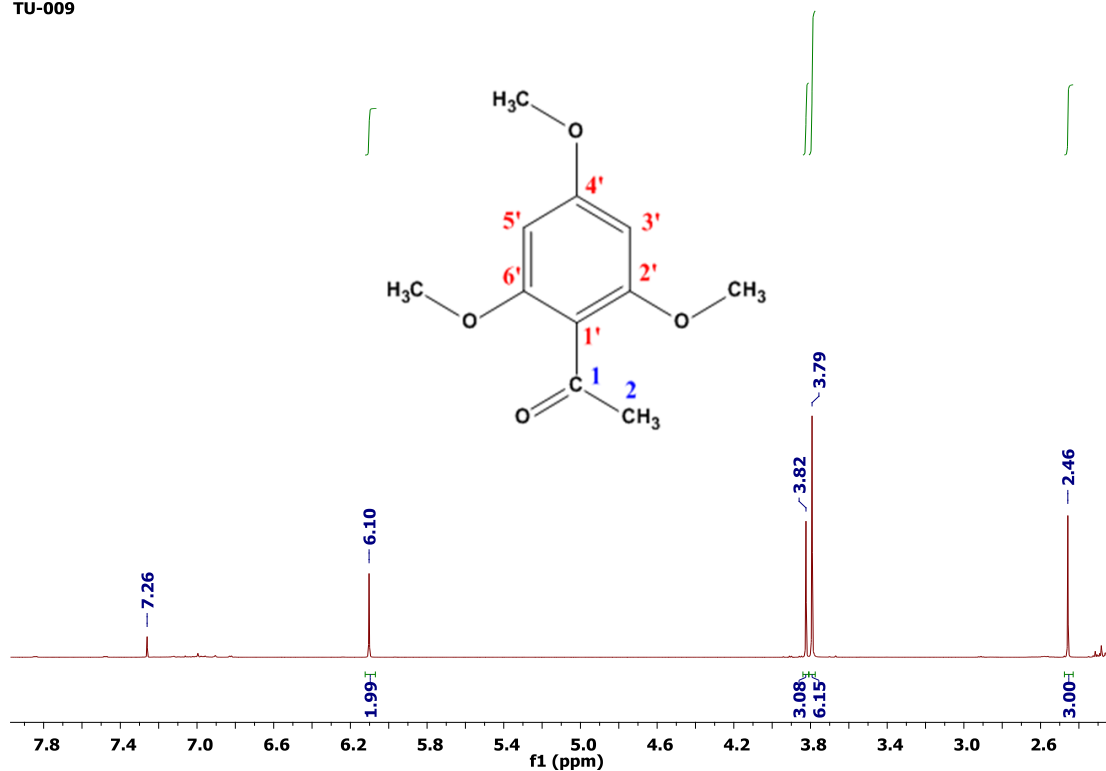
Figure 30: ^{1}H NMR spectrum of TU-009 56 in CDCl$_3$

The ^{13}C of TU-009 **56** (**Figure 31**) has eight peaks as expected. The peak at 32.5 ppm represents the methyl carbon of acetyl group and the peak at 201.7 ppm represents the cabonyl carbon of the acetyl group. The peaks of the methoxy groups are at 55.4 ppm and 55.8 ppm and the peaks of the aromatic carbon nuclei are in the interval between 90 ppm to 170 ppm. An attempt to acylate TU-009 **56** with diethyl oxalate in the presence of sodium did not yield the desired product.
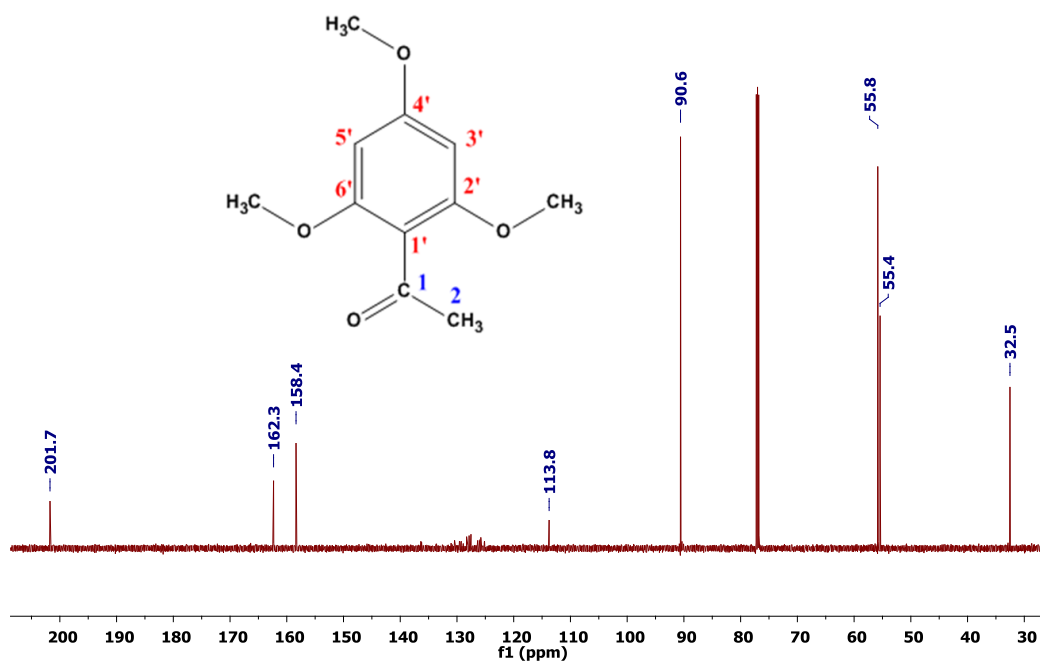
Figure 31: ^{13}C NMR spectrum of TU-009 56 in CDCl$_3$

After realizing that using sodium was not yielding the desired product **42**, we changed the base to lithium bis (trimethylsilyl) amide. Treating TU-003 **41** with lithium bis (trimethylsilyl) amide, followed by the addition of diethyl oxalate yielded the compound TU-010 **48**. Although we had aimed to synthesize compound **42**, NMR data suggested that we had obtained compound TU-010 **48**. We continued with the synthesis since the two compounds are tautomers. **(Scheme 7, page 55)**
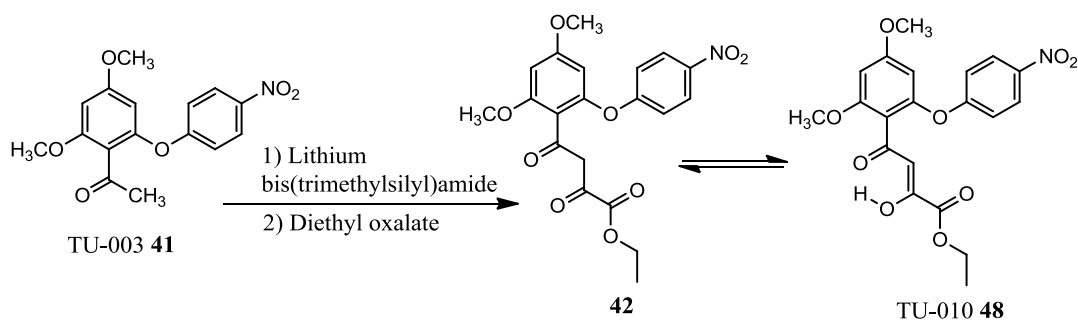
Scheme 7: Synthesis of TU-010 **48** from TU-003 **41** and diethyl oxalate

In the ^{1}H NMR spectrum of TU-010 **48** (**Figure 32**), there is a triplet at 1.34 ppm that represents the protons of the methyl group of the ethyl substituent while the methylene protons of this substituent has its quartet of signals at 4.33 ppm. These two groups of peaks have the same coupling constant ($J = 7.12$ Hz), which confirms that the protons are attached to adjacent carbon atoms.

TU-010 **48**
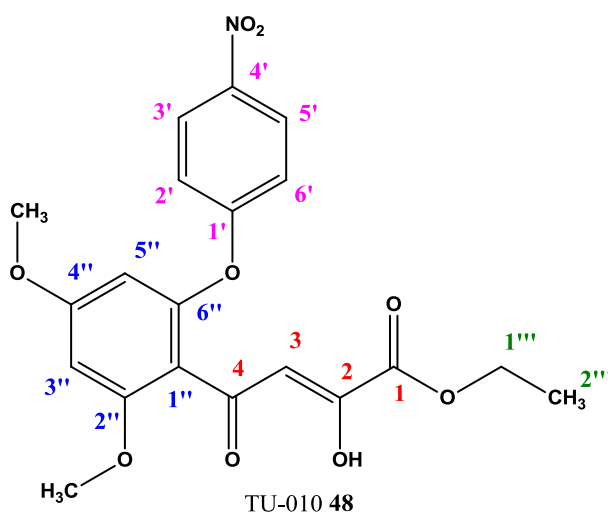
The singlets at 3.81 ppm and 3.88 ppm represent the protons of the methoxy groups and the doublets at 6.18 ppm and 6.40 ppm represent the protons (3''-H and 5''-H) of the aromatic ring. Their peaks are doublets because the two protons couple with each other. The singlet at 6.69 ppm represents the vinylic proton (3-H) and the multiplets at 7.00 ppm and 8.19 ppm represent the aromatic protons (2'-H and 6'-H, 3'-H and 5'-H) of the nitro-substituted ring. The peak at 14.25 ppm represents the enolic proton (2-OH). Its integral (0.56 instead of 1) is low because 2-OH undergoes proton exchange.
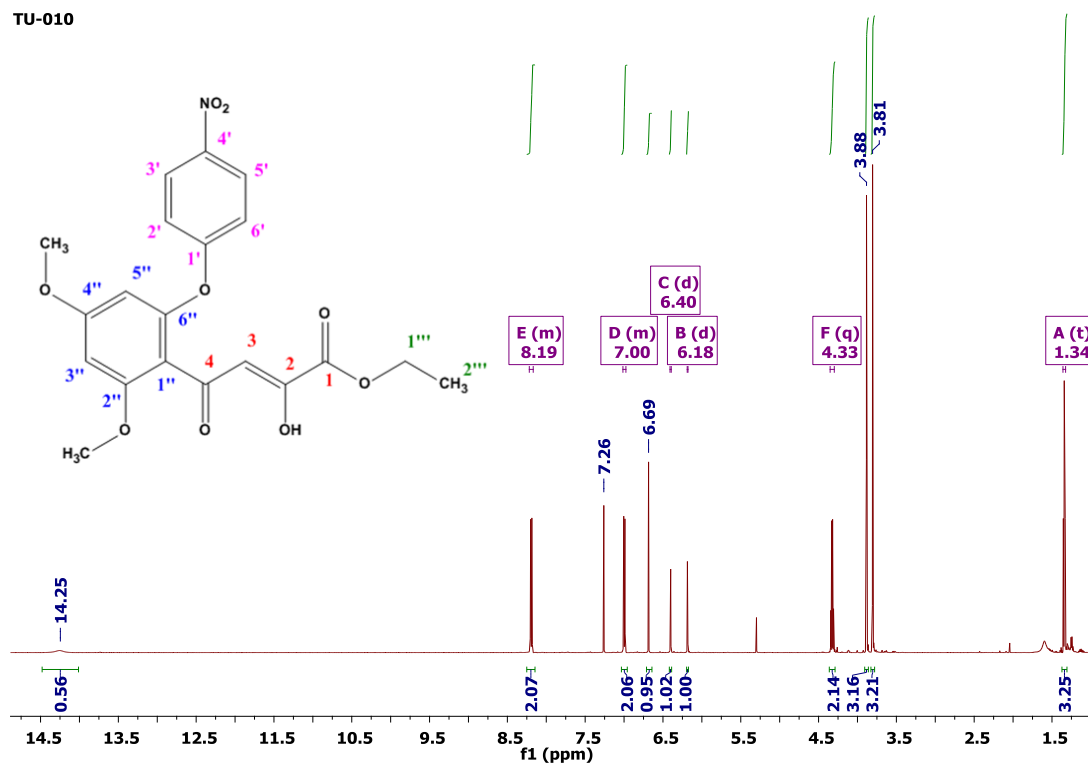
Figure 32: ^{1}H NMR spectrum of TU-010 48 in CDCl$_3$

The ^{13}C NMR spectrum of TU-010 **48 (Figure 33)** is more complicated than its ^{1}H NMR spectrum. However, some of the peaks can be easily assigned. The peak at 14.1 ppm represents the carbon nucleus of the methyl group (2'''-CH$_3$) of the ethyl substituent of the ester moiety whereas the signal of the carbon nucleus of the methylene group (1'''-CH$_2$) is at 62.5 ppm. The peaks corresponding to the carbon nuclei of the methoxy groups are at 55.8 ppm and 56.3 ppm and the peak corresponding to the carbonyl carbon nucleus of the ketone group (4-C=O) is at 192.2 ppm.
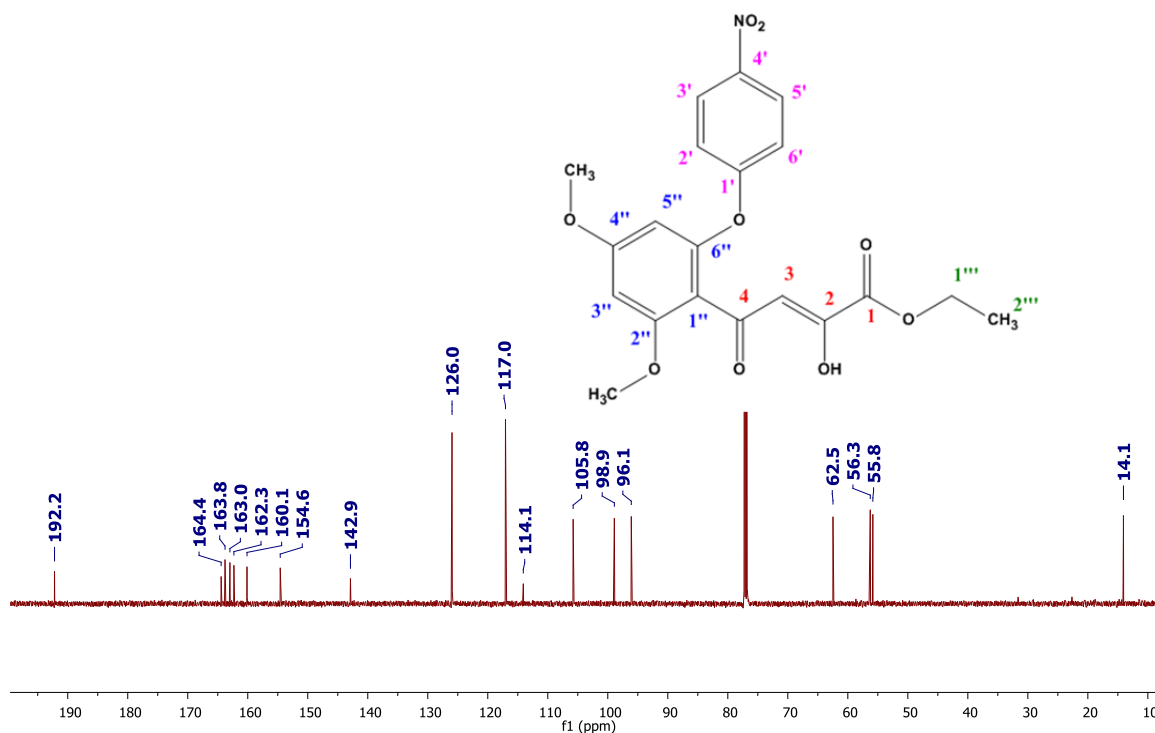
Figure 33: ^{13}C NMR spectrum of TU-010 48 in CDCl$_3$

The HSQC spectrum (**Figure 34**) corroborates our assignements of the protons and carbon nuclei of the ethyl groups of TU-010 **48**, but an HMBC experiment would be necessary to collectly assign the remaining peaks between 90 ppm and 170 ppm that represent the aromatic carbon nuclei.
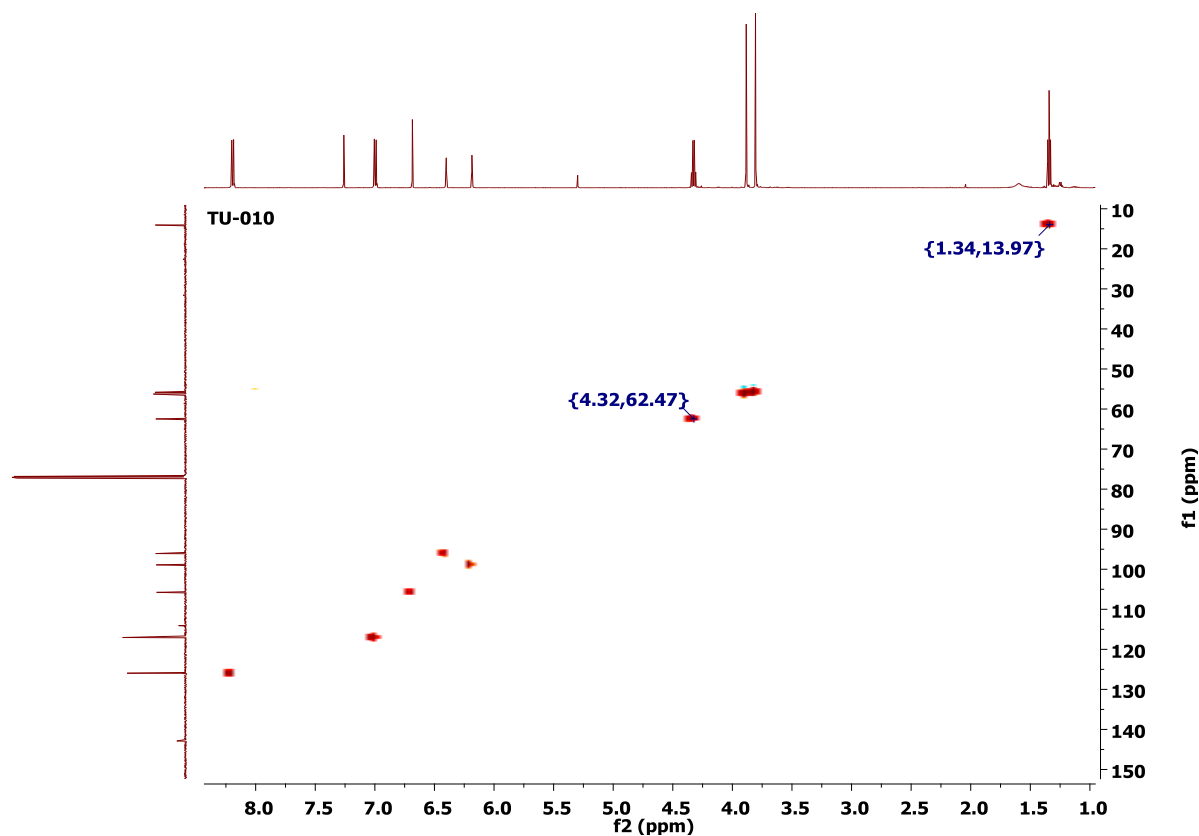
Figure 34: HSQC spectrum of TU-010 48 in CDCl$_3$

2.2.4. Synthesis of isoxazoles

The third step of our synthesis of analogues of NMS-E973 (L-1) **38** involves the formation of the isoxazole TU-011 (L-7) **43**. The isoxazole moiety is found in many synthetic Hsp90 inhibitors which are generally active against cancer cells[49,50,53] and protozoans.[31,74] One of the methods of preparation of isoxazoles is the condensation of a β-diketone with hydroxylamine hydrochloride (**Scheme 8, page 59**).[101] If the diketone is symmetrical, only one product is obtained while unsymmetrical diketones can give one or two products depending on the regioselectivity of the reaction.[101]
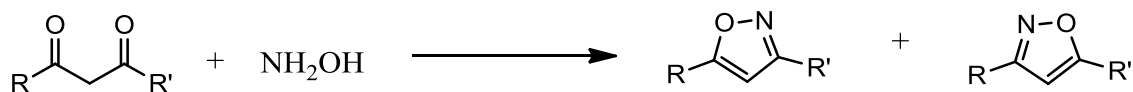
Scheme 8: Synthesis of isoxazoles from β-diketones

The isoxazoles can also be prepared by condensation of hydroxylamine with α,β-unsaturated carbonyl compounds such as chalcones.[101,102] In this case, a leaving group in position β of the carbonyl is removed.[101,103] An example of this is the synthesis of 5-arylisoxazoles in yields of up to 93% in some cases.[103] The same reactions yield pyrazoles or pyrimidines if hydroxyl amine is replaced by hydrazines or amidines respectively.[104] Therefore, these reagents can be used to synthesize pyrazole or amidine analogues of NMS-E973 (L-1) **38**.

In our study, compound TU-010 **48** was reacted with hydroxyl amine hydrochloride in ethanol to yield compound TU-011 (L-7) **43**, the precursor of different amide analogues of NMS-E973 (L-1) **38**. The two steps of synthesis of TU-010 **48** and TU-011 (L-7) **43** give yields of 65% and 77% respectively, with the overall yield of the two reactions being 50%. This is much lower than the reported value of 78% obtained where the second step was carried whithout purifying the product obtained in the first step.[61] Therefore, it is important for future researchers to omit the purification of the product after the first step.

The ^{1}H NMR spectrum of TU-011 (L-7) **43** (**Figure 35**) has the peaks corresponding to the protons of the ethyl substituent at 1.39 ppm (2'-CH$_3$) and 4.41 ppm (1'-CH$_2$-). The peaks of the methoxy groups are at 3.83 ppm and 3.92 ppm while the peaks of the protons of the aromatic ring substituted with the methoxy groups are at 6.29 ppm and 6.47 ppm. They are doublets because of *meta*-coupling which is confirmed by the coupling constant (J = 2.34 Hz). The peak at 6.88 ppm represent the proton of the isoxazole ring and the peaks at 6.99 ppm and 8.16 ppm represent the two sets of equivalent protons of the nitro-substituted ring.
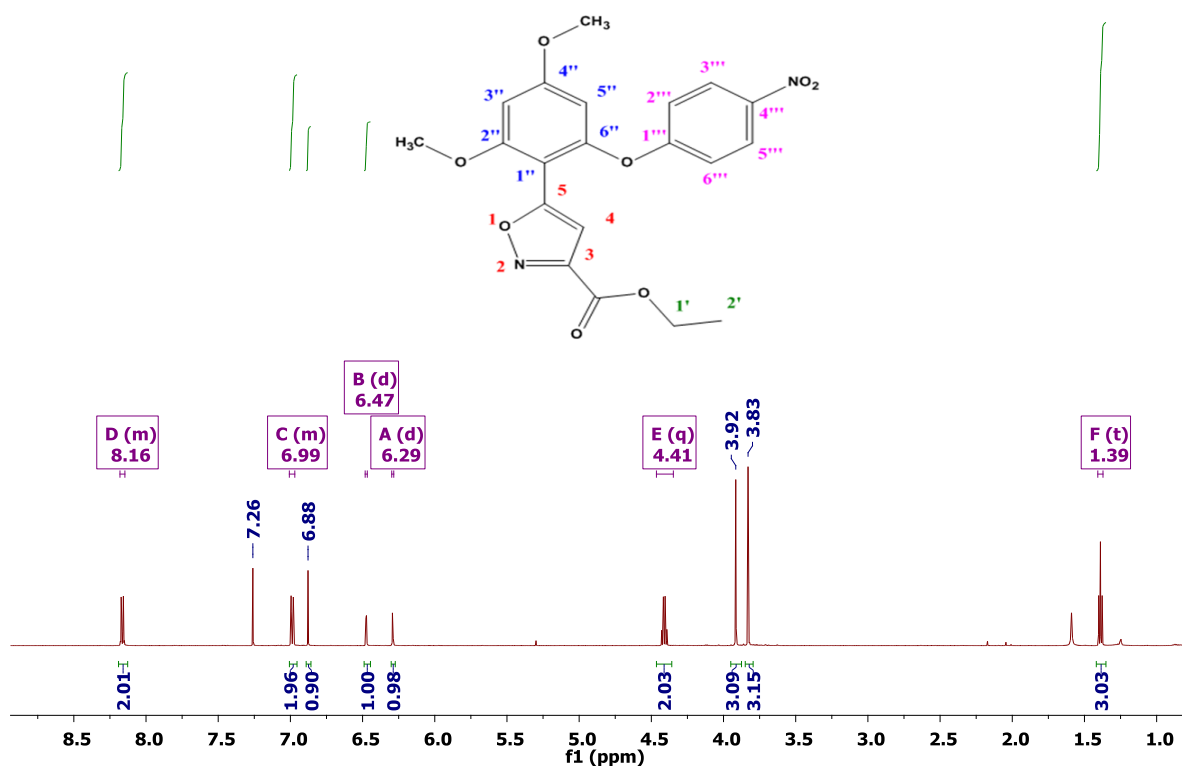
Figure 35: ^{1}H NMR spectrum of TU-011 (L-7) 43 in CDCl$_3$

The ^{13}C NMR spectrum (**Figure 36**) has signals corresponding to the carbon nuclei of the ethyl group at 14.2 ppm (2'-CH$_3$) and 62.1 ppm (1'-CH$_2$-) whereas the peaks of the carbon nuclei of the methoxy groups are at 55.8 ppm and 56.2 ppm. The peaks of the carbon nuclei of the aromatic rings (both of the phenyl rings and the isoxazole ring) are in the interval spanning 90 ppm – 170 ppm.
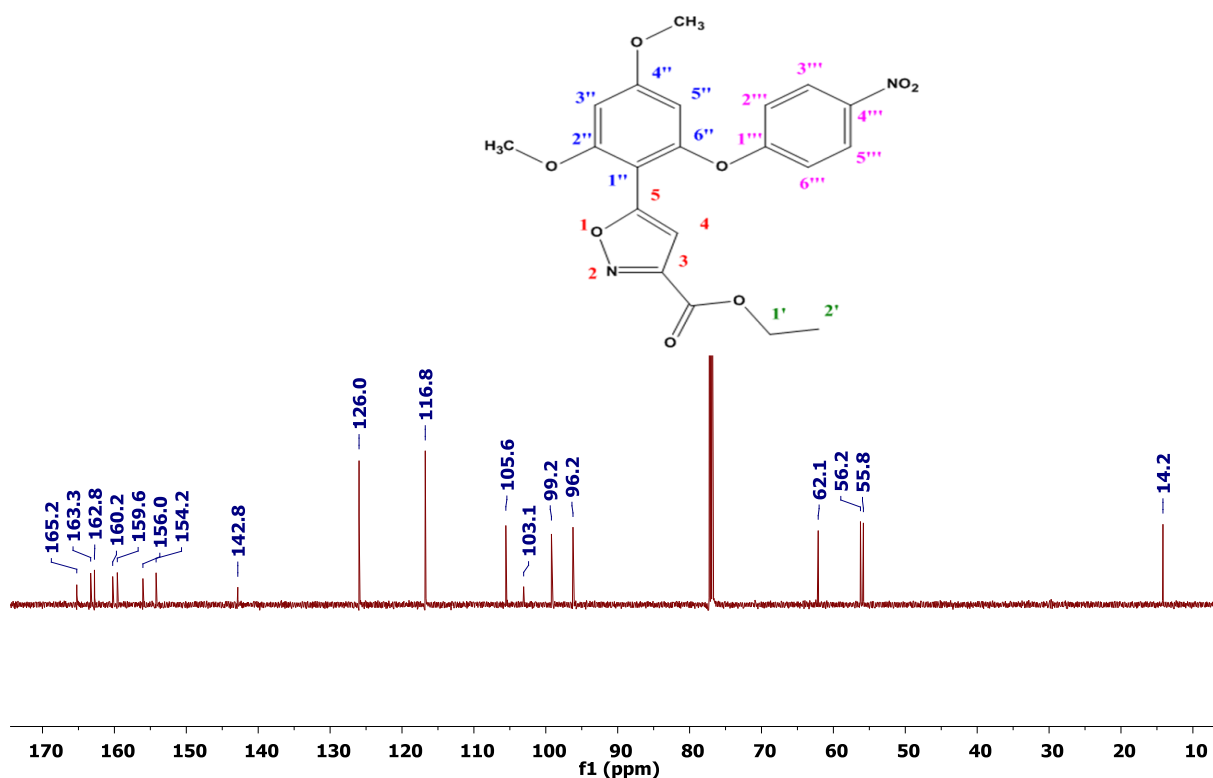
Figure 36: ^{13}C NMR spectrum of TU-011 (L-7) **43** in CDCl$_3$

HRMS (ESI) of TU-011 (L-7) **43** indicates that the mass of [M+H]$^+$ is m/z = 415.1141 as compared to the experimentally obtained value m/z = 415.1156 (**Figure 37**).

Mass	Calc. Mass	mDa	PPM	DBE	Formula	i-FIT	i-FIT Norm	Fit Conf %	C	H	N	O	Si
415.1156	415.1155	0.1	0.2	17.5	C21 H15 N6 O4	278.2	9.310	0.01	21	15	6	4	
	415.1154	0.2	0.5	20.5	C28 H19 O2 Si	290.8	21.967	0.00	28	19		2	1
	415.1159	-0.3	-0.7	16.5	C20 H19 N6 O Si2	293.5	24.659	0.00	20	19	6	1	2
	415.1160	-0.4	-1.0	-0.5	C8 H23 N4 O15	287.5	18.639	0.00	8	23	4	15	
	415.1164	-0.8	-1.9	-1.5	C7 H27 N4 O12 Si2	293.3	24.418	0.00	7	27	4	12	2
	415.1145	1.1	2.6	11.5	C19 H23 N2 O5 Si2	293.4	24.529	0.00	19	23	2	5	2
	415.1141	1.5	3.6	12.5	C20 H19 N2 O8	268.9	0.013	98.71	20	19	2	8	
	415.1173	-1.7	-4.1	7.5	C16 H23 N2 O9 Si	289.7	20.850	0.00	16	23	2	9	1
	415.1137	1.9	4.6	2.5	C10 H27 N4 O8 Si3	294.9	26.076	0.00	10	27	4	8	3

Figure 37: HRMS (ESI) spectrum of TU-011 (L-7) 43

2.2.5. Amidation of carboxylic acids and carboxylic esters

There are various methods of preparation of amides. Some of the common methods include preparation of amides by acylation of amines with acyl halides, carboxylic anhydrides, carboxylic esters or carboxylic acids, the acyl halides being the most reactive of these reagents **(Scheme 9, page 63)**.[83,105] The amidation of acyl halides is very exothermic and the temperature is usually controlled either by dilution or cooling.[83]
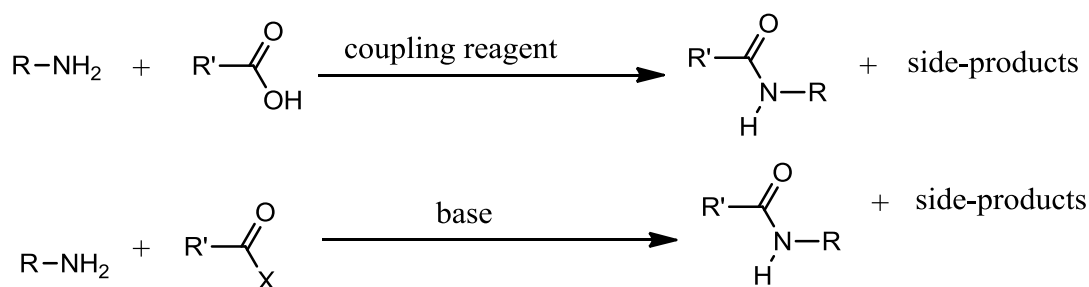
Scheme 9: Traditional methods of preparation of amides[105]

61

In some cases, amides can be prepared from esters by simply heating the amine and the ester resulting in yields above 90%.[61] Amides can be also prepared by reacting an ester with an amine in the presence of a Lewis acid such as BBr_3,[106] $MgCl_2$[107] and $MgBr_2$[107] and yields obtained in these reactions using $MgBr_2$ or $MgCl_2$ are generally above 90%. Amides have been also prepared by heating carboxylic acids and amines in the presence of dehydrating agents such as $POCl_3$ and $SOCl_2$.[108] Other catalysts used to prepare amides from carboxylic acids include molecular sieves,[109] transition metals such as ruthenium and copper,[110] Lewis acids such as $B(OCH_2CF_3)_3$[111] and coupling reagents such as *N,N,N',N'*-tetramethyl-*O*-(benzotriazol-1-yl)uronium tetrafluoroborate (TBTU).[61] Although amidation reactions catalysed with molecular sieves generally give very good yields, it requires high temperatures (> 140 °).[109] However, reactions catalysed by TBTU give good yields at lower temperatures.[61] As a result, we used this coupling reagent to synthesize many of our compounds **(Scheme 10, page 76)**. However, we also synthesized another Boc-protected amide TU-012 (L-97) **49** using a different method[61] and we obtained more amides by Boc-deprotection followed by reductive amination **(Scheme 4, page 40)**.

TU-011 (L-7) **43** was reacted with 4-amino-1-Boc-piperidine at 90 °C for 36 hours and TU-012 (L-97) **49** was obtained with a yield of 81%.

TU-012 **49**
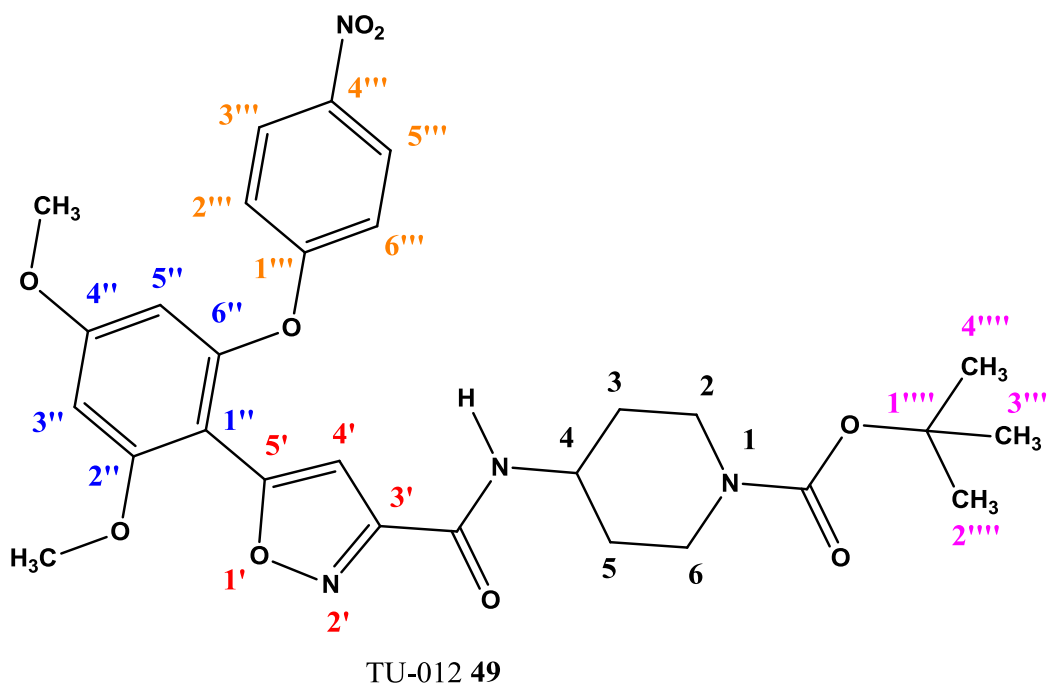
The ^{1}H NMR spectrum of TU-012 (L-97) **49** (**Figure 38**) is quite complex and the protons of the piperidine ring cannot be easily assigned because of the different but very close chemical shift values of the axial and equatorial hydrogen nuclei as well as their complex splitting patterns. The peak of the protons of the *tert*-butyl group are at 1.45 ppm, the peaks of the methoxy groups are at 3.82 ppm and 3.91 ppm and the protons (3''-H and 5''-H) of the ring substituted with methoxy groups are doublets at 6.27 ppm and 6.47 ppm with a *meta*-coupling constant of J = 2.24 Hz. The peak of the amide proton is at 6.68 ppm and the peak of the proton of the isoxazole ring is at 6.92 ppm. The peaks of the protons (2'''-H and 6'''-H, 3'''-H and 5'''-H) of the ring substituted with the nitro group are at 6.97 ppm and 8.18 ppm. The peaks corresponding to the protons of the piperidine ring are at 1.39 ppm, 1.95 ppm, 2.88 ppm and 4.06 ppm.
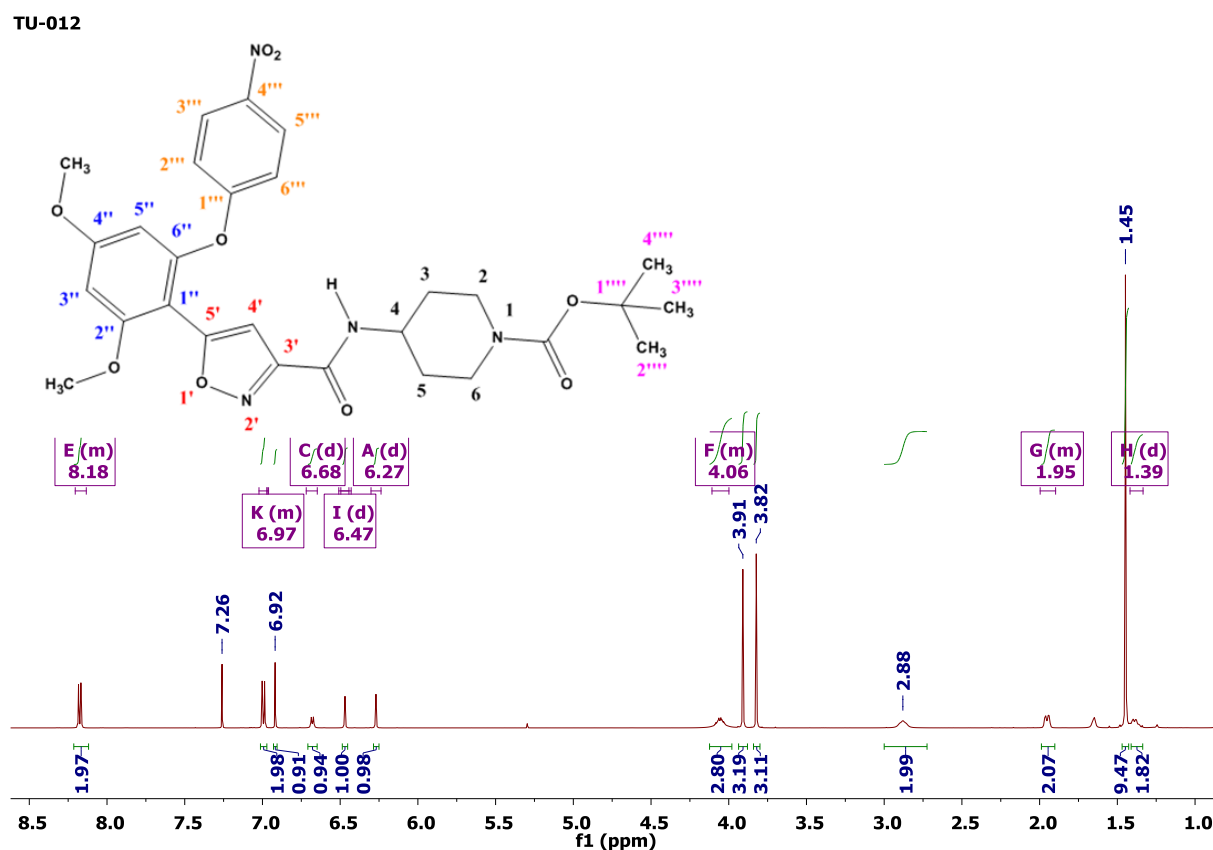
Figure 38: ^{1}H NMR spectrum of TU-012 (L-97) 49 in CDCl$_3$

The ^{13}C NMR spectrum of TU-012 (L-97) **49** (**Figure 39**) is complex and some of the peaks could not be unambiguously assigned from the HSQC spectrum (**Figure 40**), for example in

the overlapping peaks of the carbon nuclei 2-C and 6-C at 42.9 ppm. Due to this overlap, the protons of the piperidine ring could also not be unambiguously assigned.
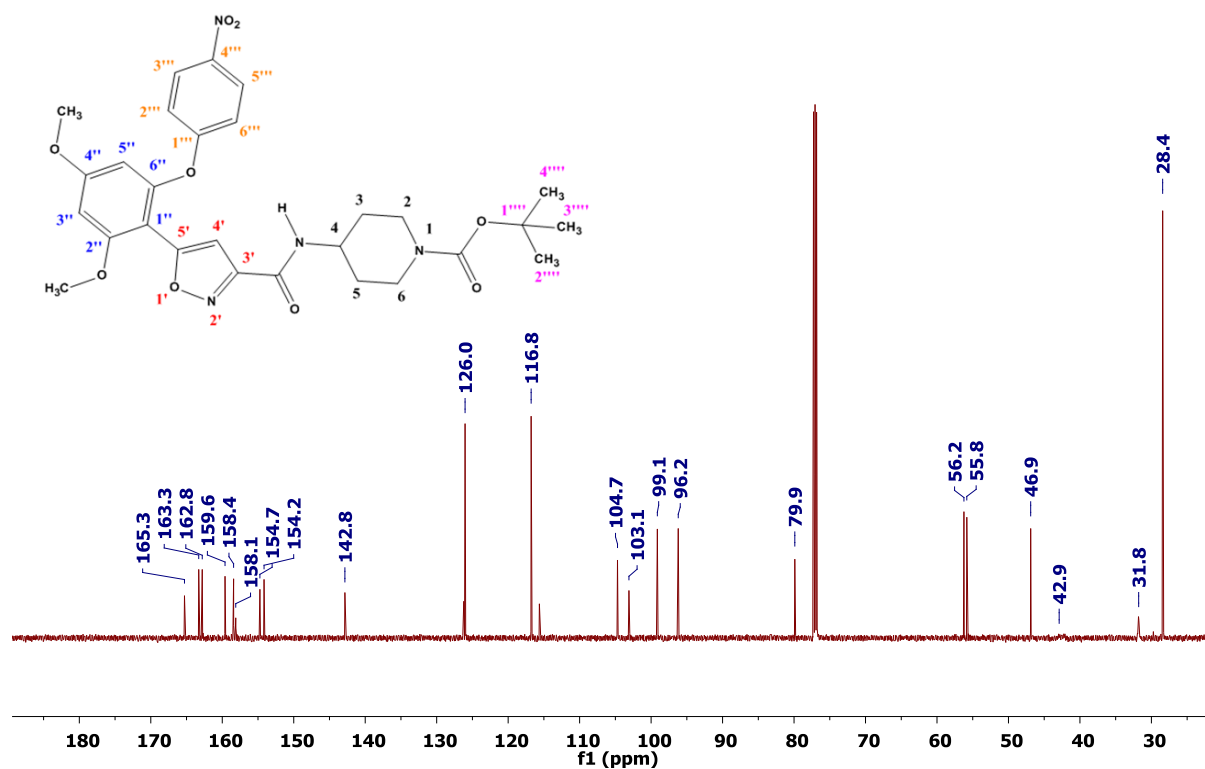
Figure 39: ^{13}C NMR spectrum of TU-012 (L-97) 49 in CDCl$_3$
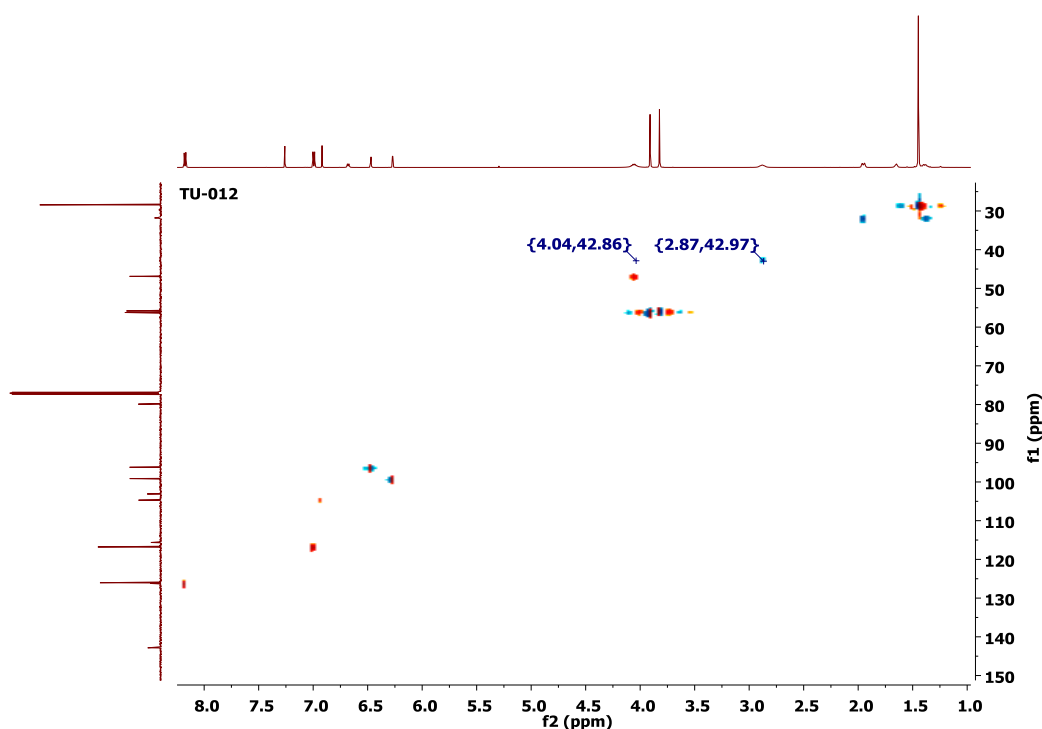
Figure 40: HSQC spectrum of TU-012 (L-97) 49

The mass of TU-012 (L-97) **49** was confirmed by HRMS (ESI) analysis. The mass of [M+H]$^+$ is m/z =569.2248) as compared to the experimental mass m/z = 569.2250 (**Figure 41**).

Mass	Calc. Mass	mDa	PPM	DBE	Formula	i-FIT	i-FIT Norm	Fit Conf %	C	H	N	O	Si
569.2250	569.2248	0.2	0.4	14.5	C28 H33 N4 O9	190.9	2.916	5.41	28	33	4	9	
	569.2252	-0.2	-0.4	13.5	C27 H37 N4 O6 Si2	199.9	11.832	0.00	27	37	4	6	2
	569.2243	0.7	1.2	4.5	C18 H41 N6 O9 Si3	201.3	13.311	0.00	18	41	6	9	3
	569.2260	-1.0	-1.8	22.5	C36 H33 N2 O3 Si	198.0	9.924	0.00	36	33	2	3	1
	569.2239	1.1	1.9	5.5	C19 H37 N6 O12 Si	197.1	9.058	0.01	19	37	6	12	1
	569.2238	1.2	2.1	8.5	C26 H41 O10 Si2	199.7	11.712	0.00	26	41		10	2
	569.2265	-1.5	-2.6	21.5	C35 H37 N2 Si3	201.4	13.398	0.00	35	37	2		3
	569.2266	-1.6	-2.8	4.5	C23 H41 O14 Si	197.0	9.024	0.01	23	41		14	1
	569.2234	1.6	2.8	9.5	C27 H37 O13	191.3	3.321	3.61	27	37		13	

Figure 41: HRMS (ESI) spectrum of TU-012 (L-97) 49

The method used to prepare TU-012 (L-97) **49** did not work well for the preparation of TU-013 (L-98) **57**. When we tried to prepare TU-013 (L-98) **57** from TU-011 (L-7) **43** by heating the mixture at 90 °C with piperidine, we obtained a very low yield (9%) of TU-013 (L-98) **57**, and we had to change the method. We first prepared TU-014 (L-99) **58** from TU-011 (L-7) **43** and from TU-014 (L-99) **58** we prepared TU-013 (L-98) **57**.

TU-014 (L-99) **58** was prepared by saponification of TU-011 (L-7) **43** followed by neutralization of the base by HCl, giving the desired product in a yield of 75%.

TU-014 **58**
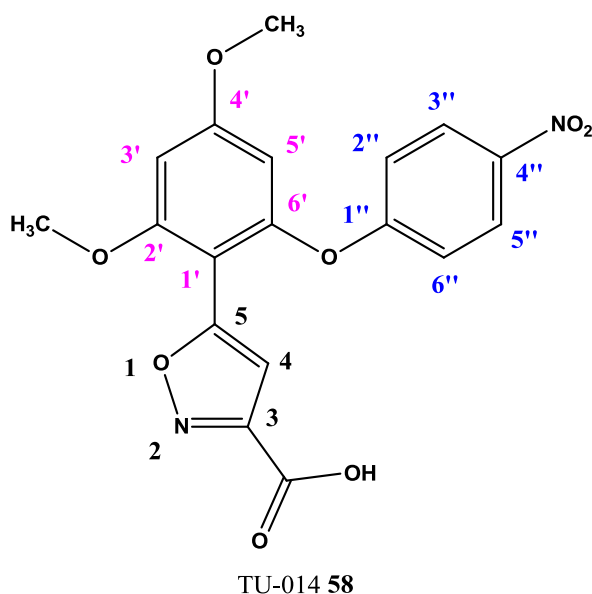
The ^{1}H NMR spectrum of TU-014 (L-99) **58** has two singlets corresponding to the protons of the methoxy groups at 3.87 ppm and 3.95 ppm, the signals of 3'-H and 5'-H of the ring substituted by the methoxy groups are doublets at 6.57 ppm and 6.77 ppm and the singlet at 6.88 ppm represents the proton of the isoxazole ring. The doublets at 7.15 ppm and 8.25 ppm correspond to the protons (2''-H and 6''-H, 3''-H and 5''-H) of the nitro-substituted ring.

66
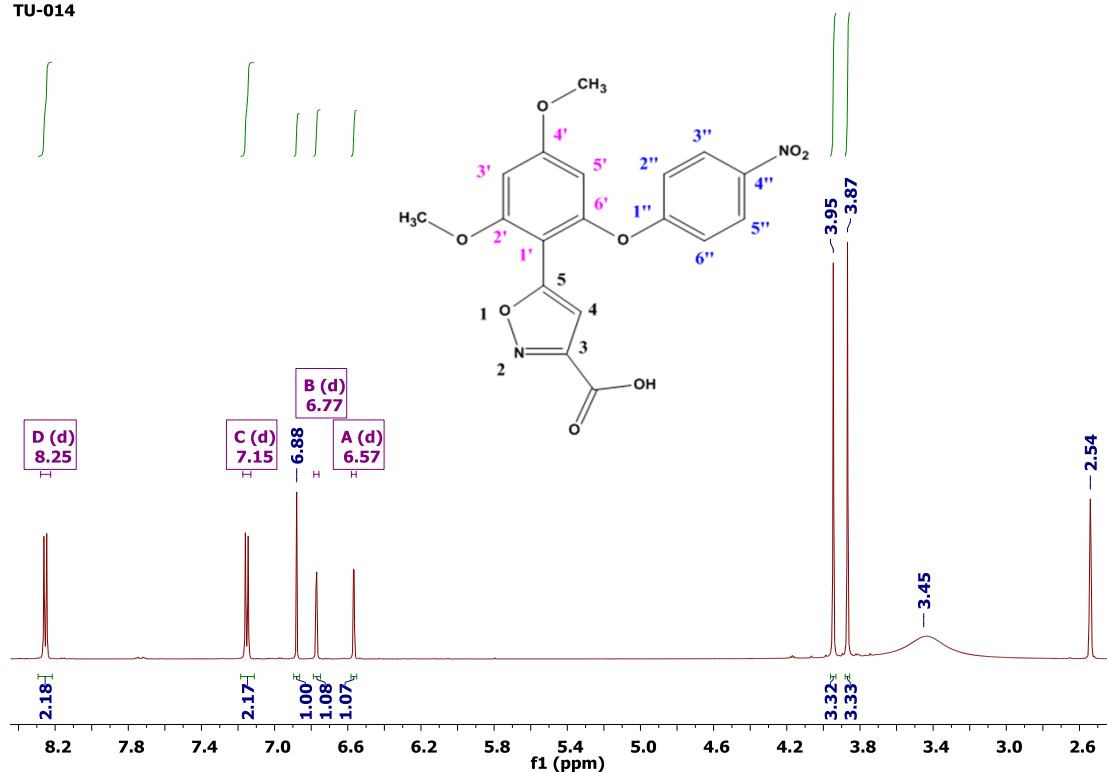
Figure 42: 1H NMR spectrum of TU-014 (L-99) 58 in DMSO-d$_6$ (deuterated dimethyl sulfoxide)

The ^{13}C NMR spectrum of TU-014 (L-99) **58** (**Figure 43**) has peaks corresponding to the carbon nuclei of the methoxy groups at 57.0 ppm and 57.5 ppm. The remaining peaks between 90 ppm and 170 ppm correspond to the aromatic carbon nuclei and one of them correspond to the carbonyl carbon nucleus of the carboxylic acid group.
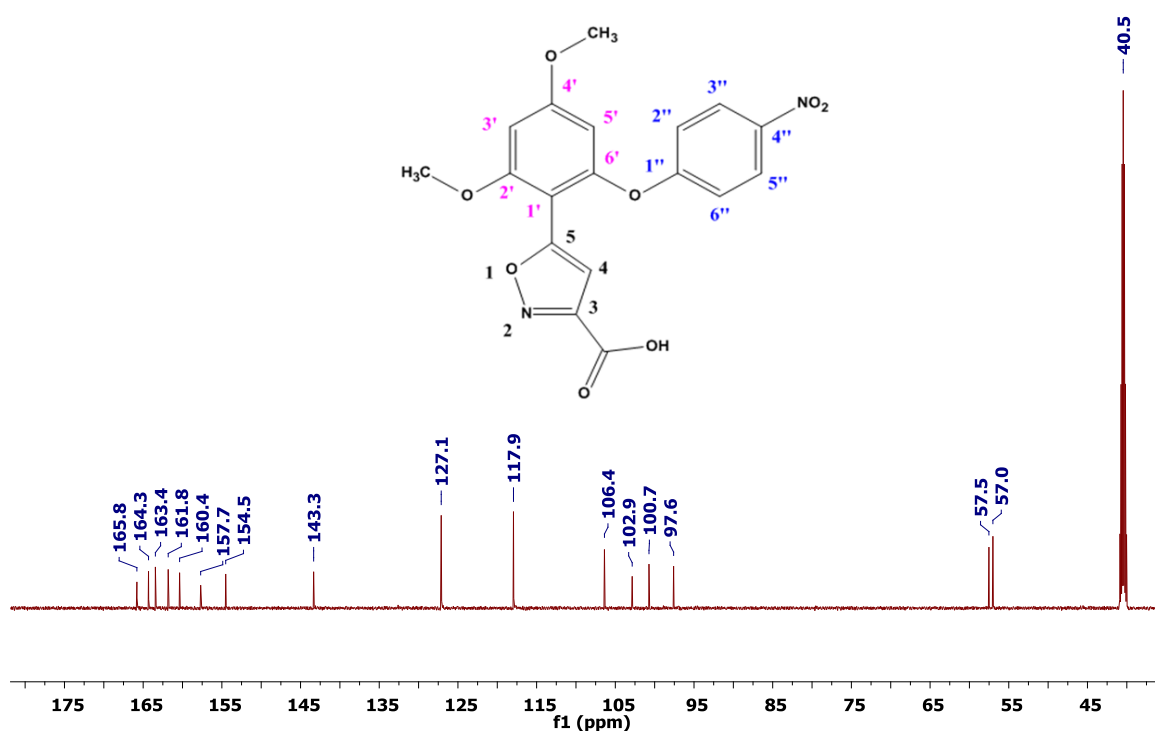
Figure 43: ^{13}C NMR spectrum of TU-014 (L-99) **58** in DMSO-d$_6$

The mass of TU-014 (L-99) **58** was confirmed by HRMS (ESI) analysis. The calculated mass of $[M+H]^+$ is m/z = 387.0828 as compared to the experimentally obtained mass m/z = 387.0820 (**Figure 44**).

Mass	Calc. Mass	mDa	PPM	DBE	Formula	i-FIT	i-FIT Norm	Fit Conf %	C	H	N	O	Si
387.0820	387.0820	0.0	0.0	3.5	C9 H19 N4 O11 Si	180.2	15.382	0.00	9	19	4	11	1
	387.0824	-0.4	-1.0	2.5	C8 H23 N4 O8 Si3	184.6	19.721	0.00	8	23	4	8	3
	387.0814	0.6	1.6	21.5	C22 H11 N6 Si	180.4	15.529	0.00	22	11	6		1
	387.0828	-0.8	-2.1	12.5	C18 H15 N2 O8	166.6	1.704	18.19	18	15	2	8	
	387.0810	1.0	2.6	25.5	C30 H11 O	172.3	7.477	0.06	30	11		1	
	387.0832	-1.2	-3.1	11.5	C17 H19 N2 O5 Si2	183.0	18.103	0.00	17	19	2	5	2
	387.0806	1.4	3.6	-1.5	C8 H23 O15 Si	180.7	15.829	0.00	8	23		15	1
	387.0805	1.5	3.9	15.5	C20 H19 N2 O Si3	184.5	19.636	0.00	20	19	2	1	3
	387.0801	1.9	4.9	16.5	C21 H15 N2 O4 Si	180.1	15.216	0.00	21	15	2	4	1

TU 014
MS_Direct_151105_144 36 (0.169) Cm (31:37)

Figure 44: HRMS (ESI) spectrum of TU-014 (L-99) 58

The preparation of TU-013 (L-98) **57** from TU-014 (L-99) **58** gave us a better yield (67%). It was prepared by reacting TU-014 (L-99) **58** with piperidine in the presence of the coupling agent *N,N,N',N'*-tetramethyl-o-(benzotriazol-1-yl) uronium tetrafluoroborate (TBTU). The reaction was done in *N,N*-dimethylacetamide (DMA) and *N,N*-diisopropylethylamine (DIPEA) was used as the base.
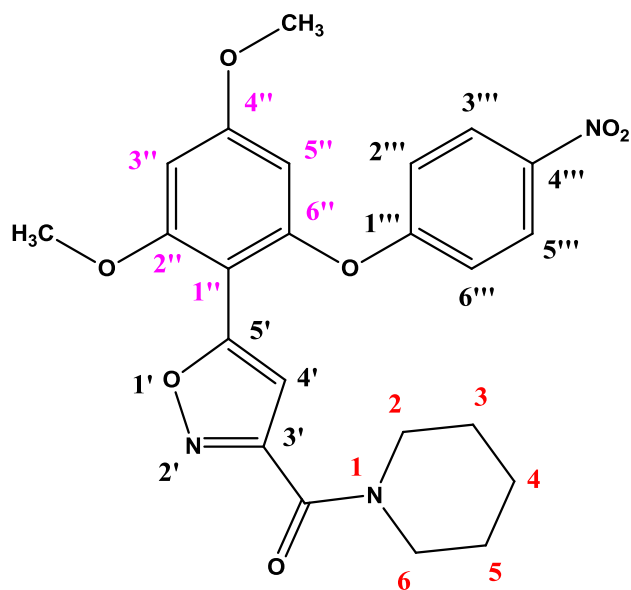
TU-013 **57**

In the ^{1}H NMR spectrum of TU-013 (L-98) **57** (**Figure 45**), the singlets corresponding to the protons of the methoxy groups are at 3.82 ppm and 3.90 ppm. The peaks at 1.55 ppm, 1.65 ppm, 3.61 ppm and 3.68 ppm represent the protons of the piperidine ring. The doublets at 6.28 ppm and 6.47 ppm represent the protons 3''-H and 5''-H of the ring substituted by the methoxy groups. The singlet at 6.72 ppm represent the proton of the isoxazole ring whereas the multiplets at 7.00 ppm and 8.16 ppm represent the protons (2'''-H and 6'''-H, 3'''-H and 5'''-H) of the nitro-substituted ring.

70
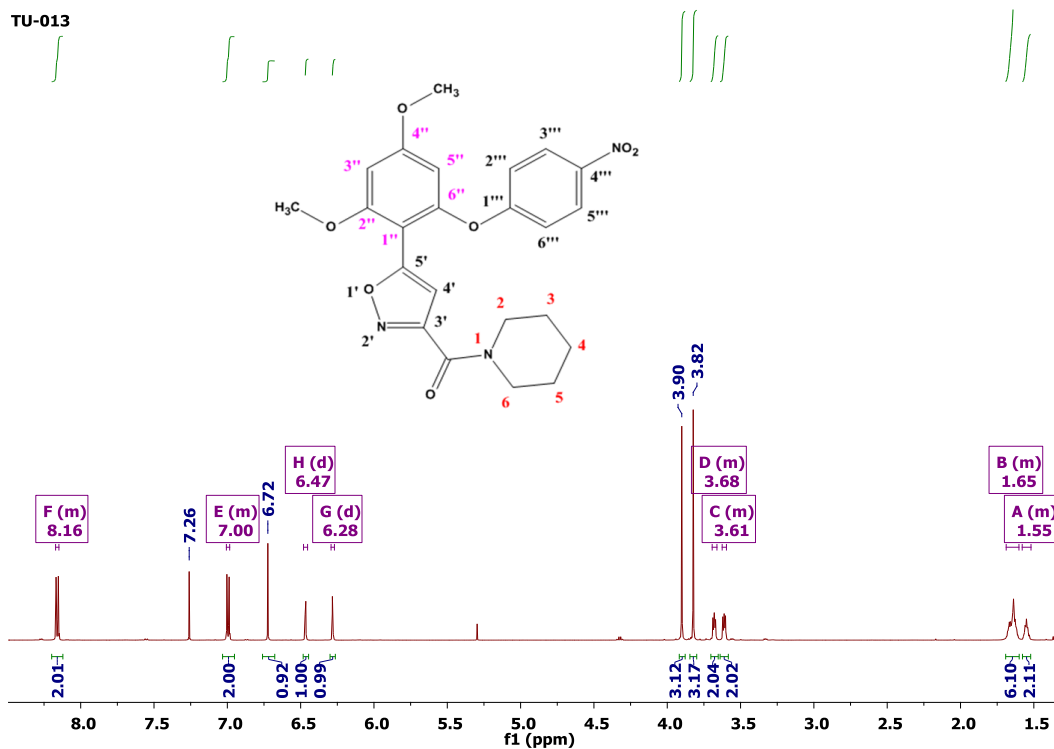
Figure 45: ^{1}H NMR spectrum of TU-013 (L-98) 57

The ^{13}C NMR spectrum of TU-013 (L-98) **57** (**Figure 46**) has the peaks at 24.5 ppm, 25.6 ppm, 26.6 ppm, 43.6 ppm and 48.1 ppm corresponding to the carbon nuclei of the piperidine ring. The peaks at 55.8 ppm and 56.2 ppm represent the carbon nuclei of the methoxy groups and the remaining peaks between 90 ppm and 170 ppm represent the carbon nuclei of the aromatic rings and the carbon nucleus of the amide group.
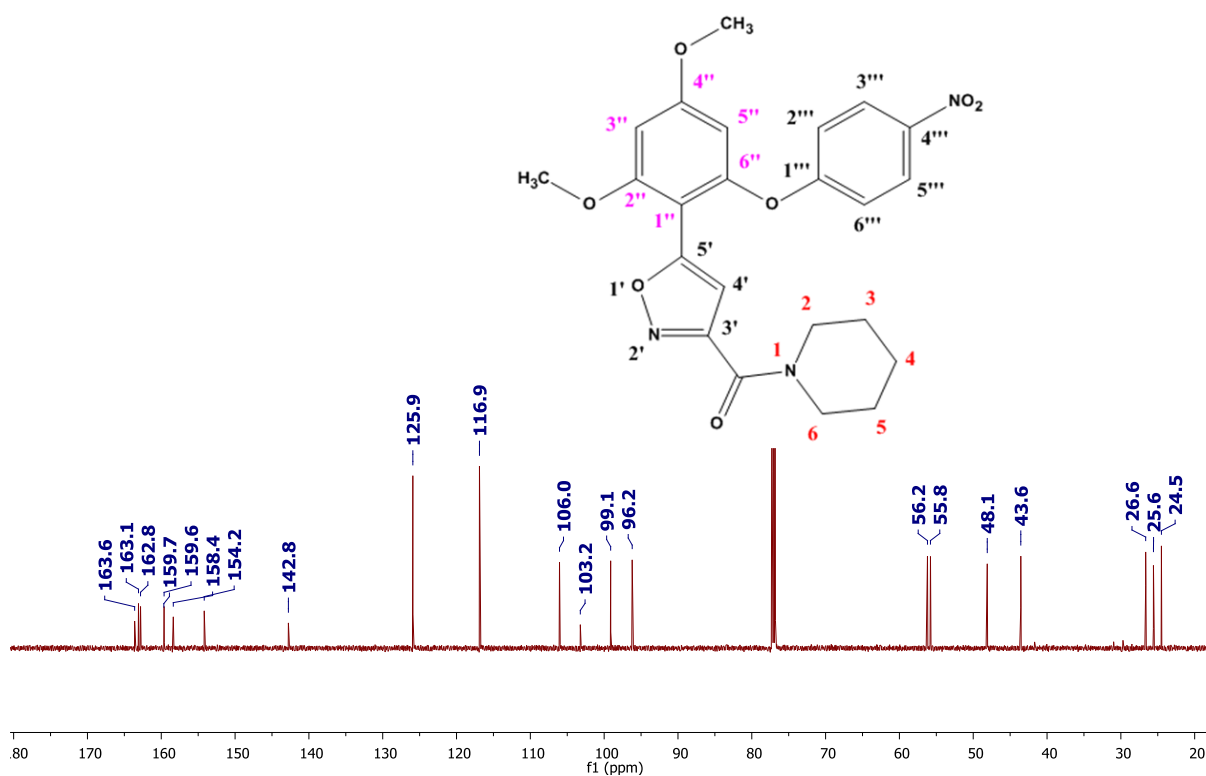
Figure 46: ^{13}C NMR spectrum of TU-013 (L-98) 57

The mass of TU-013 (L-98) **57** was confirmed by HRMS (ESI). The calculated mass of [M+H]$^+$ is m/z = 454.1614) and the experimentally obtained mass is m/z = 454.1624 (**Figure 47**).

Mass	Calc. Mass	mDa	PPM	DBE	Formula	i-FIT	i-FIT Norm	Fit Conf %	C	H	N	O	Si
454.1624	454.1627	-0.3	-0.7	21.5	C31 H24 N O Si	260.3	18.875	0.00	31	24	1	1	1
	454.1628	-0.4	-0.9	18.5	C24 H20 N7 O3	247.3	5.825	0.30	24	20	7	3	
	454.1618	0.6	1.3	12.5	C22 H28 N3 O4 Si2	262.9	21.496	0.00	22	28	3	4	2
	454.1632	-0.8	-1.8	17.5	C23 H24 N7 Si2	263.1	21.657	0.00	23	24	7		2
	454.1633	-0.9	-2.0	0.5	C11 H28 N5 O14	257.3	15.885	0.00	11	28	5	14	
	454.1614	1.0	2.2	13.5	C23 H24 N3 O7	241.9	0.470	62.48	23	24	3	7	
	454.1637	-1.3	-2.9	-0.5	C10 H32 N5 O11 Si2	262.9	21.398	0.00	10	32	5	11	2
	454.1610	1.4	3.1	3.5	C13 H32 N5 O7 Si3	264.6	23.122	0.00	13	32	5	7	3
	454.1605	1.9	4.2	4.5	C14 H28 N5 O10 Si	259.5	18.075	0.00	14	28	5	10	1

Figure 47: HRMS (ESI) spectrum of TU-013 (L-98) 57

TU-015 (L-100) **59**, TU-016 (L-14) **60** and TU-017 (L-102) **61** were all prepared following the same method as the one used to prepare TU-013 (L-98) **57** from TU-014 (L-99) **58** (**Scheme 10, page 76**). The only difference is that for each of these compounds a different amine was used.

73
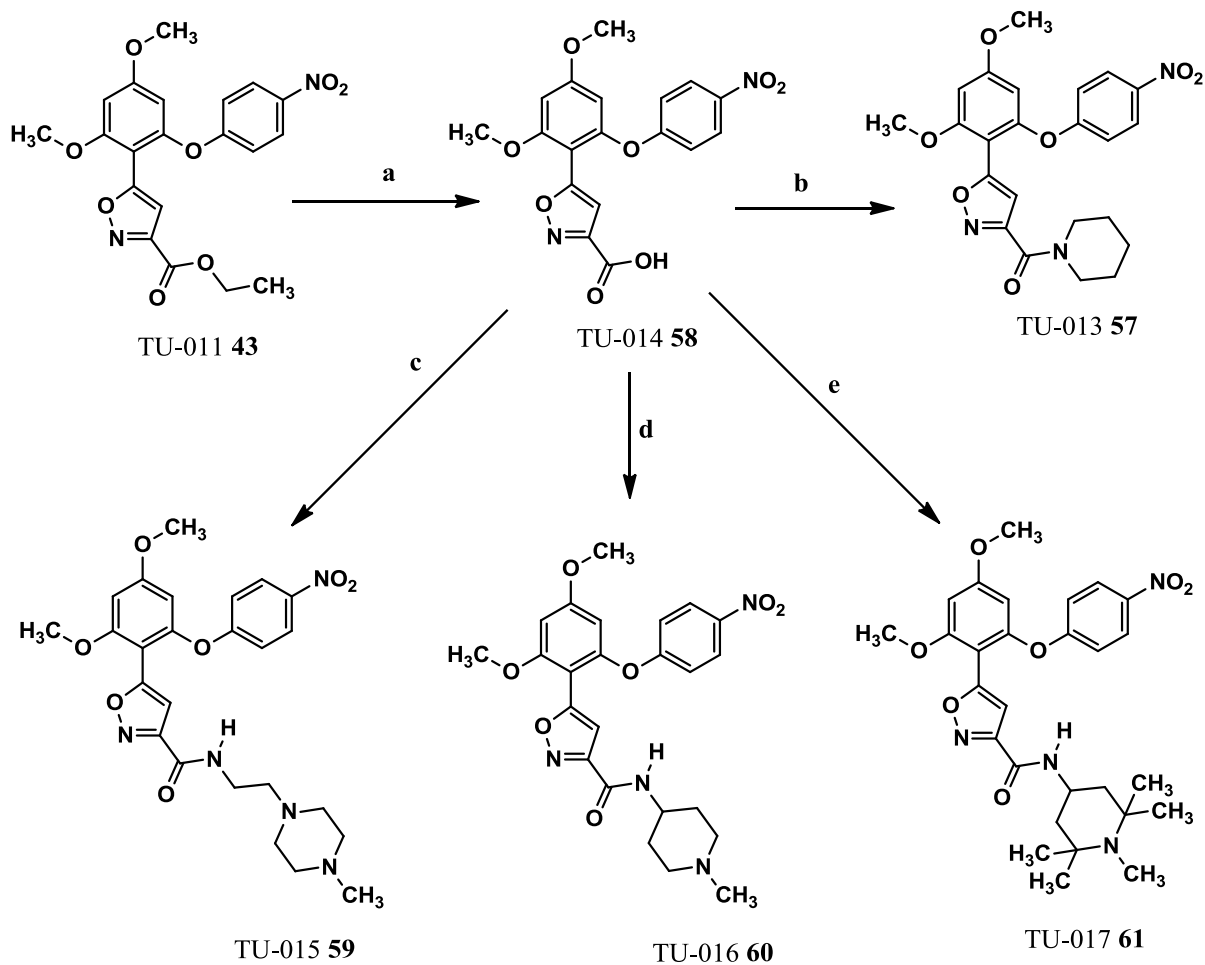
(a) KOH, 80 °C, overnight, 1 M HCl; (b) DMA, TBTU, room temperature, 15 minutes, then DIPEA, piperidine, room temperature, 48 hours; (c) DMA, TBTU, room temperature, 15 minutes, then DIPEA, 2-(4-methylpiperazin-1-yl) ethanamine, room temperature, 48 hours, (d) DMA, TBTU, room temperature, 15 minutes, then DIPEA, 1-methyl-4-piperidinamine , room temperature, 24 hours, (e) DMA, TBTU, room temperature, 15 minutes, then DIPEA, 4-amino-1, 2, 2, 6, 6-pentamethylpiperidine, room temperature, 24 hours

Scheme 10: Synthesis of analogues of NMS-E973 (L-1) **38** with the use of a coupling agent (TBTU)

TU-015 (L-100) **59** was prepared using TU-014 (L-99) **58** and 2-(4-methylpiperazin-1-yl) ethanamine. A yield of 65% for the desired product was obtained.
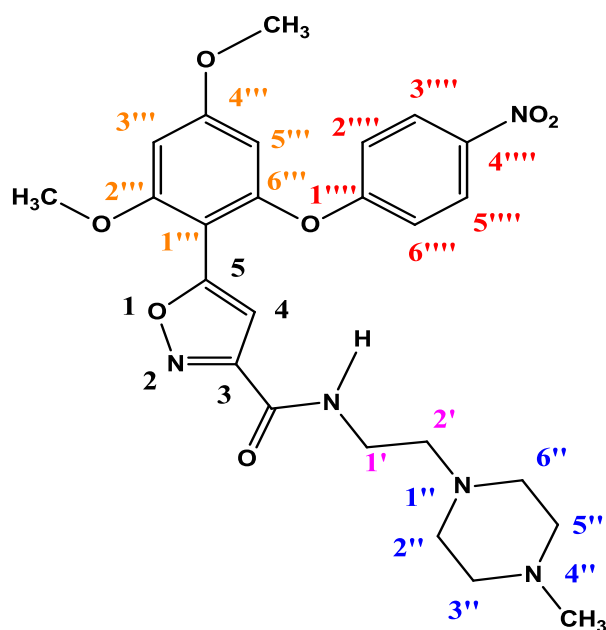
TU-015 **59**

In the ^{1}H NMR spectrum (**Figure 48**) of TU-015 (L-100) **59,** the peak of the protons of the methyl group attached to the piperazine ring is at 2.29 ppm. The peaks of the protons of the piperazine ring are at 2.55 ppm and they partially overlap with a triplet corresponding to the protons of the methylene group attached to the piperazine ring. The peak of the second methylene group (1'-CH$_2$-) is a quartet at 3.50 ppm due to coupling with the protons of the other methylene (2'-CH$_2$-) group and to the proton of the amide group. This is supported by the COSY spectrum (**Figure 50**). The peaks of the protons of the two methoxy groups are at 3.82 ppm and 3.91 ppm. The doublets at 6.27 ppm and 6.47 ppm represent the protons of the aromatic ring substituted by the methoxy groups and the peak at 6.91 ppm represents the proton of the isoxazole ring. The signal of the amide proton is at 7.23 ppm. The doublets at 7.01 ppm and 8.18 ppm represent the protons of the nitro-substituted aromatic ring.
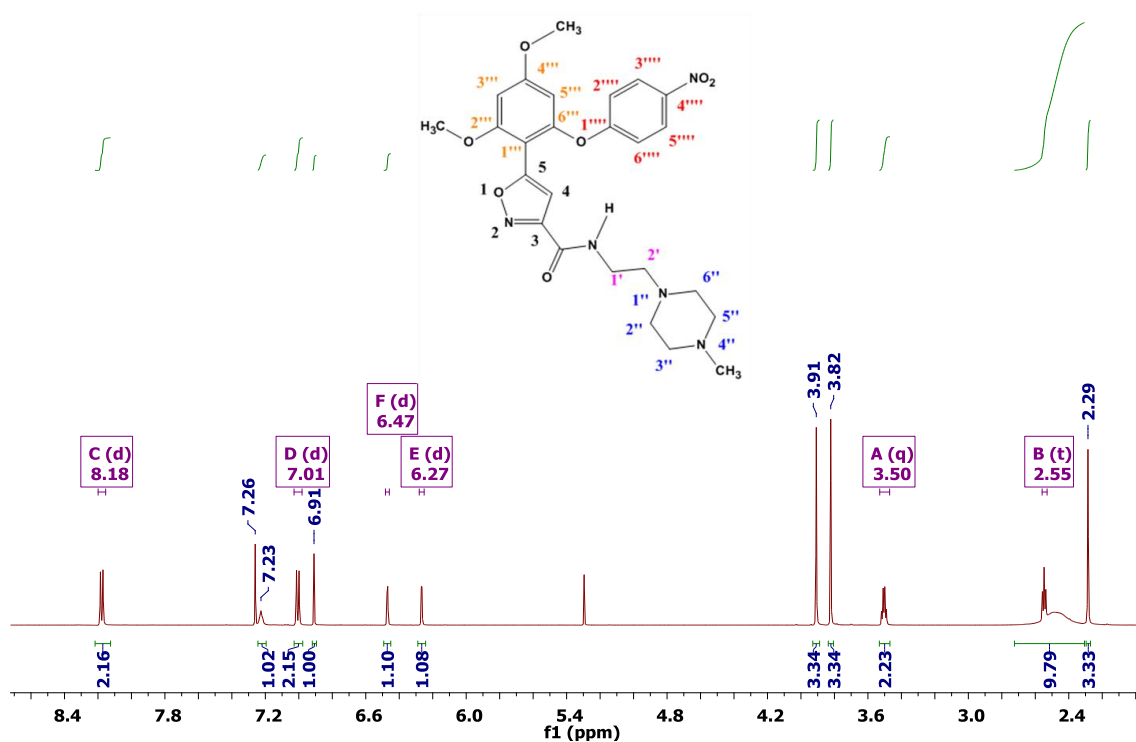
Figure 48: 1H NMR spectrum of TU-015 (L-100) 59

The ^{13}C NMR spectrum (**Figure 49**) of TU-015 (L-100) **59** is complex and peaks cannot easily be assigned without using the HSQC spectrum (**Figure 51**).
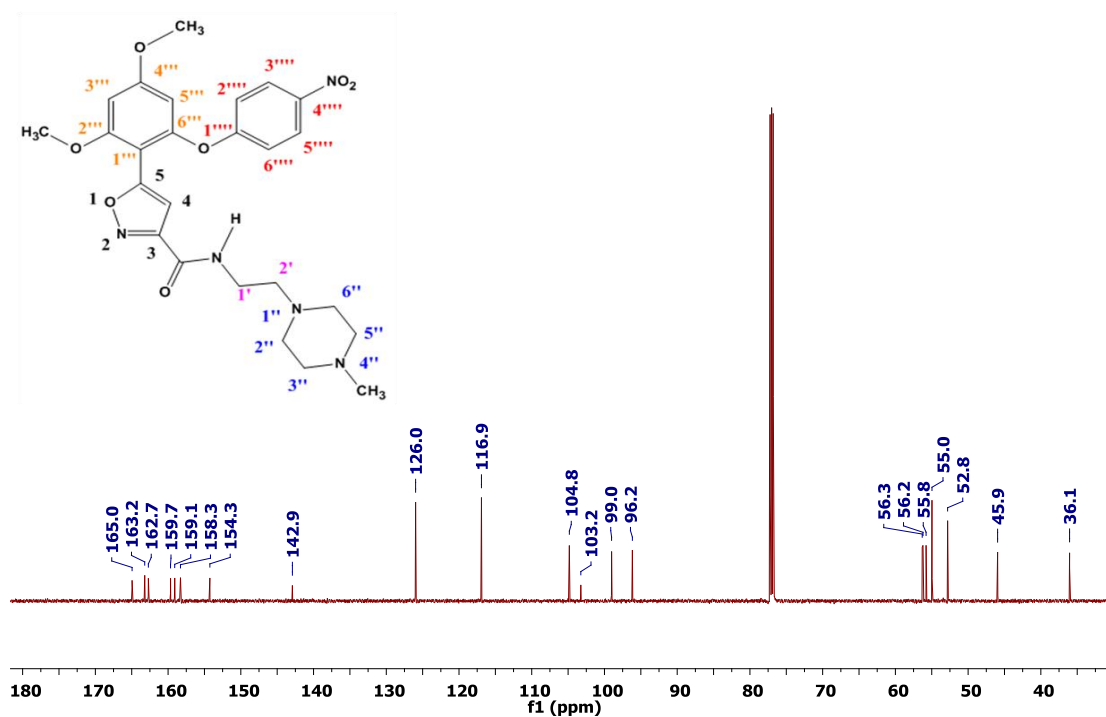
Figure 49: ^{13}C NMR spectrum of TU-015 (L-100) 59
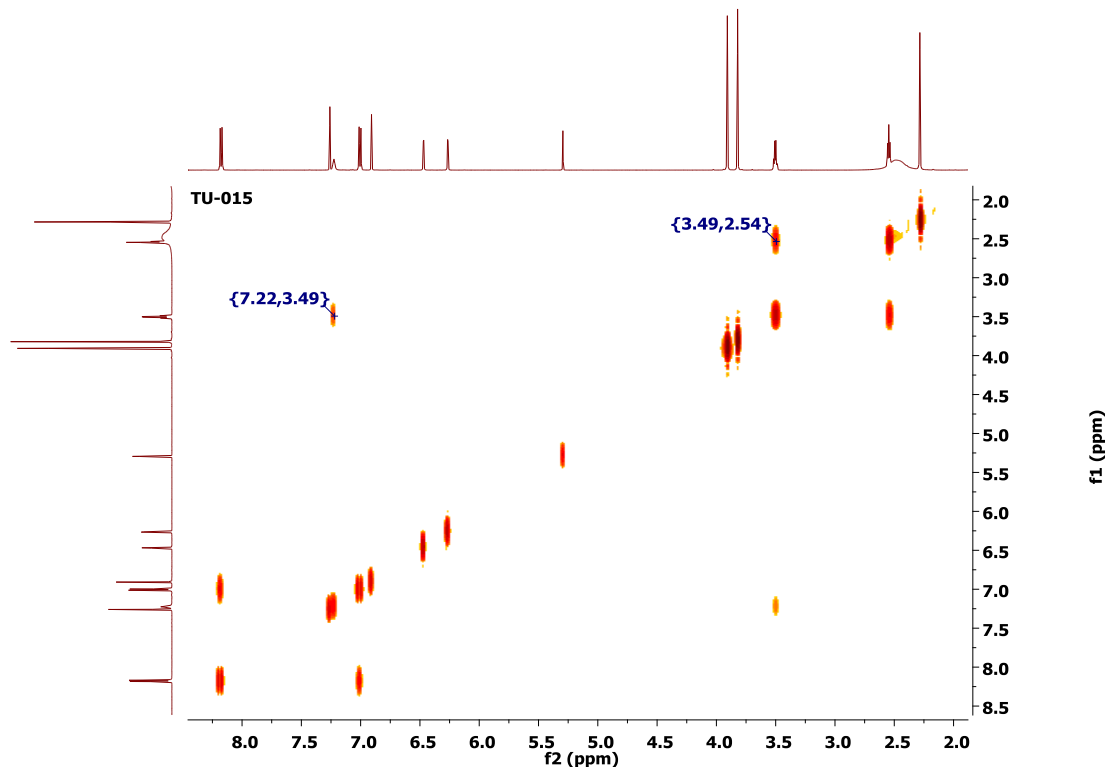
Figure 50: COSY spectrum of TU-015 (L-100) 59

The DEPT-135 spectrum was used on the F1 axis in place of the ^{13}C spectrum (**Figure 49**) on the HSQC spectrum (**Figure 51**) in order to better differentiate between the carbon nuclei of the methoxy groups and those of the methylene group that overlaps with them in the ^{13}C spectrum. The cross peak (2.55 ppm, 56.72 ppm) correlates the protons of the methylene (2'-CH$_2$-) with the carbon nucleus that they are attached to and differentiate it from the carbon nuclei of the methoxy groups with cross-peaks at (3.82 ppm, 56.11 ppm) and (3.91 ppm, 56.56 ppm).
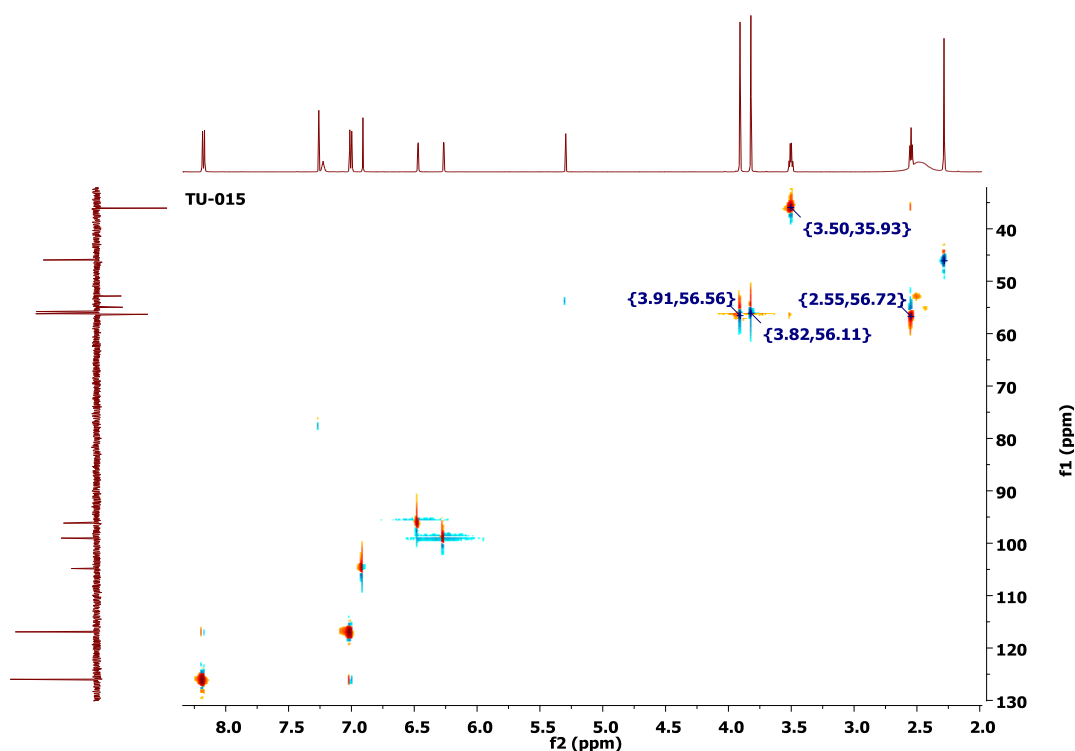
Figure 51: HSQC spectrum of TU-015 (L-100) 59

The results of HRMS (ESI) indicate that the calculated mass of [M+H]$^+$ is m/z = 512.2145 as compared to the experimentally obtained mass m/z = 512.2152 (**Figure 52**).

Mass	Calc. Mass	mDa	PPM	DBE	Formula	i-FIT	i-FIT Norm	Fit Conf %	C	H	N	O	Si
512.2152	512.2149	0.3	0.6	12.5	C24 H34 N5 O4 Si2	282.6	20.263	0.00	24	34	5	4	2
	512.2158	-0.6	-1.2	21.5	C33 H30 N3 O Si	278.7	16.349	0.00	33	30	3	1	1
	512.2145	0.7	1.4	13.5	C25 H30 N5 O7	264.8	2.507	8.16	25	30	5	7	
	512.2163	-1.1	-2.1	3.5	C20 H38 N O12 Si	278.4	16.132	0.00	20	38	1	12	1
	512.2141	1.1	2.1	3.5	C15 H38 N7 O7 Si3	284.6	22.300	0.00	15	38	7	7	3
	512.2164	-1.2	-2.3	0.5	C13 H34 N7 O14	275.0	12.660	0.00	13	34	7	14	
	512.2167	-1.5	-2.9	2.5	C19 H42 N O9 Si3	284.5	22.215	0.00	19	42	1	9	3
	512.2136	1.6	3.1	4.5	C16 H34 N7 O10 Si	278.7	16.431	0.00	16	34	7	10	1
	512.2136	1.6	3.1	7.5	C23 H38 N O8 Si2	282.5	20.202	0.00	23	38	1	8	2

TU 015
MS_Direct_151105_145 36 (0.169) Cm (32:36)

Figure 52: HRMS (ESI) spectrum of TU-015 (L-100) 59

TU-016 **60** was prepared from TU-014 (L-99) **58** and 1-methyl-4-piperidinamine and a yield of 57% was obtained.

79
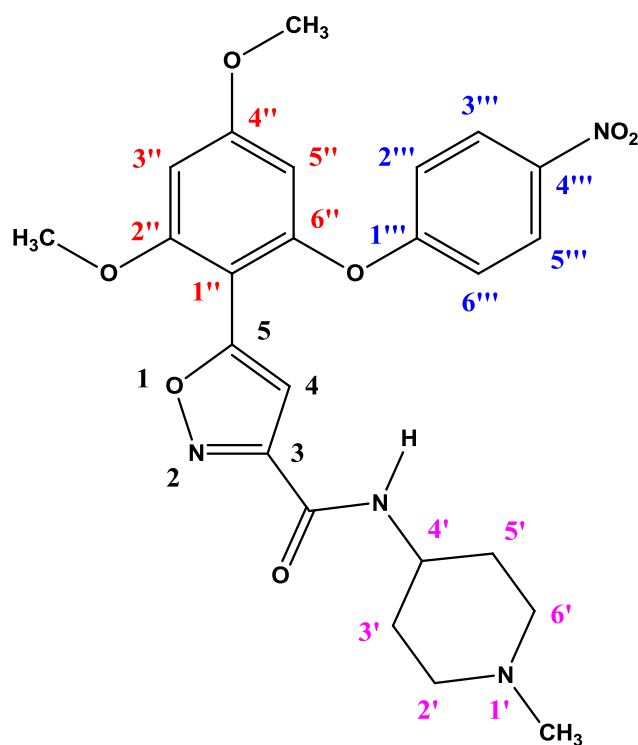
TU-016 **60**

The ^{1}H NMR spectrum of TU-016 **60** (**Figure 53**) has a peak at 2.28 ppm corresponding to the methyl group (1'-CH$_3$) connected to the piperidine ring. The peaks of the methoxy groups are at 3.82 ppm and 3.90 ppm and the peaks of the protons of the piperidine ring are at 1.57 ppm, 1.98 ppm, 2.12 ppm, 2.79 ppm and 3.90 ppm. The peak at 3.90 ppm overlaps with the peak of one of the methoxy groups. The doublets at 6.27 ppm and 6.47 ppm represent the protons of the ring substituted with methoxy groups whereas the doublet at 6.68 ppm represents the amide proton. The singlet at 6.91 ppm represents the proton of the isoxazole ring and the two sets of doublets at 6.99 ppm and 8.17 ppm represent the two sets of equivalent protons of the aromatic ring with the nitro group.
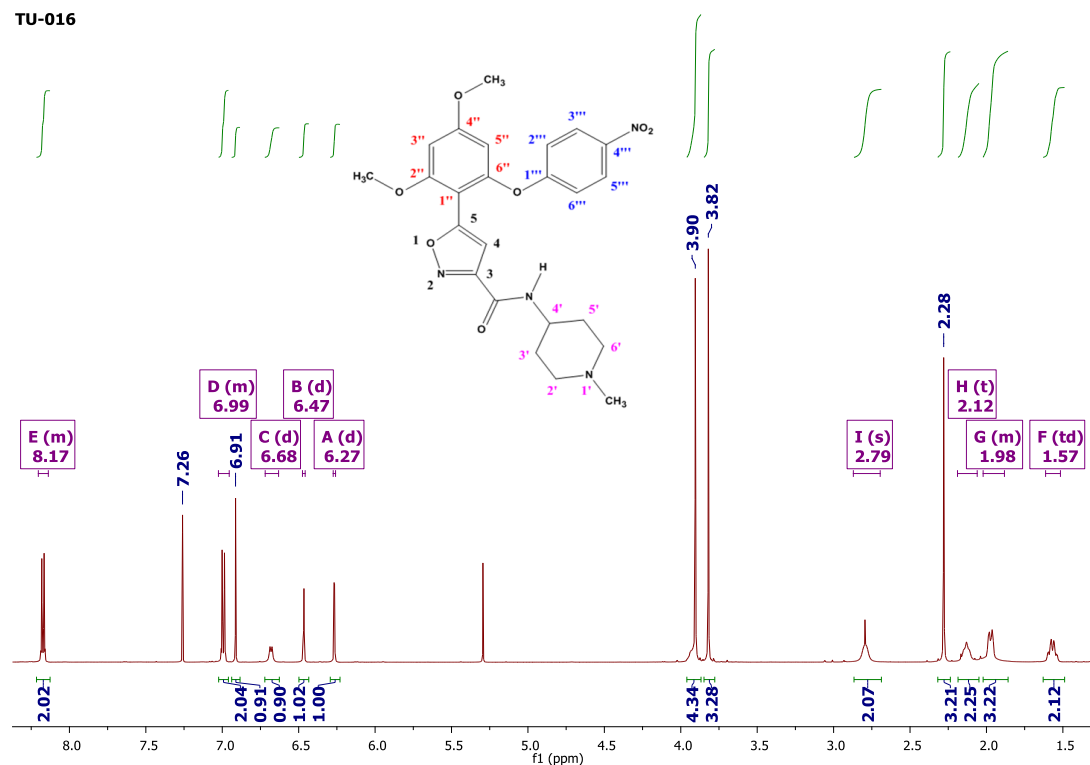
Figure 53: ¹H NMR spectrum of TU-016 (L-14) 60

The peaks of the carbon nuclei of the piperidine ring in the ^{13}C NMR spectrum (**Figure 54**) are at 31.9 ppm, 46.1 ppm and 54.3 ppm whereas those of the methoxy groups are at 55.8 ppm and 56.2 ppm. The peaks of the aromatic and the amide carbon nuclei are in the range of 90 ppm – 170 ppm.
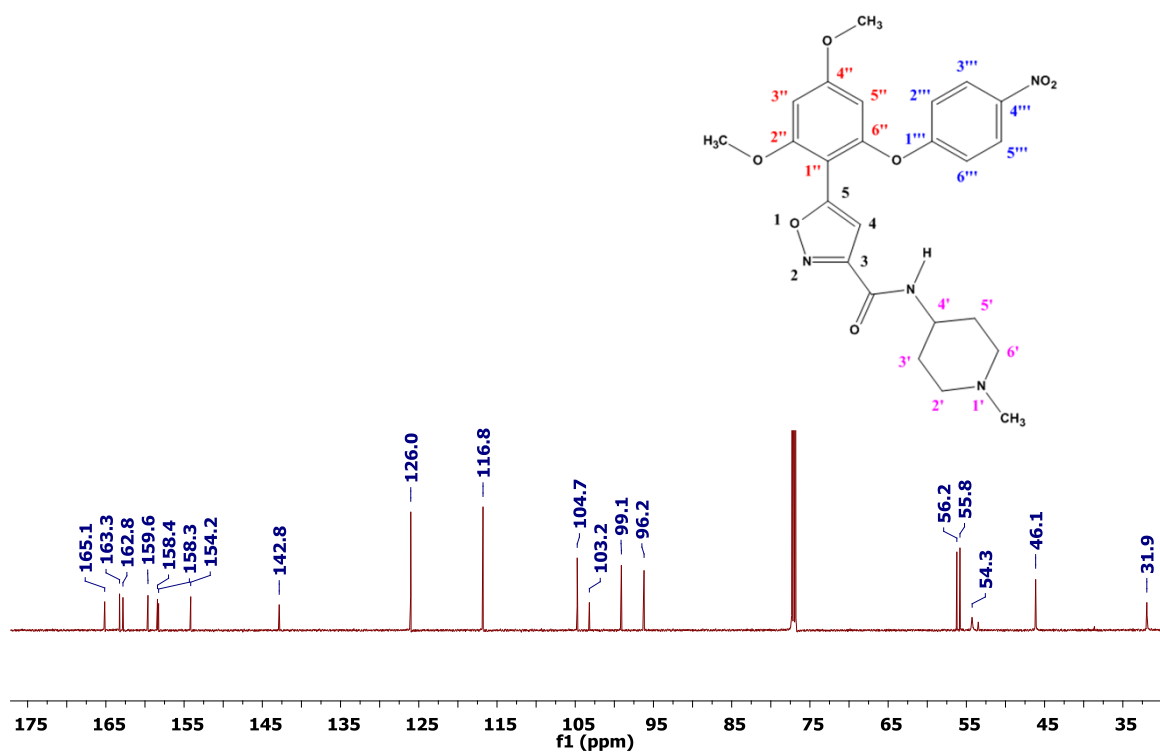
Figure 54: ^{13}C NMR spectrum of TU-016 (L-14) **60**

HRMS (ESI) of TU-016 (L-14) **60** indicates that the calculated mass of $[M+H]^+$ is m/z = 483.1880 as compared to the experimentally obtained mass m/z = 483.1879 (**Figure 55**).

Mass	Calc. Mass	mDa	PPM	DBE	Formula	i-FIT	i-FIT Norm	Fit Conf %	C	H	N	O	Si
483.1879	483.1880	-0.1	-0.2	13.5	C24 H27 N4 O7	247.9	3.905	2.01	24	27	4	7	
	483.1875	0.4	0.8	3.5	C14 H35 N6 O7 Si3	265.8	21.754	0.00	14	35	6	7	3
	483.1884	-0.5	-1.0	12.5	C23 H31 N4 O4 Si2	264.0	19.960	0.00	23	31	4	4	2
	483.1871	0.8	1.7	4.5	C15 H31 N6 O10 Si	259.9	15.908	0.00	15	31	6	10	1
	483.1870	0.9	1.9	7.5	C22 H35 O8 Si2	263.8	19.800	0.00	22	35		8	2
	483.1866	1.3	2.7	8.5	C23 H31 O11	250.5	6.478	0.15	23	31		11	
	483.1893	-1.4	-2.9	21.5	C32 H27 N2 O Si	260.9	16.936	0.00	32	27	2	1	1
	483.1862	1.7	3.5	-1.5	C13 H39 N2 O11 Si3	265.7	21.731	0.00	13	39	2	11	3
	483.1861	1.8	3.7	26.5	C36 H23 N2	255.9	11.865	0.00	36	23	2		

TU 016
MS_Direct_151105_146 39 (0.186) Cm (37:42)

Figure 55: HRMS (ESI) NMR spectrum of TU-016 (L-14) 60

TU-017 (L-102) **61** was prepared from TU-014 (L-99) **58** and 4-amino-1, 2, 2, 6, 6-pentamethylpiperidine with a yield of 57%.
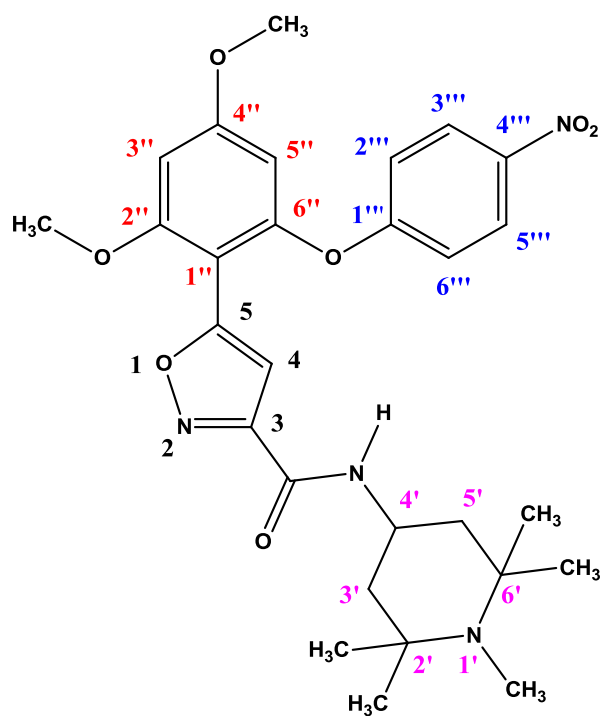
TU-017 **61**

The ^{1}H NMR spectrum of TU-017 (L-102) **61** (**Figure 56**) has a singlet at 2.27 ppm that represents the protons of the methyl group (1'-CH$_3$) connected to the nitrogen atom of the piperidine ring. The multiplet at 1.14 ppm with an integral of 12 protons represents the remaining four methyl (2'-(CH$_3$)$_2$ and 6'-(CH$_3$)$_2$) substituents of the piperidine ring.
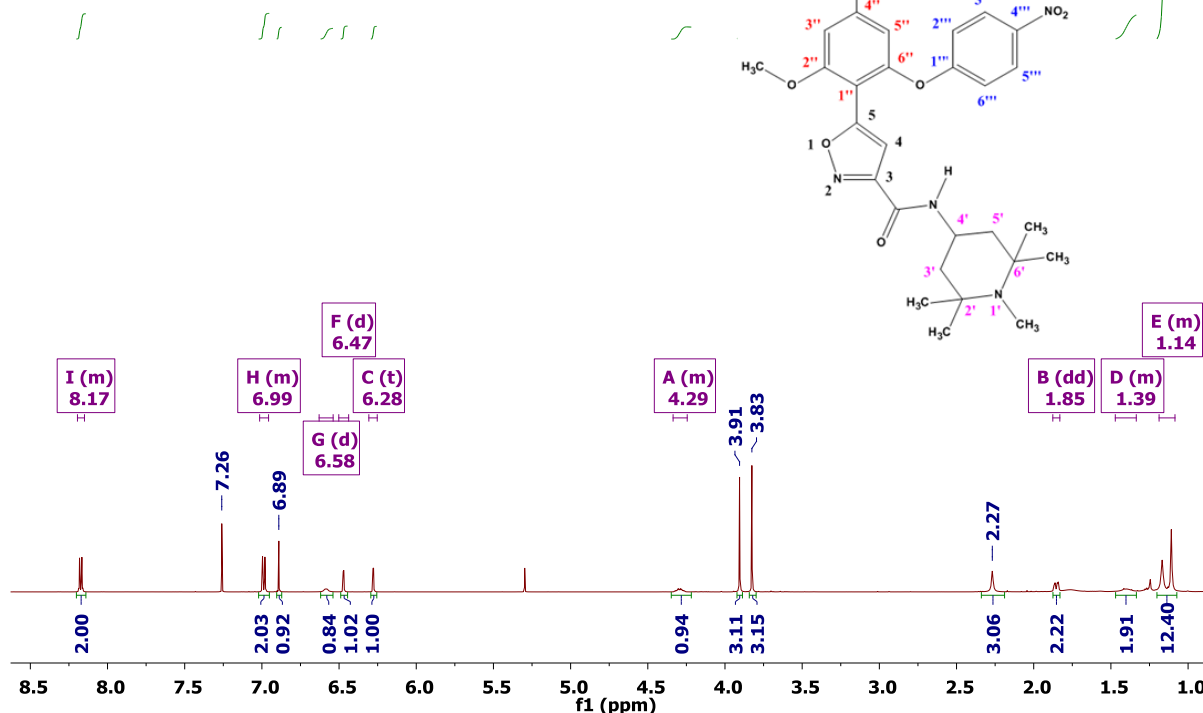
Figure 56: ¹H NMR spectrum of TU-017 (L-102) 61

The multiplets at 1.39 ppm, 1.85 ppm and 4.29 ppm represent the protons of the piperidine ring. The singlets at 3.83 ppm and 3.91 ppm represent the protons of the methoxy groups. The signals of the protons attached to the same aromatic ring as the methoxy groups are doublets at 6.28 ppm and 6.47 ppm. The doublet at 6.58 ppm represents the proton (CONH) of the amide group. It is coupled to the neighbouring proton (4'-H) of the piperidine ring. The singlet at 6.89 ppm corresponds to the proton of the isoxazole ring whereas the multiplets at 6.99 ppm and 8.17 ppm represent the protons of the aromatic ring with the nitro substituent.

The interpretation of the ¹³C NMR of TU-017 (L-102) **61** (**Figure 57**) is complicated by the low intensity of the signals of the carbon nuclei of the piperidine ring. The signals of the carbon nuclei of methoxy groups at 55.8 ppm and 56.2 ppm have clear cross peaks with their corresponding protons on the HSQC (**Figure 58**). The peak at 55.2 ppm which represents the tetra-substituted carbon nuclei of the piperidine ring is practically invisible in the ¹³C NMR. Their presence was confirmed by cross peaks between the proton signals of the protons of the methyl group (1'-CH₃) attached to the nitrogen atom of the piperidine ring and the

overlapping signals of the carbon nuclei of the piperidine ring on the HMBC spectrum (**Figure 59**).
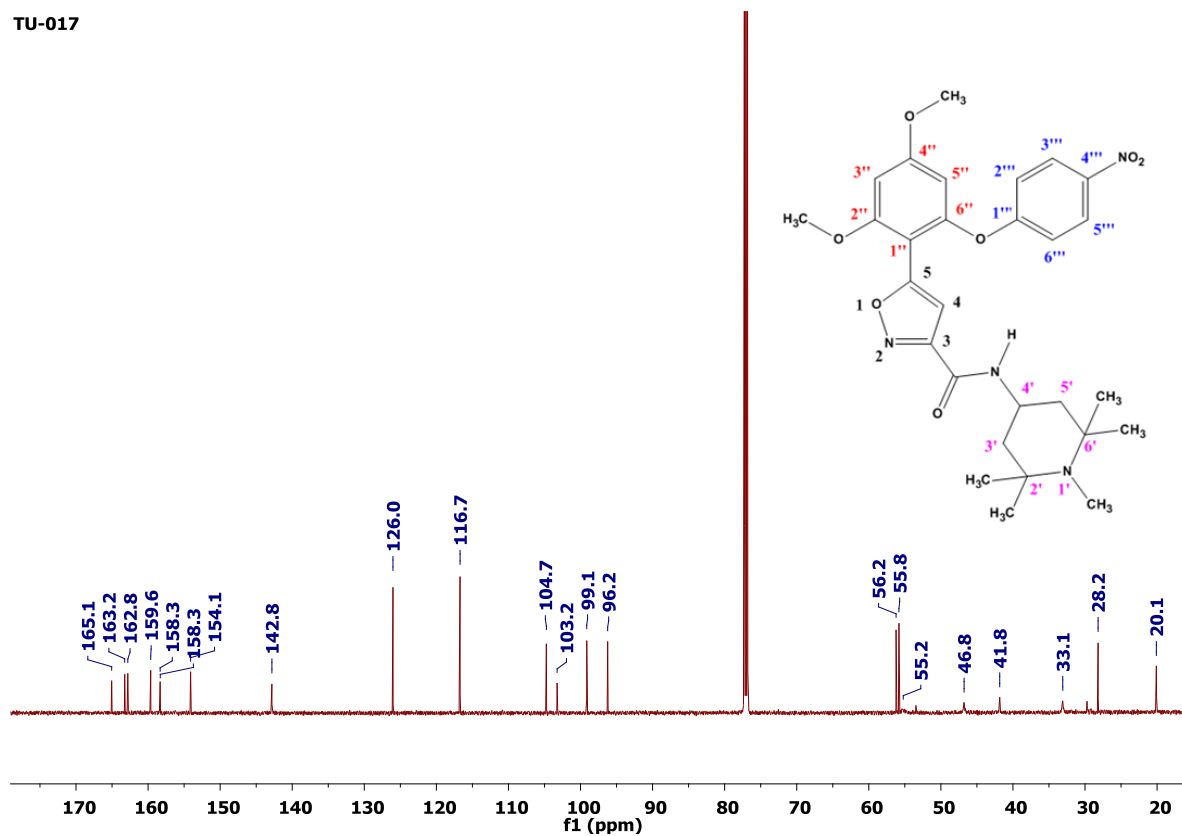
Figure 57: ^{13}C NMR spectrum of TU-017 (L-102) 61
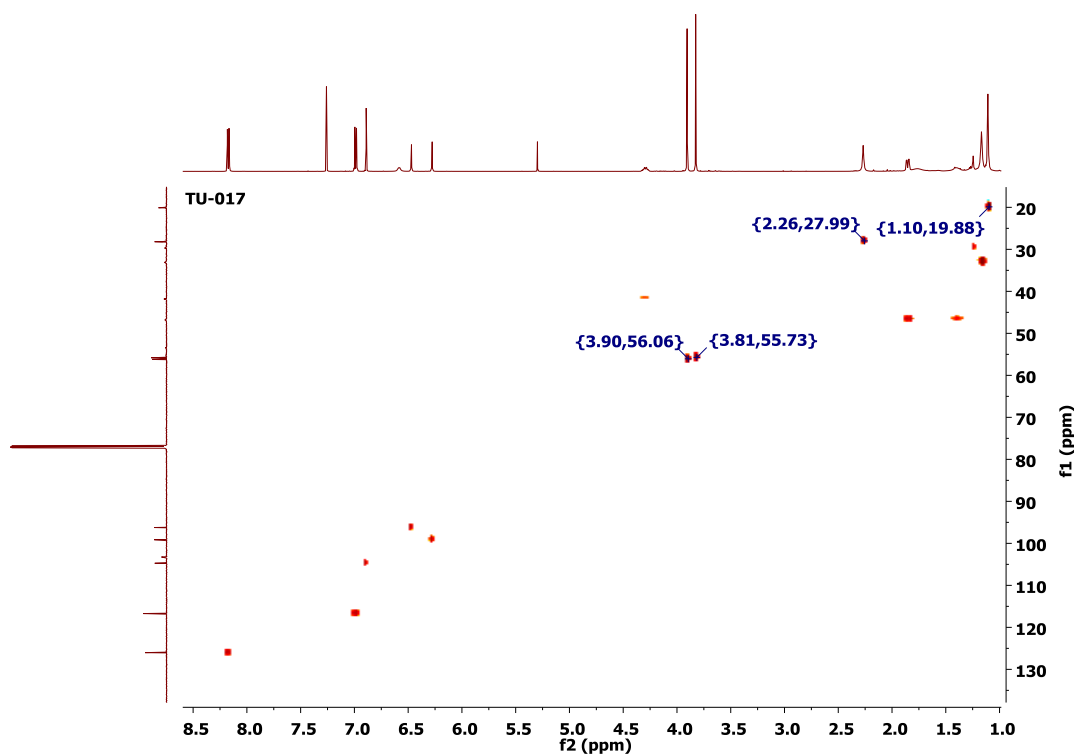
Figure 58: HSQC spectrum of TU-017 (L-102) 61
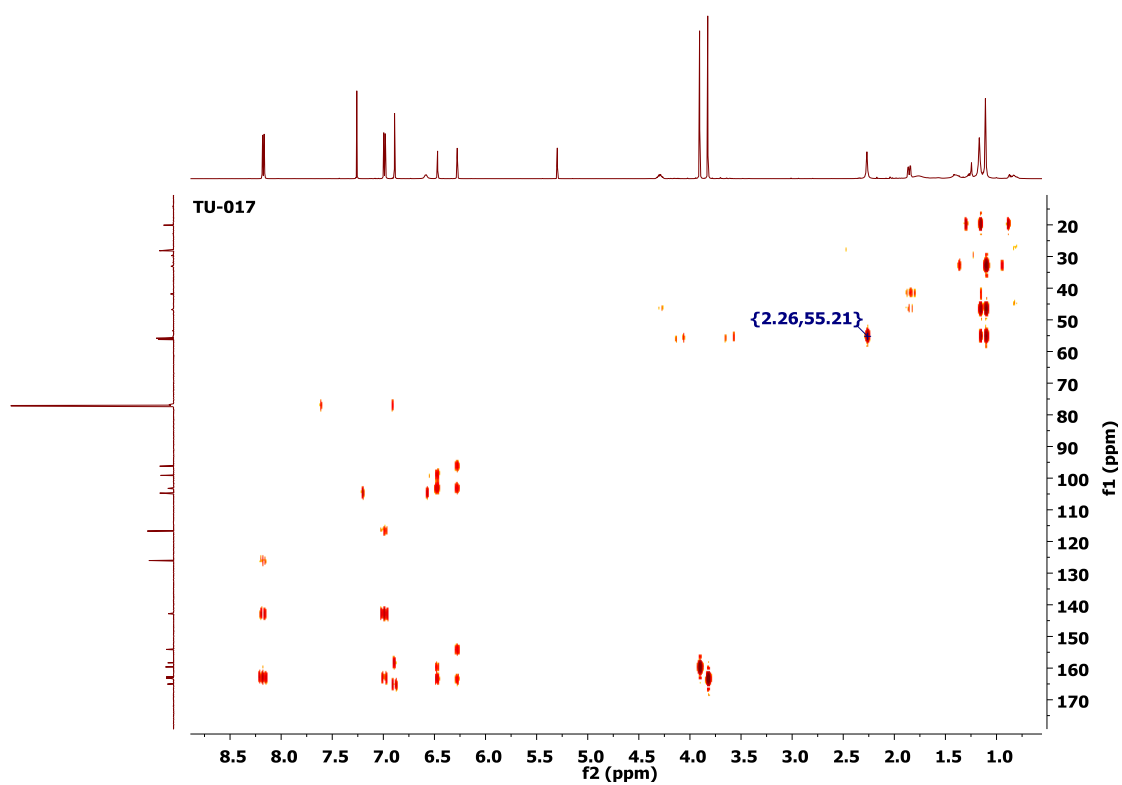
Figure 59: HMBC spectrum of TU-017 (L-102) 61

HRMS (ESI) analysis of TU-017 (L-102) **61** indicates that the calculated mass of [M+H]$^+$ is m/z = 539.2506 as compared to the experimentally obtained mass m/z =539.2520 (**Figure 60**).

Mass	Calc. Mass	mDa	PPM	DBE	Formula	i-FIT	i-FIT Norm	Fit Conf %	C	H	N	O	Si	
539.2520	539.2519	0.1	0.2	21.5	C36 H35 N2 O Si	416.8	19.095	0.00	36	35	2	1	1	
	539.2524	-0.4	-0.7	0.5	C16 H39 N6 O14	413.8	16.061	0.00	16	39	6	14		
	539.2524	-0.4	-0.7	3.5	C23 H43 O12 Si	416.1	18.326	0.00	23	43		12	1	
	539.2528	-0.8	-1.5	2.5	C22 H47 O9 Si3	422.0	24.316	0.00	22	47		9	3	
	539.2528	-0.8	-1.5	-0.5	C15 H43 N6 O11 Si2	420.1	22.328	0.00	15	43	6	11	2	
	539.2510	1.0	1.9	12.5	C27 H39 N4 O4 Si2	420.1	22.361	0.00	27	39	4	4	2	
	539.2506	1.4	2.6	13.5	C28 H35 N4 O7	404.3	6.598	0.14	28	35	4	7		
	539.2537	-1.7	-3.2	8.5	C24 H39 N4 O8 Si	415.6	17.886	0.00	24	39	4	8	1	
	539.2501	1.9	3.5	3.5	C18 H43 N6 O7 Si3	422.1	24.327	0.00	18	43	6	7	3	

TU 017
MS_Direct_151105_147 44 (0.205) Cm (44:51)

Figure 60: HRMS (ESI) spectrum of TU-017 (L-102) 61

TU-018 (L-103) **50** was prepared by Boc-deprotection of TU-012 (L-97) **49** with HCl in dioxane (**Scheme 4**) with a yield of 89%.

88
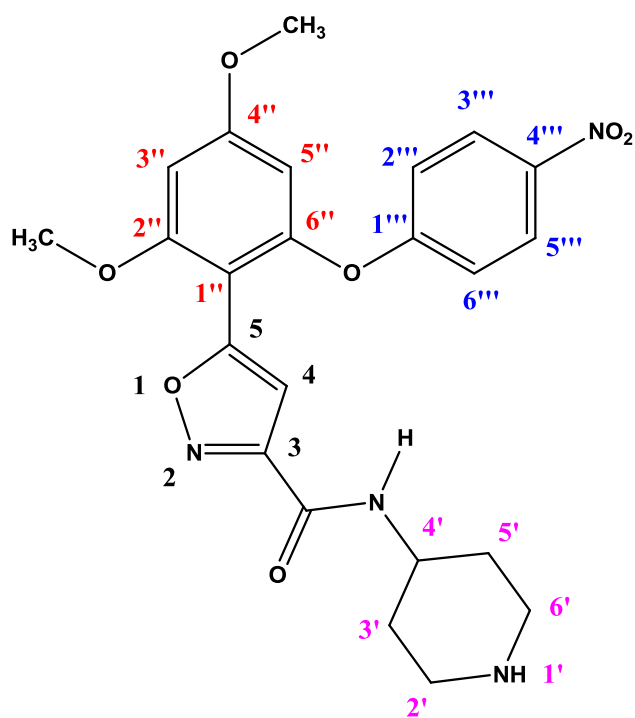
TU-018 **50**

The ^{1}H NMR spectrum of TU-018 (L-103) **50** (**Figure 61**) has peaks representing the protons of the piepridine ring at 1.40 ppm, 1.98 ppm, 2.71 ppm, 3.08 ppm and 4.02 ppm. The peaks at 3.82 ppm and 3.91 ppm represent the protons of the methoxy groups. The peaks of the aromatic protons of the ring substituted by the methoxy groups are doublets at 6.27 ppm and 6.47 ppm and the peak of the amide proton is a doublet at 6.70 ppm because it couples the neighbouring proton of the piperidine ring. The singlet at 6.92 ppm represents the proton of the isoxazole ring and the multiplets at 6.99 ppm and 8.17 ppm represent the protons of the nitro-substituted aromatic ring.
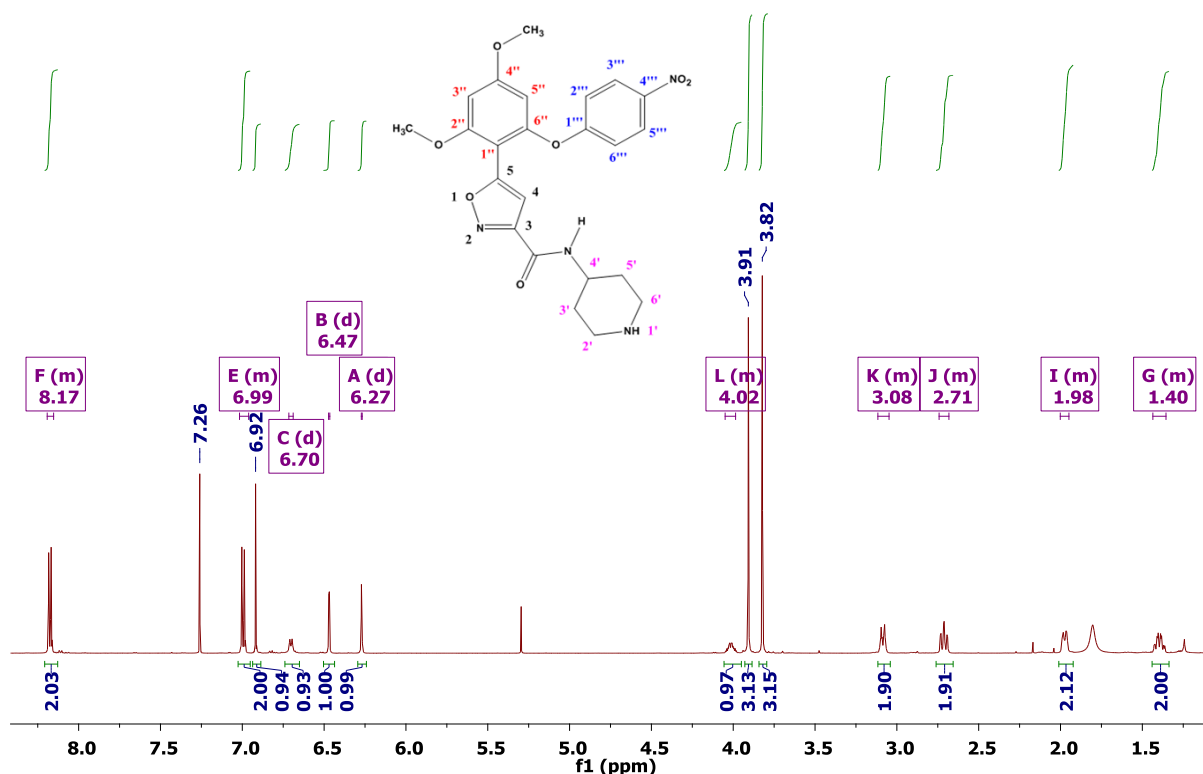
Figure 61: 1H NMR spectrum of TU-018 (L-103) 50

The ^{13}C NMR spectrum of TU-018 (L-103) **50** (**Figure 62**) has the peaks representing the carbon nuclei of the methoxy groups at 55.8 ppm and 56.2 ppm. The peaks at 33.2 ppm, 45.3 ppm and 47.0 ppm represent the carbon nuclei of the piperidine ring. The peak of the carbon nucelus of the amide functional group is identified by analysis of the HMBC spectrum (**Figure 63**). In the HMCB spectrum, a cross-peak (6.70 ppm, 158.20 ppm) is observed between the signal of the amide proton and the nucleus of the carbonyl carbon. Another cross peak (6.92 ppm, 158.27 ppm) shows the coupling of the proton of the isoxazole ring with one of the neighbouring carbon nuclei (3-C). The rest of the peaks between 90 ppm and 170 ppm represent the carbon nuclei of the different aromatic rings(including the isoxazole).
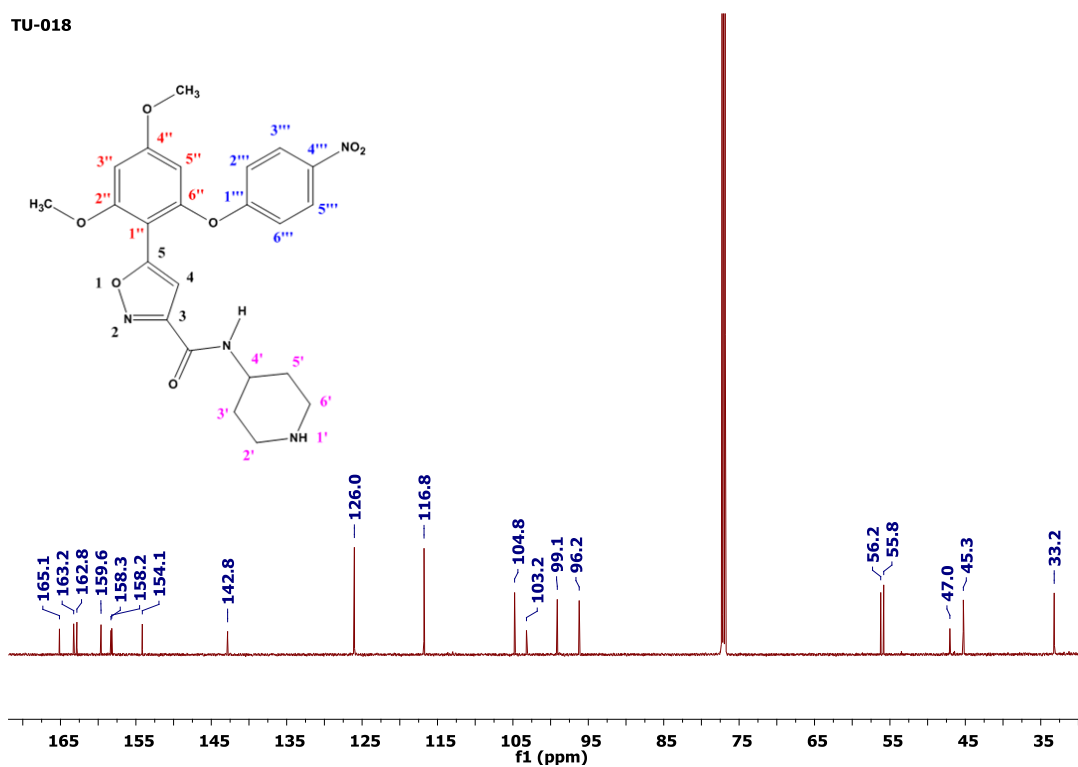
Figure 62: ^{13}C NMR spectrum of TU-018 (L-103) 50
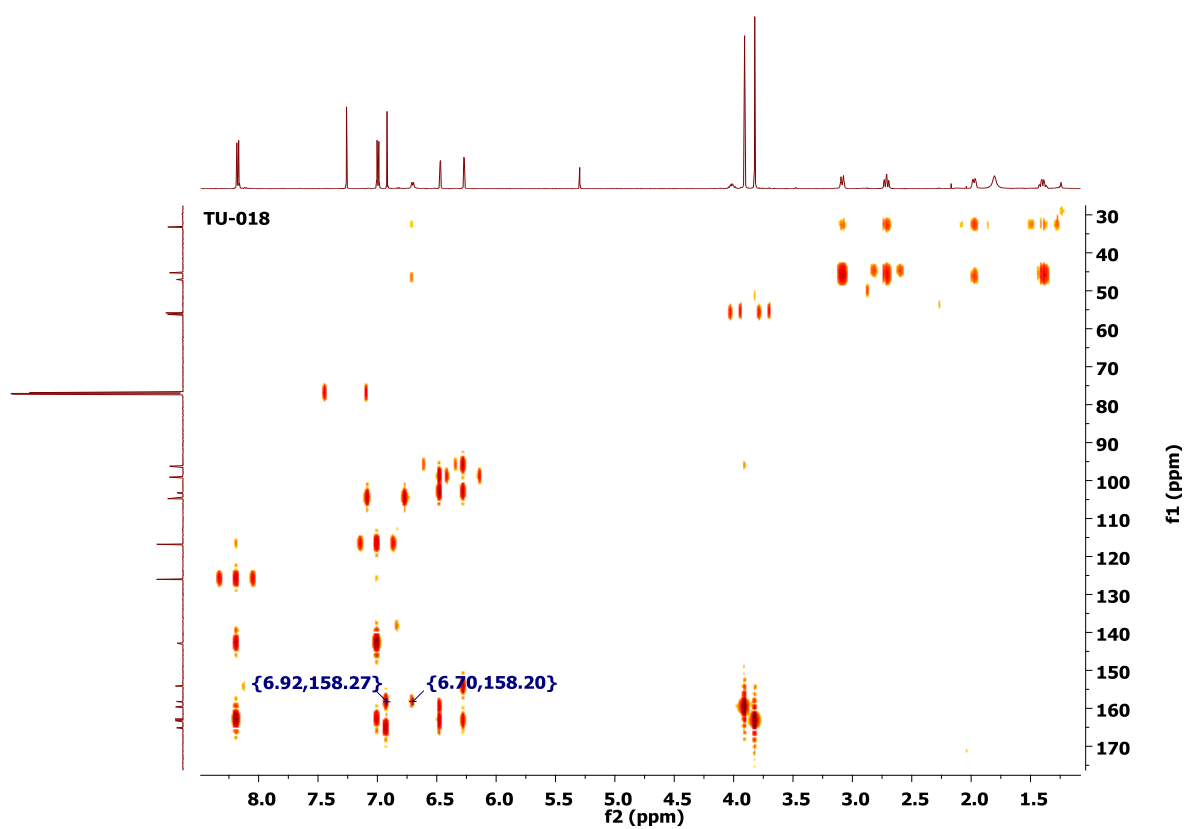
Figure 63: HMBC spectrum of TU-018 (L-103) 50

HRMS (ESI) analysis of TU-018 (L-103) **50** indicates that the calculated mass of [M+H]$^+$ m/z = 469.1723 as compared to the experimentally obtained mass m/z = 469.1732 (**Figure 64**).

Mass	Calc. Mass	mDa	PPM	DBE	Formula	i-FIT	i-FIT Norm	Fit Conf %	C	H	N	O	Si
469.1732	469.1736	-0.4	-0.9	21.5	C31 H25 N2 O Si	218.6	15.681	0.00	31	25	2	1	1
	469.1727	0.5	1.1	12.5	C22 H29 N4 O4 Si2	223.4	20.504	0.00	22	29	4	4	2
	469.1741	-0.9	-1.9	3.5	C18 H33 O12 Si	219.1	16.192	0.00	18	33		12	1
	469.1723	0.9	1.9	13.5	C23 H25 N4 O7	202.9	0.035	96.53	23	25	4	7	
	469.1742	-1.0	-2.1	0.5	C11 H29 N6 O14	216.2	13.312	0.00	11	29	6	14	
	469.1745	-1.3	-2.8	2.5	C17 H37 O9 Si3	225.3	22.443	0.00	17	37		9	3
	469.1719	1.3	2.8	3.5	C13 H33 N6 O7 Si3	225.5	22.612	0.00	13	33	6	7	3
	469.1746	-1.4	-3.0	-0.5	C10 H33 N6 O11 Si2	223.6	20.704	0.00	10	33	6	11	2
	469.1714	1.8	3.8	7.5	C21 H33 O8 Si2	223.2	20.308	0.00	21	33		8	2

Figure 64: HRMS (ESI) spectrum of TU-018 (L-103) 50

TU-019 (L-104) **51** was prepared with a 5% yield by reductive amination of TU-018 (L-103) **50** with acetone in the presence of sodium triacetoxyborohydride. The reaction was not optimized due to time constraints.
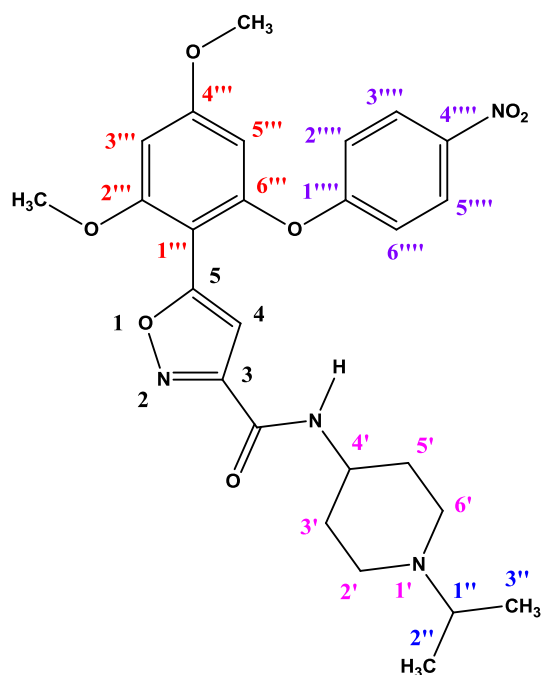
TU-019 **51**

The peaks of the protons of the methoxy groups of TU-019 (L-104) **51** are at 3.82 ppm and 3.90 ppm and the protons of the two equivalent methyl groups of the isopropyl substituent of the piperidine ring are represented by a doublet at 1.27 ppm because they couple with the neighbouring proton (1''-H). The signal of proton 1''-H is distinguished from the signal of proton 4'-H by the relevant cross peaks on the COSY spectrum (**Figure 66**). The signal of proton 4'-H at 4.08 ppm has a cross peak with the signal of the amide proton (CONH) and the signal of proton 1''-H at 3.24 ppm has a cross peak with the signal of the methyl groups of the isopropyl substituent. The peaks at 2.12 ppm, 2.67 ppm and 3.24 ppm also represent the protons of the piperidine ring.

93
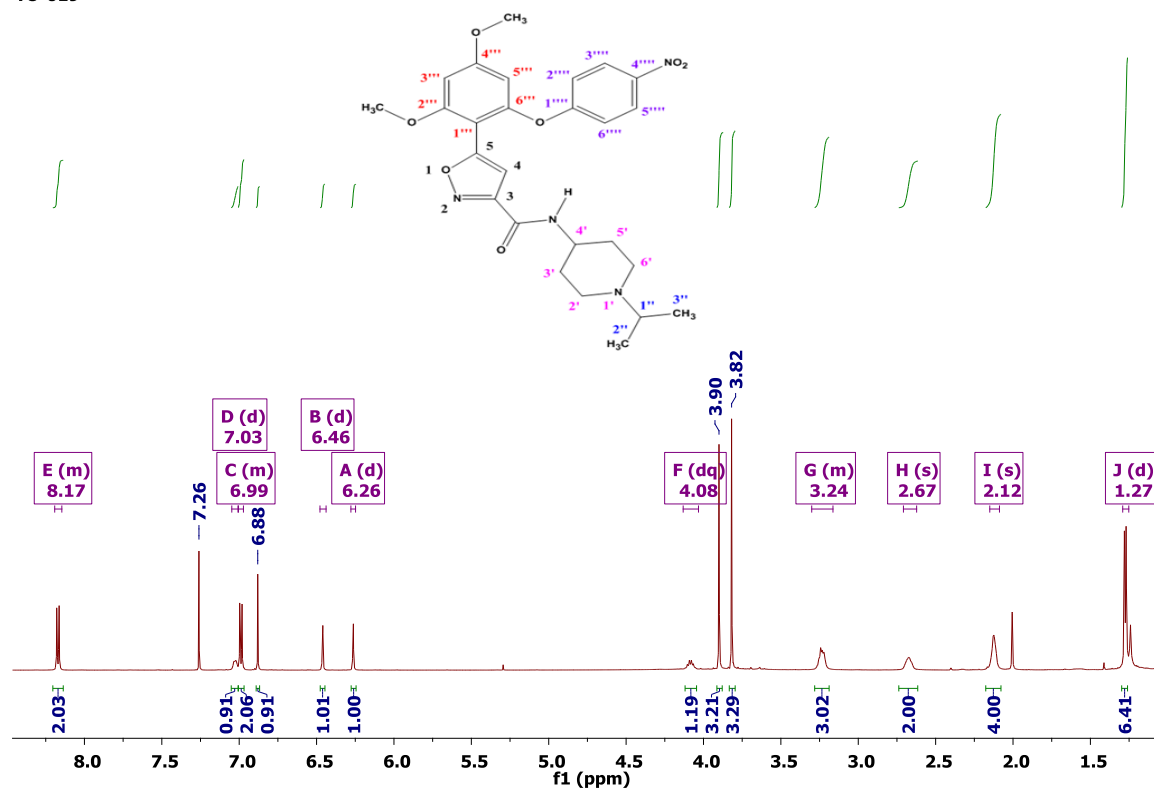
Figure 65: 1H NMR spectrum of TU-019 (L-104) 51
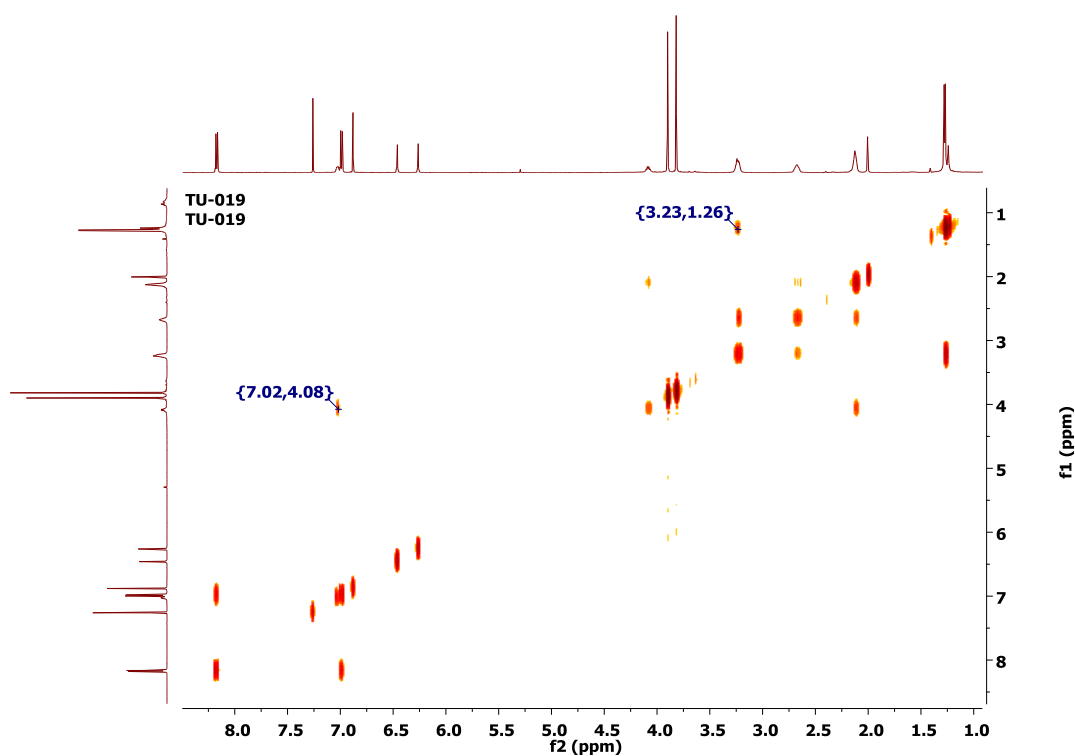
Figure 66: COSY spectrum of TU-019 (L-104) 51

The doublets at 6.26 ppm and 6.46 ppm represent the protons of the methoxy substituted aromatic ring and the doublet at 7.03 ppm represents the proton of the amide group coupled with H-4' of the piperidine ring. The singlet at 6.88 ppm represents the proton of the isoxazole ring. The doublets at 6.99 ppm and 8.17 ppm represent the two sets of equivalent protons of the aromatic ring with the nitro substituent.
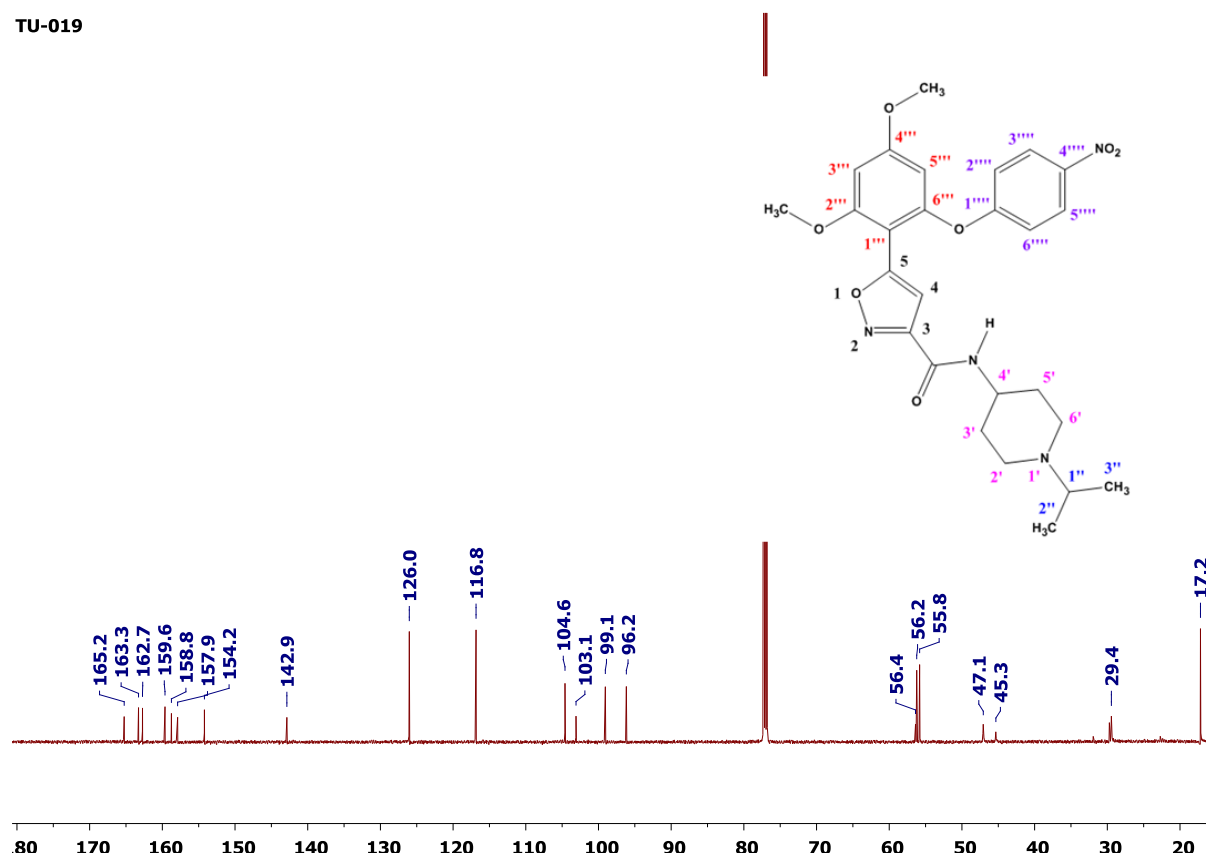
Figure 67: ^{13}C NMR spectrum of TU-019 (L-104) 51

The ^{13}C NMR spectrum of TU-019 (L-104) **51** (**Figure 66**) has the peaks representing the carbon nuclei of the methoxy groups at 55.8 ppm and 56.2 ppm. The peaks at 17.2 ppm and 56.4 ppm represent the carbon nuclei of the methyl groups (2''-C and 3''-C) and the tri-substituted carbon nucleus (1''-C) of the isopropyl substituent respectively. The signals of the aromatic ring carbon nuclei and the carbonyl carbon nucleus (158.8 ppm) are in the interval spanning 90 ppm to 170 ppm.

95

The HRMS (ESI) analysis of TU-019 (L-104) **51** indicates that the calculated mass of $[M+H]^+$ (m/z = 511.2193) is similar to the experimentally obtained mass (m/z = 511.2191) (**Figure 68**).

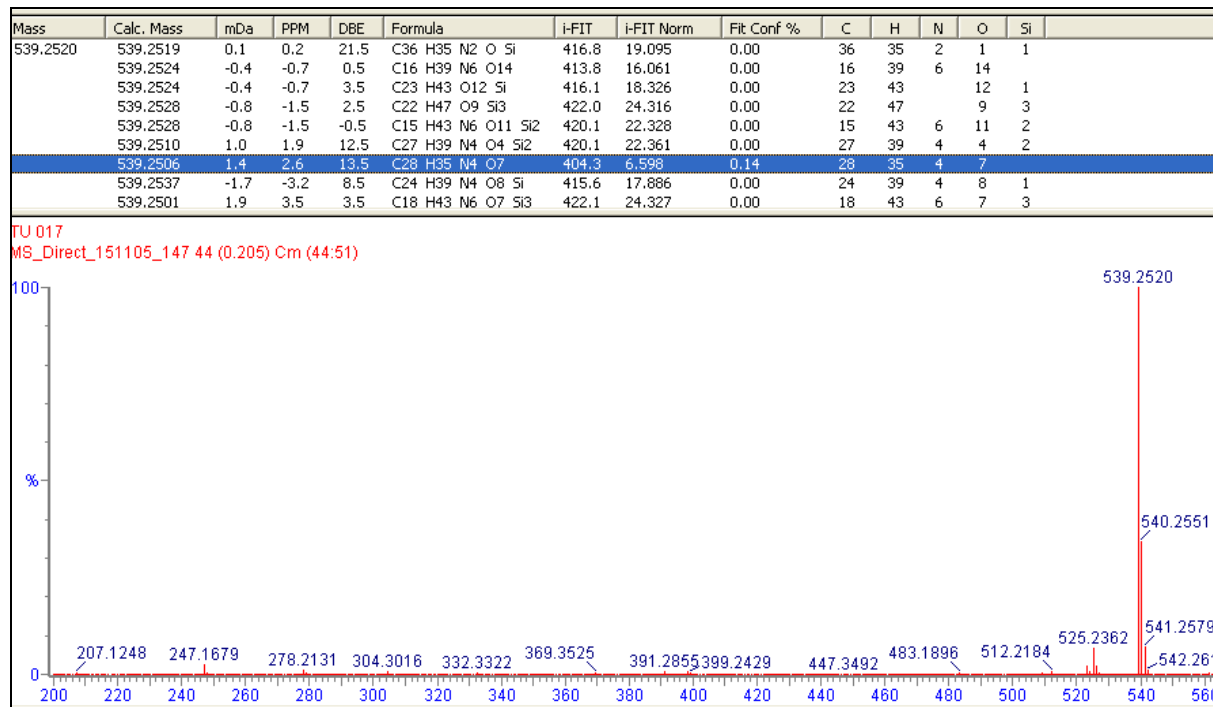| Mass	Calc. Mass	mDa	PPM	DBE	Formula	i-FIT	i-FIT Norm	Fit Conf %	C	H	N	O	Si
511.2191	511.2193	-0.2	-0.4	13.5	C26 H31 N4 O7	310.4	9.536	0.01	26	31	4	7	
	511.2188	0.3	0.6	3.5	C16 H39 N6 O7 Si3	327.4	26.505	0.00	16	39	6	7	3
	511.2197	-0.6	-1.2	12.5	C25 H35 N4 O4 Si2	325.4	24.563	0.00	25	35	4	4	2
	511.2184	0.7	1.4	4.5	C17 H35 N6 O10 Si	321.9	21.019	0.00	17	35	6	10	1
	511.2183	0.8	1.6	7.5	C24 H39 O8 Si2	325.3	24.456	0.00	24	39		8	2
	511.2179	1.2	2.3	8.5	C25 H35 O11	312.6	11.705	0.00	25	35		11	
	511.2206	-1.5	-2.9	21.5	C34 H31 N2 O Si	322.1	21.204	0.00	34	31	2	1	1
	511.2175	1.6	3.1	-1.5	C15 H43 N2 O11 Si3	327.4	26.484	0.00	15	43	2	11	3
	511.2174	1.7	3.3	26.5	C38 H27 N2	316.6	15.754	0.00	38	27	2		

Figure 68: HRMS (ESI) spectrum of TU-019 (L-104) 51

NOESY experiments of a number of the compounds in this study yielded information with regards to the spatial orientation of the methoxy groups attached to the aromatic ring. Nuclei that are within a certain distance from each other in space have cross peaks on a NOESY spectrum. For example, the signal of the aromatic proton 3'''-H of TU-019 (L-104) **51** has a cross-peak with the signal of the protons of the methoxy group 2'''-OCH$_3$. Likewise, the signal of the aromatic proton 5'''-H has a cross peak with the signal of the protons of the methoxy group 4'''-OCH$_3$.

The preparation of different dimethyl ether resorcinol analogues of NMS-E973 (L-1) **38** from their precursor TU-014 (L-99) **58** has been a straightforward process and afforded higher yields than preparing them through reductive amination because reductive amination has an additional step and this results in a lower overal yield.

2.2.6. Demethylation of aryl methyl ethers

The methyl group is widely considered an excellent protecting group for phenols in organic synthesis.[112] This is mainly due to the stability of the resulting ether bond.[112] The disadvantage is that in the past harsh conditions such as the use of concentrated HBr at high temperatures were required in order to liberate phenol[83]. The yields obtained using the system HBr/acetic acid varied between 49% and 90%.[113] Hydriodic acid or hydroiodic acid (HI) in acetic acid in the presence of red phosphorous has been also reported to demethylate aryl methyl ethers by refluxing the mixture but the yield obtained was low (49 %).[114] However, a milder method using hydroiodic acid produced *in situ* from iodocyclohexane in DMF under argon and at reflux gave generally high yields (88 % - 95 %) with relatively short reaction times (2.5 – 14 h).[115] However, HBr is usually preferred to HI due to the fact that HBr is less prone to producing side reactions.[83] Many other methods which use less severe conditions have been reported but have various disadvantages. Although less harsh, the use of BBr$_3$ requires long reaction times, and the yields (29 % - 70 %) are low due to incomplete reactions and the laborious reaction work-up.(61,72,116) BCl$_3$ has also been used for the selective deprotection of the less hindered methoxy when two methoxy groups are present.[116] However, this reaction has a very long reaction time (10 days).[116] Dimethylboron bromide (Me$_2$BBr) is another Lewis acid used to cleave aryl methyl ethers and it is a versatile reagent which can also cleave even aliphatic and cyclic ethers.[117] BF$_3$, AlCl$_3$ and AlBr$_3$ alone or in combination with NaI also constitute good aryl methyl ether demethylating agents.[118] In the case of Lewis acids, the departure of the methoxy or alkoxy in general is supported by complex formation with the Lewis acid.[83]
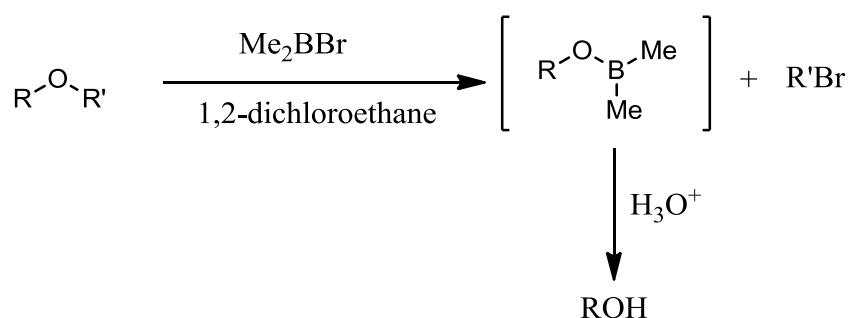
Scheme 11: Ether cleavage with Me$_2$BBr[117]

Apart from Lewis acids, lithium salts have also been used in ether cleavage. Lithium iodide (LiI) refluxed with collidine was reported to cleave aryl alkyl ethers in general[119-121] while

lithium chloride (LiCl) in boilig DMF has been used to selectively cleave alkyl aryl ethers activated with electron-withdrawing groups such as nitro, halogens, aldehydic and ester carbonyl groups in *ortho-* or *para-* positions with respect to the alkoxy group.[120] In both cases the reactions tended to be slow and required high temperatures.[119,120]

Another method which uses sodium ethanethiolate (EtSNa) in DMF at reflux temperatures give excellent yields (94 % and higher) in a relatively short time (3 hours) when compared to other methods found in the literature and is widely used.[122] Aryl alkyl ethers have also been cleaved by alkali metal thiophenoxide (PheS⁻) at 190 °C giving good yields (70 % - 90 %) in a short time (10 min – 30 min).[122] In spite of the stated benefits of this method, it has a disadvantage that N-methyl-2-pyrrolidone and hexamethylphosphoramide which are the best solvents used in this method have been reported to be teratogenic and carcinogenic respectively,[123-125] although other authors argue that N-methyl-2-pyrrolidone is no different from other solvents, that its toxicity is acute and that the benefits obtained from using it as a solvent outweigh its perceived toxicity.[126,127] Although thiolates in general are popular amongst the methods used to cleave aryl methyl ethers, if the compound contains other functionalities, the choice of the thiolate and the solvent to use must be carefully considered. Thiolates can displace the nitro group and halogen substituents.[128,129] In addition, thiolates also reduce nitro groups to the corresponding amines.[128] However, it was observed that catalytic potassium thiophenoxide (PheSK) generated *in situ* from PheSH and K_2CO_3 could selectively cleave the aryl methyl ether bond without affecting other functionalities present in the compound.[122] Sodium trimethylsilanethiolate (Me_3SiSNa) and hexamethyldisilathiane ($Me_3SiSSiMe_3$) were found to be good demethylating agents for the removal of two methoxy groups from aryl methyl ethers under alkaline conditions. Me_3SiSNa gave yields of 86 % – 92 % while $Me_3SiSSiMe_3$ gave yields of 72 % – 75 %. [130]

$$Nu^- \ + \ CH_3\text{-}OAr \longrightarrow Nu\text{-}CH_3 \ + \ ArO^-$$
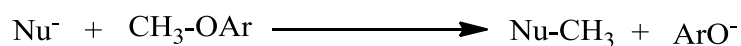
Scheme 12: Ester cleavage with nucleophiles [131]

In our study, we sought to demethylate TU-011 (L-7) **43** with PhSK[122] generated *in situ* from PhSOH and K_2CO_3 as this method[122] appeared to be the quickest and most promising in terms of yield. Unfortunately, the reaction did not yield the desired product. We then tried

to demethylate TU-012 (L-97) **49** using HBr in acetic acid (6.5% weight/volume)[113]. However instead of obtaining the desired product, we rather obtained the compound TU-018 (L-103) **50** which resulted from Boc-deprotection of TU-012 (L-97) **49** instead of demethylation. Taking into consideration that demethylated analogues of NMS-E973 (L-1) **38** would share the antiplasmodial pharmacophore with their dimethyl ether resorcinol analogues, we rather pursued the dimethyl ether resorcinol analogues due to their ease of synthesis, the constraint of time and the inadequate quantities of starting materials for the demethylation studies. We expected both the dimethyl ether resorcinol analogues and the demethylated analogues to possess the antiplasmodial activity, and for this reason we first sought to demonstrate that the dimethyl ether resorcinol analogues possessed that activity so that future researchers can further optimize these molecules by demethylation. Therefore, we synthesized the dimethyl ether resorcinol analogues and tested them for their biological activity.

2.3. Cell-based assays

After synthesis of the NMS-E973 (L-1) **38 analogues**, they were sent for bioassays in the Biossay, Parasite and Tissue Culture Laboratory at Rhodes University. They were assayed for their antiplasmodial activity and their cytotoxicity.

2.3.1. PLDH (*Plasmodium* lactate dehydrogenase) (Malaria) assay

The compounds were incubated with *P. falciparum* (strain 3D7) cells for 48 hours in a 37 °C CO_2 incubator. Afterwards, the % cell viability of the parasite was assessed in relation to the varying concentrations of each compound. (**Table 5**) Chloroquine **12** was used as a standard drug and its IC_{50} value was expected in the range 0.01 μM – 0.05 μM.

Table 5: Percentage (%) cell viability relative to the varying concentrations of the test compounds (PLDH assay)

Conc (µM)	Log(Conc)	TU-007 (L-96) 55		TU-011 (L-7) 43		TU-012 (L-97) 49		TU-013 (L-98) 57	
		% Viab	SD	% Viab	SD	% Viab	SD	% Viab	SD
100	2	94.58	9.23	97.66	7.83	99.50	1.63	90.81	7.62
25	1.39	105.69	0.15	95.14	2.80	105.65	0.75	93.48	9.54
6.25	0.79	107.05	8.07	113.05	13.16	117.77	7.25	114.25	2.16
1.56	0.19	122.55	2.63	116.58	10.15	125.51	1.23	122.12	8.68
0.39	-0.408	109.58	10.1	115.76	5.97	116.43	1.55	108.86	1.39
0.097	-1.01	105.42	7.57	110.02	8.97	113.73	10.65	113.05	5.06
0.024	-1.6	103.57	0.62	109.03	15.04	119.08	16.49	117.85	5.00
0.0061	-2.21	104.60	7.25	107.40	12.80	118.03	8.79	118.81	15.98

Table 5 (continued): Percentage (%) cell viability relative to the varying concentrations of the test compounds (PLDH assay)

Conc (µM)	Log(Conc)	TU-014 (L-99) 58		TU-015 (L-100) 59		TU-016 (L-14) 60		TU-017 (L-102) 61	
		% Viab	SD	% Viab	SD	% Viab	SD	% Viab	SD
100	2	84.79	11.20	15.52	1.00	79.39	3.59	36.80	7.08
25	1.39	113.69	3.35	19.45	2.88	111.14	2.37	32.67	0.40
6.25	0.79	114.66	7.92	98.94	3.62	120.25	5.71	44.44	1.30
1.56	0.19	108.59	6.40	112.27	6.02	115.22	8.97	121.25	8.29
0.39	-0.408	106.47	8.38	111.09	5.51	119.76	14.46	123.77	9.56
0.097	-1.01	107.04	0.06	126.24	6.10	124.06	22.25	137.91	4.59
0.024	-1.6	114.52	12.36	137.57	23.26	131.36	22.36	134.01	6.79
0.0061	-2.21	106.22	0.21	145.11	4.17	128.49	22.81	130.11	12.83

Table 5 (continued): Percentage (%) cell viability relative to the varying concentrations of the test compounds (PLDH assay)

Conc (µM)	Log(Conc)	TU-018 (L-103) 50		TU-019 (L-104) 51		Chloroquine 12
		%Viab	SD	%Viab	SD	%Viab
100	2	48.75	1.79	43.61	5.63	-5.160526
25	1.39	37.51	1.58	49.72	9.29	-3.759966
6.25	0.79	34.46	2.70	81.77	16.16	0.3770739
1.56	0.19	116.98	12.78	120.35	11.91	-6.60418
0.39	-0.408	118.15	6.29	119.52	16.05	54.374057
0.097	-1.01	124.73	11.86	122.31	16.00	97.080371
0.024	-1.6	137.93	13.94	134.36	19.85	107.07822
0.0061	-2.21	136.14	11.19	152.56	15.78	100.1616

The IC$_{50}$ values (**Table 6**) were deduced from the dose-response plots (**Figure 69** and **Figure 70**) of the % viability of the parasites versus the logarithm of the concentrations of the compounds used.

Figure 69: Dose-response plot of the % viability of *P. falciparum* (3D7) in the presence of TU-007 (L-96) 55, TU-011 (L-7) 43, TU-012 (L-97) 49, TU-013 (L-98) 57, TU-014 (L-99) 58 and chloroquine 12

Figure 70: Dose-response plot of the % viability of *P. falciparum* (3D7) in the presence of TU-015 (L-100) 59, TU-016 (L-14) 60, TU-017 (L-102) 61, TU-018 (L-103) 50, TU-019 (L-104) 51 and chloroquine 12

The IC_{50} values obtained show that the compounds TU-015 (L-100) **59**, TU-017 (L-102) **61**, TU-018 (L-103) **50** and TU-019 (L-104) **51** have IC_{50} values in the range of 1 μM to 10 μM. The rest of the compounds are not toxic to the parasite at 100 μM. The most active compound is TU-018 (L-103) **50** which has an IC_{50} value of approximately 1.830 μM. This IC_{50} value is 172 times higher than the one (IC_{50} = 0.01062 μM) obtained from the standard drug chloroquine.

Table 6: IC$_{50}$ of the compounds tested by the PLDH assay

Compound	IC$_{50}$ (μM)
TU-007 (L-96) **55**	Not toxic at 100 μM
TU-011 (L-7) **43**	Not toxic at 100 μM
TU-012 (L-97) **49**	Not toxic at 100 μM
TU-013 (L-98) **57**	Not toxic at 100 μM
TU-014 (L-99) **58**	Not toxic at 100 μM
TU-015 (L-100) **59**	9.343 μM
TU-016 (L-14) **60**	Not toxic at 100 μM
TU-017 (L-102) **61**	3.089 μM
TU-018 (L-103) **50**	~ 1.830 μM
TU-019 (L-104) **51**	6.189 μM
Chloroquine **12**	0.01062

IC$_{50}$ values were not calculated for compounds which were not toxic to the parasite at 100 μM since no curve could be drawn.

2.3.2. Cell cytotoxicity assay

The compounds were incubated with HeLa cells for 48 hours and then the percentage cell viability was determined using the resazurin reagent and reading the fluorescence. Emetine **62**, the apoptosis inducer drug,[132,133] was used as the standard drug and its IC$_{50}$ value was expected in the range 0.01 μM – 0.05 μM.

Emetine **62**

104
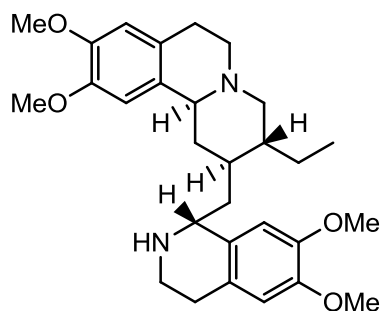
Table 7: Percentage (%) cell viability relative to the varying concentrations of the test compounds (cell cytotoxicity assay)

Conc (μM)	Log(Conc)	TU-007 (L-96) 55		TU-011 (L-7) 43		TU-012 (L-97) 49		TU-013 (L-98) 57	
		% Viab	SD	% Viab	SD	% Viab	SD	% Viab	SD
100	2	110.26	9.69	100.33	8.70	108.88	0.70	106.36	12.36
25	1.39	125.23	8.33	102.77	4.56	102.64	7.59	110.64	5.41
6.25	0.79	123.42	3.92	103.63	14.48	96.59	2.33	114.92	31.98
1.56	0.19	117.97	5.27	98.88	1.81	104.17	7.27	99.46	1.61
0.39	-0.408	114.44	8.07	100.43	0.42	97.98	8.51	99.71	5.14
0.097	-1.01	105.06	5.21	103.31	0.29	97.19	2.98	99.14	8.85
0.024	-1.6	102.81	2.97	91.26	9.97	100.49	22.02	99.16	10.28
0.0061	-2.21	114.81	4.72	108.14	0.00	106.99	3.07	101.92	2.85

Table 7 (continued): Percentage (%) cell viability relative to the varying concentrations of the test compounds (cell cytotoxicity assay)

Conc (μM)	Log(Conc)	TU-014 (L-99) 58		TU-015 (L-100) 59		TU-016 (L-14) 60		TU-017 (L-102) 61	
		% Viab	SD	% Viab	SD	% Viab	SD	% Viab	SD
100	2	69.25	2.41	78.18	7.66	107.62	6.08	27.08	0.41
25	1.39	95.14	6.71	110.12	5.30	98.82	11.82	84.86	9.78
6.25	0.79	92.59	1.31	126.77	2.92	111.52	19.56	110.66	7.96
1.56	0.19	97.56	0.70	125.39	14.27	117.28	10.39	97.74	2.45
0.39	-0.408	104.21	4.91	121.88	17.27	107.03	21.48	88.99	3.52
0.097	-1.01	97.86	0.50	128.35	7.41	123.57	19.73	98.13	4.83
0.024	-1.6	102.03	10.74	139.57	4.21	125.75	18.62	105.28	11.04
0.0061	-2.21	97.38	3.55	130.81	15.68	106.94	2.49	106.71	0.80

Table 7 (continued): Percentage (%) cell viability relative to the varying concentrations of the test compounds (cell cytotoxicity assay)

Conc (μM)	Log(Conc)	TU-018 (L-103) 50		TU-019 (L-104) 51		Emetine 62	
		% Viab	SD	% Viab	SD	% Viab	SD
100	2	-0.44	0.62	6.47	5.86	2.278003	0.890768
25	1.39	45.92	51.67	109.32	0.23	8.670643	1.188506
6.25	0.79	102.17	2.76	111.90	9.75	21.09511	2.892763
1.56	0.19	96.71	6.64	104.00	12.90	62.16879	6.409259
0.39	-0.408	100.28	21.64	109.99	7.95	123.1905	33.12945
0.097	-1.01	100.03	4.96	112.69	6.08	125.8574	11.37702
0.024	-1.6	98.34	0.56	106.98	4.90	112.3763	20.28484
0.0061	-2.21	99.01	6.61	95.60	0.87	113.67	5.664351

The results of the percentage (%) cell viability were plotted against the logarithm of the concentrations of the compounds tested for cell cytotoxicity and the IC_{50} values of those compounds were deduced from the resulting dose-response graphs.
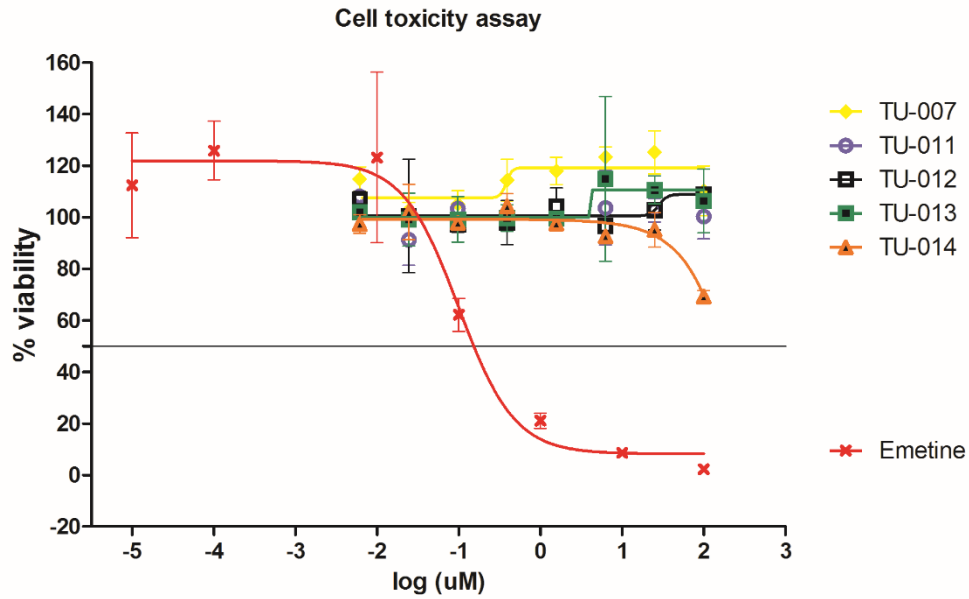
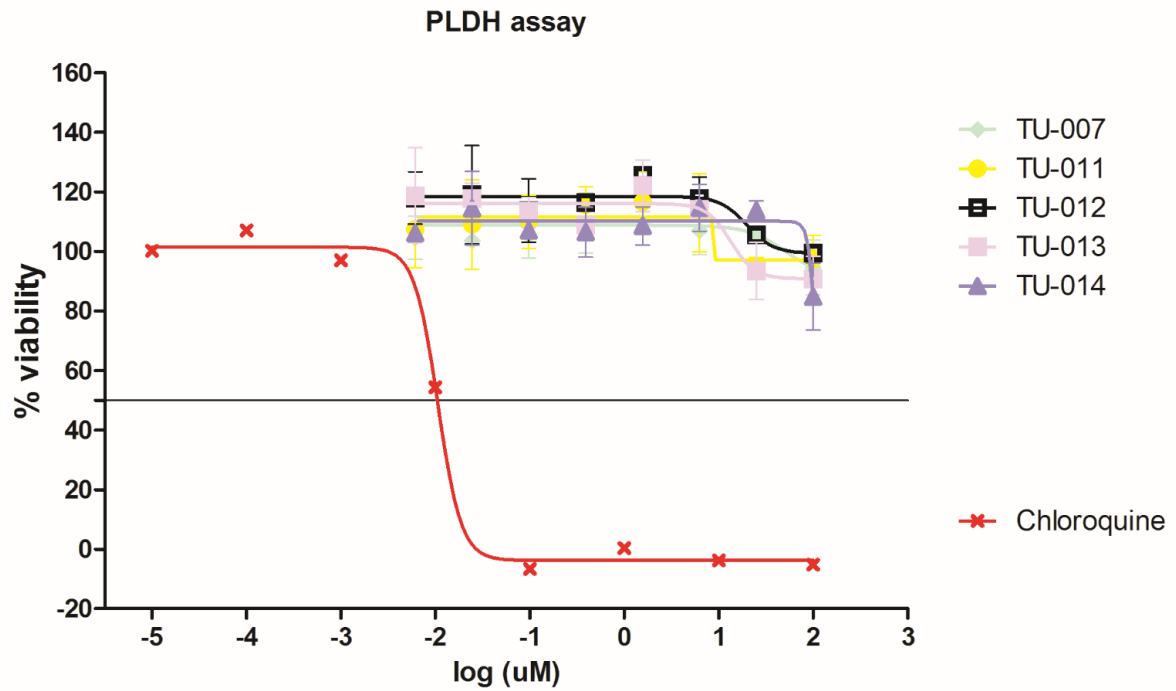**Figure 71: Dose-response plot of the % viability of HeLa cells in the presence of TU-007 (L-96) 55, TU-011 (L-7) 43, TU-012 (L-97) 49, TU-013 (L-98) 57, TU-014 (L-99) 58 and emetine 62**

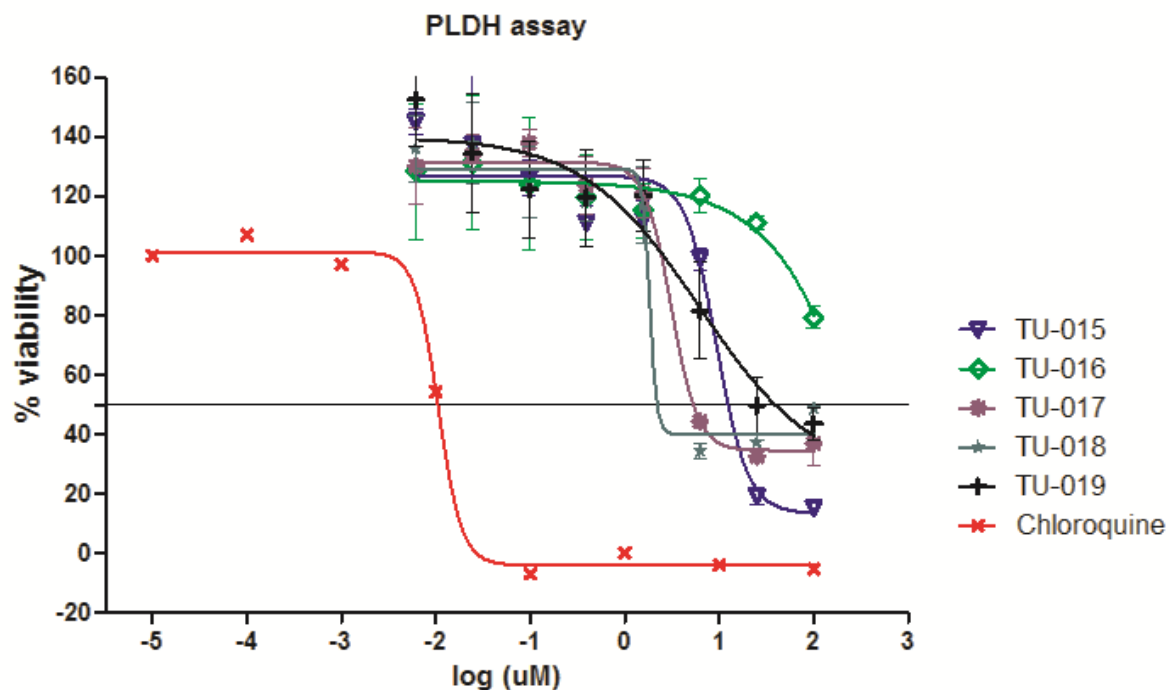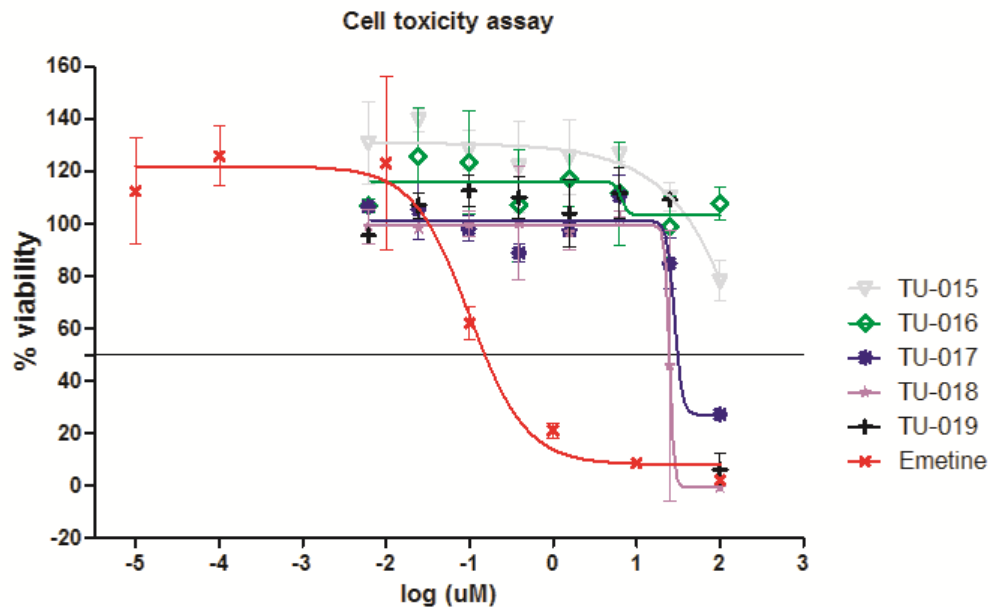**Figure 72: Dose-response plot of the % viability of HeLa cells (3D7) in the presence of TU-015 (L-100) 59, TU-016 (L-14) 60, TU-017 (L-102) 61, TU-018 (L-103) 50, TU-019 (L-104) 51 and emetine 62.**

The analysis of the IC_{50} values obtained shows that most of our compounds were not cytotoxic at 100 μM and that only compounds TU-014 (L-99) **58**, TU-017 (L-102) **61**, TU-018 (L-103) **50** and TU-019 (L-104) **51** were toxic at concentrations of 25 μM and higher. This means that the IC_{50} values of our compounds for cell cytotoxicity are at least 251 times higher than the IC_{50} value of emetine **62**.

Table 8: IC_{50} of the compounds tested for cell cytotoxicity

Compound	IC_{50} (μM)
TU-007 (L-96) **55**	Not Cytotoxic at 100 μM
TU-011 (L-7) **43**	Not Cytotoxic at 100 μM
TU-012 (L-97) **49**	Not Cytotoxic at 100 μM
TU-013 (L-98) **57**	Not Cytotoxic at 100 μM
TU-014 (L-99) **58**	Cytotoxic at 25 μM and higher
TU-015 (L-100) **59**	Not Cytotoxic at 100 μM
TU-016 (L-14) **60**	Not Cytotoxic at 100 μM
TU-017 (L-102) **61**	~ 28.49
TU-018 (L-103) **50**	~ 24.78
TU-019 (L-104) **51**	Cytotoxic above 25 μM
Emetine **62**	0.09948

2.4. Conclusion and recommendations

Our results show that the compounds TU-015 (L-100) **59**, TU-017 (L-102) **61**, TU-018 (L-103) **50** and TU-019 (L-104) **51** are active against the *P. falciparum* strain 3D7. Their activity is not related to their general toxicity since they are cytotoxic to HeLa cells only at concentration above 25 μM whereas their IC_{50} values for the anti-plasmodial activity vary between 1 and 10 μM. Although, these compounds are not as active as the standard drug chloroquine **12**, they are worth further optimization since our preliminary results suggest that they would be generally safe, which also corroborates the previous findings.[61] Moreover, these compounds are important because they represent novel scaffolds in the anti-malarial

area. *Pf*Hsp90 is also a novel anti-plasmodial target and more research is needed in order to confirm it as a drug target.

Our docking results suggest that demethylated analogues of our compounds will be more active than their dimethyl ether resorcinol analogue counterparts. In addition, the demethylated compounds will more likely selectively bind to *Pf*Hsp90 in the presence of Hsp90. However, results obtained by docking studies are approximations and should not be interpreted as if they corresponded exactly to the experimental values. It is also important for future researchers to assess whether the anti-plasmodial activity of these compounds was specifically mediated by *Pf*Hsp90 inhibition since in our case we only tested the growth inhibitory anti-plasmodial activity and not specifically the *Pf*Hsp90 inhibition.

Chapter Three: Experimental

3.1. Organic synthesis

The reagents used during our synthesis were of reagent grade while the solvents used for column chromatography were of technical grade and both were purchased from Sigma-Aldrich unless stated otherwise. We collected NMR data of our compounds using either the Bruker 300 MHz Nuclear Magnetic Resonance Spectrometer or the Bruker 400 MHz Nuclear Magnetic Resonance Spectrometer or a Bruker Avance III 600 MHz Nuclear Magnetic Resonance Spectrometer. Mass Spectrometry data were collected using a Waters Synapt G2 instrument with ESI ionisation method.

3.1.1. Synthesis of 1,3-dimethyl-5-(4-nitrophenoxy)benzene TU-001 46
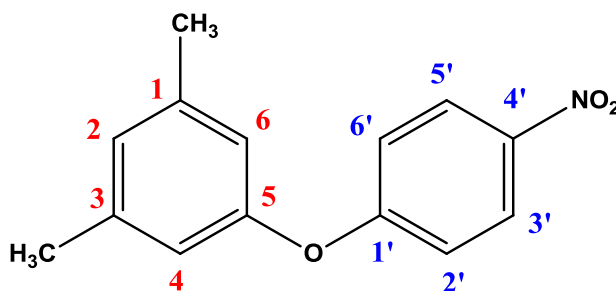
3,5-dimethylphenol (M.W.: 122.16 g.mol^{-1}; 0.13 g; 1.06 mmol), 1-fluoro-4-nitrobenzene (M.W.: 141.10 g.mol^{-1}; 0.15 g; 1.06 mmol), K_2CO_3 (M.W.: 138.21 g.mol^{-1}; 0.22 g; 1.59 mmol) and dimethyl sulfoxide (5 mL) were added to a 50 mL round-bottomed flask and stirred at 110 °C for 4 hours. After cooling down, the reaction mixture was diluted with ethyl acetate (20 mL) and then washed with brine (3 × 10 mL), dried with $MgSO_4$, filtered and finally concentrated under reduced pressure to give a crude product. The crude was purified by column chromatography (hexane: ethyl acetate 98:2; L = 5 cm; D = 1.90 cm; silica gel 0.040 – 0.063 mm) to obtain TU-001 **46** as an amorphous white solid (0.25 g, 96%). Melting point = 68 °C - 70 °C. The retention factor (Rf) of TU-001 **46** in hexane/ethyl acetate 9:1 is 0.44. ^{1}H-NMR (400.13 MHz; 30.160 °C; CDCl$_3$) δ ppm 2.33 (s, 6 H (1-CH$_3$ and 3-CH$_3$)), 6.71 (s, 2 H (4-H and 6-H)), 6.89 (s, 1 H (2-H)), 7.00 (d, J = 9.09 Hz, 2 H (2'-H and 6'-H)), 8.17 (d, J = 9.09 Hz, 2 H (3'-H and 5'-H)). ^{13}C-NMR (100.61 MHz; 30.160 °C; CDCl$_3$) δ

ppm 21.2 (1-CH$_3$ and 3-CH$_3$), 117.0 (2'-C and 6'-C), 118.1 (4-C and 6-C), 125.8 (3'-C and 5'-C), 127.1 (2-C), 140.3 (1-C and 3-C), 142.5 (4'-C), 154.7 (5-C), 163.6 (1'-C).

3.1.2. Synthesis of 1-(4-(3,5-dimethylphenoxy)phenyl)ethanone TU-002 47
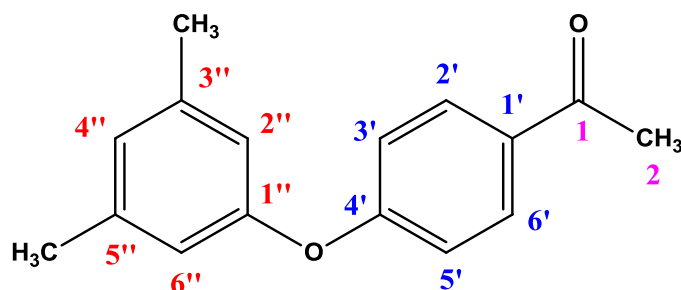
3,5-dimethylphenol (M.W.: 122.16 g.mol^{-1}; 0.13 g; 1.06 mmol), 1-(4-fluorophenyl)ethanone (M.W.: 138.14 g.mol^{-1}; 0.15 g, 1.09 mmol) and K$_2$CO$_3$ (M.W.: 138.21 g.mol^{-1}; 0.22 g; 1.59 mmol) were dissolved in dimethyl sulfoxide (5 mL) and stirred at 110 °C for 48 hours. After cooling down, the mixture was diluted with ethyl acetate (20 mL), washed with brine (10 mL × 3) and dried over MgSO$_4$. After filtration, the mixture was concentrated under reduced pressure to give a crude product. Purification of the crude was done by column flash chromatography (hexane: ethyl acetate 98: 2, L=15 cm; D = 2.0 cm, silica gel: 0.040 – 0.063 mm) to give TU-002 **47** as an amorphous white solid (0.15 g, 60%). Melting point = 67 °C – 68 °C. The retention factor of TU-002 **47** in hexane: ethyl acetate 9:1 is 0.26. ^{1}H-NMR (600.03 MHz; 25.000 °C; CDCl$_3$) δ ppm 2.31 (s, 6 H (3''-CH$_3$ and 5''-CH$_3$)), 2.57 (s, 3 H (2-CH$_3$)), 6.68 (s, 2 H (2''-H and 6''-H)), 6.83 (s, 1 H (4''-H)), 6.99 (m, 2 H (3'-H and 5'-H)), 7.93 (m, 2 H (2'-H and 6'-H)). ^{13}C-NMR (150.88 MHz; 25.000 °C; CDCl$_3$) δ ppm 21.3 (3''-CH$_3$ and 5''-CH$_3$), 26.4 (2-C), 117.2 (3'-CH and 5'-CH), 117.8 (2''-C and 6''-C), 126.3 (4''-C), 130.5 (2'-C and 6'-C), 131.7 (1'-C), 140.0 (3''-C), 155.4 (1''-C), 162.2 (4'-C-O), 196.8 (1-C=O).

3.1.3. Synthesis of 1-(2,4-dimethoxy-6-(4-nitrophenoxy)phenyl)ethanone TU-003 41
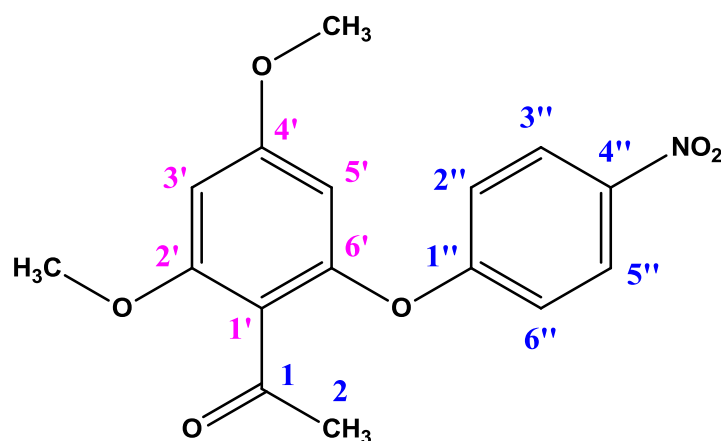
1-(2-hydroxy-4,6-dimethoxyphenyl)ethanone (M.W.: 196.20 g.mol^{-1}; 0.60 g; 3.06 mmol), 1-fluoro-4-nitrobenzene (M.W.: 141.10 g.mol^{-1}; 0.45 g; 3.19 mmol) and K$_2$CO$_3$ (M.W.: 138.21 g.mol^{-1}; 0.53 g; 3.83 mmol) were dissolved in dimethyl sulfoxide (10 mL) and stirred at 45 °C for 4 hours. After cooling down, the mixture was diluted with ethyl acetate (50 mL) and washed with brine (20 mL × 3). The mixture was then dried with MgSO$_4$, filtered and then concentrated under reduced pressure to give a crude product. The crude was purified by column chromatography (hexane/ethyl acetate 4: 1) to give TU-003 **41** as a white solid (0.86 g, 88%). The retention factor of TU-003 **41** in hexane: ethyl acetate 1:1 is 0.50. Melting point = 64 °C - 66 °C. ^{1}H-NMR (300.19 MHz; 20.500 °C; CDCl$_3$) δ ppm 2.43 (s, 3 H (2-CH$_3$)), 3.78 (s, 3 H (4'-OCH$_3$)), 3.86 (s, 3 H (2'-OCH$_3$)), 6.14 (d, J = 2.05 Hz, 1 H (5'-H)), 6.38 (d, J = 2.05 Hz, 1 H (3'-H)), 7.00 (m, 2 H (2''-H and 6''-H)), 8.19 (m, 2 H (3''-H and 5''-H)). ^{13}C-NMR (75.48 MHz; 20.500 °C; CDCl$_3$) δ ppm 32.3 (2-C), 55.7 (4'-OCH$_3$), 56.0 (2'-OCH$_3$), 96.0 (3'-C), 98.4 (5'-C), 117.0 (2''-C and 6''-C), 117.7 (1'-C), 125.9 (3''-C and 5''-C), 142.8 (4''-C), 153.0 (6'-C), 159.2 (2'-C), 162.6 (4'-C), 163.1 (1''-C), 199.4 (1-C=O).

3.1.4. The synthesis of 1-(2-hydroxy-4,6-dimethoxyphenyl)-2-(4-nitrophenyl)ethanone TU-004 52
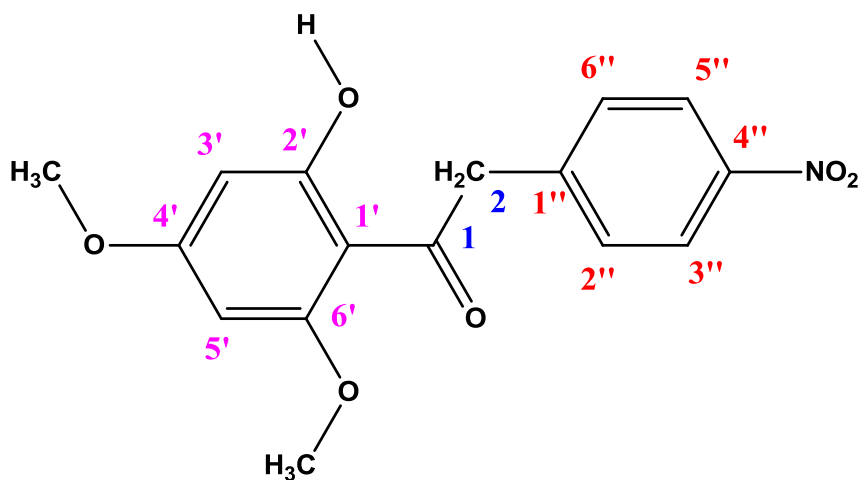
1-(2-hydroxy-4,6-dimethoxyphenyl)ethanone (M.W.: 196.20 g.mol^{-1}; 0.20 g; 1.02 mmol), 1-fluoro-4-nitrobenzene (M.W.: 141.10 g.mol^{-1}; 0.15 g; 1.06 mmol) and K_2CO_3 (M.W.: 138.21 g.mol^{-1}; 0.22 g; 1.59 mmol) were dissolved in dimethyl sulfoxide (5 mL) and stirred at 55 °C for 4 hours. After cooling down, the mixture was diluted with ethyl acetate (20 mL) and washed with brine (10 mL × 3). The mixture was then dried with $MgSO_4$, filtered and then concentrated under reduced pressure to give a crude product. The crude product was purified by column chromatography (hexane/ethyl acetate 4:1) to give TU-004 **52** as a white solid (0.023 g, 7%). Melting point = 124 °C - 126 °C. ^{1}H-NMR (300.19 MHz; 21.4 °C; CDCl$_3$) δ ppm 3.83 (s, 3 H (4'-OCH$_3$)), 3.86 (s, 3 H (6'-OCH$_3$)), 4.43 (s, 2 H (2-H)), 5.94 (d, J = 2.35 Hz, 1 H (5'-H)), 6.09 (d, J = 2.35 Hz, 1 H (3'-H)), 7.37 (m, 2 H (2''-H and 6''-H)), 8.19 (m, 2 H (3''-H and 5''-H)), 13.65 (s, 1 H (2'-OH)). ^{13}C-NMR (75.48 MHz; 20.500 °C; CDCl$_3$) δ ppm 50.0 (2-C), 55.7 (4'-OCH$_3$ and 6'-OCH$_3$), 91.1 (5'-C), 93.8 (3'-C), 105.5 (1'-C), 123.5 (3''-C and 5''-C), 130.5 (2''-C and 6''-C), 143.3 (1''-C), 146.8 (4''-C), 162.5 (6'-C), 166.7 (4'-C), 168.0 (2'-C), 200.8 (1-C=O).

3.1.5. Synthesis of 1-(2,4-dimethoxy-6-((4-nitrobenzyl)oxy)phenyl)ethanone TU-005 54
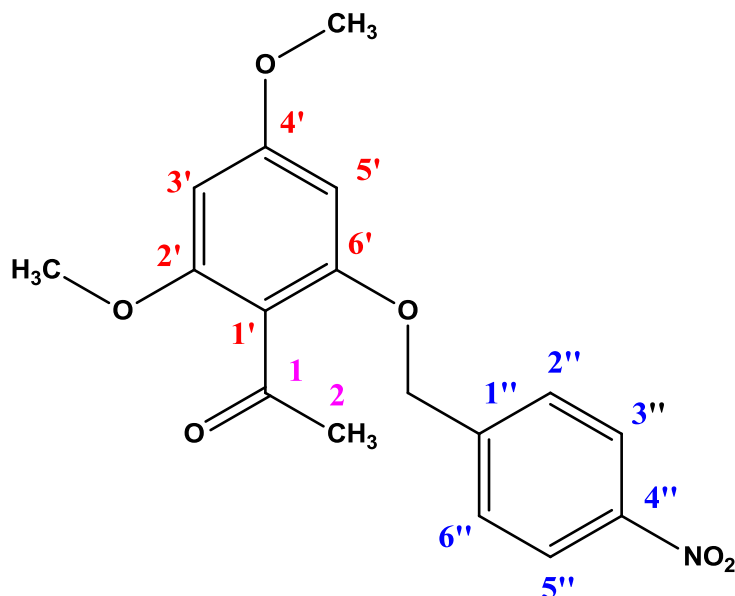
1-(2-hydroxy-4,6-dimethoxyphenyl)ethanone (M.W.: 196.20 g.mol^{-1}; 0.49 g; 2.50 mmol) and 1-(bromomethyl)-4-nitrobenzene (M.W.: 216.03 g.mol^{-1}; 0.66 g; 3.06 mmol) were added to a 25 mL round-bottomed flask. Then, K$_2$CO$_3$ (M.W.: 138.21 g.mol^{-1}; 0.59 g; 4.27 mmol) was also added and the mixture was dissolved in acetonitrile (10 mL) and afterwards refluxed for 6 hours. Then, it was cooled down, diluted with ethyl acetate (50 mL), washed with deionised water (10 mL × 3) and then with brine (10 mL × 2). The extract was further dried with MgSO$_4$, and afterwards concentrated under reduced pressure to give a residue. After purification of the mixture by column flash chromatography (first hexane/ethyl acetate 4:1; L = 12 cm; D = 2.5 cm, then hexane/ethyl acetate1:1), the collected fractions were concentrated to give TU-005 **54** as a white solid (0.23 g, 28%). Melting point = 133 °C – 135 °C.^{1}H-NMR (300.19 MHz; 17.50 °C; CDCl$_3$) δ ppm 2.49 (s, 3 H (2-CH$_3$)), 3.80 (s, 3 H (4'-OCH$_3$)), 3.81 (s, 3 H (2'-OCH$_3$)), 5.15 (s, 2 H (1''-CH$_2$-O-)), 6.08 (d, J = 2.02 Hz, 1 H (5'-H)), 6.14 (d, J = 2.02 Hz, 1 H (3'-H)), 7.56 (m, 2 H (2''-H and 6''-H)), 8.23 (m, 2 H (3''-H and 5''-H)). ^{13}C-NMR (75.48 MHz; 17.50 °C; CDCl$_3$) δ ppm 32.7 (2-C), 55.5 (4'-OCH$_3$ or 2'-OCH$_3$), 55.9 (4'-OCH$_3$ or 2'-OCH$_3$), 69.2 (1''-CH$_2$-O-), 91.1 (3'-C), 92.1 (5'-C), 114.2 (1'-C), 123.9 (3''-C and 5''-C), 127.4 (2''-C and 6''-C), 143.9 (1''-C), 147.5 (4''-C), 156.5 (6'-C), 158.6 (2'-C), 162.3 (4'-C), 201.6 (1-C=O).

3.1.6. Preparation of ethyl 2-hydroxy-4,6-dimethoxybenzoate TU-006 53
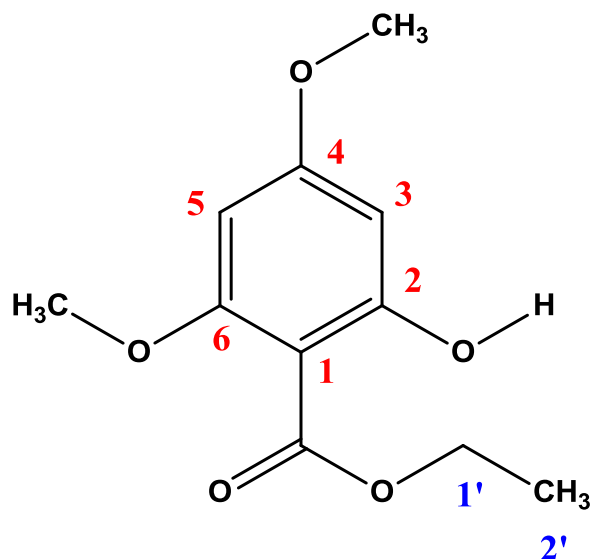
Na (M.W.: 22.99 g.mol^{-1}; 0.03 g; 1.30 mmol) was added to ethanol (3 mL) and dissolved completely. After completion of the reaction, we waited for 30 minutes to add 1-(2,4-dimethoxy-6-(4-nitrophenoxy)phenyl)ethanone (**41**, M.W.: 317.29 g.mol^{-1}; 0.20 g; 0.63 mmol) and then diethyl oxalate (M.W.: 146.14 g.mol^{-1}; 0.18 g; 1.23 mmol). After heating at 90 °C for overnight, we could not obtain any product. More sodium (M.W.: 22.99 g.mol^{-1}; 0.1 g; 4.35 mmol) was dissolved in ethanol (2 mL) and added to the reaction mixture. Within 5 minutes, a new product had formed. After stirring at room temperature for more 30 minutes, the mixture was quenched by 1M HCl (10 mL), put on a rotavapor to remove ethanol, and then extracted with dichloromethane. The extract was concentrated on a rotavapor. Purification was done by column chromatography (hexane: ethyl acetate 9: 1; L = 12 cm; D = 1.5 cm and then hexane: ethyl acetate 1:1). After concentration of the fractions on the rotavapor, the solvent was removed to give TU-006 **53** as a white solid (0.06 g, 43%). Melting point = 64. °C- 65 °C. ^{1}H-NMR (300.19 MHz; 19.30 °C; CDCl$_3$) δ ppm 1.39 (t, J = 7.09 Hz, 3 H (2'-CH$_3$)), 3.80 (s, 3 H (4-OCH$_3$/6-OCH$_3$)), 3.81(s, 3 H (6-OCH$_3$/4-OCH$_3$)), 4.37 (q, J = 7.09 Hz, 2 H (1'-CH$_2$)), 5.95 (d, J = 2.37 Hz, 1 H (5-H)), 6.10 (d, J = 2.37 Hz, 1 H (3-H)), 12.09 (s, 1 H (OH)). ^{13}C-NMR (75.48 MHz; 19.40 °C; CDCl$_3$) δ ppm 14.2 (2'-CH$_3$), 55.4 (4-OCH$_3$/6-OCH$_3$), 56.0 (6-OCH$_3$/4-OCH$_3$), 61.2 (1'-CH$_2$), 91.6 (5-C), 93.4 (3-C), 96.8 (6-C), 162.2 (4-C), 165.2 (1-C), 165.9 (2-C), 171.2 (COOEt)).

3.1.7. Preparation of 4,6-dimethoxy-3-methyl-2-(4-nitrophenyl)benzofuran TU-007 (L-96) 55
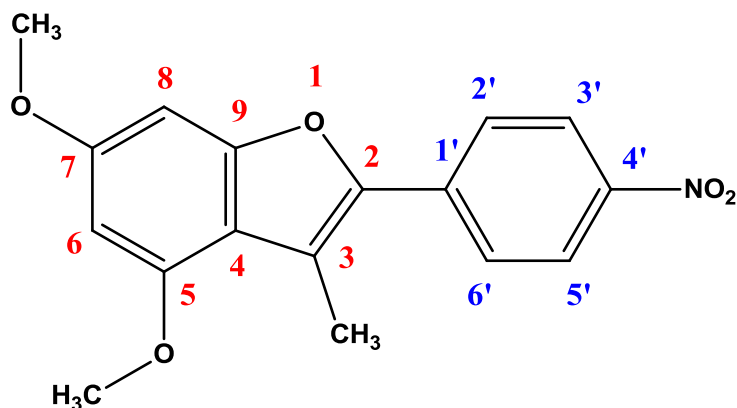
1-(2,4-dimethoxy-6-((4-nitrobenzyl)oxy)phenyl)ethanone (**54**, M.W.: 331.32 g.mol^{-1};. 0.10 g; 0.30 mmol) was dissolved in ethanol (3 mL) and the mixture brought at 90 °C. Then, Na (M.W.: 22.99 g.mol^{-1}; 0.10 g; 4.35 mmol) was dissolved in ethanol (3 mL) and added to the mixture at 90 °C. The mixture was stirred at 90 °C for 1 hour. Then, after cooling down, 1 M HCl (10 mL) was added. The mixture was concentrated and extracted with dichloromethane. The extract was concentrated on a rotavapor to give a crude product. Purification was done by gradient column chromatography (hexane: ethyl acetate 9: 1; L = 12 cm; D = 1.5 cm, then increased to hexane: ethyl acetate 1: 1 and finally to ethyl acetate: methanol 96: 4). Removal of volatiles resulted in recovery of TU-007 (L-96) **55** as an orange solid (0.06 g, 66%). Melting point = 160 °C – 162 °C. ^{1}H-NMR (300.19 MHz; 19.20 °C; CDCl$_3$) δ ppm 2.65 (s, 3 H (3-CH$_3$)), 3.86 (s, 3 H (7-OCH$_3$)), 3.90 (s, 3 H (5-OCH$_3$)), 6.29 (d, J = 1.92 Hz, 1 H (8-H)), 6.61 (d, J = 1.92 Hz, 1 H (6-H)), 7.85 (m, 2 H (3'-H and 5'-H)), 8.27 (m, 2 H (2'-H and 6'-H)). ^{13}C-NMR (75.48 MHz; 19.20 °C; CDCl$_3$) δ ppm 11.6 (3-CH$_3$), 55.5 (5-OCH$_3$), 55.8 (7-OCH$_3$), 87.7 (6-C), 94.4 (8-C), 114.0 (4-C), 116.7 (3-C) 124.0 (2'-C and 6'-C), 125.7 (3'-C and 5'-C), 137.7 (2-C), 145.7 (1'-C), 146.1 (4'-C), 155.8 (5-C), 156.3 (9-C), 160.2 (7-C). HRMS (ESI): m/z calculated for C$_{17}$H$_{15}$NO$_5$+H$^+$ 314.1028, found 314.1039.

3.1.8. Synthesis of 1-(2, 4, 6-trimethoxyphenyl)ethanone TU-009 56
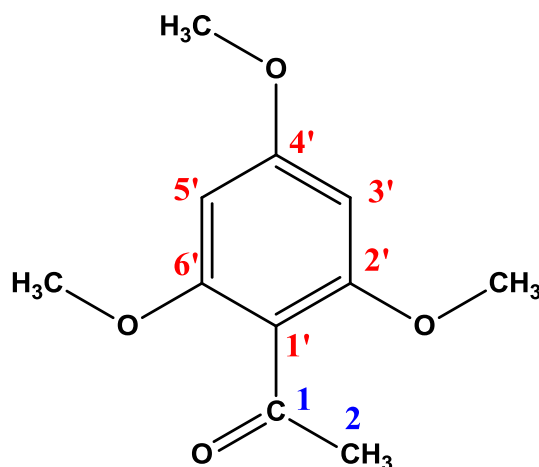
1-(2-hydroxy-4, 6-dimethoxyphenyl)ethanone (M.W. : 196.20 g.mol^{-1}; 0.20 g; 1.02 mmol), iodomethane (M.W.: 141.94 g.mol^{-1}; 0.16 g; 1.13 mmol) and K_2CO_3 (M.W. : 138.21 g.mol^{-1}; 0.18 g; 1.30 mmol) were dissolved in acetonitrile (10 mL) and refluxed for 12 hours. Thereafter, the reaction product was cooled down and acetonitrile was removed under reduced pressure. Water (20 mL) and dichloromethane (30 mL) were added to the mixture and the layers were separated. The aqueous layer was extracted further with dichloromethane (10 mL × 2). The organic extracts were combined and washed with brine (15 mL), then dried over MgSO$_4$, and afterwards concentrated under reduced pressure to give a crude product. The crude product was purified with column chromatography (hexane: ethyl acetate: 95: 5; L = 10 cm; D = 2 cm). After removing, the first spot, the column was washed with hexane: ethyl acetate 1:1. Removal of volatiles resulted in recovery of compound TU-009 **56** as a white solid (0.09 g, 43 %). Melting point = 79 °C – 80 °C. ^{1}H-NMR (600.03 MHz; 25 °C; CDCl$_3$) δ ppm 2.46 (s, 3 H (2-CH$_3$)) 3.79 (s, 6 H (2'-OCH$_3$ and 6'-OCH$_3$)), 3.82 (s, 3 H (4'-OCH$_3$)), 6.10 (s, 2 H (3'-H and 5'-H)). ^{13}C-NMR (150.89 MHz; 25 °C; CDCl$_3$) δ ppm 32.5 (2-C), 55.4 (4'-OCH$_3$), 55.8 (2'-OCH$_3$ and 6'-OCH$_3$), 90.6 (3'-C and 5'-C), 113.8 (1'-C), 158.4 (2'-C and 6'-C), 162.3 (4'-C), 201.7 (1-C=O).

3.1.9. Synthesis of (Z)-ethyl 4-(2, 4-dimethoxy-6-(4-nitrophenoxy) phenyl)-2-hydroxy-4-oxobut-2-enoate TU-010 48
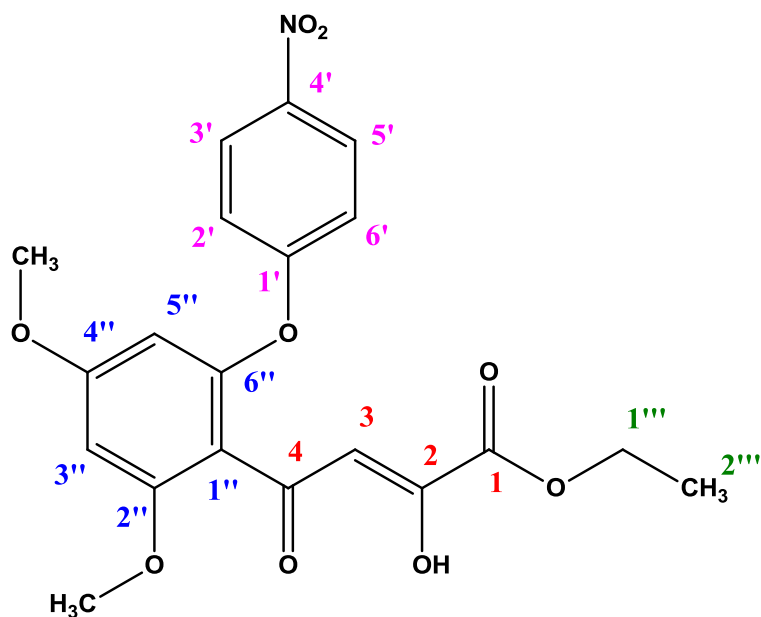
1-(2, 4-dimethoxy-6-(4-nitrophenoxy) phenyl) ethanone (**41**, M.W.: 317.29 g.mol^{-1}; 2.15 g; 6.78 mmol) was added to a two-neck flask. Then, dry tetrahydrofuran (15 mL) was added and the mixture was stirred at − 5 °C until all the starting material had dissolved. Afterwards, 1 M lithium bis (trimethylsilyl) amide in tetrahydrofuran (11.46 mL; 10.21 g; d = 0.891g/mL; 61.02 mmol) was added and the mixture left to stir for 10 minutes. Then, diethyl oxalate (M.W.: 146.14; 1.98 g, 13.55 mmol) was added and the mixture was slowly warmed up while stirring from −5 °C to room temperature under argon atmosphere. After stirring for an overnight, excess base was neutralized with 1 M HCl (15 mL) and tetrahydrofuran was removed under reduced pressure. Afterwards, brine (40 mL) and ethyl acetate (80 mL) were added and layers separated. The aqueous layer was further extracted with ethyl acetate (20 mL × 3) and the organic extracts were combined, then dried with MgSO$_4$, filtered and concentrated under reduced pressure to give a crude product. Purification was done by column chromatography (hexane: ethyl acetate 7: 3; L = 12 cm; D = 2 cm) to give TU-010 **48** as a white solid (1.84 g, 65 %). Melting point = 83 °C – 84 °C. ^{1}H-NMR (600.03 MHz; 18.4 °C; CDCl$_3$) δ ppm 1.34 (t, J = 7.12 Hz, 3 H (2'''-CH$_3$), 3.81 (s, 3 H (4''-OCH$_3$)), 3.88 (s, 3 H (2''-OCH$_3$)), 4.33 (q, J = 7.12 Hz, 2 H (1'''-CH$_2$)), 6.18 (d, J = 2.20 Hz, 1 H (5''-H)), 6.40 (d, J = 2.20 Hz, 1 H (3''-H)), 6.69 (s, 1 H (3-H)), 7.00 (m, 2 H (2'-H and 6'-H)), 8.19 (m, 2 H

(3'-H and 5'-H)), 14.25 (s, 1 H (2-OH)). ^{13}C-NMR (150.89 MHz; 18.7 °C; CDCl$_3$) δ ppm 14.1 (2'''-CH$_3$), 55.8 (4''-OCH3), 56.3 (2''-OCH3), 62.5 (1'''-CH$_2$), 96.1 (3''-C), 98.9 (5''-C), 105.8 (3-C), 114.1 (1''-C), 117.0 (2'-C and 6'-C), 126.0 (3'-C and 5'-C), 142.9 (1'-C), 154.6 (6''-C), 160.1 (2''-C), 162.3 (1-C=OO), 163.0 (4'-C), 163.8 (4''-C), 164.4 (2-C), 192.2 (4-C=O).

3.1.10. Synthesis of ethyl 5-(2, 4-dimethoxy-6-(4-nitrophenoxy) phenyl) isoxazole-3-carboxylate TU-011 (L-7) 43
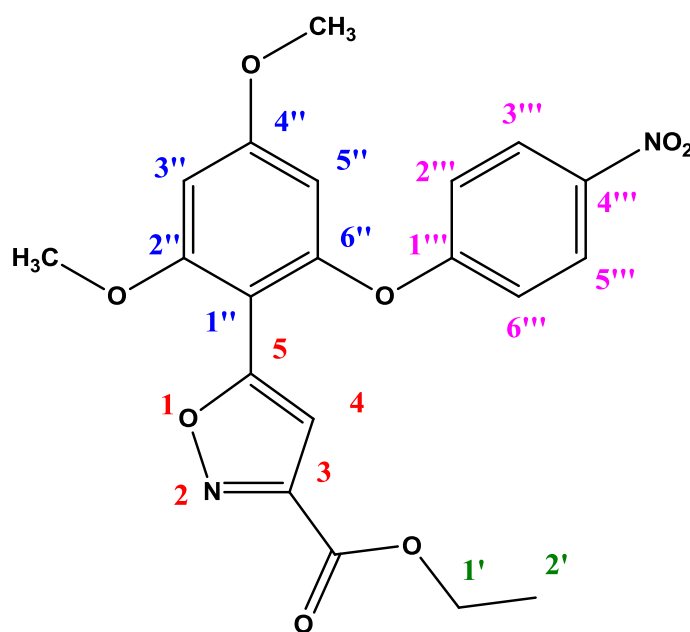
(*Z*)-Ethyl 4-(2, 4-dimethoxy-6-(4-nitrophenoxy) phenyl)-2-hydroxy-4-oxobut-2-enoate (**48**, M.W.: 417.37 g.mol^{-1}; 1.85 g; 4.43 mmol) and hydroxylamine hydrochloride (M.W.: 69.49 g.mol^{-1}; 0.40 g; 5.76 mmol) were dissolved in ethanol (20 mL) and refluxed for 5 hours. Afterwards, the mixture was cooled down and ethanol concentrated under reduced pressure. The crude was purified by column chromatography (hexane: dichloromethane 6:4; L = 15 cm; D = 2.5 cm, then changed to dichloromethane: ethyl acetate 99:1) and after concentration of the collected fractions, TU-011 (L-7) **43** was obtained as a white solid (1.42 g, 77 % yield). Melting point = 125 °C – 127 °C. ^{1}H-NMR (600.03 MHz; 18.7 °C; CDCl$_3$) δ ppm 1.39 (t, *J* = 7.16 Hz, 3 H (2'-CH$_3$)), 3.83 (s, 3 H (4''-OCH$_3$)), 3.92 (s, 3 H (2''-OCH$_3$)), 4.41 (q, *J* = 7.16 Hz, 2 H (1'-CH$_2$-)), 6.29 (d, *J* = 2.34 Hz, 1 H (5''-H)), 6.47 (d, *J* = 2.34 Hz, 1 H

(3''-H)), 6.88 (s, 1 H (4-H)), 6.99 (m, 2 H (2'''-H and 6'''-H)), 8.16 (m, 2 H (3'''-H and 5'''-H)). ^{13}C-NMR (150.89 MHz; 19.4 °C; CDCl$_3$) δ ppm 14.2 (2'-CH$_3$), 55.8 (4''-OCH$_3$), 56.2 (2''-OCH$_3$), 62.1 (1'-CH$_2$-), 96.2 (3''-C), 99.2 (5''-C), 103.1 (1''-C), 105.6 (4-C), 116.8 (2'''-C and 6'''-C), 126.0 (3'''-C and 5'''-C), 142.8 (1'''-C), 154.2 (6''-C), 156.0 (3-C), 159.6 (2''-C), 160.2 (3-C=OO), 162.8 (4'''-C), 163.3 (4''-C), 165.2 (5-C). HRMS (ESI): m/z calculated for C$_{20}$H$_{18}$N$_2$O$_8$+H$^+$ 415.1141, found 415.1156.

3.1.11. Synthesis of *tert*-butyl 4-(5-(2,4-dimethoxy-6-(4-nitrophenoxy)phenyl)isoxazole-3-carboxamido)piperidine-1-carboxylate TU-012 (L-97) 49
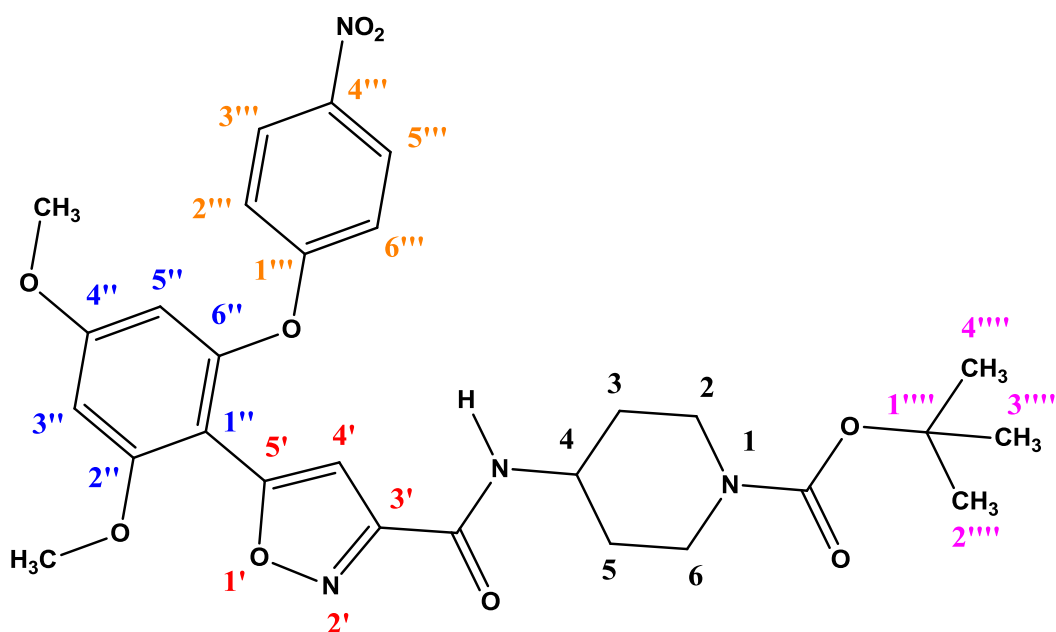
Ethyl 5-(2,4-dimethoxy-6-(4-nitrophenoxy)phenyl)isoxazole-3-carboxylate (**43**, M.W.: 414.37 g.mol^{-1}, 0.88 g; 2.12 mmol) and 4-amino-1-Boc-piperidine (1.70 g; 8.49 mmol) were dissolved in dichloromethane (10 mL) and refluxed while stirring to obtain a homogeneous solution. Then, the solvent was removed and the mixture heated at 90 °C for 36 hours. After cooling down, the reaction product was concentrated under reduced pressure to a crude product, which was purified by column chromatography (dichloromethane: ethyl acetate 80: 20; L = 12 cm; D = 2 cm) to give TU-012 (L-97) **49** as a white powder (0.98 g, 81%). Melting point = 65 °C – 68 °C. ^{1}H -NMR (600.03 MHz; 16.9 °C; CDCl$_3$) δ ppm 1.39 (d, *J* = 10.20 Hz, 2 H (3-H/5-H)), 1.45 (s, 9 H (1''''-(CH$_3$)$_3$), 1.95 (m, 2 H (5-H/ 3-H)), 2.88 (br s, 2 H (2-H/6-H)), 3.82 (s, 3 H (4''-OCH$_3$)), 3.91 (s, 3 H (2''-OCH$_3$)), 4.06 (m, (3 H (4-H and 6-

H/2-H)), 6.27 (d, J = 2.24 Hz, 1 H (5''-H)), 6.47 (d, J = 2.24 Hz, 1 H (3''-H)), 6.68 (d, J = 8.08 Hz, 1 H (CONH)), 6.92 (s, 1 H (4'-H)), 6.99 (m, 2 H (2'''-H and 6'''-H)), 8.18 (m, 2 H (3'''-H and 5'''-H)). ^{13}C-NMR (150.88 MHz; 16.9 °C; CDCl$_3$) δ ppm 28.4 (1''''-(CH$_3$)$_3$), 31.8 (3-C and 5-C), 42.9 (2-C and 6-C), 46.9 (4-C), 55.8 (4''-OCH$_3$), 56.2 (2''-OCH$_3$), 79.9 (1''''-C), 96.2 (3''-C), 99.1 (5''-C), 103.1 (1''-C), 104.7 (4'-C), 116.8 (2'''-C and 6'''-C), 126.0 (3'''-C and 5'''-C), 142.8 (1'''-C), 154.2 (6''-C), 154.7 (COO), 158.1 (3'-C), 158.4 (CONH), 159.6 (2''-C), 162.8 (4'''-C), 163.3 (4''-C), 165.3 (5'-C). HRMS (ESI): m/z calculated for C$_{28}$H$_{32}$N$_4$O$_9$+H$^+$ 569.2248, found 569.2250.

3.1.12. Synthesis of (5-(2,4-dimethoxy-6-(4-nitrophenoxy)phenyl)isoxazol-3-yl)(piperidin-1-yl)methanone TU-013 (L-98) 57

5-(2,4-dimethoxy-6-(4-nitrophenoxy)phenyl)isoxazole-3-carboxylic acid (**58**, M. W.: 386.31 g.mol^{-1}; 0.10 g; 0.26 mmol) was dissolved in *N,N*-dimethylacetamide (DMA) (3 mL) followed by addition of *N,N,N',N'*-tetramethyl-o-(benzotriazol-1-yl) uronium tetrafluoroborate (TBTU) (M.W.: 321.08; 0.15 g; 0.47 mmol). After stirring for 15 minutes at room temperature, *N,N*-diisopropylethylamine (DIPEA) (M.W.: 129.24 g.mol^{-1}; 0.10 g; 0.77 mmol) was added, which was followed by the addition of piperidine (M.W.: 85.15 g.mol^{-1}; 0.03 g; 0.35 mmol). The mixture was left to stir at room temperature for 24 hours. Then, the

resultant reaction mixture was poured into a saturated solution of NaHCO₃ (20 mL), which was extracted with ethyl acetate (20 mL × 3), washed with brine (10 mL × 3), dried with MgSO₄ and finally concentrated to give a crude product. The crude was purified by column chromatography (dichloromethane: ethyl acetate 95: 5; L = 11 cm; D = 2 cm) and removal of volatiles resulted in recovery of TU-013 (L-98) **57** as a white solid (0.08 g, 67 %). Melting point = 132 °C – 134 °C. ^{1}H -NMR (600.03 MHz; 24.9 °C; CDCl₃) δ ppm 1.55 (m, 2 H (3-H/5-H)), 1.65 (m, 4 H (4-H and 5-H/3-H)), 3.61 (m, 2 H (2-H/6-H)), 3.68 (m, 2 H (6-H/2-H)), 3.82 (s, 3 H (4''-OCH₃)), 3.90 (s, 3 H (2''-OCH₃)), 6.28 (d, J = 2.34 Hz, 1 H (5''-H)), 6.47 (d, J = 2.34 Hz, 1 H (3''-H)), 6.72 (s, 1 H (4'-H)), 7.00 (m, 2 H (2'''-H and 6'''-H)), 8.16 (m, 2 H (3'''-H and 5'''-H)). ^{13}C-NMR (150.88 MHz; 19.0 °C; CDCl₃) δ ppm 24.5 (4-C), 25.6 (5-C and 3-C), 26.6 (3-C/5-C), 43.6 (6-C/2-C), 48.1 (2-C/6-C), 55.8 (4''-OCH₃), 56.2 (2''-OCH₃), 96.2 (3''-C), 99.1 (5''-C), 103.2 (1''-C), 106.0 (4'-C), 116.9 (2'''-C and 6'''-C), 125.9 (3'''-C and 5'''-C), 142.8 (1'''-C), 154.2 (6''-C), 158.4 (3'-C), 159.6 (2''-C), 159.7 (CON), 162.8 (4'''-C), 163.1 (4''-C), 163.6 (5'-C). HRMS (ESI): m/z calculated for C₂₃H₂₃N₃O₇+H⁺ 454.1614, found 454.1624.
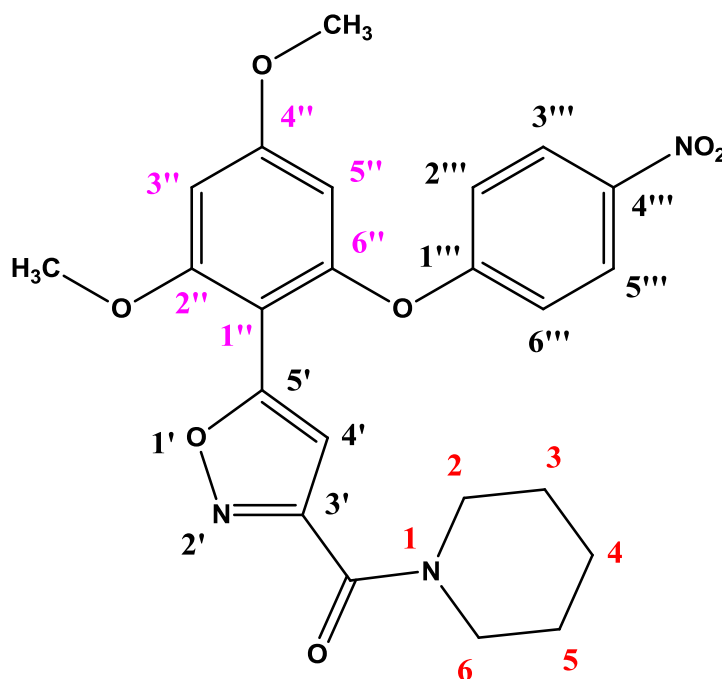
3.1.13. 5-(2, 4-dimethoxy-6-(4-nitrophenoxy) phenyl) isoxazole-3-carboxylic acid TU-014 (L-99) 58

122
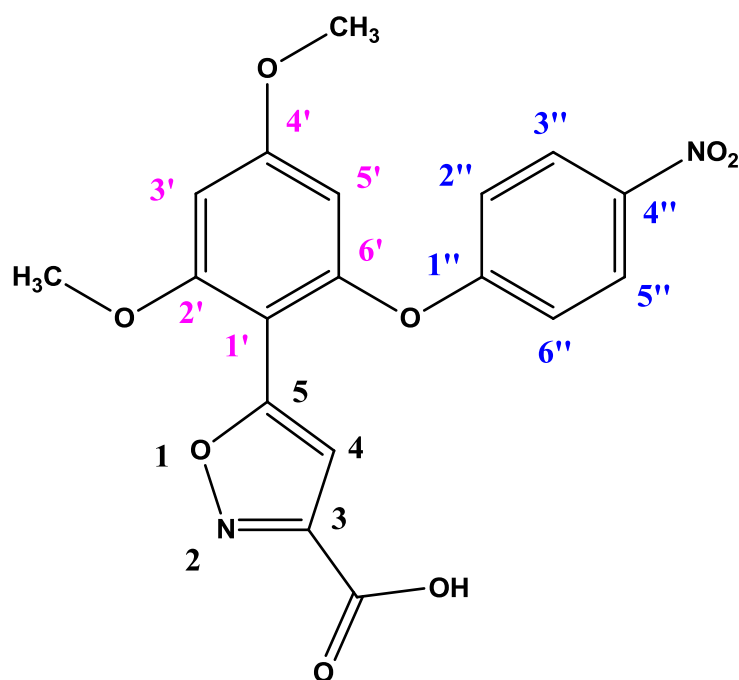
Ethyl 5-(2, 4-dimethoxy-6-(4-nitrophenoxy) phenyl) isoxazole-3-carboxylate (**43**, M.W.: 414.37 g.mol^{-1}; 0.35 g; 0.84 mmol) was dissolved in deionised water (10 mL) and KOH (M.W.: 56.11; 0.24 g; 4.28 mmol) was added. The mixture was stirred at 80 °C for an overnight. After cooling down, 1 M HCl (10 mL) was added which was accompanied by precipitating of the desired compound TU-014 (L-99) **58**. The aqueous layer was removed and the solid dried in the oven. The product was obtained as a brown solid (0.24 g, 75 %). Melting point = 153 °C – 155 °C. ^{1}H -NMR (600.03 MHz; 19.0 °C; DMSO) δ ppm 3.87 (s, 3 H (4'-OCH$_3$)), 3.95 (s, 3 H (2'-OCH$_3$)), 6.57 (d, J = 2.01 Hz, 1 H (5'-H)), 6.77 (d, J = 2.01 Hz, 1 H (3'-H)), 6.88 (s, 1 H (4-H)), 7.15 (d, J = 9.17 Hz, 2 H (2''-H and 6''-H), 8.25 (d, J = 9.17 Hz, 2 H (3''-H and 5''-H)). ^{13}C-NMR (150.88 MHz; 19.0 °C; CDCl$_3$) δ ppm 57.0 (4'-OCH$_3$), 57.5 (2'-OCH$_3$), 97.6 (3'-C), 100.7 (5'-C), 102.9 (1'-C), 106.4 (4-C), 117.9 (2''-C and 6''-C), 127.1 (3''-C and 5''-C), 143.3 (1''-C), 154.5 (6'-C), 157.7 (3-C), 160.4 (2'-C), 161.8 (COOH), 163.4 (4''-C), 164.3 (4'-C), 165.8 (5-C). HRMS (ESI): m/z calculated for C$_{18}$H$_{14}$N$_2$O$_8$+H$^+$ 387.0828, found 387.0820.

3.1.14. 5-(2, 4-dimethoxy-6-(4-nitrophenoxy) phenyl)-*N*-(2-(4-methylpiperazin-1-yl) ethyl) isoxazole-3-carboxamide TU-015 (L-100) 59

5-(2, 4-dimethoxy-6-(4-nitrophenoxy) phenyl) isoxazole-3-carboxylic acid (**58**, M.W.: 386.31 g.mol^{-1}; 0.15 g; 0.39 mmol) was dissolved in DMA (3 ml) and TBTU (M.W.: 321.08 g.mol^{-1}; 0.15 g; 0.47 mmol) was added. After stirring for 15 minutes at room temperature, DIPEA (M.W.: 129.24 g.mol^{-1}; 0.2 ml; 0.15 g; 1.16 mmol) was added. Afterwards, 2-(4-methylpiperazin-1-yl) ethanamine (M.W.: 143.23 g.mol^{-1}; 0.06 g; 0.42 mmol) was added and the reaction mixture left to stir at room temperature for 48 hours. The resultant mixture was then poured into a saturated solution of NaHCO$_3$ (20 mL), extracted with ethyl acetate (20 mL × 3), washed with brine (10 mL × 3), dried with MgSO$_4$ and finally concentrated to obtain a crude product. The crude was purified with column chromatography (CHCl$_3$: MeOH 95: 5) and solvents removed to give a white powder (0.13 g, 65 %). Melting point = 144 °C – 145 °C. ^{1}H -NMR (600.03 MHz; 25.0 °C; CDCl$_3$) δ ppm 2.29 (s, 3 H (4''-CH$_3$)), 2.55 (m, 10 H (2'-H and 2''-H and 3''-H and 5''-H and 6''-H)), 3.50 (q, J = 5.65 Hz, 2 H (1'-H)), 3.82 (s, 3 H (4'''-OCH$_3$)), 3.91 (s, 3 H (2'''-OCH$_3$)), 6.27 (d, J = 2.04 Hz, 1 H (5'''-H)), 6.47 (d, J = 2.04 Hz, 1 H (3'''-H)), 6.91 (s, 1 H (4-H)), 7.01 (d, J = 9.16 Hz, 2 H (2'''''-H and 6'''''-H)), 7.23 (s, 1 H (CONH)), 8.18 (d, J = 9.16 Hz, 2 H (3'''''-H and 5'''''-H)). ^{13}C-NMR (150.89 MHz; 25.0 °C; CDCl$_3$) δ ppm 36.1 (1'-C), 45.9 (4''-CH$_3$), 52.8 (2''-C and 6''-C), 55.0 (3''-C and 5''-C), 55.8 (4'''-OCH$_3$), 56.2 (2'''-OCH$_3$), 56.3 (2'-C), 96.2 (3'''-C), 99.0 (5'''-C), 103.2 (1'''-C), 104.8 (4-C), 116.9 (2'''''-C and 6'''''-C), 126.0 (3'''''-C and 5'''''-C), 142.9 (1'''''-C), 154.3 (6'''-C), 158.3 (3-C), 159.1 (CONH), 159.7 (2'''-C), 162.7 (4'''''-C), 163.2 (4'''-C), 165.0 (5-C). HRMS (ESI): m/z calculated for C$_{25}$H$_{29}$N$_5$O$_7$+H$^+$ 512.2145, found 512.2152.

3.1.15. Synthesis of 5-(2,4-dimethoxy-6-(4-nitrophenoxy)phenyl)-*N*-(1-methylpiperidin-4-yl)isoxazole-3-carboxamide TU-016 (L-14) 60
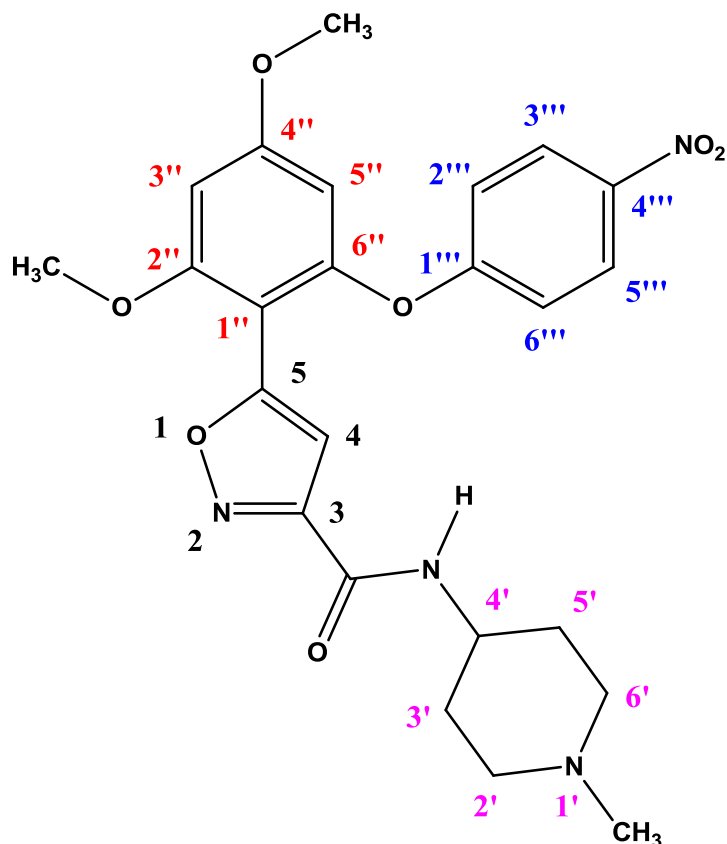
5-(2, 4-dimethoxy-6-(4-nitrophenoxy) phenyl) isoxazole-3-carboxylic acid (**58**, M.W.: 386.31 g.mol^{-1}; 0.17 g; 0.44 mmol) was dissolved in DMA (3 mL) and TBTU (M.W.: 321.08 g.mol^{-1}; 0.17 g; 0.53 mmol) added. After stirring for 15 minutes, DIPEA (M.W.: 129.24 g.mol^{-1}; 0.17 g; 1.32 mmol) and 1-methyl-4-piperidinamine (M.W.: 114.19 g.mol^{-1}; 0.05 g; 0.44 mmol) were ad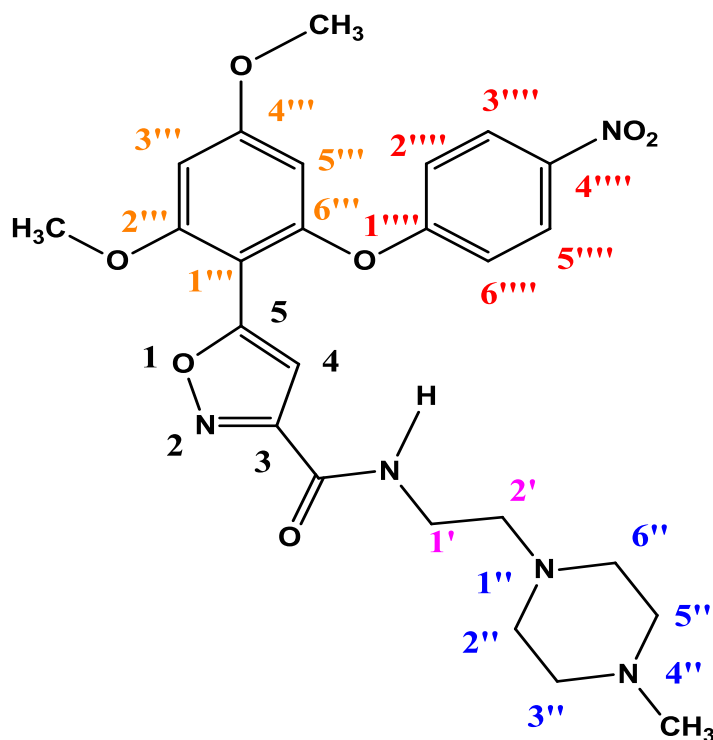ded and the mixture left to stir at room temperature for 24 hours. The resultant mixture was then poured into a saturated solution of NaHCO$_3$ (20 mL), extracted with ethyl acetate (20 mL × 3), washed with brine (10 mL × 3), dried with MgSO$_4$ and later filtered and concentrated to give a crude product. The crude was purified by column flash chromatography (CHCl$_3$: MeOH 95: 5; L = 8 cm; D = 1.75 cm) to give an orange solid (0.12 g, 57%). Melting point = 175 °C – 177 °C. ^{1}H -NMR (600.03 MHz; 25.0 °C; CDCl$_3$) δ ppm 1.57 (qd, 4 × *J* = 3.65 Hz, 2 H (3'-H/5'-H)), 1.98 (m, 2 H (5'-H/3'-H)), 2.12 (t, *J* = 9.03 Hz, 2 H (2'-H/6'-H)), 2.28 (s, 3 H (1'-CH$_3$)), 2.79 (s, 2 H (6'-H/2'-H)), 3.82 (s, 3 H (4''-OCH$_3$)), 3.90 (m, 4 H (4'-H and 2''-OCH$_3$)), 6.27 (d, *J* = 2.26 Hz, 1 H (5''-H)), 6.47 (d, *J* = 2.26 Hz, 1

H (3''-H)), 6.68 (d, J = 8.01 Hz, 1 H (CONH)), 6.91 (s, 1 H (4-H)), 6.99 (m, 2 H (2'''-H and 6'''-H)), 8.17 (m, 2 H (3'''-H and 5'''-H)). ^{13}C-NMR (150.88 MHz; 25.0 °C; CDCl$_3$) δ ppm 31.9 (3'-C and 5'-C), 46.1 (4'-C and 1'-CH$_3$), 54.3 (2'-C and 6'-C), 55.8 (4''-OCH$_3$), 56.2 (2''-OCH$_3$), 96.2 (3''-C), 99.1 (5''-C), 103.2 (1''-C), 104.7 (4-C), 116.8 (2'''-C and 6'''-C), 126.0 (3'''-C and 5'''-C), 142.8 (1'''-C), 154.2 (6''-C), 158.3 (3-C), 158.4 (CONH), 159.6 (2''-C), 162.8 (4'''-C), 163.3 (4''-C), 165.1 (5-C). HRMS (ESI): m/z calculated for C$_{24}$H$_{26}$N$_4$O$_7$+H$^+$ 483.1880, found 483.1879.

3.1.16. Synthesis of 5-(2, 4-dimethoxy-6-(4-nitrophenoxy) phenyl)-*N*-(1, 2, 2, 6, 6-pentamethylpiperidin-4-yl) isoxazole-3-carboxamide TU-017 (L-102) 61

5-(2, 4-dimethoxy-6-(4-nitrophenoxy) phenyl) isoxazole-3-carboxylic acid (**58**, M. W.: 386.31 g.mol^{-1}; 0.15 g; 0.39 mmol) was dissolved in DMA (3 mL) and TBTU (M.W.: 386.31 g.mol^{-1}; 0.15 g; 0.47 mmol) was added. After stirring for 15 minutes, DIPEA (M.W.: 129.24 g.mol^{-1}; 0.15 g; 1.16 mmol) and 4-amino-1, 2, 2, 6, 6-pentamethylpiperidine (M.W.: 170.30 g.mol^{-1}; 0.07 g; 0.41 mmol) were added and the reaction mixture left to stir at room

temperature for 24 hours. The resultant mixture was poured into a saturated solution of NaHCO$_3$, extracted with ethyl acetate (20 mL × 3), washed with brine (10 mL × 3), dried with MgSO$_4$, filtered and concentrated to give a crude product. The crude was purified by column chromatography (dichloromethane: methanol 98: 2; L = 10 cm; D = 1.75 cm) and solvents removed to give a red solid (0.12 g, 57%). Melting point = 125 °C – 127 °C. ^{1}H - NMR (600.03 MHz; 25.0 °C; CDCl$_3$) δ ppm 1.14 (m, 12 H (2'-(CH$_3$)$_2$ and 6'-(CH$_3$)$_2$)), 1.39 (m, 2 H (3'-H/5'-H)), 1.85 (dd, 2 × J = 3.56 Hz, 2 H (5'-H/3'-H)), 2.27 (s, 3 H (1'-CH$_3$)), 3.83 (s, 3 H (4''-OCH$_3$)), 3.91 (s, 3 H (2''-OCH$_3$)), 4.29 (m, 1 H (4'-H)), 6.28 (d, J = 2.30 Hz, 1 H (5''-H), 6.47 (d, J = 2.30 Hz, 1 H (3''-H), 6.58 (d, J = 6.53 Hz, 1 H (CONH)), 6.89 (s, 1 H (4-H)), 6.99 (m, 2 H (2'''-H and 6'''-H)), 8.17 (m, 2 H (3'''-H and 5'''-H)). ^{13}C-NMR (150.88 MHz; 25.0 °C; CDCl$_3$) δ ppm 20.1 (2'-(CH$_3$)$_2$)/6'-(CH$_3$)$_2$), 28.2 (1'-CH$_3$), 33.1 ((6'-CH$_3$)$_2$ or 2'-(CH$_3$)$_2$), 41.8 (4'-C), 46.8 (3'-C and 5'-C), 55.2 (2'-C and 6'-C), 55.8 (4''-OCH$_3$), 56.2 (2''-OCH$_3$), 96.2 (3''-C), 99.1 (5''-C), 103.2 (1''-C), 104.7 (4-C), 116.7 (2'''-C and 6'''-C), 126.0 (3'''-C and 5'''-C), 142.8 (1'''-C), 154.1 (6''-C), 158.3 (3-C), 158.3 (CONH), 159.6 (2''-C), 162.8 (4'''-C), 163.2 (4''-C), 165.1 (5-C). HRMS (ESI): m/z calculated for C$_{28}$H$_{34}$N$_4$O$_7$+H$^+$ 539.2506, found 539.2520.
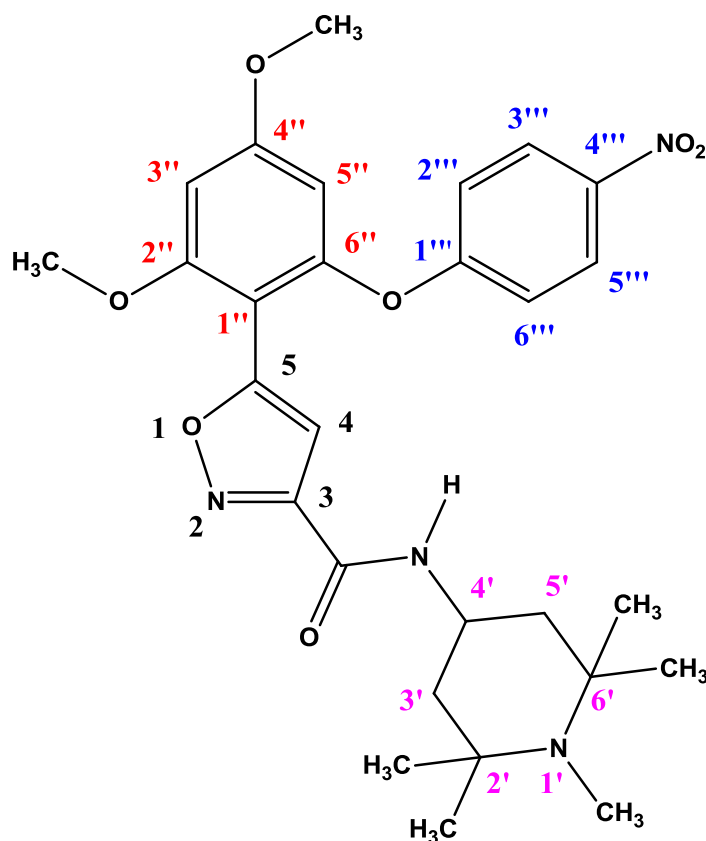
3.1.17. Synthesis of 5-(2,4-dimethoxy-6-(4-nitrophenoxy)phenyl)-*N*-(piperidin-4-yl)isoxazole-3-carboxamide TU-018 (L-103) 50

Tert-butyl 4-(5-(2,4-dimethoxy-6-(4-nitrophenoxy)phenyl)isoxazole-3-carboxamido)piperidine-1-carboxylate (**49**, M.W.: 568.58 g.mol^{-1}; 0.60 g; 1.06 mmol) was dissolved in 4.0 M HCl in dioxane (5 mL) and the mixture was left to stir overnight under argon. Then, HCl was neutralized with KOH and the mixture was poured into ice water (100 mL) and extracted with chloroform (30 mL × 3). The extracted organic layer was dried with MgSO$_4$, filtered and concentrated to give a crude product. The crude was purified by column chromatography (dichloromethane: methanol 95: 5; L = 7 cm; D = 1.75 cm) and the solvents removed to give TU-018 (L-103) **50** as a yellow solid (0.44 g, 89%). Melting point = 70 °C – 72 °C. ^{1}H -NMR (600.03 MHz; 25.0 °C; CDCl$_3$) δ ppm 1.40 (m, 2 H (3'-H/5'-H), 1.98 (m, 2 H (5'-H/3'-H)), 2.71 (td, 3 × *J* = 2.58 Hz, 2 H (2'-H/6'-H)), 3.09 (dt, 2 × *J* = 3.64 Hz, 2 H (6'-H/2'-H)), 3.82 (s, 3 H (4''-OCH$_3$)), 3.91 (s, 3 H (2''-OCH$_3$)), 4.01 (m, 1 H (4'-H)), 6.27 (d, *J* = 2.28 Hz, 1 H (5''-H)), 6.47 (d, *J* = 2.28 Hz, 1 H(3''-H)), 6.70 (d, *J* = 8.26 Hz 1 H (CONH)), 6.92 (s, 1 H (4-H)), 7.00 (m, 2 H (2'''-H and 6'''-H)), 8.18 (m, 2 H (3'''-H and 5'''-H)). ^{13}C-NMR (150.88 MHz; 25.0 °C; CDCl$_3$) δ ppm 33.2 (3'-C and 5'-C), 45.3 (2'-C

and 6'-C), 47.1 (4'-C), 55.8 (4''-OCH$_3$), 56.2 (2''-OCH$_3$), 96.2 (3''-C), 99.1 (5'-C), 103.2 (1''-C), 104.8 (4-C), 116.8 (2'''-C and 6'''-C), 126.0 (3'''-C and 5'''-C), 142.8 (1'''-C), 154.2 (6''-C), 158.2 (CONH), 158.3 (3-C), 159.6 (2''-C), 162.8 (4'''-C), 163.3 (4''-C), 165.1 (5-C). HRMS (ESI): m/z calculated for C$_{23}$H$_{24}$N$_4$O$_7$+H$^+$ 469.1723, found 469.1732.

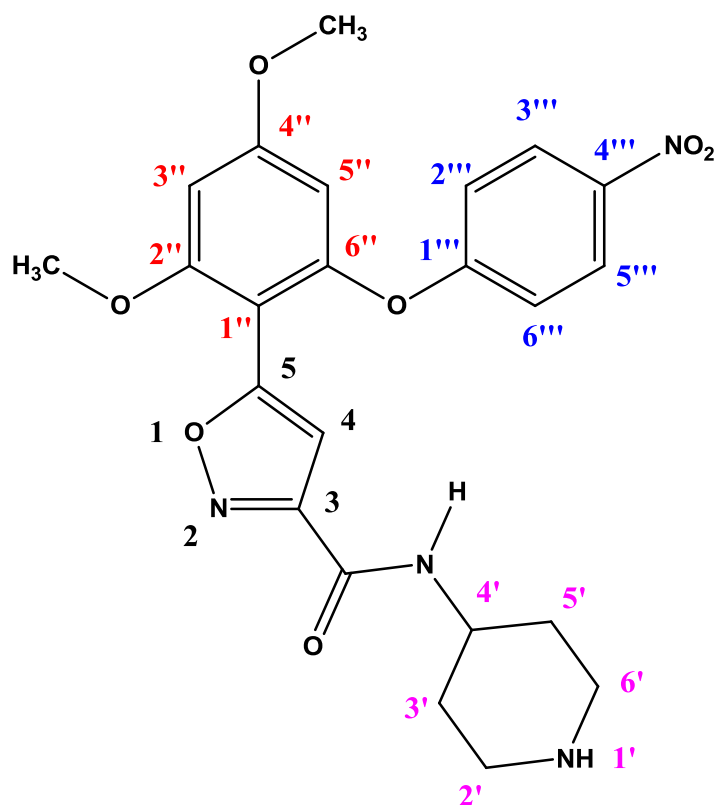### 3.1.18. Synthesis 5-(2,4-dimethoxy-6-(4-nitrophenoxy)phenyl)-*N*-(1-isopropylpiperidin-4-yl)isoxazole-3-carboxamide TU-019 (L-104) 51
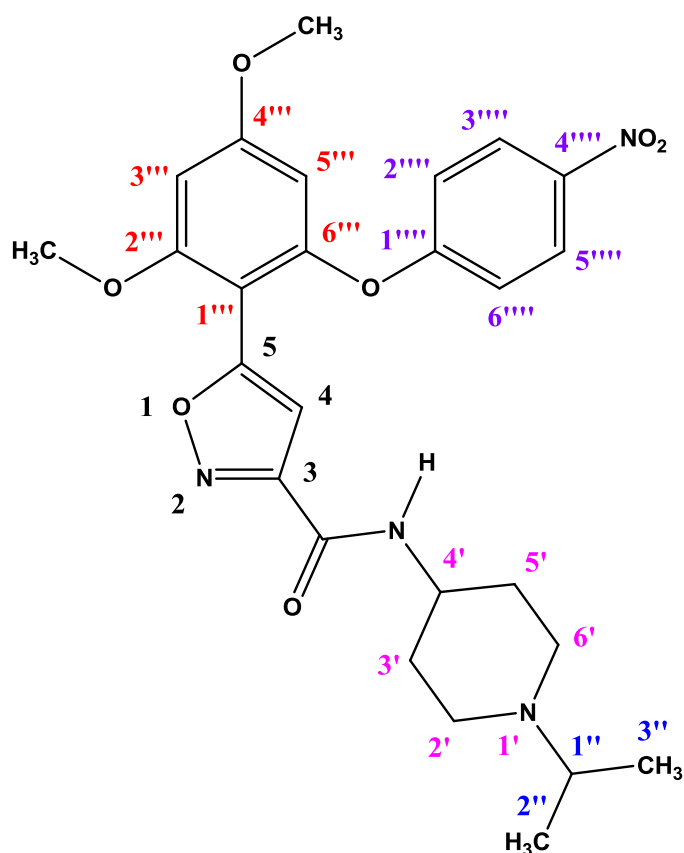
5-(2, 4-dimethoxy-6-(4-nitrophenoxy) phenyl)-N-(piperidin-4-yl) isoxazole-3-carboxamide hydrochloride (**50**, M.W.: 504.92 g.mol^{-1}; 0.19 g; 0.38 mmol) was dissolved in DMA (3 ml) and acetone (M.W.: 58.08 g.mol^{-1}; 0.10 g; 4.65 mmol) was added. After stirring for a few minutes, sodium triacetoxyborohydride (M.W.: 211.94 g.mol^{-1}; 0.36 g; 1.70 mmol) was added and the reaction mixture was left to stir at room temperature for 24 hours. The resultant mixture was then dissolved in ethyl acetate (40 mL), washed with brine (15 mL × 3), dried with MgSO$_4$, filtered and concentrated to give a crude product. The crude was purified with

column chromatography (dichloromethane: methanol 95: 5; L = 7 cm; D = 1.75 cm), and after concentration of the solvents TU-019 (L-104) **51** was isolated as a yellow solid (0.01 g, 5%). Melting point = 80 °C – 82 °C. ^{1}H -NMR (600.03 MHz; 25.0 °C; CDCl$_3$) δ ppm 1.27 (d, J = 6.66 Hz, 6 H (2''-CH$_3$ and 3''-CH$_3$)), 2.12 (br s, 4 H (3'-CH$_2$ and 5'-CH$_2$)), 2.67 (br s, 2 H (2'-CH$_2$/6'-CH$_2$)), 3.24 (m, 3 H (1''-H and 6'-CH$_2$/2'-CH$_2$)), 3.82 (s, 3 H (4'''-OCH$_3$)), 3.90 (s, 3 H (2'''-OCH$_3$)), 4.08 (m, 1 H (4'-H)), 6.26 (d, J = 2.25 Hz, (1 H (5'''-H)), 6.46 (d, J = 2.25 Hz, 1 H (3'''-H)), 6.88 (s, 1 H (4-H)), 6.99 (m, 2 H (2'''''-H and 6'''''-H)), 7.03 (d, J = 7.57 Hz, 1 H (CONH)), 8.17 (m, 2 H (3'''''-H and 5'''''-H)). ^{13}C-NMR (150.88 MHz; 25.0 °C; CDCl$_3$) δ ppm 17.2 (2''-C and 3''-C), 29.4 (3'-C and 5'-C), 45.3 (4'-C), 47.1 (2'-C and 6'-C), 55.8 (4'''-OCH$_3$), 56.2 (2'''-OCH$_3$), 56.4 (1''-C), 96.2 (3'''-C), 99.1 (5'''-C), 103.1 (1'''-C), 104.6 (4-C), 116.8 (2'''''-C and 6'''''-C), 126.0 (3'''''-C and 5'''''-C), 142.9 (1'''''-C), 154.2 (6'''-C), 157.9 (3-C), 158.8 (C=O), 159.6 (2'''-C), 162.7 (4'''''-C), 163.3 (4'''-C), 165.2 (5-C). HRMS (ESI): m/z calculated for C$_{26}$H$_{30}$N$_4$O$_7$+H$^+$ 511.2193, found 511.2191.

3.2. PLDH (malaria) assay

Plasmodium falciparum (strain 3D7) cells were maintained in RPMI (Roswell Park Memorial Institute) 1640 medium containing 2 mM L-glutamine and 25 mM Hepes (Lonza). The medium was further supplemented with 5% Albumax II, 20 mM glucose, 0.65 mM hypoxanthine, 60 μg/ml gentamycin and 2-4% hematocrit human red blood cells. The parasites were then cultured at 37 °C under an atmosphere of 5% CO$_2$, 5% O$_2$, and 90% N$_2$ in sealed T75 culture flasks. The compounds to be screened (in a range of 100 μM to 0.0061 μM) were then added in duplicate to the parasite cultures in 96-well plates and incubated for 48 hours in a 37 °C CO$_2$ incubator. After 48 hours, the plates were removed from the incubator, and then 20 μL of culture removed from each well and mixed with 125 μL of a mixture of Malstat solution and NBT/PES (nitro blue tetra-zolium + phenazine ethosulphate) solution in a fresh 96-well plate in order to measure the activity of the parasite lactate dehydrogenase (PLDH) enzyme in the cultures. Absorbance readings at 620 nm were recorded for each well, the number of parasites in that well deduced, and then the % parasite viability in comparison to the untreated controls was calculated. The anti-malarial drug chloroquine was used as a drug standard.

3.3. Cell cytotoxicity assay

The compounds to be screened (in concentrations ranging from 100 μM to 0.0061 μM) were incubated in two replicates in 96-well plates containing human cervix adenocarcinoma (HeLa) cells for 48 hours. The number of cells surviving the drug was then determined using the resazurin reagent (TOX8-Kit (Sigma)) and then reading the fluorescence in the multi-well plate reader. The percentage cell viability for each compound concentration was determined by comparing the fluorescence of the treated wells with the untreated wells. The cell apoptosis inducer drug, emetine was used as a drug standard.

3.4. Virtual screening

Virtual screening of the candidate compounds was done using Autodock vina. First, the energy of each ligand molecule was minimized with Vegazz, and then the ligand and the target protein (*Pf*Hsp90 (PDB code: 3K60) or human Hsp90 (PDB code: 1BYQ)) were prepared with Autodock tools for docking with Autodock vina. Compounds whose estimate maximum length was less than 15 Å, they were docked in a 25 Å × 25 Å × 25 Å box and those with an estimated maximum length equal to or larger than 15 Å were docked in a 30 Å × 30 Å × 30 Å box. The intention was to increase the docking speed, thus minimizing the docking time while preserving the accuracy of predictions of the binding modes of the candidate compounds. Then, the ratio between the inhibition constants of the best binding modes of each ligand for human Hsp90 and *Pf*Hsp90 was determined and used to decide which compounds would selectively bind to *Pf*Hsp90 in the presence of human Hsp90. The approximate dimensions of the ligand compounds were determined using Vegazz.

Reference List

(1) Marco A.Biamonte, Jutta Wanner, Karine G.Le Roche. Recent advances in malaria drug discovery. Bioorganic and Medicinal Chemistry Letters 2013; 23:2829-2843.

(2) WHO. World malaria report 2014. 1-228. 2014.
Ref Type: Report

(3) WHO. World malaria report 2013. 1, 1-255. 2013.
Ref Type: Report

(4) Alan F.Cowman, Drew Berry, Jake Baum. The cellular and molecular basis for malaria parasite invasion of the human red blood cell. The Journal of Cell Biology 2012; 198(6):961-971.

(5) Evelyn Siu, Alexander Ploss. Modeling malaria in humanized mice: opportunities and challenges. Annals of the New York Academy of Sciences 2015; 1342:29-36.

(6) Sinclair D., Zani B., Donegan S., Olliaro P., Garner P. Artemisinin-based combination therapy for treating uncomplicated malaria (Review). The Cochrane Collaboration 2009;(4):1-264.

(7) Angelika Sturm, Rogerio Amino, Claudia van de Sand, Tommy Regen, Silke Retzlaff, Annika Rennenberg et al. Manipulation of host hepatocytes by the malaria parasite for delivery into liver sinusoids. Science 2006; 313:1287-1291.

(8) Michelle J.Boyle, Danny W.Wilson, James G.Beeson. New approaches to studying *Plasmodium falciparum* merozoite invasion and insights into invasion biology. International Journal for Parasitology 2013; 43:1-10.

(9) Leann Tilley, Matthew W.A.Dixon, Kiaran Kirk. The *Plasmodium falciparum*-infected red blood cell. The International Journal of Biochemistry and Cell Biology 2011; 43:839-842.

(10) Arjen M.Dondorp, Shunmay Yeung, Lisa White, Chea Nguon, Nicholas P.J.Day, Duong Socheat et al. Artemisinin resistance : current status and scenarios for containment. Nature Reviews Microbiology 2010; 8:272-280.

(11) Timothy N.C.Wells, Rob Hooft van Huijsduijnen, Wesley C.Van Voorhis. Malaria medicine : a glass half full ? Nature Reviews Drug Discovery 2015; 14:424-442.

(12) Oliver Billker, Sandrine Dechamps, Rita Tewari, Gerald Wenig, Blandine Franke-Fayard, Volker Brinkmann. Calcium and a calcium-dependent protein kinase regulate gamete formation and mosquito transmission in a malaria parasite. Cell 2004; 117:503-514.

(13) David S.Guttery, Anthony A.Holder, Rita Tewari. Sexual development in *Plasmodium*: lessons from functional analyses. PLoS Pathogens 2012; 8(1):1-3.

(14) Chris J.Janse, Peter F.J.van der Klooster, Hugo J.van der Kaay, Mels van der Ploeg, J.Prosper Overdulve. DNA synthesis in *Plasmodium berghei* during asexual and sexual development. Molecular and Biochemical Parasitology 1986; 20:173-182.

(15) Victoria Carter, Adéla M.L.Nacer, Ann Underhill, Robert E.Sinden, Hilary Hurd. Minimum requirements for ookinete to oocyst transformation in *Plasmodium*. International Journal for Parasitology 2007; 37:1221-1232.

(16) Fouzia Farooq, Elke S.Bergmann-Leitner. Immune escape mechanisms are *Plasmodium*'s secret weapons foiling the success of potent and persistently efficacious malaria vaccines. Clinical Immunology 2015; 161:136-143.

(17) RTS SCTP. Efficacy and safety of RTS,S/AS01 malaria vaccine with or without a booster dose in infants and children in Africa : final results of a phase 3, individually randomised, controlled trial. Lancet 2015; 386:31-45.

(18) Kasara Na-Bangchang, Juntra Karbwang. Current status of malaria chemotherapy and the role of pharmacology in antimalarial drug research and development. Fundamental and Clinical Pharmacology 2009; 23:387-409.

(19) Ines Petersen, Richard Eastman, Michael Lanzer. Drug-resistant malaria: molecular mechanisms and implications for public health. FEBS Letters 2011; 585:1551-1562.

(20) Hasifa Bukirwa, Adoke Yeka, Moses R.Kamya, Ambrose Talisuna, Kristin Banek, Nathan Bakyaita et al. Artemisinin combination therapies for treatment of uncomplicated malaria in Uganda. PLoS Clinical Trials 2006; 1(1):1-8.

(21) S.R.Meshnick, T.E.Taylor, S.Kamchonwongpaisan. Artemisinin and the antimalarial endoperoxides: from herbal remedy to targeted chemotherapy. Microbiological Reviews 1996; 60(2):301-315.

(22) T.K.Mutabingwa. Artemisinin-based combination therapies (ACTs): Best hope for malaria treatment but inaccessible to the needy ! Acta Tropica 2005; 95:305-315.

(23) Shannon Takala-Harrison, Miriam K.Laufer. Antimalarial drug resistance in Africa: key lessons for the future. Annals of the New York Academy of Sciences 2015; 1342:62-67.

(24) Ajay Kumar, Deepika Paliwal, Deepika Saini, Aman Thakur, Shilpy Aggarwal, Dhirender Kaushik. A comprehensive review on synthetic approach for antimalarial agents. European Journal of Medicinal Chemistry 2014; 85:147-178.

(25) Susan A.Charman, Sarah Arbe-Barnes, Ian C.Bathurst, Reto Brun, Michael Campbell, William N.Charman et al. Synthetic ozonide drug candidate OZ439 offers new hope for a single-dose cure of uncomplicated malaria. Proceedings of the National Academy of Sciences 2011; 108(11):4400-4405.

(26) Hussien O.Alkadi. Antimalarial drug toxicity: a review. Chemotherapy 2007; 53:385-391.

(27) Dharmendar Rathore, Dewal Jani, Rana Nagarkatti, Sanjai Kumar. Heme detoxification and antimalarial drugs-Known mechanisms and future prospects. Drug Discovery Today: Therapeutic Strategies 2006; 3(2):153-158.

(28) Cecilia P.Sanchez, Petra Rohrbach, Jeremy E.McLean, David A.Fidock, Wilfred D.Stein, Michael Lanzer. Differences in *trans*-stimulated chloroquine efflux kinetics are linked to *Pf*CRT in *Plasmodium falciparum*. Molecular Microbiology 2007; 64(2):407-420.

(29) Michelle L.Gatton, Laura B.Martin, Qin Cheng. Evolution of resistance to sulfadoxine-pyrimethamine in *Plasmodium falciparum*. Antimicrobial Agents and Chemotherapy 2004; 48(6):2116-2123.

(30) Rajinder Kumar, Alla Musiyenko, Sailen Barik. The heat shock protein 90 of *Plasmodium falciparum* and antimalarial activity of its inhibitor, geldanamycin. Malaria Journal 2003; 2(30):1-11.

(31) Rani Pallavi, Nainita Roy, Rishi Kumar Nageshan, Pinaki Talukdar, Soundara Raghavan Pavithra, Raghunath Reddy et al. Heat shock protein 90 as a drug target against protozoan infections. Biochemical characterization of Hsp90 from *Plasmodium falciparum* and *Trypanosoma Evansi* and evaluation of its inhibitor as a candidate drug. The Journal of Biological Chemistry 2010; 285(49):37964-37975.

(32) Rinku Dutta, Masayori Inouye. GHKL, an emergent ATPase/kinase superfamily. Trends in Biochemical Sciences 2000; 25(1):24-25.

(33) Tai Wang, William H.Bisson, Pascal Mäser, Leonardo Scapozza, Didier Picard. Differences in conformational dynamics between *Plasmodium falciparum* and human Hsp90 othologues enable the structure-based discovery of pathogen-selective inhibitors. Journal of Medicinal Chemistry 2014; 57:2524-2535.

(34) Chrisostomos Prodromou, S.Mark Roe, Ronan O'Brien, John E.Ladbury, Peter W.Piper, Laurence H.Pearl. Identification and structural characterization of the ATP/ADP-binding site in the Hsp90 molecular chaperone. Cell 1997; 90:65-75.

(35) Taras Makhnevych, Walid A.Houry. The role of Hsp90 in protein complex assembly. Biochimica et Biophysica Acta 2012; 1823:674-682.

(36) Soundara Raghavan Pavithra, Ranjit Kumar, Utpal Tatu. Systems analysis of chaperone networks in the malarial parasite *Plasmodium falciparum*. Plos Computational Biology 2007; 3(9):1701-1716.

(37) Stewart H.Lecker, Alfred L.Goldberg, William E.Mitch. Protein degradation by the ubiquitin-proteasome pathway in normal and disease states. Journal of the American Society of Nephrology 2006; 17:1807-1819.

(38) Alina Röhl, Julia Rohrberg, Johannes Buchner. The chaperone Hsp90: changing partners for demanding clients. Trends in Biochemical Sciences 2013; 38(5):253-262.

(39) Shireen Vali, Rani Pallavi, Shweta Kapoor, Utpal Tatu. Virtual prototyping study shows increased ATPase activity of Hsp90 to be the key determinant of cancer phenotype. Systems and Synthetic Biology 2010; 4:25-33.

(40) Gowrishankar Banumathy, Varsha Singh, Soundara Raghavan Pavithra, Utpal Tatu. Heat shock protein 90 function is essential for *Plasmodium falciparum* growth in human erythrocytes. The Journal of Biological Chemistry 2003; 278(20):18336-18345.

(41) Marylène Péroval, Pierre Péry, Marie Labbé. The heat shock protein 90 of *Eimeria tenella* is essential for invasion of host cell and schizont growth. International Journal of Parasitology 2006; 36:1205-1215.

(42) Martina Wiesgigl, Joachim Clos. Heat shock protein 90 homeostasis controls stage differentiation in *Leishmania donovani*. Molecular Biology of the Cell 2001; 12:3307-3316.

(43) Pablo C.Echeverria, Mariana Matrajt, Omar S.Harb, María P.Zappia, Monica A.Costas, David S.Roos et al. *Toxoplasma gondii* Hsp90 is a potential drug target whose expression and subcellular localization are developmentally regulated. Journal of Molecular Biology 2005; 350:723-734.

(44) Charles E.Stebbins, Alicia A.Russo, Christine Schneider, Neal Rosen, F.Ulrich Hartl, Nikola P.Pavletich. Crystal structure of an Hsp90-geldanamycin complex: targeting of a protein chaperone by an antitumour agent. Cell 1997; 89:239-250.

(45) Kevin D.Corbett, James M.Berger. Strucutre of the ATP-binding domain of *Plasmodium falciparum* Hsp90. Proteins 2010; 78:2738-2744.

(46) Christine J.Martin, Sabine Gaisser, Iain R.Challis, Isabelle Carletti, Barrie Wilkinson, Matthew Gregory et al. Molecular characterization of macbecin as an Hsp90 inhibitor. Journal of Medicinal Chemistry 2008; 51:2853-2857.

(47) Xiao-Li Xu, Qi-chao Bao, Jian-Min Jia, Fang Liu, Xiao-Ke Guo, Ming-ye Zhang et al. CPUY201112, a novel synthetic small-molecule compound and inhibitor of heat shock protein Hsp90, induces p53-mediated apoptosis in MCF-7 cells. Scientific Reports 2016; 6(19004):1-16.

(48) Tai Wang, William H.Bisson, Pascal Mäser, Leonardo Scapozza, Didier Picard. Differences in conformational dynamics between *Plasmodium falciparum* and human Hsp90 othologues enable the structure-based discovery of pathogen-selective inhibitors. Journal of Medicinal Chemistry 2014; 57:2524-2535.

(49) Maria Gabriella Brasca, Sergio Mantegani, Nadia Amboldi, Simona Bindi, Dannica Caronni, Elena Casale et al. Discovery of NMS-E973 as novel, selective and potent

inhibitor of heat shock protein 90 (Hsp90). Bioorganic and Medicinal Chemistry 2013; 21:7047-7063.

(50) Loredana Vesci, Ferdinando Maria Milazzo, Valeria Carollo, Silvia Pace, Giuseppe Giannini. Preclinical antitumor activity of SST0116CL1: a novel heat shock protein 90 inhibitor. International Journal of Oncology 2014; 45:1421-1429.

(51) Chrisostomos Prodromou, S.Mark Roe, Ronan O'Brien, John E.Ladbury, Peter W.Piper, Laurence H.Pearl. Structural basis for inhibition of the Hsp90 molecular chaperone by the antitumor antibiotics radicicol and geldanamycin. Journal of Medicinal Chemistry 1999; 42:260-266.

(52) Dea Shahinas, Asongna Folefoc, Dylan R.Pillai. Targeting *Plasmodium falciparum* Hsp90 : towards reversing antimalarial resistance. Pathogens 2013; 2:33-54.

(53) Edward B.Garon, Richard S.Finn, Habib Hamidi, Judy Dering, Sharon Pitts, Naeimeh Kamranpour et al. The Hsp90 inhibitor NVP-AUY922 potently inhibits non-small cell lung cancer growth. Molecular Cancer Therapeutics 2013; 12(6):890-901.

(54) Dea Shahinas, Gregory MacMullin, Christan Benedict, Ian Crandall, Dylan R.Pillai. Harmine is a potent antimalarial targeting Hsp90 and synergizes with chloroquine and artemisinin. Antimicrobial Agents and Chemotherapy 2012; 56(8):4207-4213.

(55) Barry Panaretou, Chrisostomos Prodromou, S.Mark Roe, Ronan O'Brien, John E.Ladbury, Peter W.Piper et al. ATP binding and hydrolysis are essential to the function of the Hsp90 molecular chaperone *in vivo*. The EMBO Journal 1998; 17(16):4829-4836.

(56) Chrisostomos Prodromou, S.Mark Roe, Ronan O'Brien, John E.Ladbury, Peter W.Piper, Laurence H.Pearl. Structural basis for inhibition of the Hsp90 molecular chaperone by the antitumor antibiotics radicicol and geldanamycin. Journal of Medicinal Chemistry 1999; 42:260-266.

(57) Dea Shahinas, Asongna Folefoc, Dylan R.Pillai. Targeting *Plasmodium falciparum* Hsp90 : Towards reversing antimalarial resistance. Pathogens 2013; 2:33-54.

(58) Riccardo Baruchello, Daniele Simoni, Giuseppina Grisolia, Giuseppina Barbato, Paolo Marchetti, Riccardo Rondanin et al. Novel 3,4-isoxazolediamides as potent inhibitors of chaperone heat shock protein 90. Journal of Medicinal Chemistry 2011; 54:8592-8604.

(59) Paul A.Brough, Wynne Aherne, Xavier Barril, Jenifer Borgognoni, Kathy Boxal, Julie E.Cansfield et al. 4,5-Diarylisoxazole Hsp90 chaperone inhibitors: Potential therapeutic agents for the treatment of cancer. Journal of Medicinal Chemistry 2008; 51(2):196-218.

(60) Xiao-Li Xu, Qi-chao Bao, Jian-Min Jia, Fang Liu, Xiao-Ke Guo, Ming-ye Zhang et al. CPUY201112, a novel synthetic small-molecule compound and inhibitor of heat

shock protein Hsp90, induces p53-mediated apoptosis in MCF-7 cells. Scientific Reports 2016; 6(19004):1-16.

(61) Maria Gabriella Brasca, Sergio Mantegani, Nadia Amboldi, Simona Bindi, Dannica Caronni, Elena Casale et al. Discovery of NMS-E973 as novel, selective and potent inhibitor of heat shock protein 90 (Hsp90). Bioorganic and Medicinal Chemistry 2013; 21:7047-7063.

(62) Giuseppe Giannini, Gianfranco Battistuzzi. Exploring *in vitro* and *in vivo* Hsp90 inhibitors activity against human protozoan parasites . Bioorganic and Medicinal Chemistry Letters 2015; 25:462-465.

(63) A Textbook of Drug Design and Development. Copenhagen: Harwood Academic Publishers , 1992.

(64) Xuan-Yu Meng, Hong-Xing Zhang, Mihaly Mezei, Meng Cui. Molecular docking : a powerful approach for structure-based drug discovery. Current Computer Aided Drug-Design 2011; 7(2):146-157.

(65) Thomas Lengauer, Matthias Rarey. Computational methods for biomolecular docking. Current Opinion in Structural Biology 1996; 6:402-406.

(66) Pawel Szymanski, Magdalena Markowicz, Elzbieta Mikiciuk-Olasik. Adaptation of high-throughput screening in drug discovery-Toxicological screening tests. International Journal of Molecular Sciences 2012; 13:427-452.

(67) Jonathan Greer, John W.Erickson, John J.Baldwin, Michael D.Varney. Application of the three-dimensional structures of protein target molecules in structure-based drug design. Journal of Medicinal Chemistry 1994; 37(8):1035-1054.

(68) Gregory L.Warren, C.Webster Andrews, Anna-Maria Capelli, Brian Clarke, Judith LaLonde, Millard H.Lambert et al. A critical assessment of docking programs and scoring functions. Journal of Medicinal Chemistry 2005; 49:5912-5931.

(69) Oleg Trott, Arthur J.Olson. Software news and update AutoDock Vina: improving the speed and accuracy of docking with a new scoring function, efficient optimization, and multithreading. Journal of Computational Chemistry 2010; 31(2):455-461.

(70) Amy C.Anderson. The Process of structure-based drug design. Chemistry and Biology 2003; 10:787-797.

(71) Vernalis (Cambridge) Limited, Cancer Research Technology Ltd, The Institute of Cancer Research. Isoxazole compounds as inhibitors of heat shock proteins. Great Britain patent WO 2004/072051 A1. 2004 2004.

(72) Maria Gabriella Brasca, Elena Casale, Ron Ferguson, Paolo Polucci, Fabio Zuccotto. Resorcinol derivatives as Hsp90 inhibitors. patent WO 2010/121963. 2010 2010.

(73) Maria Gabriella Brasca, Elena Casale, Ron Ferguson, Paolo Polucci, Fabio Zuccotto. Resorcinol derivatives as Hsp90 inhibitors. United States patent US 2012/0046266 A1. 2012 Feb 2012.

(74) Giuseppe Giannini, Gianfranco Battistuzzi. Exploring *in vitro* and *in vivo* Hsp90 inhibitors activity against human protozoan parasites . Bioorganic and Medicinal Chemistry Letters 2015; 25:462-465.

(75) Ng.Ph.Buu-Hoi, E.Bisagni, R.Royer, C.Router. Oxygen heterocycles. Part VII. Spasmolytic ketones in the benzofuran series, and related compouds. Journal of the Chemical Society 1957;625-628.

(76) Taillefer Marc, Monnier Florian, Tlili Anis. Method for synthesising biaryl ether or biheteroaryl ether. patent WO2012/032261 A1. 2012 2012.

(77) Amita Mishra, Harikrishna Batchu, Kumkum Srivastava, Pratiksha Singh, Pravin K.Shukla, Sanjay Batra. Synthesis and evaluation of new diaryl ether and quinoline hybrids as potential antiplasmodial and antimacrobial agents. Bioorganic and Medicinal Chemistry Letters 2014; 24:1719-1723.

(78) Schnatterer Stefan, Maier Michael, Lochhaas Friederike, Knauf Werner, Seeger Karl. Pesticidal substituted phenylethers. patent WO 2006/119876 A1. 2006 2006.

(79) Qi Zhang, Deping Wang, Xianyang Wang, Ke Ding. (2-Pyridyl)acetone-promoted Cu-catalyzed O-arylation of phenols with aryl iodides, bromides, and chlorides. The Journal of Organic Chemistry 2009; 74:7187-7190.

(80) Taillefer Marc, Xia Ning, Monnier Florian. New catalytic system for cross-coupling reactions. patent WO 2009/071997 A2. 2009 Jun 2009.

(81) Amita Mishra, Harikrishna Batchu, Kumkum Srivastava, Pratiksha Singh, Pravin K.Shukla, Sanjay Batra. Synthesis and evaluation of new diaryl ether and quinoline hybrids as potential antiplasmodial and antimicrobial agents. Bioorganic and Medicinal Chemistry Letters 2014; 24:1719-1723.

(82) Francis A.Carey, Richard J.Sundberg. Aromatic substitution. Advanced Organic Chemistry. Part A : Structure and Mechanisms. New York: Springer Science+Business Media, 2007: 1-1999.

(83) Michael B.Smith, Jerry March. March's Advanced Organic Chemistry. Reactions, mechanisms and structure. New York: John Wiley and Sons, Inc., 2001: 1-2083.

(84) Zhang Yugen, Ying Jackie Y., Zhao Lan. Poly-*N*-heterocyclic carbene transition metal complexes and *N*-heterocyclic carbene transition metal complexes for carbon-sulfur and carbon-oxygen coupling reactions. patent WO 2008/136770 A1. 2008 2008.

(85) Anis Tlili, Florian Monnier, Marc Taillefer. Selective one-pot access to symmetrical or unsymmetrical diaryl ethers by copper-catalysed double arylation of a simple oxygen source. Chemistry-A European Journal 2010; 16:12299-12302.

(86) Sofia Benyahya, Florian Monnier, Michel Wong Chi Man, Catherine Bied, Fouad Ouazzani, Marc Taillefer. Sol-gel immobilized and reusable copper-catalyst for arylation of phenols from aryl bromides. Green Chemistry 2009; 11:1121-1123.

(87) Kassem Beydoun, Henri Doucet. Palladium catalytic system for inhibition of *O*-arylation type reaction and regioselective direct arylation at C2 of phenols. Catalysis Science and Technology 2011; 1:1243-1249.

(88) Manfred Hesse, Herbert Meier, Bernd Zeeh. Spectroscopic Methods in Organic Chemistry. 1st Edition ed. New York: Georg Thieme Verlag, 1997.

(89) Michel Keller, Mykhailo Ianchuk, Sonia Ladeira, Marc Taillefer, Anne-Marie Caminade, Jean-Pierre Majoral et al. Synthesis of dendritic β-diketones and their application in copper-catalyzed diaryl ether formation. European Journal of Organic Chemistry 2012;1056-1062.

(90) Ning Xia, Marc Taillefer. Copper- or Iron-catalyzed arylation of phenols from respectively aryl chlorides and aryl iodides. Chemistry-A European Journal 2008; 14:6037-6039.

(91) Laszlo Borka, John K.Haleblian. Crystal polymorphism of pharmaceuticals. Acta Pharmaceutica Jugoslavica 1990; 40:71-94.

(92) Joe T.Adams, Charles R.Hauser. The acylation of methyl ketones with aliphatic esters by means of sodium amide. Synthesis of β-diketones of the type $RCOCH_{2COR}$. Journal of the American Chemical Society 1944; 66(7):1220-1222.

(93) Eugene H.Man, Frederic W.Swamer, Charles R.Hauser. The Claisen acylation of methyl ketones with branched chain aliphatic esters. Journal of American Chemical Society 1951; 73(3):901-903.

(94) Jingbao Liu, Faqin Jiang, Yan Jin, Yong Zhang, Jingjing Liu, Wenlu Liu et al. Design, synthesis, and evaluation of 2-substituted ethenesulfonic acid ester derivatives as protein tyrosine phosphatase 1 B inhibitors. European Journal of Organic Chemistry 2012; 57:10-20.

(95) Jun Yuan, Michael Gulianello, Stéphane De Lombaert, Robbin Brodbeck, Andrzej Kieltyka, Kevin J.Hodgetts. 3-aryl pyrazolo[4,3-d]pyrimidine derivatives: nonpeptide CRF-1 antagonists. Bioorganic and Medicinal Chemistry Letters 2002; 12:2133-2136.

(96) Alas Michel, Favreliere Didier, Chassaing Serge, Barrier Alain, Henrio Francoise. Preparation de composes beta-dicarbonyles comprenant deux etapes successives mettant en jeu des agents alcalins de nature differente. France patent 2842519. 2002 Jul 2002.

(97) Proteostasis theurapeutics I. Methods of modulating CFTR activity. US patent WO 2014/210159. 2014 2014.

(98) Drysdale Martin James, Dymock Brian William, Finch Harry, Webb Paul, McDonald Edward, James Karen Elizabeth et al. Isoxazole compounds as inhibitors of heat shock proteins. Great Britain patent WO 2004/072051 A1. 2004 2004.

(99) Zbigniew Grobelny. Chemical methods for ether-bond cleavage by electron-transfer reagents. European Journal of Organic Chemistry 2004;2973-2982.

(100) Alexey Fedorov, Anton A.Toutov, Nicholas A.Swisher and Robert H.Grubbs. Lewis-base silane activation: from reductive cleavage of aryl ethers to selective *ortho*-silylation. Chemical Science 2013; 4:1640-1645.

(101) Vinod Kumar, Kamalneet Kaur. Fluorinated isoxazolines and isoxazoles : A synthetic perspective. Journal of Fluorine Chemistry 2015; 180:55-97.

(102) A.Voskiene, V.Mickevicius. Cyclization of chalcones to isoxazole and pyrazole derivatives. Chemistry of Heterocyclic Compounds 2009; 45(12):1485-1488.

(103) Guolan Dou, Pan Xu, Qiang Li, Yukun Xi, Zhibin Huang, Daqing Shi. Clean and efficient synthesis of isoxazole derivatives in aqueous media. Molecules 2013; 18:13645-13653.

(104) Alan R.Katritzky, Daryl L.Ostercamp, Taher I.Yousaf. The mechanism of heterocyclic ring closure. Tetrahedron 1987; 43(22):5171-5186.

(105) Qian Han, Xingquan Xiong, Sizhong Li. An efficient, green and scale-up synthesis of amides from esters and amines catalyzed by Ru-MACHO catalyst under mild conitions. Catalysis Communications 2015; 58:85-88.

(106) Hisatoyo Yazawa, Kunihiko Tanaka, Kazuo Kariyone. The reaction of carboxylic esters with boron tribromide. A convenient method for the synthesis of amides and transesterification. Tetrahedron Letters 1974; 46:3995-3996.

(107) Zhenrong Guo, Eric D.Dowdy, Wen-Sen Li, Richard Polniaszek, Edward Delaney. A novel method for the mild and selective amidation of diesters and the amidation of monoesters. Tetrahedron Letters 2001; 42:1843-1845.

(108) Richard Frank Goldstein. Process for the production of carboxylic acid amides. United States patent 1,972,142. 1934 1934.

(109) J.Cossy, C.Pale-Grosdemange. A convenient synthesis of amides from carboxylic acids and primary amines. Tetrahedron Letters 1989; 30(21):2771-2774.

(110) Vijaya R.Pattabiraman, Jeffrey W.Bode. Rethinking amide bond synthesis. Nature 2011; 480:471-479.

(111) Rachel M.Lanigan, Pavel Starkov, Tom D.Sheppard. Direct synthesis of amides from carboxylic acids and amines using $B(OCH_2CF_3)_3$. The Journal of Organic Chemistry 2013; 78:4512-4523.

(112) Jeffrey A.Dodge, Mark G.Stocksdale, Kennan J.Fahey, C.David Jones. Regioselectivity in the alkaline thiolate deprotection of aryl methyl ethers. The Journal of Organic Chemistry 1995; 60:739-741.

(113) Chun-Lan Zou, Hong Ji, Guang-Bo Xie, Dong-Lin Chen, Feng-Peng Wang. An effective O-demethylation of some C_{19}-diterpenoid alkaloids with HBr-glacial acetic acid. Journal of Asian Natural Products Research 2008; 10(11):1063-1067.

(114) L.Canonica, B.Rindone, E.Santaniello, C.Scolastico. A total synthesis of mycophenolic acid. Tetrahedron Letters 1971; 28:2691-2692.

(115) Li Zuo, Shanyan Yao, Wei Wang, Wenhu Duan. An efficient method for demethylation of aryl methyl ethers. Tetrahedron Letters 2008; 49:4054-4056.

(116) L.Canonica, B.Rindone, E.Santaniello, C.Scolastico. A total synthesis of mycophenolic acid, some analogues and some biogenetic intermidiates. Tetrahedron 1972; 28(Demethylation; BBr$_3$):4395-4404.

(117) Yvan Guindon, Christiane Yoakim, Howard E.Morton. Cleavage of carbon-oxygen bonds. Dimethylboron bromide. A new reagent for ether cleavage. Tetrahedron Letters 1983; 24(29):2969-2972.

(118) Steven A.Weissman, Daniel Zewge. Recent advances in ether dealkylation. Tetrahedron 2005; 61:7833-7863.

(119) I.T.Harrison. Cleavage of alkyl aryl ethers with lithium iodide. Chemical Communications 1969;616.

(120) Angela M.Bernard, M.Rossella Ghiani, Pier Paolo Piras, Antonio Rivoldini. Dealkylation of activated alkyl aryl ethers using lithium chloride in dimethylformamide. Communications 1989;287-289.

(121) Michael B.Smith, Jerry March. March's Advanced Organic Chemistry. Reactions, Mechanisms and Structure. New York: John Wiley and Sons, Inc., 2001: 1-2083.

(122) Mrinal K.Nayak, Asit K.Chakraborti. Chemoselective aryl alkyl ether cleavage by thiophenolate anion through its *in situ* generation in catalytic amount. Tetrahedron Letters 1997; 38(50):8749-8752.

(123) State of California. California safe drinking water and toxic enforcement act of 1986 (Proposition 65). Section 1-Section 8. 1986.

Ref Type: Bill/Resolution

(124) Robert R.Dystra. Hexamethylphosphoric triamide. e-EROS Encyclopedia of Reagents for Organic Synthesis. John Wiley and Sons, Ltd, 2001.

(125) Douglas A.Keller, Craig E.Marshall, K.P.Lee. Subchronic nasal toxicity of hexamethylphosphoramide administered to rats orally for 90 days. Fundamental and applied toxicology 1997; 40:15-29.

(126) K.P.Lee, N.C.Chromey, R.Culik, J.R.Barnes, P.W.Schneider. Toxicity of N-methyl-2-pyrrolidone (NMP) : Teratogenic, subchronic, and two-year inhalation studies. Toxicological Sciences 1987; 9(2):222-235.

(127) Abolghasen Jouyban, Mohammad A.A.Fakhree, Ali Shayanfar. Review of pharmaceutical applications of N-methyl-2-pyrrolidone. Journal of Pharmacy and Pharmaceutical Sciences 2010; 13(4):524-535.

(128) Pietro Cogolli, Lorenzo Testaferri, Marco Tingoli, Marcello Tiecco. Alkyl thioether activation of the nitro displacement by alkanethiol anions. A useful process for the synthesis of poly[(alkylthio)benzenes]. Journal of Organic Chemistry 1979; 44(15):2636-2642.

(129) Pietro Cogolli, Filippo Maiolo, Lorenzo Testaferri, Marco Tingoli, Marcello Tiecco. Nucleophilic aromatic substitution reactions of unactivated aryl halides with thiolate ions in hexamethylphosphoramide. Journal of Organic Chemistry 1979; 44(15):2642-2646.

(130) Jih Ru Hwu, Shwu-Chen Tsay. Counterattack reagents sodium trimethylsilanethiolate and hexamethyldisilathiane in the bis-O-demethylation of aryl mehtyl ethers. The Journal of Organic Chemistry 1990; 55:5987-5991.

(131) G.I.Feutrill, R.N.Mirrington. Demethylation of aryl methyl ethers with thioethoxide ion in dimethylformamide. Tetrahedron Letters 1970; 16:1327-1328.

(132) Emmanuel S.Akinboye, Oladapo Bakare. Biological activities of emetine. The Open Natural Products Journal 2011; 4:8-15.

(133) Mihail S.Iordanov, Olga P.Ryabinina, John Wong, et.al. Molecular determinants of apoptosis induced by the cytotoxic ribonuclease onconase: evidence for cytotoxic mechanisms different from inhibition of protein synthesis. Cancer Research 2000; 60:1983-1994.

Appendices

Appendix I: Calculated binding energies (in kcal/mol) of different ligands bound to human Hsp90 (1BYQ)

Code of ligand	Experiment no										Mean	S.D.	Ki(μM)
	1	2	3	4	5	6	7	8	9	10			
L-1	-9.3	-9.4	-9.4	-9.4	-9.4	-9.4	-9.4	-9.4	-9.4	-9.4	**-9.4**	**0.0**	0.1
L-2	-8.4	-8.4	-8.3	-8.4	-8.4	-8.3	-8.4	-8.3	-8.3	-8.4	**-8.4**	**0.1**	0.7
L-3	-6.7	-6.7	-6.7	-6.7	-6.7	-6.7	-6.7	-6.7	-6.7	-6.7	**-6.7**	**0.0**	12.3
L-4	-8.3	-8.3	-8.3	-8.4	-8.3	-8.4	-8.4	-8.1	-8.4	-8.4	**-8.3**	**0.1**	0.8
L-5	-6.9	-7.0	-7.0	-7.0	-7.0	-7.0	-7.0	-7.0	-7.0	-6.9	**-7.0**	**0.0**	7.6
L-6	-6.9	-6.9	-6.9	-6.9	-6.9	-6.9	-6.9	-6.9	-6.9	-6.8	**-6.9**	**0.0**	8.9
L-7	-7.7	-7.8	-7.7	-7.7	-7.7	-7.7	-7.7	-7.7	-7.7	-7.7	**-7.7**	**0.0**	2.2
L-8	-7.8	-7.7	-7.7	-7.7	-7.7	-7.8	-7.8	-7.8	-7.6	-7.7	**-7.7**	**0.1**	2.2
L-9	-7.5	-7.4	-7.6	-7.4	-7.4	-7.5	-7.5	-7.5	-7.5	-7.5	**-7.5**	**0.1**	3.3
L-10	-7.7	-7.7	-7.7	-7.7	-7.7	-7.8	-7.8	-7.7	-7.7	-7.7	**-7.7**	**0.0**	2.2
L-11	-8.0	-8.2	-8.0	-7.9	-8.0	-8.0	-8.2	-8.0	-7.9	-7.9	**-8.0**	**0.1**	1.3
L-12	-6.9	-6.8	-6.8	-6.9	-7.0	-7.0	-6.9	-6.9	-6.9	-6.7	**-6.9**	**0.1**	9.1
L-13	-6.7	-6.8	-6.7	-6.7	-6.9	-7.0	-6.6	-6.8	-6.7	-6.7	**-6.8**	**0.1**	11.1
L-14	-8.4	-8.4	-8.4	-8.4	-8.6	-8.4	-8.4	-8.4	-8.4	-8.4	**-8.4**	**0.1**	0.7
L-15	-7.3	-7.3	-7.4	-7.4	-7.3	-7.3	-7.3	-7.3	-7.3	-7.3	**-7.3**	**0.0**	4.3
L-16	-7.4	-7.5	-7.5	-7.5	-7.4	-7.5	-7.3	-7.5	-7.5	-7.4	**-7.5**	**0.1**	3.5
L-17	-7.9	-7.9	-8.0	-7.8	-7.8	-7.9	-7.9	-7.9	-7.9	-8.0	**-7.9**	**0.1**	1.6
L-18	-6.9	-6.9	-6.9	-6.8	-6.9	-6.9	-6.9	-6.9	-6.9	-6.9	**-6.9**	**0.0**	8.9
L-19	-7.4	-7.5	-7.4	-7.4	-7.4	-7.4	-7.4	-7.4	-7.4	-7.4	**-7.4**	**0.0**	3.7
L-20	-8.6	-8.5	-8.6	-8.6	-8.6	-8.6	-8.6	-8.5	-8.5	-8.5	**-8.6**	**0.1**	0.5
L-21	-8.4	-8.4	-8.4	-8.4	-8.4	-8.4	-8.5	-8.4	-8.4	-8.4	**-8.4**	**0.0**	0.7
L-22	-6.5	-6.5	-6.5	-6.5	-6.5	-6.5	-6.5	-6.5	-6.5	-6.5	**-6.5**	**0.0**	17.2
L-23	-6.6	-6.6	-6.6	-6.6	-6.6	-6.6	-6.6	-6.6	-6.5	-6.6	**-6.6**	**0.0**	14.8
L-24	-6.6	-6.7	-6.6	-6.5	-6.5	-6.6	-6.6	-6.5	-6.5	-7.0	**-6.6**	**0.2**	14.3
L-25	-7.8	-7.7	-7.7	-7.7	-7.7	-7.7	-7.7	-7.8	-7.7	-7.7	**-7.7**	**0.0**	2.2
L-26	-8.7	-8.6	-8.6	-8.6	-8.6	-8.5	-8.6	-8.6	-8.5	-8.6	**-8.6**	**0.1**	0.5
L-27	-8.6	-7.6	-7.6	-8.6	-8.6	-8.6	-8.6	-8.6	-7.6	-8.6	**-8.3**	**0.5**	0.8
L-28	-8.1	-8.1	-8.1	-8.1	-8.1	-8.1	-8.1	-8.1	-8.1	-8.1	**-8.1**	**0.0**	1.2
L-29	-9.0	-9.0	-9.0	-9.0	-9.0	-9.0	-9.0	-9.0	-8.9	-9.0	**-9.0**	**0.0**	0.3
L-30	-8.4	-8.3	-8.3	-8.4	-8.4	-8.3	-8.3	-8.4	-8.4	-8.4	**-8.4**	**0.1**	0.7
L-31	-8.1	-8.1	-8.2	-8.1	-8.1	-8.1	-8.1	-8.1	-8.1	-8.2	**-8.1**	**0.0**	1.1
L-32	-7.7	-7.7	-7.7	-7.7	-7.7	-7.7	-7.7	-7.7	-7.7	-7.7	**-7.7**	**0.0**	2.3
L-33	-7.5	-7.5	-7.7	-7.4	-7.5	-7.5	-7.4	-7.5	-7.5	-7.4	**-7.5**	**0.1**	3.2

L-34	-8.0	-8.0	-8.1	-8.1	-8.0	-8.1	-8.1	-8.0	-8.0	-8.0	**-8.0**	**0.1**	1.3
L-35	-7.9	-7.8	-7.8	-7.8	-7.8	-7.8	-7.8	-7.8	-7.8	-7.9	**-7.8**	**0.0**	1.9
L-36	-8.0	-7.9	-7.7	-8.0	-8.0	-7.9	-8.0	-8.0	-7.7	-8.0	**-7.9**	**0.1**	1.6
L-37	-8.0	-8.0	-8.0	-8.1	-8.0	-8.0	-8.0	-8.0	-8.0	-8.1	**-8.0**	**0.0**	1.3
L-38	-7.8	-7.8	-7.8	-7.8	-7.8	-7.8	-7.8	-7.8	-7.8	-7.8	**-7.8**	**0.0**	1.9
L-39	-7.7	-7.7	-7.7	-7.6	-7.7	-7.7	-7.7	-7.7	-7.7	-7.7	**-7.7**	**0.0**	2.3
L-40	-7.8	-7.7	-7.9	-7.8	-7.8	-7.9	-7.8	-7.8	-7.8	-7.8	**-7.8**	**0.1**	1.9
L-41	-7.5	-7.5	-7.5	-7.5	-7.5	-7.5	-7.5	-7.5	-7.5	-7.5	**-7.5**	**0.0**	3.2
L-42	-7.5	-7.5	-7.5	-7.5	-7.5	-7.5	-7.5	-7.6	-7.5	-7.5	**-7.5**	**0.0**	3.1
L-43	-7.4	-7.5	-7.4	-7.4	-7.3	-7.4	-7.4	-7.4	-7.4	-7.5	**-7.4**	**0.1**	3.7
L-44	-7.5	-7.6	-7.5	-7.6	-7.6	-7.6	-7.5	-7.5	-7.5	-7.5	**-7.5**	**0.1**	3.0
L-45	-7.5	-7.5	-7.5	-7.5	-7.6	-7.6	-7.5	-7.5	-7.5	-7.6	**-7.5**	**0.0**	3.0
L-46	-6.8	-6.7	-6.7	-6.7	-6.7	-6.7	-6.8	-6.7	-6.8	-6.7	**-6.7**	**0.0**	11.7
L-47	-7.0	-7.2	-6.9	-6.9	-6.9	-7.3	-6.9	-6.9	-7.0	-7.2	**-7.0**	**0.2**	7.1
L-48	-7.9	-7.9	-7.8	-7.9	-7.9	-7.9	-7.9	-7.9	-7.9	-7.8	**-7.9**	**0.0**	1.7
L-49	-7.9	-7.9	-8.0	-7.6	-8.0	-7.9	-7.9	-7.9	-7.9	-7.8	**-7.9**	**0.1**	1.7
L-50	-7.9	-7.9	-7.8	-7.9	-7.9	-7.9	-7.8	-7.9	-7.9	-8.2	**-7.9**	**0.1**	1.6
L-51	-7.8	-7.8	-7.9	-7.9	-7.9	-7.6	-7.8	-7.8	-7.9	-7.7	**-7.8**	**0.1**	1.9
L-52	-8.2	-8.2	-8.2	-8.2	-8.2	-8.2	-8.2	-8.2	-8.2	-8.1	**-8.2**	**0.0**	1.0
L-53	-8.0	-7.6	-7.6	-7.8	-8.1	-7.6	-7.9	-7.8	-7.6	-8.0	**-7.8**	**0.2**	1.9
L-54	-8.2	-8.2	-8.2	-8.2	-8.2	-8.2	-8.2	-8.2	-8.2	-8.2	**-8.2**	**0.0**	1.0
L-55	-8.3	-7.9	-8.3	-8.3	-8.2	-8.3	-8.2	-8.1	-8.3	-8.3	**-8.2**	**0.1**	0.9
L-56	-8.0	-7.7	-7.7	-7.7	-7.9	-8.0	-7.8	-8.0	-7.7	-8.0	**-7.9**	**0.1**	1.8
L-57	-9.0	-8.4	-8.7	-8.6	-9.0	-8.7	-8.7	-8.6	-8.7	-8.6	**-8.7**	**0.2**	0.4
L-58	-8.6	-8.6	-8.5	-8.6	-8.5	-8.6	-8.6	-8.6	-8.6	-8.6	**-8.6**	**0.0**	0.5
L-59	-8.4	-8.3	-8.3	-8.3	-8.6	-8.9	-8.8	-8.2	-8.3	-8.3	**-8.4**	**0.2**	0.7
L-60	-8.8	-8.8	-8.8	-8.8	-8.8	-8.9	-8.8	-8.8	-8.8	-8.8	**-8.8**	**0.0**	0.3
L-61	-8.8	-8.7	-8.7	-8.7	-8.7	-8.8	-8.8	-8.7	-8.7	-8.7	**-8.7**	**0.0**	0.4
L-62	-8.3	-8.3	-8.3	-8.3	-8.3	-8.3	-8.3	-8.3	-8.3	-8.3	**-8.3**	**0.0**	0.8
L-63	-8.4	-8.4	-8.3	-8.4	-8.4	-8.3	-8.4	-8.3	-8.4	-8.0	**-8.3**	**0.1**	0.8
L-64	-8.8	-8.9	-8.8	-8.9	-9.0	-8.8	-8.9	-8.8	-8.9	-8.8	**-8.9**	**0.1**	0.3
L-65	-8.6	-8.6	-8.6	-8.6	-8.5	-8.6	-8.6	-8.6	-8.6	-8.6	**-8.6**	**0.0**	0.5
L-66	-8.7	-8.7	-8.7	-8.7	-8.8	-8.7	-8.6	-8.7	-8.7	-8.7	**-8.7**	**0.0**	0.4
L-67	-8.2	-8.2	-7.8	-8.0	-8.1	-7.9	-8.2	-7.9	-8.2	-8.0	**-8.1**	**0.2**	1.3
L-68	-8.2	-8.3	-8.2	-8.2	-8.2	-8.2	-8.2	-8.2	-8.2	-8.2	**-8.2**	**0.0**	1.0
L-69	-7.9	-8.1	-7.7	-7.7	-8.5	-8.1	-8.4	-7.7	-7.8	-7.7	**-8.0**	**0.3**	1.5
L-70	-8.7	-8.7	-8.7	-8.7	-8.7	-8.7	-8.7	-8.7	-8.7	-8.7	**-8.7**	**0.0**	0.4
L-71	-8.5	-8.3	-8.5	-8.2	-8.3	-8.5	-8.4	-8.4	-8.5	-8.4	**-8.4**	**0.1**	0.7
L-72	-8.0	-8.2	-8.0	-8.0	-8.0	-8.2	-8.0	-8.1	-8.1	-8.2	**-8.1**	**0.1**	1.2
L-73	-8.6	-8.6	-8.6	-8.5	-8.5	-8.5	-8.6	-8.5	-8.4	-8.4	**-8.5**	**0.1**	0.6
L-74	-8.3	-8.8	-8.9	-8.5	-8.7	-8.7	-8.3	-8.6	-8.7	-8.5	**-8.6**	**0.2**	0.5
L-75	-8.9	-8.8	-8.8	-8.9	-8.7	-8.8	-8.8	-8.7	-8.8	-8.8	**-8.8**	**0.1**	0.4
L-76	-7.9	-7.9	-7.9	-7.9	-7.9	-7.9	-8.2	-7.8	-8.4	-8.4	**-8.0**	**0.2**	1.3

L-77	-8.8	-9.1	-9.1	-9.1	-8.6	-9.0	-8.8	-9.0	-9.2	-9.2	**-9.0**	**0.2**	0.3
L-78	-8.6	-8.5	-8.5	-8.4	-8.6	-8.4	-8.3	-8.4	-8.6	-8.4	**-8.5**	**0.1**	0.6
L-79	-9.7	-9.7	-9.2	-9.7	-9.6	-8.6	-9.1	-9.6	-9.6	-8.0	**-9.3**	**0.6**	0.2
L-80	-8.8	-9.0	-8.9	-8.8	-8.9	-8.8	-8.9	-9.0	-9.0	-8.9	**-8.9**	**0.1**	0.3
L-81	-9.1	-8.8	-8.6	-8.9	-9.1	-9.0	-8.9	-8.8	-8.7	-8.9	**-8.9**	**0.2**	0.3
L-82	-7.8	-7.8	-7.9	-7.8	-7.7	-7.7	-7.7	-7.7	-7.8	-7.7	**-7.8**	**0.1**	2.1
L-83	-7.4	-7.4	-7.8	-7.4	-7.4	-7.4	-7.4	-7.4	-7.7	-7.8	**-7.5**	**0.2**	3.1
L-84	-9.4	-9.4	-9.4	-9.4	-9.3	-9.4	-9.2	-9.5	-9.3	-9.3	**-9.4**	**0.1**	0.1
L-85	-9.1	-9.1	-9.1	-9.2	-9.1	-8.9	-9.5	-9.2	-9.5	-9.1	**-9.2**	**0.2**	0.2
L-86	-9.3	-9.5	-9.2	-9.5	-9.3	-9.5	-9.5	-9.5	-9.4	-9.5	**-9.4**	**0.1**	0.1
L-87	-8.1	-8.1	-8.1	-8.1	-8.1	-8.1	-8.1	-8.2	-8.1	-8.1	**-8.1**	**0.0**	1.1
L-88	-9.5	-9.6	-9.6	-9.6	-9.6	-9.5	-9.6	-9.6	-9.7	-9.4	**-9.6**	**0.1**	0.1
L-89	-9.8	-9.7	-9.8	-9.8	-9.4	-9.8	-9.8	-9.8	-9.8	-9.7	**-9.7**	**0.1**	0.1
L-90	-7.7	-7.6	-7.6	-7.7	-7.7	-7.7	-7.8	-7.6	-7.7	-7.8	**-7.7**	**0.1**	2.3
L-91	-8.9	-8.8	-7.9	-8.6	-8.5	-8.8	-7.9	-7.9	-8.8	-8.9	**-8.5**	**0.4**	0.6
L-92	-7.2	-7.7	-7.7	-7.8	-8.0	-7.8	-7.4	-7.8	-7.8	-7.7	**-7.7**	**0.2**	2.3
L-93	-8.4	-8.4	-8.4	-8.4	-8.4	-8.4	-8.4	-8.4	-8.4	-8.4	**-8.4**	**0.0**	0.7
L-94	-8.5	-8.6	-8.5	-8.5	-8.5	-8.6	-8.5	-8.5	-8.5	-8.5	**-8.5**	**0.0**	0.6
L-95	-9.1	-9.1	-9.1	-9.1	-9.1	-9.1	-9.1	-9.1	-9.1	-9.1	**-9.1**	**0.0**	0.2
L-96	-7.0	-7.0	-7.0	-6.9	-7.0	-7.1	-7.0	-7.0	-7.0	-7.0	**-7.0**	**0.0**	7.4
L-97	-8.3	-8.3	-8.4	-8.4	-8.2	-8.3	-8.3	-8.4	-8.5	-8.4	**-8.4**	**0.1**	0.8
L-98	-8.6	-8.5	-8.5	-8.6	-8.5	-8.5	-8.5	-8.5	-8.6	-8.5	**-8.5**	**0.0**	0.6
L-99	-7.9	-7.9	-7.8	-7.9	-7.8	-7.8	-7.8	-7.8	-7.8	-7.9	**-7.8**	**0.1**	1.8
L-100	-8.3	-8.0	-8.2	-8.2	-8.2	-8.3	-8.2	-8.2	-8.3	-8.2	**-8.2**	**0.1**	1.0
L-102	-8.7	-8.5	-8.8	-8.6	-8.7	-8.5	-8.6	-8.6	-8.6	-8.6	**-8.6**	**0.1**	0.5
L-103	-7.9	-7.7	-7.9	-7.7	-8.2	-7.8	-7.9	-7.8	-7.8	-7.7	**-7.8**	**0.2**	1.8
L-104	-8.5	-8.3	-8.2	-8.5	-8.3	-8.2	-8.3	-8.3	-8.2	-8.5	**-8.3**	**0.1**	0.8

Appendix II: Calculated binding energies (in kcal/mol) of different ligands bound to
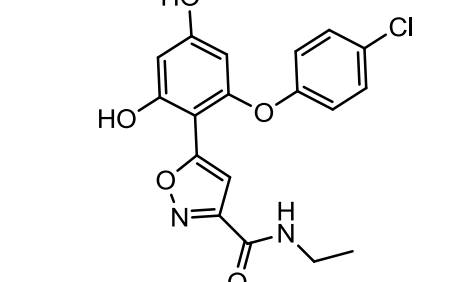***Pf*Hsp90 (3K60)**
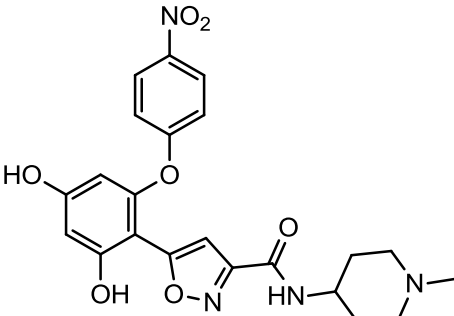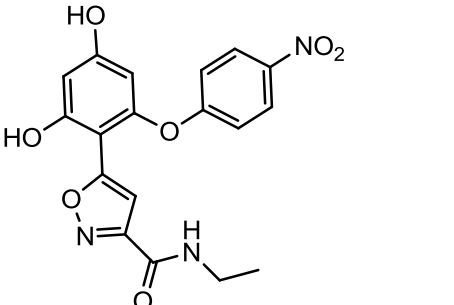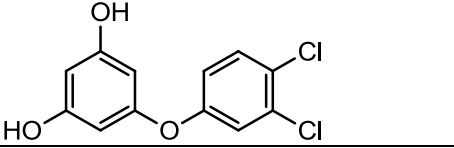
Code of ligand	Experiment no										Mean	S.D.	Ki (μM)
	1	2	3	4	5	6	7	8	9	10			
L-1	-9.0	-9.0	-8.9	-9.0	-9.0	-9.0	-9.0	-9.0	-9.0	-9.0	**-9.0**	**0.0**	0.3
L-2	-8.1	-8.3	-8.6	-7.8	-8.5	-7.9	-7.8	-7.9	-7.8	-7.9	**-8.1**	**0.3**	1.2
L-3	-6.9	-6.9	-6.9	-6.9	-6.9	-6.9	-6.9	-6.9	-6.9	-6.9	**-6.9**	**0.0**	8.8
L-4	-8.3	-7.8	-8.0	-7.8	-8.0	-7.9	-7.9	-7.9	-7.9	-7.9	**-7.9**	**0.1**	1.5
L-5	-6.8	-6.8	-6.8	-6.5	-6.8	-6.8	-6.8	-6.5	-6.8	-6.8	**-6.7**	**0.1**	11.5
L-6	-6.5	-6.5	-6.5	-6.5	-6.5	-6.5	-6.5	-6.5	-6.5	-6.5	**-6.5**	**0.0**	17.2
L-7	-7.6	-7.6	-7.3	-7.5	-7.6	-7.6	-7.6	-7.6	-7.6	-7.5	**-7.6**	**0.1**	2.9
L-8	-7.9	-7.8	-7.8	-7.9	-7.8	-7.8	-7.9	-7.8	-7.9	-7.8	**-7.8**	**0.1**	1.8
L-9	-7.5	-7.6	-7.6	-7.7	-7.6	-7.6	-7.5	-7.6	-7.4	-7.5	**-7.6**	**0.1**	2.9

L-10	-7.5	-7.5	-7.5	-7.5	-7.7	-7.5	-7.7	-7.5	-7.5	-7.6	**-7.6**	**0.1**	2.9
L-11	-8.1	-8.0	-8.1	-8.1	-8.0	-8.1	-8.1	-8.1	-8.1	-8.0	**-8.1**	**0.0**	1.2
L-12	-6.6	-6.6	-6.6	-6.6	-6.6	-6.6	-6.6	-6.6	-6.6	-6.6	**-6.6**	**0.0**	14.5
L-13	-6.6	-6.7	-6.7	-6.7	-6.6	-6.7	-6.6	-6.7	-6.6	-6.6	**-6.7**	**0.1**	13.4
L-14	-8.1	-8.3	-8.6	-8.3	-8.7	-8.7	-8.7	-8.5	-8.6	-8.7	**-8.5**	**0.2**	0.6
L-15	-7.4	-7.4	-7.4	-7.3	-7.3	-7.5	-7.5	-7.4	-7.3	-7.2	**-7.4**	**0.1**	4.0
L-16	-7.4	-7.2	-7.3	-7.4	-7.4	-7.3	-7.3	-7.4	-7.3	-7.5	**-7.4**	**0.1**	4.1
L-17	-7.5	-7.5	-7.7	-7.6	-7.6	-7.5	-7.6	-7.7	-7.6	-7.6	**-7.6**	**0.1**	2.7
L-18	-7.3	-7.3	-7.3	-7.3	-7.3	-7.2	-7.3	-7.3	-7.3	-7.3	**-7.3**	**0.0**	4.5
L-19	-7.2	-7.2	-7.3	-7.3	-7.3	-7.3	-7.3	-7.2	-7.2	-7.2	**-7.3**	**0.1**	4.8
L-20	-8.4	-8.1	-8.4	-8.4	-8.4	-8.4	-8.1	-8.4	-8.4	-8.4	**-8.3**	**0.1**	0.8
L-21	-8.3	-8.3	-8.3	-8.3	-8.3	-8.3	-8.3	-8.3	-8.3	-8.3	**-8.3**	**0.0**	0.8
L-22	-6.4	-6.4	-6.4	-6.4	-6.5	-6.4	-6.5	-6.4	-6.4	-6.4	**-6.4**	**0.0**	19.7
L-23	-6.6	-6.6	-6.6	-6.6	-6.6	-6.6	-6.6	-6.6	-6.6	-6.6	**-6.6**	**0.0**	14.5
L-24	-6.5	-6.5	-6.5	-6.5	-6.5	-6.5	-6.5	-6.5	-6.5	-6.5	**-6.5**	**0.0**	17.2
L-25	-7.8	-7.9	-7.8	-7.8	-7.8	-7.9	-7.9	-7.8	-7.8	-7.8	**-7.8**	**0.0**	1.8
L-26	-8.8	-8.8	-8.8	-8.8	-8.8	-8.8	-8.8	-8.8	-8.8	-8.7	**-8.8**	**0.0**	0.4
L-27	-8.6	-8.6	-8.5	-8.6	-8.6	-8.5	-8.6	-8.6	-8.5	-8.6	**-8.6**	**0.0**	0.5
L-28	-8.1	-8.2	-8.1	-8.1	-8.1	-8.2	-8.2	-8.2	-8.1	-8.2	**-8.2**	**0.1**	1.1
L-29	-8.8	-8.8	-8.8	-8.8	-8.9	-8.9	-8.8	-8.9	-8.9	-8.8	**-8.8**	**0.1**	0.3
L-30	-8.5	-8.5	-8.5	-8.5	-8.5	-8.5	-8.5	-8.5	-8.5	-8.5	**-8.5**	**0.0**	0.6
L-31	-9.3	-9.3	-9.3	-9.3	-9.2	-9.3	-9.3	-9.3	-9.3	-9.3	**-9.3**	**0.0**	0.2
L-32	-7.8	-7.8	-7.8	-7.9	-7.9	-7.8	-7.8	-7.9	-7.9	-7.9	**-7.9**	**0.1**	1.8
L-33	-8.0	-7.8	-8.0	-7.7	-7.8	-7.8	-7.8	-8.0	-7.8	-8.0	**-7.9**	**0.1**	1.7
L-34	-7.4	-7.4	-7.6	-7.4	-7.5	-7.5	-7.5	-7.5	-7.5	-7.5	**-7.5**	**0.1**	3.3
L-35	-7.8	-8.0	-8.0	-7.8	-7.7	-7.8	-7.9	-7.7	-7.9	-8.0	**-7.9**	**0.1**	1.7
L-36	-8.0	-7.9	-7.9	-8.0	-8.0	-7.9	-7.9	-8.0	-7.9	-8.0	**-8.0**	**0.1**	1.5
L-37	-8.1	-8.1	-8.1	-8.1	-8.1	-8.2	-8.1	-8.1	-8.1	-8.2	**-8.1**	**0.0**	1.1
L-38	-7.8	-7.4	-7.4	-7.4	-7.3	-7.8	-7.9	-7.9	-7.4	-7.9	**-7.6**	**0.3**	2.6
L-39	-7.7	-7.7	-7.7	-7.7	-7.8	-7.7	-7.7	-7.7	-7.7	-7.7	**-7.7**	**0.0**	2.2
L-40	-7.3	-7.3	-7.3	-7.9	-7.3	-7.9	-7.3	-7.9	-7.2	-7.3	**-7.5**	**0.3**	3.3
L-41	-7.3	-7.2	-7.3	-7.3	-7.3	-7.3	-7.3	-7.3	-7.3	-7.3	**-7.3**	**0.0**	4.5
L-42	-7.6	-7.6	-7.6	-7.6	-7.6	-7.6	-7.6	-7.6	-7.6	-7.6	**-7.6**	**0.0**	2.7
L-43	-7.1	-7.1	-7.1	-6.9	-7.1	-7.1	-7.1	-7.1	-7.1	-7.1	**-7.1**	**0.1**	6.5
L-44	-7.4	-7.4	-7.3	-7.1	-7.4	-7.3	-7.3	-7.3	-7.4	-7.3	**-7.3**	**0.1**	4.3
L-45	-7.4	-7.4	-7.4	-7.4	-7.4	-7.4	-7.4	-7.4	-7.4	-7.4	**-7.4**	**0.0**	3.8
L-46	-7.2	-7.2	-7.2	-7.2	-7.2	-7.0	-7.2	-7.1	-7.2	-7.2	**-7.2**	**0.1**	5.6
L-47	-7.2	-7.2	-7.2	-7.0	-7.0	-7.2	-7.2	-7.3	-7.0	-7.2	**-7.2**	**0.1**	5.7
L-48	-7.9	-7.9	-7.8	-7.8	-7.8	-7.7	-7.7	-7.7	-7.7	-7.9	**-7.8**	**0.1**	1.9
L-49	-7.4	-7.9	-7.8	-7.7	-7.7	-7.6	-7.6	-7.4	-7.5	-7.9	**-7.7**	**0.2**	2.5
L-50	-8.4	-8.4	-8.4	-8.4	-8.4	-8.4	-8.4	-8.4	-8.4	-8.4	**-8.4**	**0.0**	0.7
L-51	-7.8	-7.5	-7.8	-7.8	-7.8	-7.8	-7.8	-7.8	-7.8	-7.8	**-7.8**	**0.1**	2.0
L-52	-8.1	-8.1	-8.1	-8.1	-8.0	-8.0	-8.1	-8.1	-8.1	-8.1	**-8.1**	**0.0**	1.2
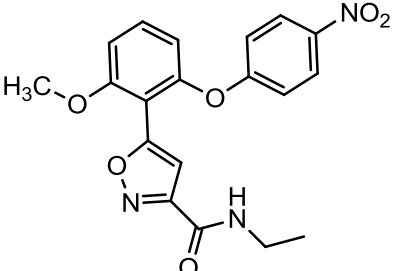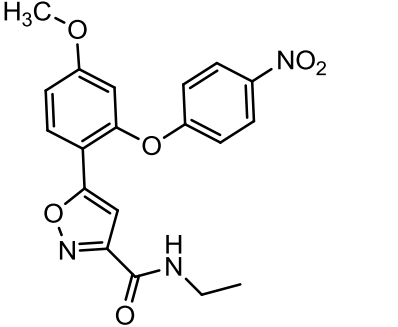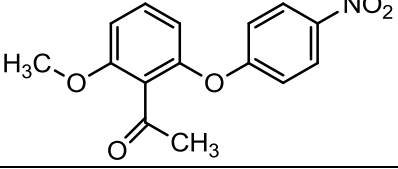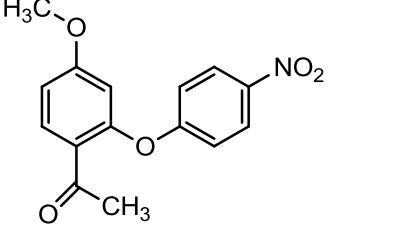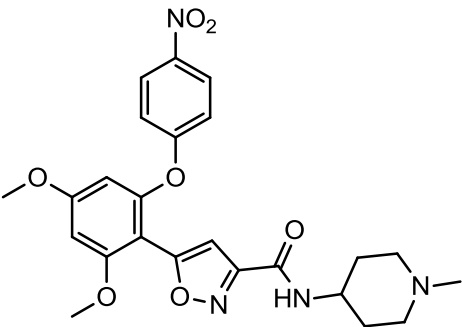
L-53	-7.8	-7.8	-7.8	-7.8	-7.8	-7.8	-7.8	-7.8	-7.8	-7.7	**-7.8**	**0.0**	1.9
L-54	-8.4	-8.4	-8.4	-8.4	-8.2	-8.3	-8.3	-8.4	-8.4	-8.2	**-8.3**	**0.1**	0.8
L-55	-8.4	-7.6	-8.3	-8.4	-8.3	-8.4	-8.3	-8.0	-8.4	-8.3	**-8.2**	**0.3**	0.9
L-56	-8.3	-8.3	-8.2	-8.0	-8.3	-8.2	-8.2	-8.2	-8.1	-8.1	**-8.2**	**0.1**	1.0
L-57	-8.6	-9.0	-8.9	-9.1	-8.9	-9.0	-9.0	-9.0	-9.0	-9.0	**-9.0**	**0.1**	0.3
L-58	-9.0	-9.2	-9.1	-9.2	-9.3	-9.1	-9.2	-9.2	-9.2	-9.2	**-9.2**	**0.1**	0.2
L-59	-9.1	-8.8	-9.2	-9.1	-9.1	-9.1	-9.1	-8.9	-9.1	-9.0	**-9.1**	**0.1**	0.2
L-60	-9.0	-9.6	-9.0	-8.9	-9.0	-8.9	-9.5	-9.0	-8.9	-9.0	**-9.1**	**0.3**	0.2
L-61	-8.9	-8.9	-8.9	-9.4	-9.5	-8.9	-8.8	-8.9	-8.9	-8.9	**-9.0**	**0.2**	0.3
L-62	-9.2	-9.2	-9.2	-9.2	-9.2	-9.2	-9.2	-9.2	-9.3	-9.2	**-9.2**	**0.0**	0.2
L-63	-9.4	-9.5	-9.4	-9.5	-9.5	-9.5	-9.4	-9.5	-9.5	-9.5	**-9.5**	**0.0**	0.1
L-64	-9.3	-9.2	-8.9	-9.3	-9.2	-9.4	-9.4	-8.4	-9.3	-9.2	**-9.2**	**0.3**	0.2
L-65	-8.9	-8.9	-8.9	-8.8	-8.9	-9.0	-8.8	-8.7	-8.7	-8.8	**-8.8**	**0.1**	0.3
L-66	-8.5	-8.5	-8.5	-8.5	-8.4	-8.5	-8.5	-8.3	-8.5	-8.5	**-8.5**	**0.1**	0.6
L-67	-7.5	-7.9	-8.1	-8.0	-7.2	-7.3	-7.1	-7.9	-7.4	-7.9	**-7.6**	**0.4**	2.6
L-68	-8.1	-8.1	-8.1	-8.1	-8.1	-8.0	-8.1	-8.1	-8.1	-8.1	**-8.1**	**0.0**	1.2
L-69	-8.9	-8.6	-8.6	-8.1	-9.0	-9.2	-7.9	-8.6	-8.1	-8.0	**-8.5**	**0.5**	0.6
L-70	-8.4	-8.4	-8.2	-8.4	-8.3	-8.3	-8.4	-8.4	-8.4	-8.4	**-8.4**	**0.1**	0.7
L-71	-8.9	-8.8	-8.9	-8.9	-9.0	-8.9	-8.8	-8.9	-8.9	-8.9	**-8.9**	**0.1**	0.3
L-72	-9.1	-9.1	-9.1	-9.1	-9.1	-9.1	-9.1	-9.1	-9.1	-9.1	**-9.1**	**0.0**	0.2
L-73	-9.0	-9.0	-9.0	-9.0	-9.0	-9.0	-8.9	-9.0	-9.0	-9.0	**-9.0**	**0.0**	0.3
L-74	-8.3	-9.0	-8.5	-9.2	-8.4	-8.4	-9.0	-8.2	-8.7	-8.5	**-8.6**	**0.3**	0.5
L-75	-9.3	-9.3	-9.4	-9.4	-9.4	-9.5	-9.3	-9.4	-9.5	-9.4	**-9.4**	**0.1**	0.1
L-76	-9.2	-8.9	-8.7	-8.6	-8.5	-9.1	-8.6	-8.8	-8.7	-8.7	**-8.8**	**0.2**	0.4
L-77	-8.8	-8.8	-8.9	-8.8	-8.7	-8.6	-8.6	-9.1	-8.8	-8.7	**-8.8**	**0.1**	0.4
L-78	-8.3	-7.9	-8.3	-8.3	-8.9	-8.3	-8.4	-8.3	-8.8	-8.4	**-8.4**	**0.3**	0.7
L-79	-9.1	-9.3	-8.9	-9.1	-9.9	-10	-9.9	-10	-9.7	-10	**-9.6**	**0.4**	0.1
L-80	-8.5	-8.7	-8.5	-8.1	-8.7	-8.7	-8.6	-8.6	-8.7	-8.6	**-8.6**	**0.2**	0.5
L-81	-9.6	-9.6	-9.6	-9.8	-9.7	-10.1	-9.8	-9.6	-10	-9.8	**-9.8**	**0.2**	0.1
L-82	-8.7	-8.5	-8.4	-8.4	-8.5	-8.9	-9.1	-8.9	-8.7	-9.1	**-8.7**	**0.3**	0.4
L-83	-8.5	-8.4	-8.4	-8.4	-8.5	-8.5	-8.3	-8.5	-8.4	-8.4	**-8.4**	**0.1**	0.7
L-84	-8.7	-8.7	-8.8	-8.7	-8.7	-8.7	-8.7	-8.7	-8.8	-8.7	**-8.7**	**0.0**	0.4
L-85	-9.1	-8.8	-8.7	-8.8	-8.9	-8.7	-8.8	-8.9	-8.8	-8.7	**-8.8**	**0.1**	0.3
L-86	-8.8	-9.0	-9.7	-9.5	-9.3	-9.5	-9.6	-9.1	-9.0	-9.1	**-9.3**	**0.3**	0.2
L-87	-9.2	-9.2	-9.3	-9.1	-9.2	-9.3	-9.2	-9.2	-9.3	-9.2	**-9.2**	**0.1**	0.2
L-88	-9.9	-9.9	-9.8	-9.8	-10.0	-9.8	-10.0	-10.0	-9.9	-9.8	**-9.9**	**0.1**	0.1
L-89	-9.4	-9.4	-9.4	-8.9	-9.4	-9.4	-9.4	-9.3	-9.3	-9.3	**-9.3**	**0.2**	0.1
L-90	-7.1	-7.6	-7.6	-7.6	-7.6	-7.6	-7.0	-7.6	-7.6	-7.7	**-7.5**	**0.2**	3.2
L-91	-7.3	-8.3	-8.1	-8.4	-8.5	-8.2	-8.2	-8.3	-8.5	-8.2	**-8.2**	**0.3**	1.0
L-92	-7.9	-7.9	-7.9	-7.8	-8.0	-7.8	-8.0	-8.0	-8.0	-7.8	**-7.9**	**0.1**	1.6
L-93	-8.2	-8.9	-8.9	-8.4	-8.4	-9.2	-9.1	-8.3	-9.1	-9.2	**-8.8**	**0.4**	0.4
L-94	-8.6	-8.3	-8.4	-8.6	-8.4	-8.6	-8.6	-8.5	-8.6	-8.4	**-8.5**	**0.1**	0.6
L-95	-9.4	-9.4	-9.3	-9.4	-8.5	-9.2	-9.3	-9.2	-8.4	-8.8	**-9.1**	**0.4**	0.2

L-96	-7.4	-7.3	-7.3	-7.3	-7.3	-7.3	-7.3	-7.1	-7.3	-7.3	**-7.3**	**0.1**	4.5
L-97	-8.7	-8.6	-8.7	-8.5	-8.6	-8.6	-8.5	-8.5	-8.5	-8.6	**-8.6**	**0.1**	0.5
L-98	-8.0	-8.5	-8.0	-8.2	-8.5	-8.1	-8.1	-8.1	-8.2	-8.5	**-8.2**	**0.2**	0.9
L-99	-7.4	-7.2	-7.5	-7.4	-7.4	-7.4	-7.4	-7.5	-7.4	-7.3	**-7.4**	**0.1**	3.8
L-100	-8.7	-7.7	-7.6	-8.4	-7.8	-8.5	-7.7	-8.4	-8.6	-7.6	**-8.1**	**0.5**	1.2
L-102	-8.5	-8.7	-8.7	-8.7	-8.6	-8.5	-8.6	-8.6	-8.5	-8.5	**-8.6**	**0.1**	0.5
L-103	-8.0	-7.5	-8.0	-7.4	-7.6	-7.6	-7.6	-8.3	-8.2	-7.8	**-7.8**	**0.3**	1.9
L-104	-9.2	-8.7	-7.8	-8.0	-8.9	-7.9	-8.6	-7.8	-8.6	-7.9	**-8.3**	**0.5**	0.8

Appendix III: List of the molecules screened by molecular docking
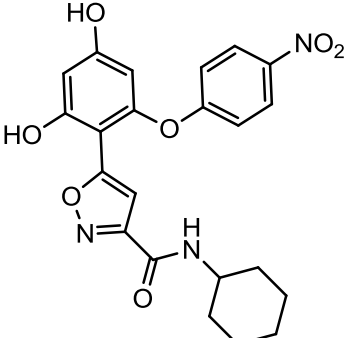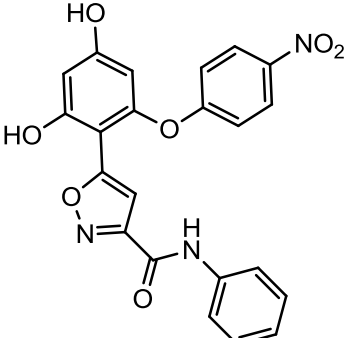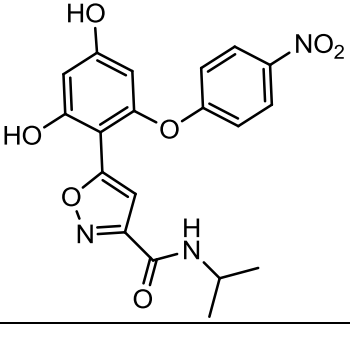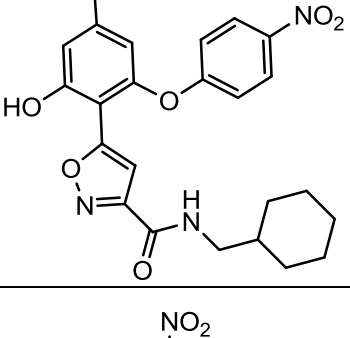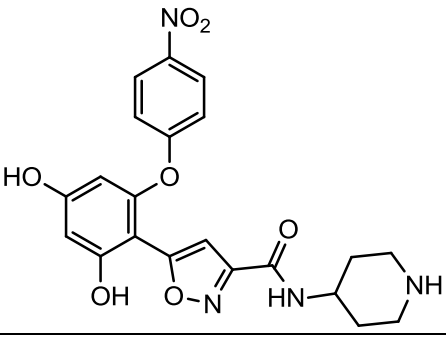
Code	Formula	Smiles	M.W.	Maximum Approximate length (Å)
L-1		O=C(C1=NOC(C2=C(OC3=CC=C([N+]([O-])=O)C=C3)C=C(O)C=C2O)=C1)NC4CCN(C)CC4	454.43	16
L-2		OC1=CC(OC2=CC=C([N+]([O-])=O)C=C2)=C(C3=CC(C(NCC)=O)=NO3)C(O)=C1	385.33	17
L-3		OC1=CC(O)=CC(OC2=CC(Cl)=C(Cl)C=C2)=C1	271.10	11
L-4		ClC1=CC=C(OC2=C(C3=CC(C(NCC)=O)=NO3)C(O)=CC(O)=C2)C=C1	374.78	16

148

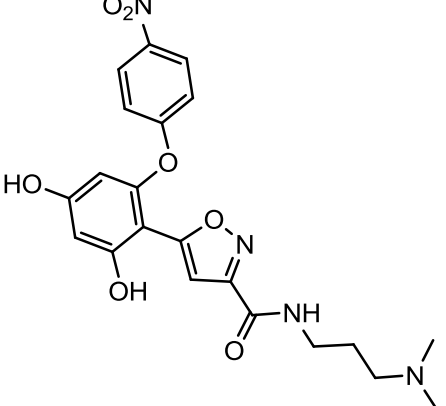| L-5 | | CC(C1=C(OC2=CC=C([N+]([O-])=O)C=C2)C=C(OC)C=C1OC)=O | 317.29 | 11 |
L-6		CC(C1=C(OC2=CC=C(Cl)C=C2)C=C(OC)C=C1OC)=O	306.74	11
TU-011 (L-7) **43**		COC1=CC(OC2=CC=C([N+]([O-])=O)C=C2)=C(C3=CC(C(OCC)=O)=NO3)C(OC)=C1	414.37	15
L-8		COC1=CC(OC2=CC=C([N+]([O-])=O)C=C2)=C(C3=CC(C(NCC)=O)=NO3)C(OC)=C1	413.38	16
L-9		ClC1=CC=C(OC2=C(C3=CC(C(NCC)=O)=NO3)C(OC)=CC(OC)=C2)C=C1	402.83	16

L-10		COC1=CC=CC(OC2=CC=C([N+]([O-])=O)C=C2)=C1C3=CC(C(NCC)=O)=NO3	383.35	13
L-11		COC1=CC(OC2=CC=C([N+]([O-])=O)C=C2)=C(C3=CC(C(NCC)=O)=NO3)C=C1	383.35	15
L-12		CC(C1=C(OC2=CC=C([N+]([O-])=O)C=C2)C=CC=C1OC)=O	287.27	13
L-13		CC(C1=C(OC2=CC=C([N+]([O-])=O)C=C2)C=C(OC)C=C1)=O	287.27	12
TU-016 (L-14) **60**		O=C(C1=NOC(C2=C(OC3=CC=C([N+]([O-])=O)C=C3)C=C(OC)C=C2OC)=C1)NC4CCN(C)CC4	482.49	20
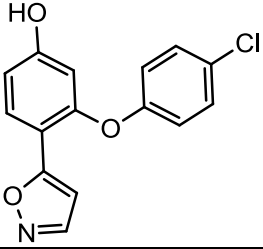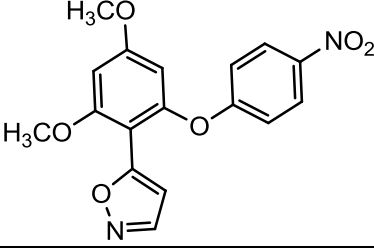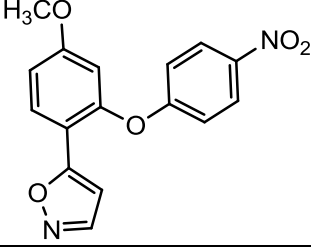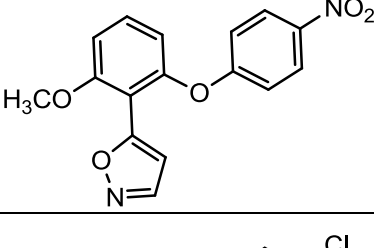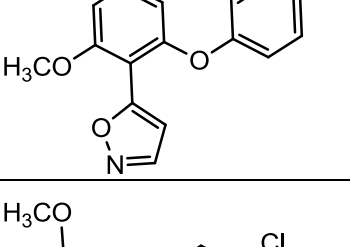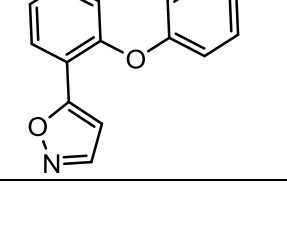
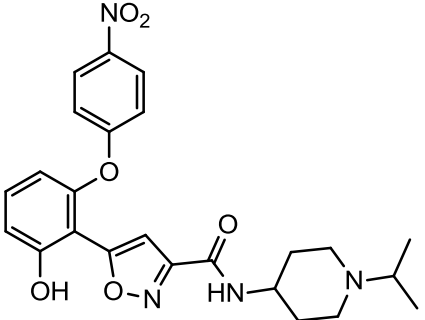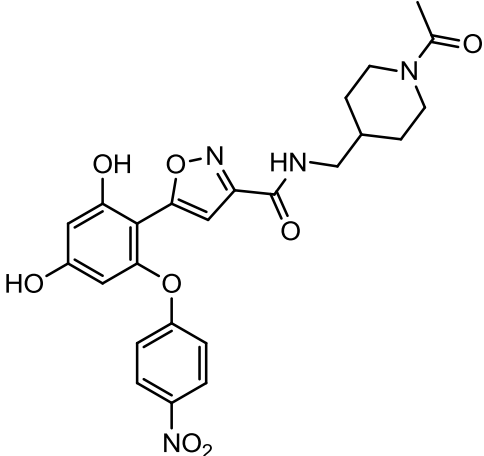| L-15		ClC1=CC=C(OC2=C(C3=CC(C(OCC)=O)=NO3)C(OC)=CC(OC)=C2)C=C1	403.81	14
L-16		COC1=CC=CC(OC2=CC=C([N+]([O-])=O)C=C2)=C1C3=CC(C(OCC)=O)=NO3	384.34	12
L-17		COC1=CC(OC2=CC=C([N+]([O-])=O)C=C2)=C(C3=CC(C(OCC)=O)=NO3)C=C1	384.34	17
L-18		ClC1=CC=C(OC2=C(C3=CC=NO3)C(OC)=CC(OC)=C2)C=C1	331.75	13
L-19		ClC1=CC=C(OC2=C(C3=CC=NO3)C(O)=CC(O)=C2)C=C1	303.70	12

L-20		OC1=CC=CC(OC2=CC=C([N+]([O-])=O)C=C2)=C1C3=CC(C(NCC)=O)=NO3	369.33	14
L-21		OC1=CC(OC2=CC=C([N+]([O-])=O)C=C2)=C(C3=CC(C(NCC)=O)=NO3)C=C1	369.33	15
L-22		CC(C1=C(OC2=CC=C(N)C=C2)C=C(OC)C=C1OC)=O	287.31	12
L-23		CC(C1=C(OC2=CC=C(N)C=C2)C=CC=C1OC)=O	257.28	11
L-24		CC(C1=C(OC2=CC=C(N)C=C2)C=C(OC)C=C1)=O	257.28	12
L-25		OC1=CC(OCC2=CC=C([N+]([O-])=O)C=C2)=C(C3=CC(C(NCC)=O)=NO3)C(O)=C1	399.35	16
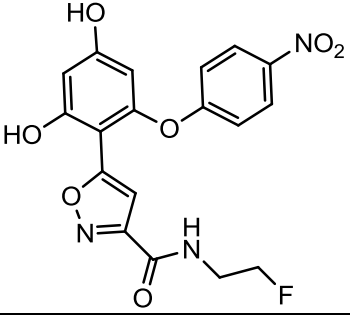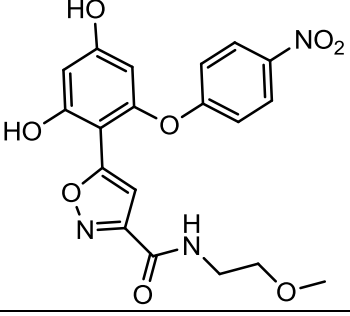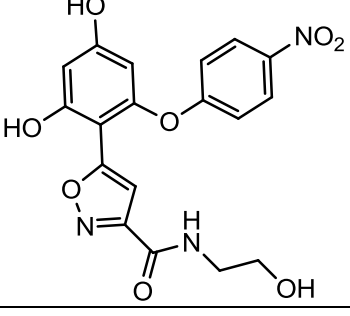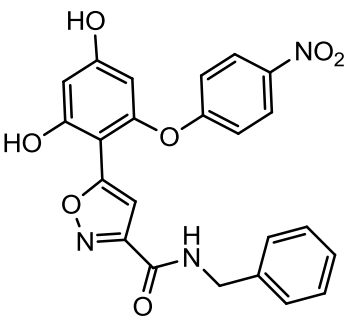
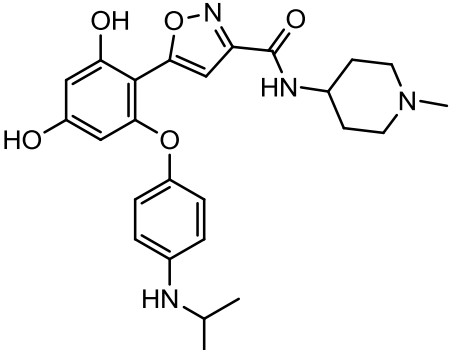| L-26		OC1=CC(OC2=CC=C([N+]([O-])=O)C=C2)=C(C3=CC(C(NC4CCCCC4)=O)=NO3)C(O)=C1	439.42	17
L-27		OC1=CC(OC2=CC=C([N+]([O-])=O)C=C2)=C(C3=CC(C(NC4=CC=CC=C4)=O)=NO3)C(O)=C1	433.37	14
L-28		OC1=CC(OC2=CC=C([N+]([O-])=O)C=C2)=C(C3=CC(C(NC(C)C)=O)=NO3)C(O)=C1	399.35	15
L-29		OC1=CC(OC2=CC=C([N+]([O-])=O)C=C2)=C(C3=CC(C(NCC4CCCCC4)=O)=NO3)C(O)=C1	453.44	14
L-30		O=C(C1=NOC(C2=C(OC3=CC=C([N+]([O-])=O)C=C3)C=C(O)C=C2O)=C1)NC4CCNCC4	440.41	15

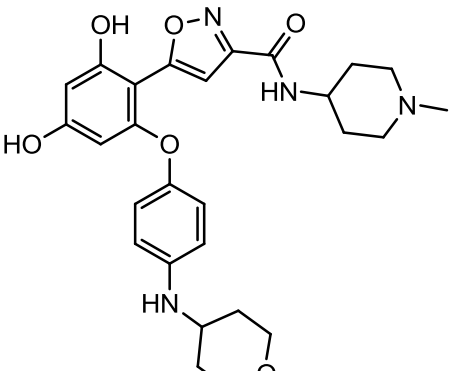| L-31		O=C(C1=NOC(C2=C(OC3=CC=C([N+]([O-])=O)C=C3)C=C(O)C=C2O)=C1)NC4CCN(C(C)C)CC4	482.49	18
L-32		ClC1=CC=C(OC2=C(C3=CC(C(OCC)=O)=NO3)C(O)=CC(O)=C2)C=C1	375.76	12
L-33		ClC1=CC=C(OC2=C(C3=CC(C(OCC)=O)=NO3)C=CC(O)=C2)C=C1	359.76	12
L-34		ClC1=CC=C(OC2=C(C3=CC(C(OCC)=O)=NO3)C(O)=CC=C2)C=C1	359.76	12
L-35		OC1=CC(OC2=CC=C([N+]([O-])=O)C=C2)=C(C3=CC(C(OCC)=O)=NO3)C(O)=C1	386.31	16

L-36		OC1=CC(OC2=CC=C([N+]([O-])=O)C=C2)=C(C3=CC(C(OCC)=O)=NO3)C=C1	370.31	13
L-37		OC1=CC=CC(OC2=CC=C([N+]([O-])=O)C=C2)=C1C3=CC(C(OCC)=O)=NO3	370.31	12
L-38		OC1=CC(OC2=CC=C([N+]([O-])=O)C=C2)=C(C3=CC=NO3)C(O)=C1	314.25	12
L-39		OC1=CC(OC2=CC=C([N+]([O-])=O)C=C2)=C(C3=CC=NO3)C=C1	298.25	12
L-40		OC1=CC=CC(OC2=CC=C([N+]([O-])=O)C=C2)=C1C3=CC=NO3	298.25	13
L-41		ClC1=CC=C(OC2=C(C3=CC=NO3)C(O)=CC=C2)C=C1	287.70	12

L-42		ClC1=CC=C(OC2=C(C3=CC=NO3)C=CC(O)=C2)C=C1	287.70	12
L-43		O=[N+]([O-])C1=CC=C(OC2=C(C3=CC=NO3)C(OC)=CC(OC)=C2)C=C1	342.30	14
L-44		O=[N+]([O-])C1=CC=C(OC2=C(C3=CC=NO3)C=CC(OC)=C2)C=C1	312.28	13
L-45		O=[N+]([O-])C1=CC=C(OC2=C(C3=CC=NO3)C(OC)=CC=C2)C=C1	312.28	12
L-46		ClC1=CC=C(OC2=C(C3=CC=NO3)C(OC)=CC=C2)C=C1	301.72	13
L-47		ClC1=CC=C(OC2=C(C3=CC=NO3)C=CC(OC)=C2)C=C1	301.72	12
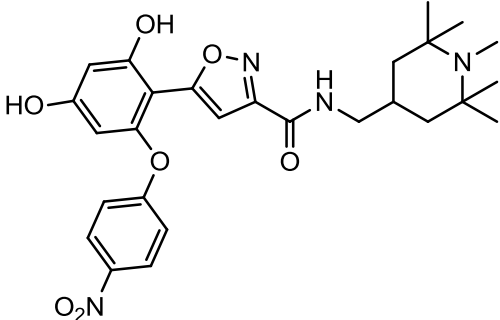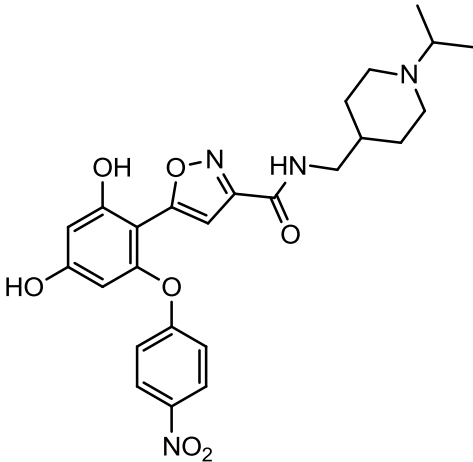
ID	Structure	SMILES		
L-48		OC1=CC(OC2=CC=C([N+]([O-])=O)C=C2)=C(C3=CC(C(OC)=O)=NO3)C(O)=C1	372.29	15
L-49		ClC1=CC=C(OC2=C(C3=CC(C(OC)=O)=NO3)C(O)=CC(O)=C2)C=C1	361.73	14
L-50		OC1=CC(OC2=CC=C([N+]([O-])=O)C=C2)=C(C3=CC(C(O)=O)=NO3)C(O)=C1	358.26	13
L-51		ClC1=CC=C(OC2=C(C3=CC(C(O)=O)=NO3)C(O)=CC(O)=C2)C=C1	347.71	12
L-52		OC1=CC(OC2=CC=C([N+]([O-])=O)C=C2)=C(C3=CC(C(N(C)C)=O)=NO3)C(O)=C1	385.33	15

L-53		OC1=CC(OC2=CC=C([N+]([O-])=O)C=C2)=C(C3=CC(C(NCCF)=O)=NO3)C(O)=C1	403.32	14
L-54		OC1=CC(OC2=CC=C([N+]([O-])=O)C=C2)=C(C3=CC(C(NCCOC)=O)=NO3)C(O)=C1	415.35	17
L-55		OC1=CC(OC2=CC=C([N+]([O-])=O)C=C2)=C(C3=CC(C(NCCO)=O)=NO3)C(O)=C1	401.33	17
L-56		O=C(C1=NOC(C2=C(OC3=CC=C([N+]([O-])=O)C=C3)C=C(O)C=C2O)=C1)NCCCN(C)C	442.42	13
L-57		OC1=CC(OC2=CC=C([N+]([O-])=O)C=C2)=C(C3=CC(C(NCC4=CC=CC=C4)=O)=NO3)C(O)=C1	447.40	17

158
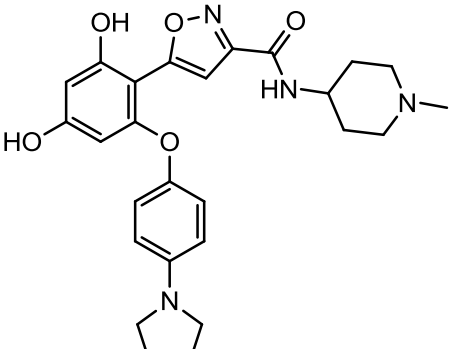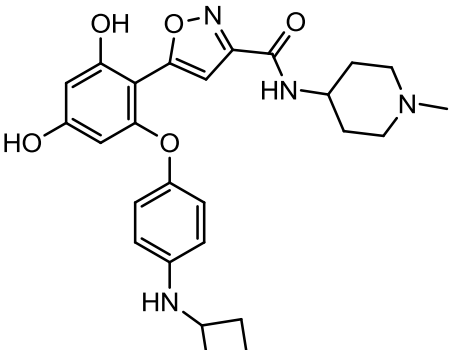
L-58		OC1=CC(OC2=CC=C([N+]([O-])=O)C=C2)=C(C3=CC(C(NCC4CCCNC4)=O)=NO3)C(O)=C1	454.43	18
L-59		OC1=CC(OC2=CC=C([N+]([O-])=O)C=C2)=C(C3=CC(C(NCC4CCNCC4)=O)=NO3)C(O)=C1	454.43	17
L-60		OC1=CC(OC2=CC=C([N+]([O-])=O)C=C2)=C(C3=CC(C(NCC4CCCN(C)C4)=O)=NO3)C(O)=C1	468.46	14
L-61		OC1=CC(OC2=CC=C([N+]([O-])=O)C=C2)=C(C3=CC(C(NCC4CCN(C)CC4)=O)=NO3)C(O)=C1	468.46	17
L-62		OC1=CC(OC2=CC=C([N+]([O-])=O)C=C2)=C(C3=CC(C(NC4CC(C)(C)N(C)C(C)(C)C4)=O)=NO3)C(O)=C1	510.54	17
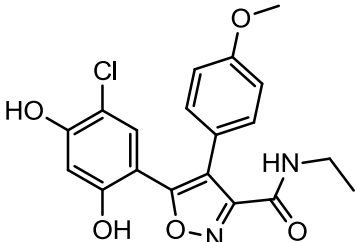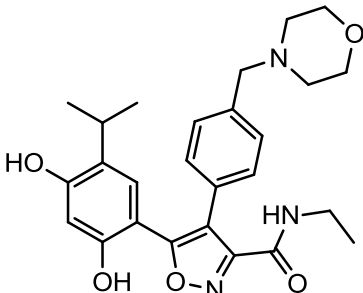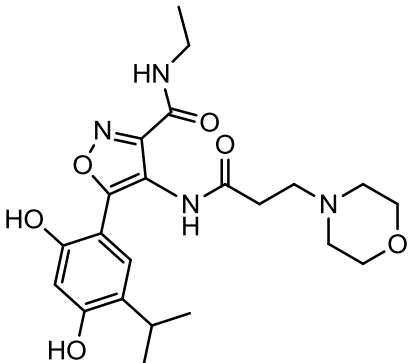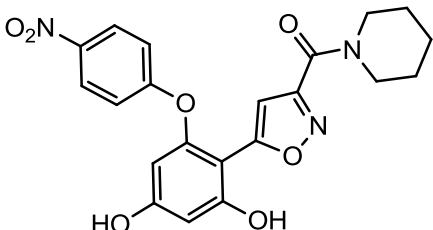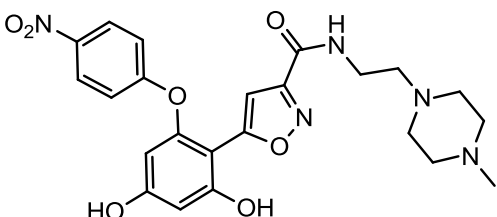
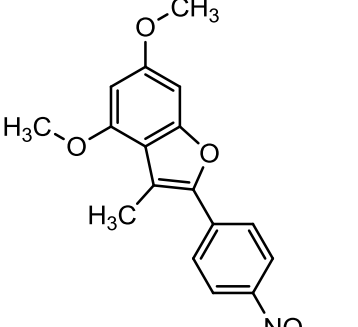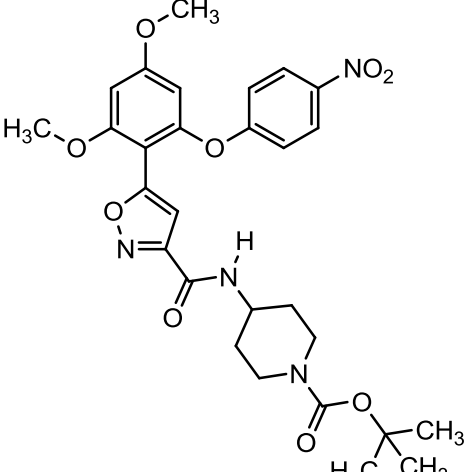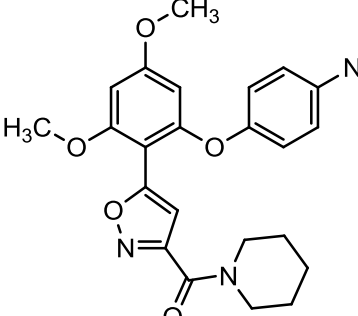| L-63 | | OC1=CC(OC2=CC=C([N+]([O-])=O)C=C2)=C(C3=CC(C(NC4CCN(C(C)=O)CC4)=O)=NO3)C(O)=C1 | 482.44 | 19 |
L-64		OC1=CC(OC2=CC=C([N+]([O-])=O)C=C2)=C(C3=CC(C(NC4CCN(CCCC(F)(F)F)CC4)=O)=NO3)C(O)=C1	550.48	20
L-65		OC1=CC(OC2=CC=C([N+]([O-])=O)C=C2)=C(C3=CC(C(NC4CCN(C5CCCCC5)CC4)=O)=NO3)C(O)=C1	522.55	17
L-66		OC1=CC(OCC2=CC=C([N+]([O-])=O)C=C2)=C(C3=CC(C(NC4CCN(C)CC4)=O)=NO3)C(O)=C1	468.46	16
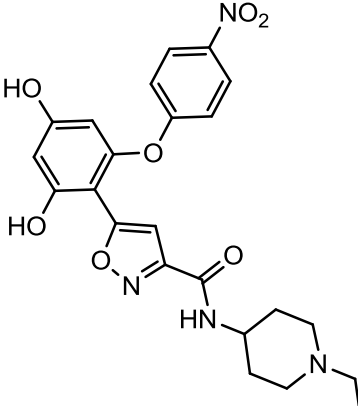
L-67		OC1=CC(OCC2=CC=C(C=C2)[N+]([O-])=O)=C(C=C1)C3=CC(C(NCC)=O)=NO3	383.35	13
L-68		[O-][N+](C(C=C1)=CC=C1COC(C=CC=C2O)=C2C3=CC(C(NCC)=O)=NO3)=O	383.35	13
L-69		OC1=CC(OCC2=CC=C(C=C2)[N+]([O-])=O)=C(C=C1)C3=CC(C(NC4CCN(CC4)C)=O)=NO3	452.46	16
L-70		[O-][N+](C(C=C1)=CC=C1COC(C=CC=C2O)=C2C3=CC(C(NC4CCN(CC4)C)=O)=NO3)=O	452.46	16
L-71		O=C(NC1CCN(CC1)C(C)C)C2=NOC(C3=C(C=C(C=C3)O)OC4=CC=C(C=C4)[N+]([O-])=O)=C2	466.49	19

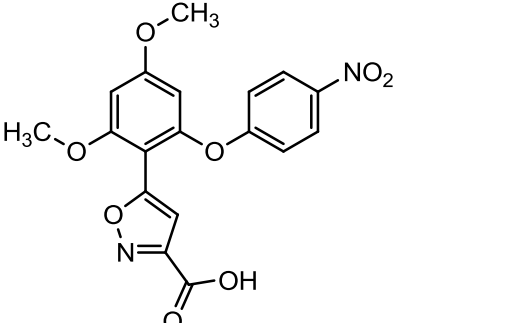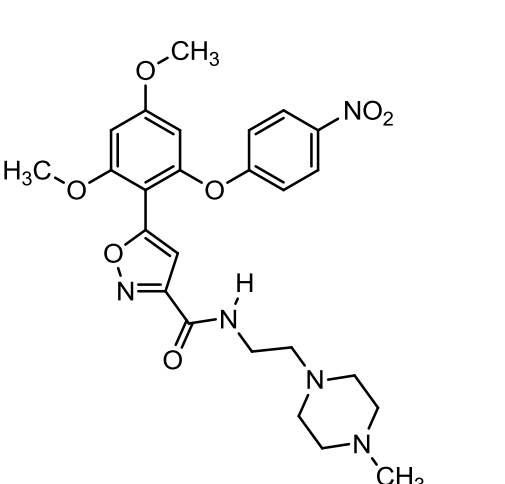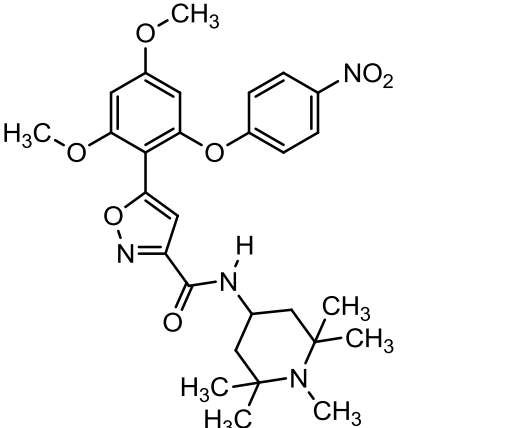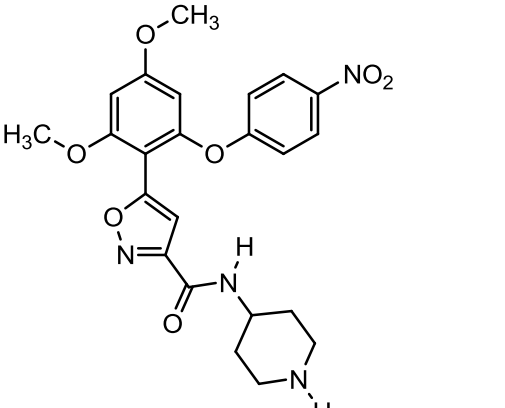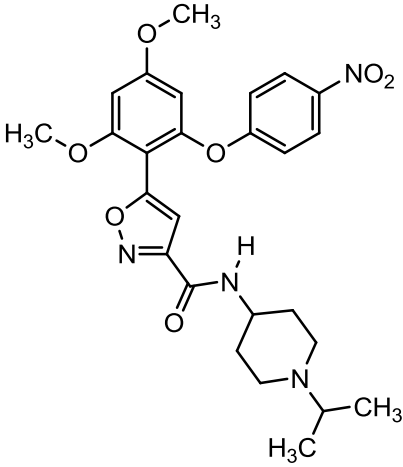| L-72		O=C(NC1CCN(CC1)C(C)C)C2=NOC(C3=C(C=CC=C3O)OC4=CC=C(C=C4)[N+]([O-])=O)=C2	466.49	21
L-73		OC1=CC(OC2=CC=C(C=C2)[N+]([O-])=O)=C(C(O)=C1)C3=CC(C(NCC4CC(C)(C)N(C)C(C)(C)C4)=O)=NO3	524.57	15
L-74		O=C(NCC1CCN(C(C)C)CC1)C2=NOC(C3=C(C=C(C=C3O)O)OC4=CC=C(C=C4)[N+]([O-])=O)=C2	496.51	14
L-75		OC1=CC(OC2=CC=C(C=C2)[N+]([O-])=O)=C(C(O)=C1)C3=CC(C(NCC4CCN(C(C)=O)CC4)=O)=NO3	496.47	14

L-76		OC1=CC(OC2=CC=C(C=C2)[N+]([O-])=O)=C(C(O)=C1)C3=CC(C(NC4CCN(C5CCCC5)CC4)=O)=NO3	508.52	13
L-77		OC1=CC(OC2=CC=C(C=C2)[N+]([O-])=O)=C(C(O)=C1)C3=CC(C(NC4CCN(C5CCCCC5)CC4)=O)=NO3	536.58	15
L-78		OC1=CC(OC2=CC=C(C=C2)[N+]([O-])=O)=C(C(O)=C1)C3=CC(C(NC4CCN(C5CCN(C)CC5)CC4)=O)=NO3	537.56	19
L-79		OC1=CC(OC2=CC=C(C=C2)[N+]([O-])=O)=C(C(O)=C1)C3=CC(C(NC4CCN(C5CCC6(OCCO6)CC5)CC4)=O)=NO3	580.59	21
L-80		OC1=CC(OC2=CC=C(C=C2)[N+]([O-])=O)=C(C(O)=C1)C3=CC(C(NC4CCN(CC5CCCCC5)CC4)=O)=NO3	536.58	18

L-81		OC1=CC(OC2=CC=C(C=C2)[N+]([O-])=O)=C(C(O)=C1)C3=CC(C(NC4CCN(CC5=CC=CC=C5)CC4)=O)=NO3	530.53	14
L-82		OC1=CC(OC2=CC=C(C=C2)N(C)C)=C(C(O)=C1)C3=CC(C(NC4CCN(C)CC4)=O)=NO3	452.50	14
L-83		OC1=CC(OC2=CC=C(C=C2)N(C)C)=C(C(O)=C1)C3=CC(C(NC4CCNCC4)=O)=NO3	438.48	18
L-84		OC1=CC(OC2=CC=C(C=C2)N(C)C)=C(C(O)=C1)C3=CC(C(NC4CCN(C5CCCCC5)CC4)=O)=NO3	520.62	19
L-85		OC1=CC(OC2=CC=C(C=C2)N(C)C)=C(C(O)=C1)C3=CC(C(NC4CCN(C5CCC6(OCCO6)CC5)CC4)=O)=NO3	578.66	17

L-86		OC1=CC(OC2=CC=C(C=C2)NC(C)C)=C(C(O)=C1)C3=CC(C(NC4CCN(C)CC4)=O)=NO3	466.53	18
L-87		OC1=CC(OC2=CC=C(C=C2)N3CCCC3)=C(C(O)=C1)C4=CC(C(NC5CCN(C)CC5)=O)=NO4	478.54	17
L-88		OC1=CC(OC2=CC=C(C=C2)NC3CCC3)=C(C(O)=C1)C4=CC(C(NC5CCN(C)CC5)=O)=NO4	478.54	20
L-89		OC1=CC(OC2=CC=C(C=C2)NC3CCOCC3)=C(C(O)=C1)C4=CC(C(NC5CCN(C)CC5)=O)=NO4	508.57	14

L-90 or VER-50589		OC1=C(Cl)C=C(C(O)=C1)C2=C(C3=CC=C(OC)C=C3)C(C(NCC)=O)=NO2	388.80	15
L-91 or NVP-AUY922		OC1=C(C(C)C)C=C(C(O)=C1)C2=C(C3=CC=C(CN4CCOCC4)C=C3)C(C(NCC)=O)=NO2	465.54	15
L-92 or SST0116 CL1		CC(C)C1=C(O)C=C(O)C(C2=C(N(C(CCN3CCOCC3)=O)[H])C(C(N([H])CC)=O)=NO2)=C1	446.50	16
L-93		O=C(C1=NOC(C2=C(OC3=CC=C([N+]([O-])=O)C=C3)C=C(O)C=C2O)=C1)N4CCCCC4	425.39	17
L-94		O=C(C1=NOC(C2=C(OC3=CC=C([N+]([O-])=O)C=C3)C=C(O)C=C2O)=C1)NCCN4CCN(C)CC4	483.47	15

L-95		OC1=CC(OC2=CC=C(C=C2)[N+]([O-])=O)=C(C(O)=C1)C3=CC(C(NC4CCN(CC4)CC)=O)=NO3	468.46	18
TU-007 (L-96) **55**		COC1=CC(OC)=CC2=C1C(C)=C(C3=CC=C([N+]([O-])=O)C=C3)O2	313.30	13
TU-012 (L-97) **49**		COC1=CC(OC2=CC=C([N+]([O-])=O)C=C2)=C(C3=CC(C(N([H])C4CCN(C(OC(C)(C)C)=O)CC4)=O)=NO3)C(OC)=C1	568.58	17
TU-013 (L-98) **57**		COC1=CC(OC)=CC(OC2=CC=C([N+]([O-])=O)C=C2)=C1C3=CC(C(N4CCCCC4)=O)=NO3	453.44	15

TU-014 (L-99) **58**		COC1=CC(OC)=CC(OC2=CC=C([N+]([O-])=O)C=C2)=C1C3=CC(C(O)=O)=NO3	386.31	14
TU-015 (L-100) **59**		COC1=CC(OC2=CC=C([N+]([O-])=O)C=C2)=C(C3=CC(C(N([H])CCN4CCN(C)CC4)=O)=NO3)C(OC)=C1	511.53	13
TU-017 (L-102) **61**		COC1=CC(OC2=CC=C([N+]([O-])=O)C=C2)=C(C3=CC(C(N([H])C4CC(C)(C)N(C)C(C)(C)C4)=O)=NO3)C(OC)=C1	538.59	18
TU-018 (L-103) **50**		COC1=CC(OC2=CC=C([N+]([O-])=O)C=C2)=C(C3=CC(C(N([H])C4CCN([H])CC4)=O)=NO3)C(OC)=C1	468.46	16

| TU-019 (L-104) **51** | | COC1=CC(OC2=CC=C([N+]([O-])=O)C=C2)=C(C3=CC(C(N([H])C4CCN(C(C)C)CC4)=O)=NO3)C(OC)=C1 | 510.54 | 17 |